uOttawa

L'Université canadienne
Canada's university

FACULTÉ DES ÉTUDES SUPÉRIEURES ET POSTOCTORALES

uOttawa

L'Université canadienne
Canada's university

FACULTY OF GRADUATE AND POSDOCTORAL STUDIES

Patrick Boily

AUTEUR DE LA THÈSE / AUTHOR OF THESIS

Ph.D. (Mathematics)

GRADE / DEGREE

Department of Mathematics and Statistics

FACULTÉ, ÉCOLE, DÉPARTEMENT / FACULTY, SCHOOL, DEPARTMENT

Spiral Wave Dynamics under Full Euclidean Symmetry-breaking: A Dynamical System Approach

TITRE DE LA THÈSE / TITLE OF THESIS

Victor LeBlanc

DIRECTEUR (DIRECTRICE) DE LA THÈSE / THESIS SUPERVISOR

CO-DIRECTEUR (CO-DIRECTRICE) DE LA THÈSE / THESIS CO-SUPERVISOR

EXAMINATEURS (EXAMINATRICES) DE LA THÈSE / THESIS EXAMINERS

Benoit Dionne

Björn Sandstede

Frithjof Lutscher

Sam Melkonian

Gary W. Slater

Le Doyen de la Faculté des études supérieures et postdoctorales / Dean of the Faculty of Graduate and Postdoctoral Studies

SPIRAL WAVE DYNAMICS UNDER FULL EUCLIDEAN SYMMETRY-BREAKING: A DYNAMICAL SYSTEM APPROACH

By
Patrick Boily, B.Sc., M.S., Ph.D.
November 2005

A Thesis
submitted to the School of Graduate Studies and Research
in partial fulfillment of the requirements
for the degree of
Doctor of Philosophy in Mathematics[1]

by Patrick Boily, B.Sc., M.S., Ph.D., Ottawa, Canada

[1]The Ph.D. Program is a joint program with Carleton University, administered by the Ottawa-Carleton Institute of Mathematics and Statistics.

Your file Votre référence
ISBN: 978-0-494-18575-9
Our file Notre référence
ISBN: 978-0-494-18575-9

I certify that I have read this thesis and that in my opinion it is fully adequate, in scope and in quality, as a dissertation for the degree of Doctor of Philosophy.

Victor G. LeBlanc, University of Ottawa
(Principal Advisor)

Benoit Dionne, University of Ottawa

Frithjof Lutscher, University of Ottawa

Sam Melkonian, Carleton University

Björn Sandstede, University of Surrey

Approved for the University Committee on Graduate Studies:

Gary Slater
Dean of Graduate Studies & Research

In darkness you make out a spiraling shape
Putting all reason aside you exchange
What you got for a thing that's hypnotic and strange
The spiraling shape will make you go insane

— They Might Be Giants, *Spiraling Shape*

Abstract

Spirals are common in Nature: the snail's shell and the ordering of seeds in the sunflower are amongst the most widely-known occurrences. While these are static, dynamic spirals can also be observed in excitable systems such as heart tissue, retina, certain chemical reactions, slime mold aggregates, flame fronts, etc. The images associated with these spirals are often breathtaking, but spirals have also been linked to cardiac arrhythmias, a potentially fatal heart ailment.

In the literature, very specific models depending on the excitable system of interest are used to explain the observed behaviour of spirals (such as anchoring or drifting). Barkley [5] first noticed that the Euclidean symmetry of these models, and not the model itself, is responsible for the observed behaviour. But in experiments, the physical domain is never Euclidean. The heart, for instance, is finite, anisotropic and littered with inhomogeneities. To capture this loss of symmetry, LeBlanc and Wulff [48,51] introduced forced Euclidean symmetry-breaking (FESB) in the analysis.

To accurately model the physical situation, two basic types of symmetry-breaking perturbations are used: translational symmetry-breaking (TSB) and rotational symmetry-breaking (RSB) terms. LeBlanc and Wulff, [51] and LeBlanc [48] have studied the effects of these individual perturbations, and they have shown that phenomena such as anchoring and quasi-periodic meandering can be explained by FESB. However, these specific perturbations only tell part of the story.

In this thesis, the effects of multiple TSB perturbations, as well as those of combined TSB-RSB perturbations are studied and provide a more complete explanation for two aspects of spiral dynamics: anchoring and boundary drifting. Higher codimension phenomena are also considered.

Acknowledgements

I would like to thank Victor G. LeBlanc who suggested a very rich thesis topic and guided me through the meandering field of spiral dynamics; Richard Levine who helped me bring this work to its conclusion in spite of all my efforts to the contrary; Alain Vinet who spontaneously offered his academic kinship at a time of need; Christiane Laperrière who made it all interesting again; Marc Ethier and Eric Matsui who helped with numerics, and Mark Power and Sarah Rayfield who gave of themselves so relentlessly, from half a world away.

J'aimerais aussi remercier Marcel Boily, qui m'a initié très tôt aux mystères des mathématiques; Danyelle Bertrand, qui m'a encouragé à essayer de les comprendre dès mon enfance, et surtout (surtout!) Elowyn Boily, qui a prêté son nom et son enthousiasme à une section très colorée de cet ouvrage et pour qui le sacrifice en vaudra définitivement toujours la peine. Je t'aime et t'aimerai toujours, ma grande.

Finally, I would like to express my gratitude to the examining committee for reading this document and improving its contents.

Dedication

À Tara. Let's not kid ourselves: I couldn't have done this without you. I owe you more than you will ever know.

Contents

Abstract v

List of Figures xiii

List of Tables xiv

1 Introduction 1

1.1 Historical Perspective 2

1.1.1 The Dynamical System Approach 5

1.1.2 The Effects of Euclidean Symmetry Breaking 9

1.2 Thesis Overview 12

2 Preliminaries 14

2.1 Reaction-Diffusion Systems on $\mathbb{R}^2$ 14

2.1.1 Existence and Uniqueness of Solutions 16

2.1.2 $\mathbb{SE}(2)-$Equivariance of Solutions 17

2.2 The Center Manifold Reduction Theorem 18

2.3 Integral Manifolds and Averaging Methods 21

2.4 The Implicit Function Theorem 24

2.5 Bifurcations of Fixed Points 25

2.5.1 The Saddle-Node Singularity 25

2.5.2 The Cusp Singularity 26

2.5.3 The Bogdanov-Takens Singularity 27

2.6 Other Notions and Results 28

2.7 Appendix: Technical Details 29

3 The Center Bundle Equations **34**
3.1 General Form of the Perturbations 34
3.2 Specific Form of the Perturbations 37
3.3 Appendix: Technical Details 40

4 Analysis of the Center Bundle Equations **42**
4.1 Spiral Anchoring 43
4.2 Epicyclic Drifting 47
4.3 Higher Codimension Phenomena 54
4.4 Appendix: Technical Details 61

5 Characterization of Spiral Anchoring $(n = 2)$ **69**
5.1 A Specific Mapping 70
5.2 The Search for Fixed Points 72
5.3 The Visual Criterion 76
5.3.1 The Elowyn-Bonhomme Map 78
5.3.2 Back to the Criterion 82
5.4 The General Mapping 85
5.5 Appendix: Technical Details 90

6 Combined TSB and RSB Perturbations **93**
6.1 Center Bundle Equations 94
6.2 Analysis of the Center Bundle Equations 96
6.2.1 The Case $\ell = 1$ 97
6.2.2 The Case $\ell > 1$ 101
6.3 Characterization of Spiral Anchoring $(\ell = 1)$ 103
6.4 Appendix: Technical Details 106

7 Examples and Simulations **107**
7.1 PDE and Semi-Flows 107
7.1.1 Spiral Anchoring 108
7.1.2 Homotopy and Hysteresis of Rotating Waves 115
7.2 Dynamics on the Center Bundle 118
7.2.1 Anchoring at Infinity 119
7.2.2 Saddle-Node Bifurcation of Rotating Waves 121

7.2.3 Collapse of the Epicycle Manifold 125
7.2.4 Combined TSB and RSB Perturbations 128
7.3 Wedges and Catastrophes 130
7.4 Appendix: Technical Details 135

8 Conclusion **140**
8.1 Conjectures 140
8.2 Remarks 142
8.3 Possible Applications 143
8.4 Future and Related Work 144

A Article Summaries **146**
A.1 Summary of [5] 146
A.2 Summary of [51] 147
A.3 Summary of [48] 151

B Spirals in the Literature **153**

Bibliography **154**

Permissions

Figures 1.1 (left) on p. 2, 1.3 on p. 5 and 1.5 (bottom) on p. 11 are reproduced from [39], [6] and [59], respectively, with the consent of the authors and of the American Physical Society.

Figure 1.1 (right) on p. 2 is reproduced from [10], with the consent of the author and of Princeton University Press.

Figures 1.2 on p. 3 and 1.5 (top) on p. 11 are reproduced from [51], with the consent of the authors and of Springer-Verlag.

Figure 1.4 on p. 8 is reproduced from [7], with the consent of the authors and of the American Institute of Physics.

List of Figures

1.1 Spirals in excitable media. 2
1.2 Possible paths of the spiral wave tip. 3
1.3 Bifurcation diagram of spiral wave dynamics in (1.1.2). 5
1.4 Bifurcation diagram of (1.1.5). 8
1.5 Non-standard motions of the spiral wave tip. 11

2.1 Bifurcation diagram near a saddle-node singularity. 25
2.2 Neighbourhood of a cusp singularity. 26
2.3 Neighbourhood of a BT singularity; homoclinic tangencies. 27

5.1 Wedges in parameter space. 70
5.2 The four wedge angles in parameter space. 74
5.3 The set $\kappa(\mathfrak{Z})$ for the EB map. 79
5.4 Fixed point branches of P_ρ for the EB map. 80
5.5 Intersections of the zero-level sets $\kappa(\mathfrak{Z})$ and $\mathcal{R}_j$, $j = 1, 2$. 81
5.6 Fixed point branches along $\gamma_{0.01}$ for the perturbed EB map. 88
5.7 Wedges W_0 and $\mathfrak{W}_0$ for the EB maps. 89

7.1 Isolated spiral and spiral tip path in excitable media. 108
7.2 Anchoring in (7.1.1) with ϕ as in (7.1.2); $n = 1$. 109
7.3 Anchoring in (7.1.3) with ϕ as in (7.1.4); $n = 2$. 110
7.4 Anchoring in (7.1.5) with pert. as in (7.1.6); $n = 2$. 111
7.5 Anchoring in (7.1.5) with pert. as in (7.1.7); $n = 2$. 112
7.6 Anchoring in (7.1.5) with pert. as in (7.1.7); $n = 2$ (RK2). 113
7.7 Anchoring in (7.1.8); $n = 4$. 114
7.8 Anchoring in (7.1.11); $\ell = 1$. 116

7.9 Homotopy of the spiral tip path in (7.1.12). 117
7.10 Hysteresis of the spiral tip path in (7.1.12). 118
7.11 Phase diagrams of (7.2.6). 124
7.12 Epicycle manifold and rotating wave in (7.2.12). 126
7.13 Epicycle manifold and three rotating waves of (7.2.13). 127
7.14 Collapse of the epicycle manifold. 128
7.15 Epicycle manifold in (6.1.5), with H as in (7.2.14). 129
7.16 Spiral anchoring with $\mathbb{Z}_5-$symmetry; epicyclic drifting. 130
7.17 Wedges and catastrophes: the first example. 131
7.18 Wedges and catastrophes: the second example. 132
7.19 Wedges and catastrophes: the third example. 133
7.20 Wedges and catastrophes: the fourth example. 134
7.21 Wedges and catastrophes: the fifth example. 135

List of Tables

2.1 Real conic sections. 29

5.1 Fold catastrophes of P_ρ along C_0 and C_ξ for the EB map. 82
5.2 Partial bifurcation diagrams of P_ρ when $C_0 \neq C_\xi$. 84
5.3 Partial bifurcation diagrams of P_ρ when $C_0 = C_\xi$. 86

Chapter 1

Introduction

The spiral is an integral part of Nature: it can be seen in a snail's shell, in the layout of a sunflower's seeds and in the path of a falcon on a hunt, to name but a few. These particular instances are fixed in space, but spirals can also evolve in time: hurricanes and galaxies are common examples that come to mind. It is, however, rather arduous to conduct experiments on the latter physical objects, for obvious reasons.

On a smaller scale, where experiments are easier to control, spirals in evolution have also been observed in **excitable media** such as heart tissue, slime-mold aggregates, the retina or certain chemical reactions (such as the famed Belousov-Zhabotinsky (BZ) reaction). In these systems, waves propagate by 'exciting' a 'cell', which in turn 'excites' some of its neighbours before falling into a 'refractory' or 'unexcitable' state, followed by a 'resting' state, ready to be 'excited' should the wave come its way again.

These systems give rise to beautiful images (as can be attested to in Figure 1.1). While this in itself might yield enough interest to study them, there is also (at least) one serious reason to do so: spiral waves have been linked to **cardiac arrhythmias**, *i.e.*, to disruptions of the heart's normal electrical cycle [74, 75]. Most arrhythmias are harmless but if they are 're-entrant in nature and [...] occur [in the ventricles] because of the spatial distribution of cardiac tissue [44, p. 401]', they can seriously hamper the pumping mechanism of the heart and so lead to death. As a result, a full understanding of spiral wave dynamics in these media becomes imperative.

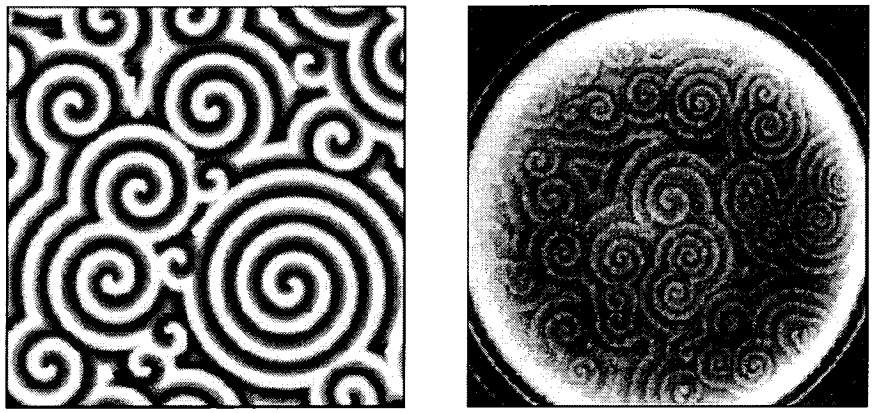

Figure 1.1: Spirals in excitable media. On the left, spirals in a solution of the Ginzburg-Landau equation (from Hendrey, Ott and Antonsen [39]), on the right, spirals in colonies of the slime-mold aggregate *Dictyostelium discoideum* (from Ball [4]).

1.1 Historical Perspective

Numerous experiments and simulations have been performed with excitable media, see for instance [5, 6, 8, 24, 52] (a selected bibliography is presented in appendix B). The various spiral motions observed have been classified according to their **tip path**, an arbitrary point on the wave front that is followed in time. Some of the standard possibilities are shown in figure 1.2.

In the literature (see [7, 59, 73] for instance), specific systems of partial differential equations (PDE) have been used to attempt to explain the observed phenomena: for instance, the **FitzHugh-Nagumo** equations

$$\begin{aligned} u_t &= \tfrac{1}{\varsigma}(u - \tfrac{1}{3}u^3 - v) + \Delta u \\ v_t &= \varsigma(u + \beta - \gamma v) \end{aligned}$$

of cardiology, where ς, β and γ are model parameters, u represents an electric potential and v a measure of permeability, or the **Oregonator**

$$\begin{aligned} u_t &= \tfrac{1}{\varsigma}(u - u^2 - fv\tfrac{u-q}{u+q}) + \Delta u \\ v_t &= u - v + D\Delta v \end{aligned}$$

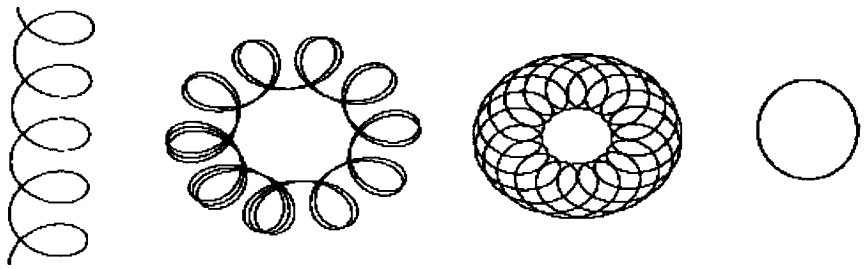

Figure 1.2: Possible paths of the spiral wave tip. From left to right: linear drifting, outer epicycle motion, inner epicycle motion and rigid rotation (from LeBlanc and Wulff [51]).

for the Belousov-Zhabotinsky reaction, where f, ς and q (small) are the model parameters, D is a diffusion coefficient and u and v represent the concentrations of certain chemical reactants. In both cases, u and v vary in terms of spatial position and time. These two systems of partial differential equations are instances of a general class of PDE, defined by

$$u_t(x,t) = f(u(x,t)) + D\Delta u(x,t), \tag{1.1.1}$$

where $x \in \mathbb{R}^2$, $u : \mathbb{R}^2 \times \mathbb{R}_0^+ \to \mathbb{R}^m$ is bounded and uniformly continuous, D is an $m \times m$ diagonal matrix and $f : \mathbb{R}^m \to \mathbb{R}^m$ is some sufficiently smooth function. The matrix D is the **diffusion coefficient matrix** and f is the **reaction term**. A general system of the form (1.1.1) is a **reaction-diffusion system** (RDS). These systems are used to model excitable media: Winfree provides a very complete survey of the topic in [73].

There are four types of solutions of (1.1.1) that are of particular interest in the context of wave and spiral wave dynamics:

Rotating waves (RW) are rigidly rotating periodic solutions that are fixed in a **co-rotating** frame of reference (*i.e.*, the frame rotates uniformly with the same frequency as the solution). In physical and numerical experiments, the tip path is circular. RW are sometimes called *vortices* or *rotors* in the literature [73,75].

Traveling waves (TW) are linearly propagating solutions[1] that are fixed in a **co-translating** frame of reference (*i.e.*, the frame translates linearly and uniformly with the solution). In experiments, the tip path of such a solution is a line.

[1]Strictly speaking, TW are not spiral waves as they do not have a rotating component; they are sometimes referred to as **retracting tip waves** [7].

Modulated rotating waves (MRW) are two-frequency quasi-periodic solutions that are periodic in a co-rotating frame of reference that rotates uniformly with one of the frequencies of the solution. The tip path of such a solution is a closed epicycle when the ratio of the frequencies is rational; otherwise the tip path densely fills a ring over time, with an epicycle-like motion. In the literature, MRW are sometimes called *meandering waves*.

Modulated traveling waves (MTW) are rotating solutions, superimposed with a linearly propagating motion, that are periodic in a co-translating frame of reference that travels uniformly with the linear component of the solution. The tip path of such a solution is a helix-shaped two-dimensional curve.

RW and TW are instances of what are known as **relative equilibria**, whereas MRW and MTW are **relative periodic solutions**. The former refers to solutions that are stationary in an appropriate frame of reference while the latter are solutions that are periodic in an appropriate frame of reference.

As an illustration of spiral dynamics, consider the reaction-diffusion system

$$\begin{aligned} u_t &= \tfrac{1}{\varsigma} u(1-u)\left(u - \tfrac{v+b}{a}\right) + \Delta u \\ v_t &= u - v, \end{aligned} \tag{1.1.2}$$

where a, b and ς are system parameters with ς small. This system was first studied by Barkley [6]. Figure 1.3 shows a bifurcation diagram of the spiral dynamics of (1.1.2) for $\varepsilon = \frac{1}{50}$. There are three regions of interest labeled `N`, `RW` and `MRW`. Note that this last region is divided in two sub-regions by a curve labeled `MTW`.

In `N`, no wave propagation is observed; in `RW`, observed solutions are RW and in `MRW`, observed solutions are MRW, with petality (the orientation of the spiral "petals") determined by the side of the curve `MTW` on which the parameters fall. The intersection of this curve with the boundary of `MRW` is a point that deserves special consideration: in every one of its neighbourhoods, the three types of spiral behaviours can be observed.

An *a priori* surprising feature of reaction-diffusion systems is that Figure 1.3 is a generic bifurcation diagram: most experimental results are strikingly similar [7, 73],

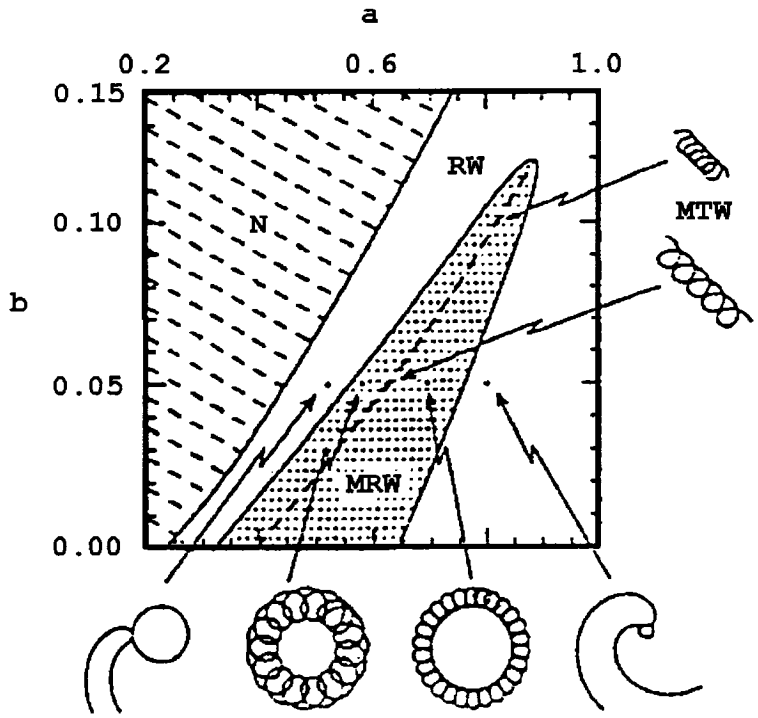

Figure 1.3: Bifurcation diagram of spiral wave dynamics in (1.1.2) (from Barkley [6]).

which suggests they are a consequence of excitable media and their geometry, and not of the particular models that aim to describe the dynamics [5, 30, 48, 51].[2]

1.1.1 The Dynamical System Approach

Let Γ be a group acting linearly on a vector space X. A function $f : X \to X$ is $\Gamma-$**equivariant** if f commutes with the action of Γ, *i.e.*,

$$\gamma \cdot f(x) = f(\gamma \cdot x), \quad \forall \gamma \in \Gamma, x \in X.$$

Equivariant vector fields (with compact Γ) have been studied by many authors: notable amongst them are Golubitsky and Schaeffer [32], Golubitsky, Stewart and Schaeffer [33] and Vanderbauwhede [69, 70]. The main feature of these $\Gamma-$equivariant

[2]It should be noted that reaction-diffusion systems are not the sole models of excitable media, nor were they the first: Wiener and Rosenblueth originally defined and modeled excitable media using cellular automata [71]. Their model was later formalized and expanded by Greenberg, Hassard and Hastings [34]. More can be found on this topic in [9, pp. 194 – 203].

vector fields is that solutions of $\dot{x} = f(x)$ get carried to solutions of that same vector field by the action of Γ, thus whenever $x(t)$ is a solution, so is $\gamma x(t)$, for all $\gamma \in \Gamma$.

The **(special) Euclidean group** $\mathbb{SE}(2) = \mathbb{C}\dot{+}\mathbb{S}^1$ is a non-compact subset of all the distance-preserving transformations of the plane, with multiplication defined by

$$(p_1, \varphi_1) \cdot (p_2, \varphi_2) = (e^{i\varphi_1} p_2 + p_1, \varphi_1 + \varphi_2), \quad \forall (p_1, \varphi_1), (p_2, \varphi_2) \in \mathbb{SE}(2). \tag{1.1.3}$$

It acts on the space of bounded uniformly continuous functions from $\mathbb{R}^2$ to $\mathbb{R}^m$, which we will denote by $\mathrm{BC}_u(\mathbb{R}^2, \mathbb{R}^m)$, according to

$$(\gamma \cdot v)(x) = ((p, \varphi) \cdot v)(x) = v(R_{-\varphi}(x - p)), \quad \forall (p, \varphi) \in \mathbb{SE}(2), \tag{1.1.4}$$

where R_θ represents a rotation by angle θ around the origin. Reaction-diffusion systems on $\mathrm{BC}_u(\mathbb{R}^2, \mathbb{R}^m)$ are $\mathbb{SE}(2)-$equivariant under the action of (1.1.4), but that action is not smooth over $\mathrm{BC}_u(\mathbb{R}^2, \mathbb{R}^m)$: the problem arises with rotations as a small shift in θ produces a large displacement at far distances. However, there is a closed set $\mathrm{BC}_e(\mathbb{R}^2, \mathbb{R}^m) \subsetneq \mathrm{BC}_u(\mathbb{R}^2, \mathbb{R}^m)$ over which (1.1.4) is smooth [76].

Barkley [5,6] was the first to realize that this Euclidean symmetry (as opposed to the specifics of a given model) could explain most of the spiral wave dynamics observed in experiments and simulations, and succinctly presented in Figure 1.3. His key observation is that for any reaction-diffusion system, the linearization at a RW at the onset of a Hopf bifurcation (hence at the boundary of MRW) has five isolated leading eigenvalues on the imaginary axis: $\lambda_R = 0$ (due to rotational symmetry), $\lambda_T = \pm i\omega$ (due to translational symmetry) and $\lambda_B = \pm i\beta_0$ (responsible for the Hopf bifurcation from RW to MRW or *vice-versa*). A summary of his ground-breaking article [5] is provided on p. 146.

The pairs of complex conjugate eigenvalues λ_T and λ_B can be made to coincide by varying two or more system parameters. The corresponding (interesting) codimension-two point is then found to lie precisely at the intersection of MTW and the boundary of MRW. Based on this observation, Barkley and Kevrekidis [7] constructed an *ad hoc* $5-$dimensional system of ordinary differential equations (ODE) which replicates the above resonant Hopf bifurcation.

It is given by

$$\begin{aligned} \dot{p} &= v \\ \dot{v} &= v\left[f(|v|^2, w^2) + iw\gamma_0\right] \\ \dot{w} &= wg(|v|^2, w^2) \end{aligned} \tag{1.1.5}$$

where $p, v \in \mathbb{C}$, $w \in \mathbb{R}$ and

$$f(\xi, \zeta) = -\frac{1}{4} + \alpha_1\xi + \alpha_2\zeta - \xi^2, \quad g(\xi, \zeta) = \xi - \zeta - 1$$

and $\gamma_0 \in \mathbb{R}$.

In their model, the variable p represents the position of the spiral tip, while v is its linear velocity and $\gamma_0 w$ its instantaneous rotational frequency rate. Note the absence of p in the right-hand side of (1.1.5) as position plays no role in a Euclidean system.

This system has RW solutions[3] that undergo a Hopf bifurcation to MRW solutions and it also has a codimension-two resonant Hopf point. Furthermore, it is equivariant under the distance-preserving planar transformations generated by

$$R_\gamma \begin{pmatrix} p \\ v \\ w \end{pmatrix} = \begin{pmatrix} e^{i\gamma}p \\ e^{i\gamma}v \\ w \end{pmatrix} \quad \text{and} \quad T_{\alpha,\beta} \begin{pmatrix} p \\ v \\ w \end{pmatrix} = \begin{pmatrix} p + \alpha + i\beta \\ v \\ w \end{pmatrix},$$

where R_γ and $T_{\alpha,\beta}$ represent a rotation by angle γ around the origin and a translation by the vector $\alpha + i\beta$, respectively. Figure 1.4 shows the bifurcation diagram of (1.1.5) for $\gamma_0 = 5.6$. The similarities with figure 1.3 are readily apparent, in particular when it comes to the presence of a codimension-two organizing center around which the four types of spirals can be found.

Then, in what has been hailed a "major mathematical work on spirals [30]", Wulff [76] rigourously proved that the resonant unbounded growth observed by many authors (such as [5, 7]) does indeed occur near the codimension-two point.

Following Krupa's [46] center bundle construction for relative equilibria and periodic solutions for compact symmetry groups and its extension to non-compact symmetry group by Sandstede, Scheel and Wulff [61, 62], Golubitsky, LeBlanc and Melbourne [30] gave a general 5−dimensional system of ODE on the center bundle

[3]Defined for ODE as they were for PDE.

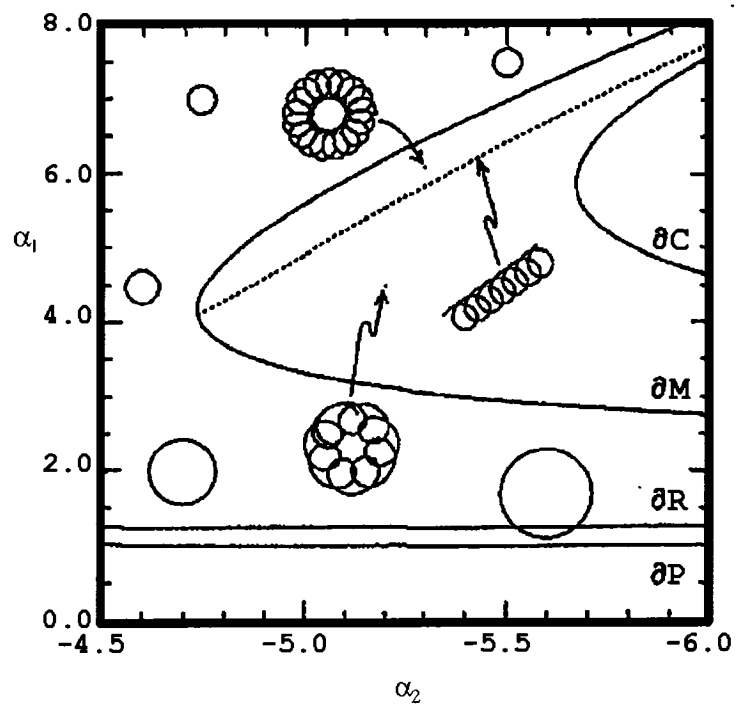

Figure 1.4: Bifurcation diagram of (1.1.5) (from Barkley and Kevrekidis [7]).

$\mathbb{SE}(2) \times \mathbb{C}$ describing the essential dynamics for Hopf bifurcation from $\ell-$armed spirals. For $\ell = 1$, the general system has the form

$$\begin{aligned} \dot{p} &= e^{i\varphi} F^p(q, \overline{q}) \\ \dot{\varphi} &= F^\varphi(q, \overline{q}) \\ \dot{q} &= F^q(q, \overline{q}), \end{aligned} \tag{1.1.6}$$

where $p \in \mathbb{C}$ represents the position of the spiral tip, $\varphi \in \mathbb{S}^1$ the angle of rotation of the spiral, $q \in \mathbb{C}$ regulates the "Hopf" bifurcation from RW to WRW, $F^\varphi(0) = \omega_{\text{rot}} \in \mathbb{R}$, $F^q(0) = 0$ and $DF^q(0) = i\omega_{\text{per}}$ is purely imaginary.[4] The Euclidean action on $\mathbb{SE}(2) \times \mathbb{C}$ is given by

$$(x, \theta) \cdot (p, \varphi, q) = (e^{i\theta} p + x, \varphi + \theta, q), \quad \forall (x, \theta) \in \mathbb{SE}(2). \tag{1.1.7}$$

The results of Barkley and Wulff concerning the Hopf bifurcation from a RW and resonant growth are then recovered. This **dynamical system approach** facilitates the

[4]The frequencies ω_{rot} and ω_{per} in (1.1.6) play similar roles to the parameters ω and β_0 in [5].

study of more complex bifurcations, as the authors demonstrate with the Bogdanov-Takens bifurcation from 1−armed spirals.

Using the same techniques, Golubitsky, LeBlanc and Melbourne [31] later show that Euclidean symmetry is generically necessary if one is to observe the spiral behaviour previously described.

1.1.2 The Effects of Euclidean Symmetry Breaking

However, physical experiments can never be perfectly Euclidean, if only because of their finite nature. In the heart, this reality is obvious. Cardiac tissue is **anisotropic** (*i.e.*, heart fibres have a preferred orientation and electrical conductivity is direction-dependent). Furthermore, tissue distribution is not uniform: there are zones of relatively high density that affect cardiac activity [44].

Similarly, introducing light pulses in a light-sensitive BZ reaction changes the geometry of the system. Moreover, the boundary cannot be ignored when the size of the spiral core is 'comparable' to that of the domain.

Yet, the heart and the BZ reaction retain a partly Euclidean local structure. At distances 'far' from the inhomogeneities, is their effect truly felt? If the anisotropy ratio is such that the 'preferred' direction is only slightly so 'preferred', are spiral dynamics really affected? Can the Oregonator distinguish the boundary from infinity if it is 'very distant' from the spiral core?

Spiral anchoring appears when local inhomogeneities are present: spirals are attracted or repelled by a RW, which rotates around the site of the inhomogeneity. This has been observed in cardiac tissue [24] and in numerical simulations of a modified Oregonator [55].

Boundary drifting can be observed when the sizes of the physical domain and of the spiral core are comparable: the latter is then attracted to the boundary of the domain and rotates around it in a meandering fashion. This has been observed in experiments and numerical simulations in a light-sensitive BZ reaction [77, 80].[5]

[5]In this work, we will also use the term **epicyclic drifting**.

Quasi-periodic anchoring is witnessed in periodically-forced reaction-diffusion systems: the results are similar to spiral anchoring, with the attracting/repelling structure consisting of either two- or three-frequency quasi-periodic motion.[6] These have been observed in a light-sensitive BZ reaction that is periodically hit by light pulses and the corresponding modified Oregonator model [18, 35].

Discrete RW and MRW can be seen in systems that incorporate the notion of anisotropy (*i.e.*, the system has a 'preferred direction').[7] In general, the tip path has discrete two-fold symmetry. These have been observed in numerical experiments on the bidomain model of cardiac electrophysiology [59].

Phase-locking can also be seen in systems that incorporate anisotropy: the rotation and meander frequencies can lock and this motion can be superimposed with a slow drift. This has been observed in the bidomain model as well [59].

The above phenomena are illustrated in Figure 1.5. Euclidean symmetry alone cannot explain them; clearly, any model hoping to do so should incorporate **forced Euclidean symmetry-breaking**, or have a 'partly Euclidean structure'.

Using the Center Manifold Reduction Theorem (CMRT) of [61, 62], LeBlanc and Wulff [51] showed that translational symmetry-breaking (TSB) from Euclidean symmetry generically leads to anchoring or quasi-periodic anchoring and that TW, MTW, boundary drifting and quasi-periodic attractors could also occur.

They did so by studying a general perturbed ODE system on the center bundle $\mathbb{SE}(2) \times \mathbb{C}$ taking the form

$$\begin{aligned} \dot{p} &= e^{i\varphi}\left[F^p(q,\overline{q}) + \varepsilon G^p(pe^{-i\varphi}, \overline{p}e^{i\varphi}, q, \overline{q}, \varepsilon)\right] \\ \dot{\varphi} &= F^\varphi(q,\overline{q}) + \varepsilon G^\varphi(pe^{-i\varphi}, \overline{p}e^{i\varphi}, q, \overline{q}, \varepsilon) \\ \dot{q} &= F^q(q,\overline{q}) + \varepsilon G^q(pe^{-i\varphi}, \overline{p}e^{i\varphi}, q, \overline{q}, \varepsilon) \end{aligned} \tag{1.1.8}$$

where $\varepsilon \in \mathbb{R}$ is small and the $G-$perturbations are bounded and uniformly continuous in p and q. When $\varepsilon = 0$, (1.1.8) is $\mathbb{SE}(2)-$equivariant under the action of (1.1.7), but for $\varepsilon \neq 0$, the system is generally only $\mathbb{SO}(2)-$equivariant: the translational symmetry of the model has been broken. A detailed summary is provided on p. 147.

[6] They are then called **entrainment** and **resonance attractors**, respectively.

[7] Generically, discrete RW and MRW cannot occur in $\mathbb{SE}(2)-$equivariant reaction-diffusion systems [8].

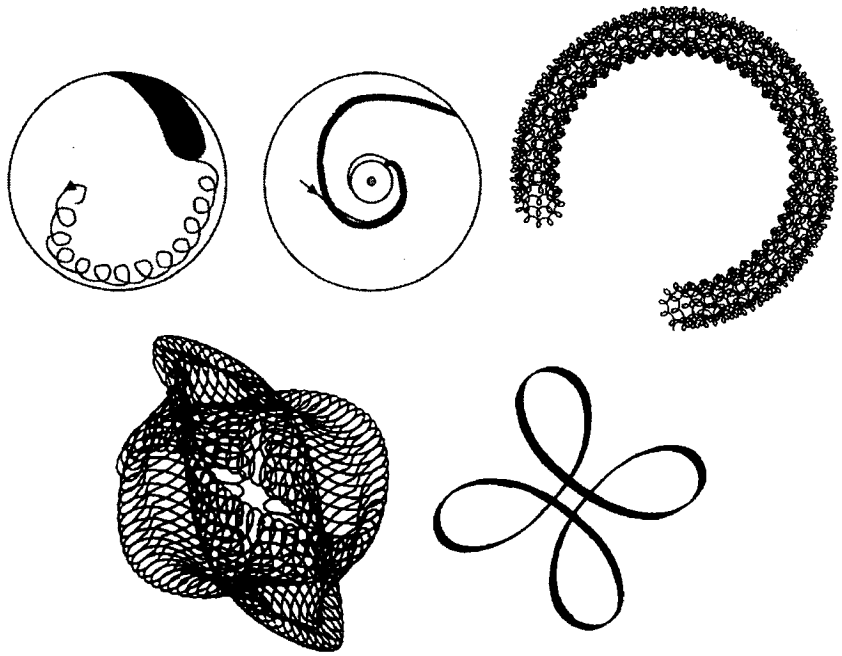

Figure 1.5: Non-standard motions of the spiral wave tip. Top row (from left to right): boundary drifting, spiral anchoring, and a three-frequency attractor (from LeBlanc and Wulff [51]). Bottom row (from left to right): a discrete MRW with $\mathbb{Z}_2-$symmetry and phase-locking with small drift (from Roth [59]).

LeBlanc [48] then showed that rotational symmetry-breaking (RSB) from Euclidean symmetry could be used to explain the presence of discrete RW, discrete MRW and phase-locking in excitable media with anisotropy. He did so by studying a general perturbed ODE system on the center bundle $\mathbb{SE}(2) \times \mathbb{C}$ given by

$$\begin{aligned} \dot{p} &= e^{i\varphi}\left[F^p(q,\overline{q}) + \varepsilon G^p(\varphi, q, \overline{q}, \varepsilon)\right] \\ \dot{\varphi} &= F^{\varphi}(q,\overline{q}) + \varepsilon G^{\varphi}(\varphi, q, \overline{q}, \varepsilon) \\ \dot{q} &= F^{q}(q,\overline{q}) + \varepsilon G^{q}(\varphi, q, \overline{q}, \varepsilon) \end{aligned} \tag{1.1.9}$$

where $\varepsilon \in \mathbb{R}$ is small and the $G-$perturbations are bounded and uniformly continuous in p and q and $\frac{2\pi}{\ell}-$periodic in φ, $\ell \in \mathbb{N}$. When $\varepsilon = 0$, (1.1.9) is $\mathbb{SE}(2)-$equivariant under the action of (1.1.7), but for $\varepsilon \neq 0$, the system is generally only $\mathbb{C}\dot{+}\mathbb{Z}_\ell-$equivariant: the rotational symmetry of the model has been broken. A detailed summary is provided on p. 151.

Center manifold reductions, symmetry and forced symmetry-breaking are powerful tools: with their help, it becomes possible to predict the dynamics in a system of PDE simply by studying a finite-dimensional model-independent ODE system.

1.2 Thesis Overview

In a model of cardiac tissue, the G-perturbations in (1.1.8) could model the presence of an inhomogeneity, for instance. Meanwhile the $G-$perturbations in (1.1.9) with $\ell = 2$ could represent anisotropy. But in reality (or at least in an idealized version of it) the heart contains more than one inhomogeneity, and anisotropy and inhomogeneities are present simultaneously. In other words, (1.1.8) and (1.1.9) do not constitute the whole picture when it comes to forced Euclidean symmetry-breaking.

In this thesis, we will study the effects of the following two scenarios: in scenario A, system (1.1.6) is perturbed by n TSB terms, for $n \geq 2$, while in scenario B, system (1.1.6) is perturbed by a TSB term and a RSB term. One might think that the results from [48, 51] would carry over, but we shall see that there are many surprises and technical issues.

In the second chapter, preliminary definitions and results concerning the existence and uniqueness of the solution of the reaction-diffusion system (1.1.1), its Euclidean symmetry, the CMRT of Sandstede, Scheel and Wulff [61,62], a (modified) averaging theorem of Hale [37,38], the (classical) Implicit Function Theorem, some results from singularity theory, a characterization of (real) conic sections and various notions and notations are presented.

In the third chapter, we derive the center bundle equations for scenario A around a (hyperbolic) rotating wave; the corresponding TSB perturbations of the $\mathbb{SE}(2)-$equivariant ODE system on the center bundle $\mathbb{SE}(2)$ take the form

$$\lambda_j H_j((p-\xi_j)e^{-i\varphi}, \overline{(p-\xi_j)}e^{i\varphi}, \lambda_j), \quad \text{for } j = 1, \ldots, n$$

where $\xi_1, \ldots, \xi_n$ represent the n inhomogeneities and $\lambda = (\lambda_1, \ldots, \lambda_n) \in \mathbb{R}^n$ is a vector determining the weight of each of the perturbations.

We state and prove our main results for scenario A in the fourth chapter: to wit, spiral anchoring is generic in a parameter wedge. However the center of anchoring does not necessarily lie at one of the ξ_j, $j = 1, \ldots, n$, which defies experimental wisdom:

it has yet to be observed in the laboratory, but we have reproduced it in numerical simulations of various systems of partial differential equations (see Chapter 7). A sufficient condition for boundary and epicyclic drifting to occur in a parameter wedge is then given. In both of these cases, we recover the results from [51] for $n = 1$. Finally, we present secondary results about the occurrence of saddle-node and Bogdanov-Takens bifurcations of rotating waves if $n \geq 4$ and $n \geq 5$, respectively.

In the fifth chapter, we provide a visual criterion characterizing the anchoring wedges in the case $n = 2$. The criterion is derived through a study of a class of mappings sharing the essential qualities of the Poincaré maps used in the proof of the anchoring wedges' existence.

We state and prove our main results for scenario B in the sixth chapter. Only certain aspects of the proofs are given to avoid duplicating the proofs of Chapter 4. In this case, the TSB term is assumed to be centered at the origin and the RSB perturbation preserves rotations by angle $\frac{2\pi k}{\ell}$, where $\ell \geq 1$ and k are co-prime integers. When $\ell = 1$, there is a parameter wedge in which spiral anchoring (or repelling) is generic, but not centered at the origin. Under certain conditions an epicycle manifold also appears. Generically, when $\ell > 1$, spirals with $\mathbb{Z}_\ell-$symmetry are anchored at (or repelled by) the origin; under certain conditions an epicycle manifold, with the same discrete symmetry, also appears. A visual criterion characterizing the anchoring wedges in the case $\ell = 1$ also finds its way in these pages.

In the seventh chapter, numerical experiments are performed on partial differential equations and on center bundle equations to illustrate and validate our results. Examples of wedges and catastrophes are also provided.

In the eighth and final chapter, we discuss possible applications of our results, such as the eventual creation of a so-called 'cardiac forecast system; we also make conjectures about MRW, based on our analysis of RW. Finally, we conclude with a brief list of problems whose resolution will further our understanding of spiral waves in excitable media.[8]

It should be noted that, throughout the thesis, parts of the text (mostly technical results and summaries) have been lifted to facilitate the reading flow. The missing links are found at the end of the appropriate chapters, or in appendix A.

[8] A lot of the results in this work can also be found in [11, 12, 14, 15].

Chapter 2

Preliminaries

In this chapter, we present some basic technical results which will find use in subsequent parts of this work.[1]

2.1 Reaction-Diffusion Systems on $\mathbb{R}^2$

Consider the reaction-diffusion system

$$u_t(x,t) = \tilde{D}\Delta u(x,t) + f(u(x,t),\varsigma), \tag{2.1.1}$$

where $x \in \mathbb{R}^2$, $u : \mathbb{R}^2 \times \mathbb{R}_0^+ \to \mathbb{R}^m$, $\tilde{D} \geq 0$ is a diagonal matrix, $\varsigma \in \mathbb{R}^M$, Δ is the Laplacian and f is C^{k+2} for some $0 \leq k \leq \infty$. If $\det \tilde{D} \neq 0$, let $Y = \mathrm{BC}_u(\mathbb{R}^2, \mathbb{R}^m)$ be the Banach space of **uniformly continuous, bounded functions**[2] **from** $\mathbb{R}^2$ **to** $\mathbb{R}^m$. The **semi-linear differential equation on** Y **associated to (2.1.1)** is

$$\frac{du}{dt} = -Au + F(u,t,\varsigma), \tag{2.1.2}$$

where $F(u,t,\varsigma) = f(u(\cdot,t),\varsigma)$ and

$$A = \mathrm{diag}(-d_1\Delta, \ldots, -d_m\Delta). \tag{2.1.3}$$

Solutions of (2.1.2) are in one-to-one correspondence with solutions of (2.1.1).

[1] The intent here is not to reproduce these highly technical results; rather, it is to show how the center bundle equations can be derived from them for multiple sites of inhomogeneities. Consequently, the proofs are omitted.

[2] Otherwise, if f satisfies some additional growth conditions, the choice $Y = L^2(\mathbb{R}^2, \mathbb{R}^m)$ can also be used, with slight variations (see [40, 62] for details). However, physical considerations demand that spiral waves in an infinitely extended medium be located in $\mathrm{BC}_u(\mathbb{R}^2, \mathbb{R}^m)$ [76].

We start with numerous definitions and results from operator theory and abstract differential equations before stating theorems on the $\mathbb{SE}(2)-$equivariance of (2.1.1) as well as on the existence and uniqueness of its solutions; these are mostly taken from [3, 40, 76].

Throughout this section, X is a Banach space and A is a linear operator on X. The **domain**, **range**, **spectrum** and **resolvent set** of A are the sets

$$\begin{aligned} \mathrm{dom}(A) &= \{x \in X : Ax \in X\}, \\ \mathrm{range}(A) &= \{Ax : x \in \mathrm{dom}(A)\}, \\ \sigma(A) &= \{\lambda \in \mathbb{C} : (\lambda \,\mathrm{id}_X - A) \text{ is not invertible}\} \end{aligned}$$

and $\Omega(A) = \mathbb{C} - \sigma(A)$, respectively.

A set $\sigma \subseteq \sigma(A) \cup \{\infty\} = \hat{\sigma}(A)$ is a **spectral set for** A if both σ and $\hat{\sigma}(A) - \sigma$ are closed in the extended complex plane $\mathbb{C} \cup \{\infty\}$. The associated **spectral projection** is the integral

$$P_\sigma = \int_\gamma (\lambda \,\mathrm{id}_X - A)^{-1} \, d\lambda, \tag{2.1.4}$$

where γ is a closed positively oriented Jordan curve in $\mathbb{C}$ such that σ lies in the interior of γ. The operator A is **sectorial** in X if

i) $\mathrm{dom}(A)$ is dense in X;

ii) for any sequence (x_n) in $\mathrm{dom}(A)$ such that $\lim x_n = x$ and $\lim Ax_n = z$, it follows that $Ax = z$, and

iii) there exists a pair $(\zeta, \phi) \in \mathbb{R} \times (0, \frac{\pi}{2})$ and a real number $K \geq 1$ such that the sector

$$S_{\zeta,\phi} = \{\lambda \in \mathbb{C} : \phi < |\arg(\lambda - \zeta)| \leq \pi, \lambda \neq \zeta\}$$

lies in $\Omega(A)$ and $\|(\lambda \,\mathrm{id}_X - A)^{-1}\| \leq \frac{K}{|\lambda - \zeta|}$ for all $\lambda \in S_{\zeta,\psi}$.

If A is sectorial, let $\zeta \in \mathbb{R}$ be such that $\sigma(A + \zeta \,\mathrm{id}_X)$ lies entirely in the half-plane $\mathrm{Re}\,\lambda > 0$. For $\alpha > 0$, define the **fractional powers associated to** A **and** ζ by

$$A_1^{-\alpha}(\zeta) = (A + \zeta \,\mathrm{id}_X)^{-\alpha} = \frac{1}{\Gamma(\alpha)} \int_0^\infty t^{\alpha-1} e^{-(A+\zeta \,\mathrm{id}_X)t} \, dt,$$

where Γ is the classical $\Gamma-$function from analysis, and set $A_1^\alpha(\zeta) = \left(A_1^{-\alpha}(\zeta)\right)^{-1}$. By convention, $A_1^0(\zeta) = \mathrm{id}_X$. The **fractional spaces** $X^\alpha = \mathrm{dom}\,(A_1^\alpha(\zeta))$ are Banach spaces when endowed with the graph norm $\|x\|_\alpha = \|A_1^\alpha(\zeta)x\|$ for all $x \in X^\alpha$.[3]

Proposition 2.1.1 [76] *Let A be given by* (2.1.3), $Y = \mathrm{BC}_u(\mathbb{R}^2, \mathbb{R}^m)$, $\alpha \in (\frac{1}{2}, 1)$ *and* $A_1 = \mathrm{id}_Y - \tilde{D}\Delta$, *where $\tilde{D}$ is as in* (2.1.1). *Then A is sectorial in Y^α and $\frac{\partial}{\partial x_1}A_1^{-\alpha}, \frac{\partial}{\partial x_2}A_1^{-\alpha}$ are bounded on Y.*

2.1.1 Existence and Uniqueness of Solutions

Let Y, A, A_1 and α be as in Proposition (2.1.1), U be a subset of $Y^\alpha \times \mathbb{R} \times \mathbb{R}^M$ and F be as in (2.1.2), locally Lipschitz in its first variable and continuous in the remaining variables.

The function $u(t) = u(t; u_0, t_0, \varsigma)$ is a **mild solution** of the initial value problem

$$\frac{du(t)}{dt} = -Au(t) + F(u(t), t, \varsigma), \quad u(t_0; u_0, t_0, \varsigma) = u_0, \quad (u_0, t_0, \varsigma) \in U \tag{2.1.5}$$

on $[t_0, t_1]$ if

i) $u \in C\left([t_0, t_1], Y^\alpha\right)$, and

ii) u satisfies the associated integral equation

$$u(t) = e^{-At}u_0 + \int_0^t e^{-A(t-s)}F(u(s), s, \varsigma)\, ds.$$

It is a **(classical) solution** of (2.1.5) on $[t_0, t_1]$ if it is a mild solution of (2.1.5) that also satisfies the initial value problem on $(t_0, t_1]$.[4] Finally, let $k \in \mathbb{N}$. Then u is a **(classical) C^k-solution** of (2.1.5) on $[t_0, t_1]$ if

i) $u \in Y^\alpha$ is a (classical) solution of (2.1.5),

ii) u is C^k in $(u_0, t_0, \varsigma) \in U$ for $t \in [t_0, t_1]$ fixed, and

iii) u is C^k in $(t, u_0, t_0, \varsigma) \in (t_0, t_1] \times U$.

[3] The dependance on ζ is omitted as different choices give rise to equivalent norms on X^α.

[4] In particular, this implies $u \in \mathrm{dom}(A)$ and $\frac{du(t)}{dt}$ is well-defined on $(t_0, t_1]$ [76].

Theorem 2.1.2 [40, 76] *For any* $(u_0, t_0, \varsigma) \in U$, (2.1.2) *has a unique (classical)* $C^{k+2}-$*solution* $u(t; u_0, t_0, \varsigma)$ *on* $[t_0, t_1]$, *where* $t_1 = t_1(u_0, t_0, \varsigma) > t_0$ *and* $0 \leq k \leq \infty$ *is the smoothness of the nonlinearity* f *in* (2.1.1).

2.1.2 $\mathbb{SE}(2)-$Equivariance of Solutions

A **smooth local semi-flow** $\{\Phi_t\}_{t\geq 0}$ on X is a smooth family of operators satisfying $\Phi_0 = \mathrm{id}_X$ and

$$\Phi_{t+s} = \Phi_t \circ \Phi_s = \Phi_s \circ \Phi_t \quad \text{for all } s, t \geq 0.$$

If

$$\lim_{t\to 0^+} \Phi_t x = x$$

for all $x \in X$, then $\{\Phi_t\}_{t\geq 0}$ is a C^0-**semi-group** on X. A **smooth semi-group** on X is a C^0-semi-group for which the map $\Psi_x : (0, \infty) \to X$ defined by $\Psi_x(t) = \Phi_t(x)$ is smooth for all $x \in X$.

Let $\{T_t\}_{t\geq 0}$ be a smooth semi-group on X. The **infinitesimal generator** L_T of $\{T_t\}_{t\geq 0}$ is defined as

$$L_T x = \lim_{t\to 0^+} \frac{1}{t} (\Phi_t x - x). \tag{2.1.6}$$

The notation $T_t = e^{L_T t}$ is commonly used.

Consider the **special Euclidean group** $\mathbb{SE}(2)$, parameterized by $\mathbb{SE}(2) = \mathbb{SO}(2) \dot{+} \mathbb{R}^2$, with multiplication given by

$$(R_1, S_1) \cdot (R_2, S_2) = (R_1 R_2, S_1 + R_1 S_2). \tag{2.1.7}$$

The **standard** $\mathbb{SE}(2)-$**action on** $\mathrm{BC}_u(\mathbb{R}^2, \mathbb{R}^m)$ is

$$(R, S)\,(v(x,t)) = v\left(R^{-1}(x - S), t\right). \tag{2.1.8}$$

Note that $\mathbb{SE}(2)$ is generated by the families $\{S_\mu\}$, $\{T_\nu\}$ and $\{R_\theta\}$, where

$$S_\mu = \begin{pmatrix} \mu \\ 0 \end{pmatrix}, \quad T_\nu = \begin{pmatrix} 0 \\ \nu \end{pmatrix} \quad \text{and} \quad R_\theta = \begin{pmatrix} \cos\theta & -\sin\theta \\ \sin\theta & \cos\theta \end{pmatrix}$$

satisfy $S_{\mu_1} \circ S_{\mu_2} = S_{\mu_1+\mu_2}$, $T_{\nu_1} \circ T_{\nu_2} = T_{\nu_1+\nu_2}$ and $R_{\theta_1} \circ R_{\theta_2} = R_{\theta_1+\theta_2}$ for $\mu_j, \nu_j, \theta_j \in \mathbb{R}$, $j = \varnothing, 1, 2$. Then $\{S_\mu\}_{\mu\geq 0}$ and $\{T_\nu\}_{\nu\geq 0}$ are smooth semi-groups on $\mathrm{BC}_u(\mathbb{R}^2, \mathbb{R}^m)$, with infinitesimal generators

$$L_S = -\frac{\partial}{\partial x_1} \quad \text{and} \quad L_T = -\frac{\partial}{\partial x_2},$$

respectively [76].

However, $\{R_\theta\}_{\theta\geq 0}$ is not a smooth semi-group (see [76, lemma 2.14]); the action of $\mathbb{SE}(2)$ on $\mathrm{BC}_u(\mathbb{R}^2, \mathbb{R}^m)$ is not even continuous. Still, the formal evaluation of (2.1.6) yields

$$L_R = x_2 \frac{\partial}{\partial x_1} - x_1 \frac{\partial}{\partial x_2}.$$

Set

$$\tilde{Y} = \mathrm{BC}_e(\mathbb{R}^2, \mathbb{R}^m) = \overline{\mathrm{dom}(L_R)} \quad \text{in } \mathrm{BC}_u(\mathbb{R}^2, \mathbb{R}^m). \tag{2.1.9}$$

The reaction-diffusion system (2.1.1) is well-posed on $\tilde{Y}$, and Proposition (2.1.1) and Theorem 2.1.2 still hold after substituting $\tilde{Y}$ for Y [76]. Furthermore, (2.1.8) is continuous on $\tilde{Y}$. As a result, we get the following.

Theorem 2.1.3 *Under the action* (2.1.8), *system* (2.1.1) *is* $\mathbb{SE}(2)-$*equivariant over* $\mathrm{BC}_e(\mathbb{R}^2, \mathbb{R}^m)$.

Proof: The Laplacian Δ is the only partial differential operator of degree less or equal to 2 which commutes with (2.1.8) (see [26, p. 265] and [68,76] for details). Furthermore, let $h_\varsigma(u(x,t)) = f(u(x,t), \varsigma)$, where f is as in (2.1.1) and $u \in \mathrm{BC}_e(\mathbb{R}^2, \mathbb{R}^m)$. Then

$$\begin{aligned} f((R,S)u(x,t),\varsigma) &= h_\varsigma((R,S)u(x,t)) = h_\varsigma\left(u(R^{-1}(x-S),t)\right) = (h_\varsigma \circ u)\left(R^{-1}(x-S),t\right) \\ &= (R,S)(h_\varsigma \circ u^\varsigma)(x,t) = (R,S)h_\varsigma(u^\varsigma(x,t)) = (R,S)f(u^\varsigma(x,t),\varsigma), \end{aligned}$$

for all $(R,S) \in \mathbb{SE}(2)$. ∎

2.2 The Center Manifold Reduction Theorem

In this section, we give a general overview of the center manifold reduction theorems (CMRT) of Sandstede, Scheel and Wulff [27, 61–63], which provide a rigourous link between (2.1.1) and the ODE system studied by Barkley and Kevrekidis [7] (see Chapter 1 for details). We focus specifically on their application to $1-$armed rotating

spiral waves, which have already been used to explain certain aspects of spiral wave dynamics [30,31,48,51].

Set $\mathfrak{se}(2) = \mathfrak{so}(2) \times \mathbb{R}^2$, where $\mathfrak{so}(2)$ is the Lie algebra of $\mathbb{SO}(2)$, consisting of the 2×2 anti-symmetric matrices on $\mathbb{R}$, and define $\exp_{\mathfrak{so}(2)} : \mathfrak{so}(2) \to \mathbb{SO}(2)$ by

$$\exp_{\mathfrak{so}(2)}\left(\begin{pmatrix} 0 & b \\ -b & 0 \end{pmatrix}\right) = \sum_{k=0}^{\infty} \frac{1}{k!} \begin{pmatrix} 0 & b \\ -b & 0 \end{pmatrix}^k = \begin{pmatrix} \cos b & \sin b \\ -\sin b & \cos b \end{pmatrix}.$$

Then, $\mathfrak{se}(2)$ is the Lie algebra of $\mathbb{SE}(2)$ when the commutator and exponential maps are defined as follows. Let I_2 be the 2×2 identity matrix. Then

$$\begin{aligned} [(r_1, s_1), (r_2, s_2)] &= (r_1 r_2 - r_2 r_1, r_1 s_2 - r_2 s_1) \\ \exp((r, s)t) &= (\exp_{\mathfrak{so}(2)}(rt), r^{-1}(\exp_{\mathfrak{so}(2)}(rt) - I_2)s), \end{aligned}$$

for $t \in \mathbb{R}$, $0 \neq r_j \in \mathfrak{so}(2)$ and $s_j \in \mathbb{R}^2$, $j = \varnothing, 1, 2$ [27,62].

For a fixed ς, a **relative equilibrium** of (2.1.1) is a solution $u(x,t)$ whose time orbit, or semi-flow orbit, is contained in its group orbit under $\mathbb{SE}(2)$. More precisely, it satisfies

$$u(x,t) = \exp((r,s)t)u(x,0) \tag{2.2.1}$$

for some $(r,s) \in \mathfrak{se}(2)$. The **isotropy subgroup** of such solutions is

$$\Sigma_u = \{\sigma \in \mathbb{SE}(2) : \sigma u(x,t) = u(x,t)\}.$$

If $\Sigma_u \cong \mathbb{Z}_\ell$, then $u(x,t)$ is an ℓ**−armed spiral**.

A **rigidly rotating wave** $u_*(x,t)$ is a relative equilibrium with no translation component; after a change of coordinates bringing the center of rotation to the origin, (2.2.1) becomes

$$u_*(x,t) = (\exp_{\mathfrak{so}(2)}(r_* t), 0)u_*(x,0) \tag{2.2.2}$$

for some non-trivial $r_* \in \mathfrak{so}(2)$.[5]

[5]The related concepts of **traveling wave** (TW), **relative periodic solution** (RPS) , **modulated rotating wave** (MRW) and **modulated traveling wave** will not be analyzed in this work. For the sake of completeness, the definitions are presented in the appendix (see p. 29 for details).

Standard center bundle results (such as those presented in [46]) cannot be applied to (2.1.1) because $\mathbb{SE}(2)$ is neither compact nor is the action (2.1.8) continuous on X. For instance, a small rotation produces large displacements far from the center of rotation; if the uniformly continuous bounded function u on which the rotation acts is not "nice enough," the action may not be continuous.[6] However, the action of $\mathbb{SE}(2)$ is continuous on a rigidly rotating wave or a modulated rotating wave (see preceding section and [76] for details).

Hypothesis 2.2.1 *For the parameter ς_*, assume u_* is a $1-$armed (normally hyperbolic) rotating wave of* (2.1.1) *with $0 \neq r_*$ as in* (2.2.2). *If $\tilde{D}$ is singular, assume further that u_* is $k+2-$times uniformly continuously differentiable.*

Scheel [64] has shown that such rotating wave solutions can arise from Hopf bifurcations in a large class of planar reaction-diffusion equations.

Hypothesis 2.2.2 *Assume that $\{\mu : |\mu| \geq 1\}$ is a spectral set for the linearization $\exp_{\mathfrak{so}(2)}(-r_*)D\Phi_{1,\varsigma_*}(u_*)$ and that $\dim(\mathrm{range}(P_*)) = 3$, where P_* is the associated spectral projection.*

Barkley [5] has performed a numerical experiment which suggests that Hypothesis 2.2.2 can hold: away from the Hopf bifurcation point, the eigenvalues of the linearization at u_* all lie within the unit circle, except for the three critical eigenvalues imposed by the Euclidean symmetry of (2.1.1) (see p. 146 for details). It should be noted, however, that Scheel [64] has also shown that this hypothesis fails to hold for a large class of spiral waves, including all asymptotically Archimedean spirals.

The following result establishes the existence of an invariant center manifold that is contained in an $\mathbb{SE}(2)-$invariant neighbourhood of the group orbit of u_*.

Theorem 2.2.3 ([62], Theorem 4, p. 142) *For any ς close enough to ς_*, there exists an $\mathbb{SE}(2)-$invariant, locally semi-flow-invariant manifold M_ς^{cu}. Both M_ς^{cu} and the action of $\mathbb{SE}(2)$ on M_ς^{cu} are C^{k+1} and depend $C^{k+1}-$smoothly on ς. Furthermore, M_ς^{cu} contains all solutions which stay close to the group orbit of u_* for all negative times. Finally, M_ς^{cu} is locally exponentially attracting.*

[6] Wulff exhibits $u(x) = \cos(x_1)$ as a simple example [76].

As $\Sigma_{u_*} \cong \{1\}$ the structure of the equations on M_ς^{cu} is described by the following result (see [30], Corollary 3.2, p. 563 and [62], Theorem 5, p. 143).

Theorem 2.2.4 *The manifold M_ς^{cu} is diffeomorphic to the bundle $V_* = \mathbb{C} \times \mathbb{S}^1$. Furthermore, the pull-back of the vector field on M_ς^{cu} to V_* is of the form*

$$\begin{aligned} \dot{p} &= e^{i\varphi} v \\ \dot{\varphi} &= \omega_{rot}, \end{aligned} \tag{2.2.3}$$

where $(p, \varphi) \in \mathbb{C} \times \mathbb{S}^1$, $v \in \mathbb{C}$ and $0 \neq \omega_{rot} \in \mathbb{R}$. As the semi-flow on M_ς^{cu} is $\mathbb{SE}(2)-$equivariant, there is an action of $\mathbb{SE}(2)$ on V_*, defined in (2.2.5), under which (2.2.3) is also $\mathbb{SE}(2)-$equivariant.

If we identify $\mathbb{SE}(2)$ with $\mathbb{C}\dot{+}\mathbb{S}^1$ (and its lie algebra $\mathfrak{se}(2)$ with $\mathbb{C} \times \mathbb{R}$), then the Euclidean group structure is given by

$$(p_1, \varphi_1)(p_2, \varphi_2) = (e^{i\varphi_1} p_2 + p_1, \varphi_1 + \varphi_2), \tag{2.2.4}$$

and the **standard group action of $\mathbb{SE}(2)$ on V_*** is given respectively by

$$(x, \psi) \cdot (p, \varphi) = (e^{i\psi} p + x, \varphi + \psi), \tag{2.2.5}$$

for $(x, \psi) \in \mathbb{SE}(2)$ and $(p, \varphi) \in \mathbb{C} \times \mathbb{S}^1$. The specific form of the equations in (2.2.3) is due to the $\mathbb{SE}(2)-$equivariance of the flow; see [30, lemma 4.1, pp. 565 – 566].

2.3 Integral Manifolds and Averaging Methods

Averaging methods are used to determine whether a particular system has a non-trivial invariant solution manifold (or **integral manifold**) by studying a simpler modified system, called the **averaged system**. As numerous results have been formulated on the subject of integral manifolds, we present only the one that will be used in the course of this work. First, some necessary definitions.

A (hyperbolic) integral manifold is **stable** if it has a neighbourhood in which all originating positive-time solutions approach the manifold exponentially. Let $\alpha_0 > 0$, $\Delta > 0$, $V \subseteq \mathbb{R}^p$, $\Sigma = \mathbb{R} \times V \times [0, \alpha_0]$, $f : \Sigma \to \mathbb{R}^q$, $g : V \to \mathbb{R}^q$ and $h : \mathbb{R} \times V \to \mathbb{R}^q$.

We say that f is **Lipschitz over a set Σ, with Lipschitz constant $\lambda(\alpha, V)$** or **Lipschitz in Hale's sense**, which we denote by $f \in \text{Lip}(x; \Sigma, \lambda(\alpha, V))$, if f is continuous in all of its arguments and is Lipschitz in x for $(t, x, \alpha) \in \Sigma$ with Lipschitz constant $\lambda(\alpha, V)$, where λ is continuous in α and the parameters describing V.

Next we say that g is **bounded by Δ over** V, which we denote by $g \in \mathcal{B}(\Delta; V)$, if $\|g(x)\| \leq \Delta$ for all $x \in V$. Finally, we denote the fact that h is $T-$periodic in $\phi \in \mathbb{R}$ by $h \in \mathfrak{P}_\phi^T$.

When the sets Σ and V are understood from the context, they are omitted.

We are now in position to state and prove the following theorem, which is a modified version of one of Hale's theorems. The essence of the proof remains the same, but enough significant differences are present to warrant a new presentation.

Theorem 2.3.1 (modified from [37], Theorem 6.1, pp. 526 – 527) *Let $\sigma_0 > 0$. Consider the system of equations*

$$\begin{aligned} \dot{x} &= \varepsilon\gamma_{\varepsilon,\mu}x + \varepsilon\Lambda(t, \psi, x, \varepsilon, \mu) \\ \dot{\psi} &= d(\varepsilon, \mu) + \Theta(t, \psi, x, \varepsilon, \mu), \end{aligned} \tag{2.3.1}$$

where $\psi \in \mathbb{R}$, $x \in [-\sigma_0, \infty)$, $\gamma_{\varepsilon,\mu} \neq 0$ depends continuously on (ε, μ), and d is defined over $S_0 = [-\varepsilon_0, \varepsilon_0] \times [-\mu_0, \mu_0]$, with $d(0, 0) = 1$. For $\sigma > 0$, let

$$\Sigma_\sigma = \mathbb{R} \times \mathbb{R} \times [-\sigma, \sigma] \times S_0 \quad \textit{and} \quad \Sigma_0 = \mathbb{R} \times \mathbb{R} \times \{0\} \times S_0.$$

Suppose $\Theta, \Lambda \in \mathfrak{P}_t^\chi \cap \mathfrak{P}_\psi^\omega$ and that

i. Θ and Λ are real-valued over Σ_{σ_0};

ii. $\Theta, \Lambda \in \mathcal{B}(\Xi(\varepsilon, \mu); \Sigma_0)$ where $\Xi(\varepsilon, \mu) = O(\varepsilon, \mu)$;

iii. for all $0 \leq \sigma \leq \sigma_0$, $\Theta \in \text{Lip}(\psi, x; \Sigma_\sigma, \theta(\varepsilon, \mu, \sigma))$ and $\Lambda \in \text{Lip}(\psi, x; \Sigma_\sigma, \lambda(\varepsilon, \mu, \sigma))$, with $\theta(\varepsilon, \mu, \sigma) = O(\varepsilon, \mu, \sigma)$ and $\lambda(\varepsilon, \mu, \sigma) = O(\varepsilon, \mu, \sigma)$.

Then, there exists $(\varepsilon_1, \mu_1) \in (0, \varepsilon_0] \times (0, \mu_0]$ such that for all

$$(\varepsilon, \mu) \in S_1 = [-\varepsilon_1, \varepsilon_1] \times [-\mu_1, \mu_1]$$

with $\varepsilon \neq 0$, (2.3.1) has a (hyperbolic) integral manifold $\mathcal{T}_{\varepsilon,\mu}$ which can be represented as an invariant torus $x = \Upsilon_{\varepsilon,\mu}(t,\psi)$, where

$$\Upsilon_{\varepsilon,\mu} \in \mathcal{B}(D(\varepsilon,\mu)) \cap \mathrm{Lip}(\psi, \Omega(\varepsilon,\mu)) \cap \mathfrak{P}_t^{\chi} \cap \mathfrak{P}_{\psi}^{\omega},$$

with $D(\varepsilon,\mu), \Omega(\varepsilon,\mu) \to 0$ uniformly as $(\varepsilon,\mu) \to 0$. Furthermore, the stability of $\mathcal{T}_{\varepsilon,\mu}$ is exactly determined by the sign of $\varepsilon\gamma_{0,0}$.

Proof: In [37], Hale proves this result for $\mu = 0$. In our proof, we only consider the case where both the parameters ε, μ are positive; the proof for the remaining cases is nearly identical.

Pick $\sigma \in (0, \sigma_0)$. Let D, Ω be positive numbers such that $D \in [-\sigma, \sigma]$. Define

$$\mathcal{X}(D,\Omega) = \{F(t,\psi) : F \in \mathcal{B}(D) \cap \mathrm{Lip}(\psi,\Omega) \cap \mathfrak{P}_t^{\chi} \cap \mathfrak{P}_{\psi}^{\omega}\}.$$

Endowed with the metric

$$m(F,G) = \sup_{\psi,t}\{|F(t,\psi) - G(t,\psi)|\},$$

$\mathcal{X}(D,\Omega)$ is a complete metric space. Let $\psi_0, t \in \mathbb{R}$. For $F \in \mathcal{X}(D,\Omega)$, let the solution of

$$\dot{\psi} = d(\varepsilon,\mu) + \Theta(y+t, \psi, F(y+t,\psi), \varepsilon, \mu) \tag{2.3.2}$$

through ψ_0 be denoted by $\psi_{y,t}^F = \psi_{y,t}^F(\psi_0)$. Finally, define the operator $\mathcal{L}_{\psi,t}$ on $\mathcal{X}(D,\Omega)$ by

$$\mathcal{L}_{\psi,t}(F) = \varepsilon \int_{-\infty}^{+\infty} K(\varepsilon y)\Lambda(y+t, \psi_{y,t}^F(\psi), F(y+t, \psi_{y,t}^F(\psi)), \varepsilon, \mu)\, dy, \tag{2.3.3}$$

where

$$K(z) = \begin{cases} -e^{-\gamma_{\varepsilon,\mu} z} & \text{if } z \geq 0 \\ 0 & \text{if } z < 0 \end{cases} \quad \text{or} \quad K(z) = \begin{cases} 0 & \text{if } z > 0 \\ e^{-\gamma_{\varepsilon,\mu} z} & \text{if } z \leq 0 \end{cases},$$

depending on whether $\gamma_{\varepsilon,\mu} > 0$ or $\gamma_{\varepsilon,\mu} < 0$, respectively. In either case, there is a positive constant $\alpha = |\gamma_{\varepsilon,\mu}|$ such that $|K(z)| \leq e^{-\alpha|z|}$, $\forall z \in \mathbb{R}$.

For an appropriate choice of the constants $D = D(\varepsilon,\mu)$ and $\Omega = \Omega(\varepsilon,\mu)$ satisfying the conditions in the conclusion of the theorem, $\mathcal{L}_{\psi,t}$ is a contraction on $\mathcal{X}(D,\Omega)$ whenever ε and μ are positive and small enough (see p. 30 for details).

By the Banach Fixed Point Theorem, $\mathcal{L}_{\psi,t}$ has a unique fixed point $\mathcal{T}_{\varepsilon,\mu} \in \mathcal{X}(D,\Omega)$, which we will denote by $x_t = \Upsilon_{\varepsilon,\mu}(t,\psi)$. By construction, x_t must satisfy the relation

$$x_t = \varepsilon \int_{-\infty}^{+\infty} K(\varepsilon y)\Lambda(y+t, \psi_{y,t}^{\Upsilon}, x_{y+t}, \varsigma, \mu)\, dy.$$

Set $y + t = s$. Then $\psi^{\Upsilon}_{y,t} = \psi^{\Upsilon}_{y+t,0} = \psi^{\Upsilon}_s$ (see [37], p. 510 for details) and

$$\begin{aligned} x_t &= \varepsilon \int_{-\infty}^{+\infty} K(\varepsilon(s-t))\Lambda(s, \psi^{\Upsilon}_s, x_s, \varepsilon, \mu)\, ds \\ &= \varepsilon \int_{-\infty}^{t} K(\varepsilon(s-t))\Lambda(s, \psi^{\Upsilon}_s, x_s, \varepsilon, \mu)\, ds + \varepsilon \int_{t}^{+\infty} K(\varepsilon(s-t))\Lambda(s, \psi^{\Upsilon}_s, x_s, \varepsilon, \mu)\, ds. \end{aligned}$$

If $\gamma_{\varepsilon,\mu} > 0$, the above equation becomes

$$\begin{aligned} x_t &= -\varepsilon \int_{t}^{+\infty} e^{-\gamma_{\varepsilon,\mu}(s-t)}\Lambda(s, \psi^{\Upsilon}_s, x_s, \varepsilon, \mu)\, ds \\ &= -\varepsilon e^{\gamma_{\varepsilon,\mu}t} \int_{t}^{+\infty} e^{-\gamma_{\varepsilon,\mu}s}\Lambda(s, \psi^{\Upsilon}_s, x_s, \varepsilon, \mu)\, ds = \varepsilon e^{\gamma_{\varepsilon,\mu}t} \int_{+\infty}^{t} e^{-\gamma_{\varepsilon,\mu}s}\Lambda(s, \psi^{\Upsilon}_s, x_s, \varepsilon, \mu)\, ds \end{aligned}$$

To show x_t is indeed an integral manifold for (2.3.1), it remains only to show that it satisfies the $\dot{x}$ equation in (2.3.1). Since

$$\begin{aligned} \dot{x}_t &= \varepsilon e^{\gamma_{\varepsilon,\mu}t} e^{-\gamma_{\varepsilon,\mu}t}\Lambda(t, \psi^{\Upsilon}_t, x_t, \varepsilon, \mu) + \varepsilon\gamma_{\varepsilon,\mu} e^{\gamma_{\varepsilon,\mu}t} \int_{+\infty}^{t} e^{-\gamma_{\varepsilon,\mu}s}\Lambda(s, \psi^{\Upsilon}_s, x_s, \varepsilon, \mu)\, ds \\ &= \varepsilon\gamma_{\varepsilon,\mu} x_t + \varepsilon\Lambda(t, \psi^{\Upsilon}_t, x_t, \varepsilon, \mu), \end{aligned}$$

this is indeed the case. Similarly, $\mathcal{T}_{\varepsilon,\mu}$ is also an integral manifold if $\gamma_{\varepsilon,\mu} < 0$. Finally, the stability is uniquely determined by the sign of $\varepsilon\gamma_{0,0}$, as can be assessed by [37, lemma 2.3]. ∎

Theorem 2.3.1 can easily be extended to the case where μ is a parameter vector, simply by modifying the constants appearing in the proof that $\mathcal{L}_{\psi,t}$ is a contraction; the rest then proceeds as above.

2.4 The Implicit Function Theorem

The Implicit Function Theorem is a well-known and oft-used result; as such, it is presented without proof.

Theorem 2.4.1 [20,54] *Let $F : \mathbb{R}^n \times \mathbb{R}^m \to \mathbb{R}^n$ be of class C^r, $r \geq 1$ (resp. analytic). If $F(x_0, \varepsilon_0) = 0$ and $\det(D_x F(x_0, \varepsilon_0)) \neq 0$, then there is a neighbourhood U_0 of ε_0 and a unique C^r (resp. analytic) map $X : U_0 \to \mathbb{R}^n$ such that $X(\varepsilon_0) = x_0$ and $F(X(\varepsilon), \varepsilon) = 0$ for all $\varepsilon \in U_0$.*

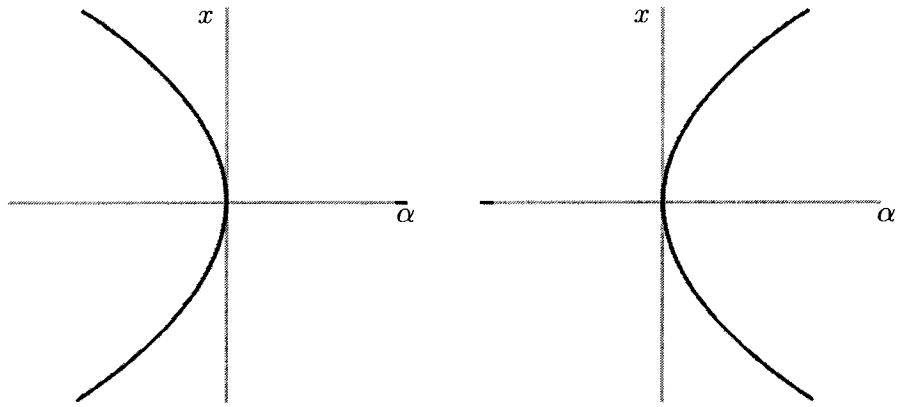

Figure 2.1: Bifurcation diagram near a saddle-node singularity.

2.5 Bifurcations of Fixed Points

Let $f : \mathbb{R}^m \times \mathbb{R}^n \to \mathbb{R}^m$ be a smooth map of $(x, \alpha) \in \mathbb{R}^m \times \mathbb{R}^n$. A **fixed point** x_0 **of** f **for** α_0 is a pair $(x_0, \alpha_0) \in \mathbb{R}^m \times \mathbb{R}^n$ for which $f(x_0, \alpha_0) = x_0$. The eigenvalues $\mu_1, \ldots, \mu_m$ of $D_x f(x_0, \alpha_0)$ are the **multipliers** of the fixed point (x_0, α_0); if none of the multipliers have modulus 1, the fixed point is said to be **hyperbolic**.

Generically, at a non-hyperbolic fixed point, the discrete-time dynamical system

$$x \mapsto f(x, \alpha) \tag{2.5.1}$$

undergoes drastic qualitative changes. Such points are called **bifurcation points** or **singularities** of (2.5.1). The **codimension** of a singularity is the number of independent conditions necessary in order to realize the singularity [47, p. 63].

We will encounter three types of singularity in this work: saddle-nodes, of codimension 1, and cusps and Bogdanov-Takens points, of codimension 2.

2.5.1 The Saddle-Node Singularity

Theorem 2.5.1 ([47], Theorem 4.1, pp. 104 – 108) *Let $m = n = 1$. Suppose the origin is a fixed point of f for $\alpha_0 = 0$, with multiplier $\mu_1 = D_x f(0,0) = 1$. If the non-degeneracy conditions $D_{xx} f(0,0), D_\alpha f(0,0) \neq 0$ are satisfied, then the bifurcation diagram of* (2.5.1) *is topologically equivalent near the origin to one of the diagrams presented in Figure* 2.1.

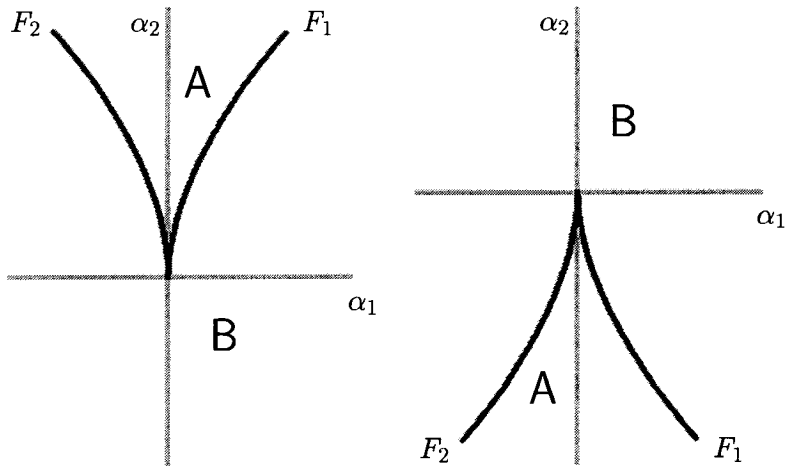

Figure 2.2: Neighbourhood of a cusp singularity in parameter space.

The singularity at the origin is called a **saddle-node** or a **fold**; it provides a generic mechanism for the creation and destruction of fixed points in (2.5.1).

Theorem 2.5.1 also characterizes folds in $m-$dimensional systems: after a center manifold reduction (and the accompanying change of coordinates) and a translation of the fold at the origin, (2.5.1) satisfies all required hypotheses.

2.5.2 The Cusp Singularity

Theorem 2.5.2 ([47], Theorem 9.1, pp. 351 – 353) *Let $m = 1$ and $n = 2$. Suppose the origin is a fixed point of f for $\alpha_0 = (0,0)$, with multiplier $\mu_1 = D_x f(0,0) = 1$, such that $D_{xx} f(0,0) = 0$. If the non-degeneracy conditions $D_{xxx} f(0,0) \neq 0$ and*

$$D_{\alpha_1} f(0,0) D_{x\alpha_2} f(0,0) - D_{\alpha_2} f(0,0) D_{x\alpha_1} f(0,0) \neq 0$$

are satisfied, then the neighbourhood of the origin in parameter space is topologically equivalent to one of the diagrams presented in Figure 2.2 (see explanations below).

The singularity at the origin is called a **cusp**: (2.5.1) has three fixed points in region A, two of which disappear at a fold singularity while crossing F_1 or F_2 into region B, where a lone fixed point remains.

As was the case for the fold singularity, Theorem 2.5.2 also characterizes cusps in generic $m-$dimensional systems.

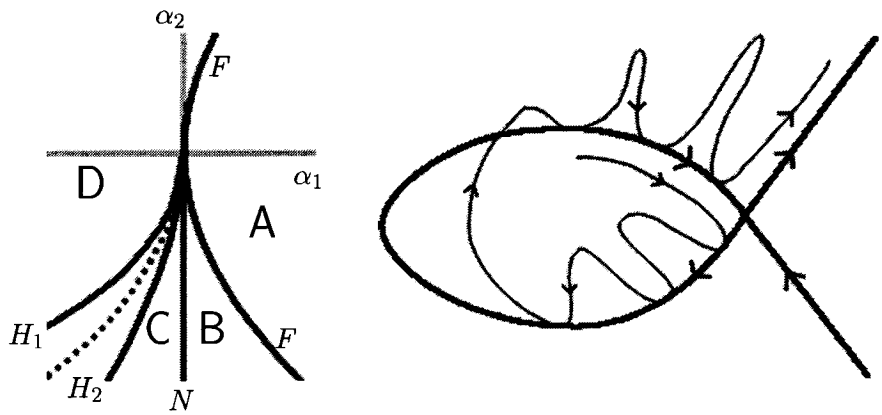

Figure 2.3: Neighbourhood of a Bogdanov-Takens singularity in parameter space (on the left) and homoclinic tangencies on H_1 (on the right).

2.5.3 The Bogdanov-Takens Singularity

Theorem 2.5.3 ([47], lemma 9.6, pp. 364 – 368) *Let $m = 2$ and $n = 2$. Suppose the origin is a fixed point of f for $\alpha_0 = (0,0)$, with multipliers $\mu_{1,2} = 1$. Let v_1, v_2 be the (linearly independent) generalized eigenvectors of $D_x f(0,0)$ associated with the double eigenvalue $\mu_{1,2} = 1$. Then, there exists a change of variables $x = g(y)$ for which (2.5.1) becomes $y \mapsto \Lambda y + G(y,\alpha)$, where $\Lambda_{2,1} = 0$ and $\Lambda_{i,j} = 1$ otherwise.*

Set $a_{20} = 2D_{y_1y_1}G_1(0,0)$, $b_{20} = 2D_{y_1y_1}G_2(0,0)$, $b_{11} = D_{y_1y_2}G_2(0,0)$. If the non-degeneracy conditions $a_{20} + b_{11} - b_{20} \neq 0$ and $b_{20} \neq 0$ are satisfied and if

$$s = \text{sign}\left[a_{20}b_{20} + b_{20}b_{11} - b_{20}^2\right] = -1,$$

then the neighbourhood of the origin in parameter space is topologically equivalent to the (partial) diagram presented in figure 2.3 (see explanations below).

The singularity at the origin is called a **Bogdanov-Takens singularity** or a **strong 1:1 resonance point**. The behaviour of (2.5.1) in a neighbourhood of the origin is complicated; Arnol'd tongues (which we will not discuss) and homoclinic tangles are part of the picture (see Figure 2.3, on the right), which remains incomplete [47, p. 412].

In region A, (2.5.1) has no fixed point. Two fixed points are created in a fold bifurcation as F is crossed into region B. For small parameter values in region C, (2.5.1) has a closed invariant curve as a result of a Neimark-Sacker bifurcation along N.

If we cross from region A into region D, two fixed points appear in a fold bifurcation along F. The invariant closed curve of region C disappears in a homoclinic bifurcation,

but there is an "exponentially narrow parameter region [...] bounded by two smooth bifurcation curves H_1 and H_2 (corresponding to homoclinic tangencies) [47, p. 368]" in which (2.5.1) has a homoclinic tangled structure. These structures are linked to chaos *via* Smale's horseshoes [72]; thus, there is a small region in parameter space for which (2.5.1) behaves chaotically.

As was the case for both previous singularities, Theorem 2.5.3 also characterizes the Bogdanov-Takens singularity in generic $m-$dimensional systems.

2.6 Other Notions and Results

Conics have been studied since Antiquity [2]; the following characterization will be of use in Chapters 5 and 7.

Theorem 2.6.1 *For $i, j = 0, 1, 2$, let $\alpha_{i,j} \in \mathbb{R}$ and define*

$$C(x, y) = \alpha_{00} + \alpha_{10}x + \alpha_{01}y + \alpha_{20}x^2 + \alpha_{11}xy + \alpha_{02}y^2.$$

Now, set

$$\begin{aligned}
\Delta &= 4\alpha_{00}\alpha_{20}\alpha_{02} - \left(\alpha_{01}^2\alpha_{20} + \alpha_{00}\alpha_{11}^2 + \alpha_{10}^2\alpha_{02}\right) + \alpha_{10}\alpha_{01}\alpha_{11}, \\
J &= 4\alpha_{20}\alpha_{02} - \alpha_{11}^2, \\
I &= \alpha_{20} + \alpha_{02}, \\
K &= 4\alpha_{00}\left(\alpha_{20} + \alpha_{02}\right) - \left(\alpha_{10}^2 + \alpha_{01}^2\right).
\end{aligned}$$

Then the (real) zero-level set of $C(x, y)$,

$$Z_{\mathbb{R}^2}\left(C(x, y)\right) = \left\{(x, y) \in \mathbb{R}^2 : C(x, y) = 0\right\},$$

is a (possibly degenerate) conic whose type is given by Table 2.1. In all other instances, $Z_{\mathbb{R}^2}\left(C(x, y)\right) = \varnothing$.

Proof: This is a classic result, see [79] for instance. ∎

Let $x \in \mathbb{R}^n$ and $f : E \subseteq \mathbb{R}^n \to \mathbb{R}^m$. We shall write $f(x) = O\big(g(x)\big)$ as $x \to 0$ if there are numbers $\delta, M > 0$ such that $\|f(x)\| \leq M\|g(x)\|$ whenever $\|x\| < \delta$. When the context allows no ambiguity, the term $x \to 0$ will usually be omitted.

Let $F : \mathbb{R}^n \to \mathbb{R}^m$. We will say that $x^* \in \mathbb{R}^n$ is a **regular solution of** F or a **transverse intersection of** F if both $F(x^*) = 0$ and $\operatorname{rank} DF(x^*) = \min\{m, n\}$.

	Δ	J	$\Delta \cdot I$	K	$Z_{\mathbb{R}^2}(C(x,y))$
1)	$\neq 0$	< 0			hyperbola
2)	$\neq 0$	> 0	< 0		ellipse
3)	$\neq 0$	0			parabola
4)	0	< 0			pair of intersecting lines
5)	0	> 0			point
6)	0	0		< 0	pair of distinct parallel lines
7)	0	0		0	line

	α_{20}	α_{11}	α_{02}	α_{10}	α_{01}	α_{00}	$Z_{\mathbb{R}^2}(C(x,y))$
8)	0	0	0	$\neq 0$			line
9)	0	0	0		$\neq 0$		line
10)	0	0	0	0	0	0	plane

Table 2.1: Characterization of the (real) conic sections.

A smooth mapping $P : \mathbb{R}^n \to \mathbb{R}^m$, with $n \geq m$ is **t−regular at the origin** if $\operatorname{rank} DP(x) = m$ for all $x \in P^{-1}(\{0\})$. It follows from the Implicit Function Theorem that if P is t−regular at the origin, then $P^{-1}(\{0\})$ is a smooth $(n-m)$−submanifold of $\mathbb{R}^n$ [25].

The notation 'c. c.' will sometimes be used to indicate that a particular quantity is the complex conjugate of the quantity that immediately precedes it; 'h. o. t.' is reserved for the expression "higher order terms" (the terms in question will be clear from the context).

Finally, we shall assume that the reader is familiar with traditional concepts of dynamical systems such as the Poincaré map or local topological equivalence of bifurcation diagrams. Results that have not been introduced in this chapter will be presented as needed.

2.7 Appendix: Technical Details

Technical Definition 1

A TW $u_*(x,t)$ is a relative equilibrium of (2.1.1) with no rotation component; in that case, (2.2.1) becomes $u_*(x,t) = (0, ts_*)u_*(x,0)$ for some non-trivial $s_* \in \mathbb{R}^2$.

A RPS of (2.1.1) is a solution $u(x,t)$ satisfying $u(x,t) = \exp(z^*t)w(x,t)$ for some $z^* \in \mathfrak{se}(2)$, where w is a non-constant $T-$periodic function in t.

A MRW $u^*(x,t)$ is a RPS of (2.1.1) with no translation component; it can be written as $u^*(x,t) = (\exp_{\mathfrak{so}(2)}(r^*t), 0)w(x,t)$ for some non-trivial $r^* \in \mathfrak{so}(2)$, where w is a non-constant $T-$periodic function in t, after a change of coordinates bringing the center of rotation to the origin.

A MTW $u^*(x,t)$ is a RPS of (2.1.1) for which both the rotation and the translation components are uniform in time. ∎

Technical Result 1 The operator $\mathcal{L}_{\psi_0,t_0}$ defined in (2.3.3) is a contraction on $\mathcal{X}(D,\Omega)$.

Proof: Let all terms be as in the statement and the proof of Theorem 2.3.1. Let $\varepsilon_1, \mu_1 > 0$ and define $D = D(\varepsilon,\mu)$ and $\Omega = \Omega(\varepsilon,\mu)$ to be such that $D(\varepsilon,\mu)$ and $\Omega(\varepsilon,\mu) \to 0$ as $(\varepsilon,\mu) \to 0$ and

$$\theta(\varepsilon,\mu,D)(1+\Omega) < \varepsilon\frac{\alpha}{2} < \frac{\alpha}{2} \tag{2.7.1}$$

$$\frac{4}{\alpha}\lambda(\varepsilon,\mu,D)(1+\Omega) < \Omega \tag{2.7.2}$$

$$\frac{4}{\alpha}\lambda(\varepsilon,\mu,D) < \frac{1}{2} \tag{2.7.3}$$

$$\frac{2}{\alpha}(\Xi(\varepsilon,\mu) + D\lambda(\varepsilon,\mu,D)) < D \tag{2.7.4}$$

for all $0 < \varepsilon \leq \varepsilon_1$ and $0 < \mu \leq \mu_1$. This can always be done because of the properties of the functions λ and θ. Let $F, F^* \in \mathcal{X}(D,\Omega)$, and $\psi_0, \psi_0^*, t_0 \in \mathbb{R}$. Denote the solutions of

$$\dot{\psi} = d(\varepsilon,\mu) + \Theta(t,\psi,F(t,\psi),\varepsilon,\mu)$$
$$\dot{\psi} = d(\varepsilon,\mu) + \Theta(t,\psi,F^*(t,\psi),\varepsilon,\mu)$$

through ψ_0 and ψ_0^* at time t_0 by $\psi^F_{t-t_0,t_0} = \psi^F_{t-t_0,t_0}(\psi_0)$ and $\psi^{F^*}_{t-t_0,t_0} = \psi^{F^*}_{t-t_0,t_0}(\psi_0^*)$, respectively.[7]

By definition,

$$\mathcal{L}_{\psi_0+\omega,t_0}(F) = \varepsilon\int_{-\infty}^{\infty} K(\varepsilon y)\Lambda(y+t_0, \psi^F_{y,t_0}(\psi_0+\omega), F(t_0, \psi^F_{y,t_0}(\psi_0+\omega)), \varepsilon, \mu)\, dy.$$

Since Λ and F are $\omega-$periodic in ψ, and since $\psi^F_{y,t_0}(\psi_0+\omega) = \psi^F_{y,t_0}(\psi_0) + \omega$ (as both sides satisfy the differential equation (2.3.2) with the same initial condition $\psi_0+\omega$), then $\mathcal{L}_{\psi_0+\omega,t_0}(F) = \mathcal{L}_{\psi_0,t_0}(F)$. Thus $\mathcal{L}_{\psi_0,t_0}(F) \in \mathfrak{P}^\omega_\psi$.

[7]Whenever it will be convenient to do so, we will write $y = t - t_0$. Then $dy = dt$ and $\psi^F_{y,t_0}(\psi_0)$ satisfies (2.3.2).

Now, let $\psi_0^* = \psi_0$. Note that

$$|F(y + t_0, \psi^F_{y,t_0}) - F(y + t_0 + \chi, \psi^F_{y,t_0+\chi})| \leq \Omega |\psi^F_{y,t_0} - \psi^F_{y,t_0+\chi}|$$

as $F \in \mathcal{X}(D, \Omega)$. Then

$$\begin{aligned}
\left| \frac{d(\psi^F_{y,t_0} - \psi^F_{y,t_0+\chi})}{dy} \right| &= |\Theta(y + t_0, \psi^F_{y,t_0}, F(y + t_0, \psi^F_{y,t_0}), \varepsilon, \mu) \\
&\qquad - \Theta(y + t_0 + \chi, \psi^F_{y,t_0+\chi}, F(y + t_0 + \chi, \psi^F_{y,t_0+\chi}), \varepsilon, \mu)| \\
&\leq \theta(\varepsilon, \mu, D) \left[|\psi^F_{y,t_0} - \psi^F_{y,t_0+\chi}| + |F(y + t_0, \psi^F_{y,t_0}) - F(y + t_0 + \chi, \psi^F_{y,t_0+\chi})| \right] \\
&\leq \theta(\varepsilon, \mu, D)(1 + \Omega) |\psi^F_{y,t_0} - \psi^F_{y,t_0+\chi}|
\end{aligned}$$

and so $|\psi^F_{y,t_0} - \psi^F_{y,t_0+\chi}| \leq |\psi_0 - \psi_0| e^{\theta(\varepsilon,\mu,D)(1+\Omega)|y|} = 0$, by a variant of Gronwall's Lemma. This in turn implies that $\psi^F_{y,t_0} = \psi^F_{y,t_0+\chi}$. Then

$$\begin{aligned}
\mathcal{L}_{\psi_0,t_0+\chi}(F) &= \varepsilon \int_{-\infty}^{\infty} K(\varepsilon y) \Lambda(y + t_0 + \chi, \psi^F_{y,t_0+\chi}, F(t_0 + \chi, \psi^F_{y,t_0+\chi}), \varepsilon, \mu)\, dy \\
&= \varepsilon \int_{-\infty}^{\infty} K(\varepsilon y) \Lambda(y + t_0 + \chi, \psi^F_{y,t_0}, F(t_0 + \chi, \psi^F_{y,t_0}), \varepsilon, \mu)\, dy.
\end{aligned}$$

Since Λ and F are $\chi-$periodic in t (and so also in y), then $\mathcal{L}_{\psi_0,t_0+\chi}(F) = \mathcal{L}_{\psi_0,t_0}(F)$. Thus $\mathcal{L}_{\psi_0,t_0}(F) \in \mathfrak{P}_t^\chi$.

By definition,

$$\begin{aligned}
|\mathcal{L}_{\psi_0,t_0}(F)| &\leq \varepsilon \int_{-\infty}^{\infty} |K(\varepsilon y)| \left| \Lambda(y + t_0, \psi^F_{y,t_0}(\psi_0), F(y + t_0, \psi^F_{y,t_0}(\psi_0)), \varepsilon, \mu) \right| dy \\
&\leq \varepsilon \int_{-\infty}^{\infty} e^{-\alpha\varepsilon|y|} \left| \Lambda(y + t_0, \psi^F_{y,t_0}(\psi_0), F(y + t_0, \psi^F_{y,t_0}(\psi_0)), \varepsilon, \mu) \right| dy.
\end{aligned}$$

But $\Lambda \in \mathcal{B}(\Xi(\varepsilon, \mu); \Sigma_0) \cap \mathrm{Lip}(\psi, x; \Sigma_D; \lambda(\varepsilon, \mu, D))$, so there exists $|\tilde{x}(x)| \leq |x| \leq D$ such that

$$\begin{aligned}
|\Lambda(s, \psi, x, \varepsilon, \mu)| &= \left| \Lambda(s, \psi, 0, \varepsilon, \mu) + x \frac{\partial \Lambda}{\partial x}(s, \psi, \tilde{x}, \varepsilon, \mu) \right| \\
&\leq |\Lambda(s, \psi, 0, \varepsilon, \mu)| + |\tilde{x}| \left| \frac{\partial \Lambda}{\partial x}(s, \psi, \tilde{x}, \varepsilon, \mu) \right| \\
&\leq \Xi(\varepsilon, \mu) + D\lambda(\varepsilon, \mu, D),
\end{aligned}$$

where the last inequality comes from the Lipschitz nature of Λ. Since $F \in \mathcal{B}(D)$,

$$\left| \Lambda(y + t_0, \psi^F_{y,t_0}(\psi_0), F(y + t_0, \psi^F_{y,t_0}(\psi_0)), \varepsilon, \mu) \right| \leq \Xi(\varepsilon, \mu) + D\lambda(\varepsilon, \mu, D)$$

and so

$$|\mathcal{L}_{\psi_0,t_0}(F)| \le \varepsilon \int_{-\infty}^{\infty} e^{-\alpha\varepsilon|y|}(\Xi(\varepsilon,\mu) + D\lambda(\varepsilon,\mu,D))\,dy = 2\varepsilon \int_0^{\infty} e^{-\alpha\varepsilon y}(\Xi(\varepsilon,\mu) + D\lambda(\varepsilon,\mu,D))\,dy$$
$$= \frac{2}{\alpha}(\Xi(\varepsilon,\mu) + D\lambda(\varepsilon,\mu,D)) \le D$$

when ε and μ are small enough, as per condition (2.7.4). Thus $\mathcal{L}_{\psi_0,t_0}(F) \in \mathcal{B}(D)$.

Note that $|F^*(y+t_0,\psi^{F^*}_{y,t_0}) - F^*(y+t_0,\psi^F_{y,t_0})| \le \Omega|\psi^{F^*}_{y,t_0} - \psi^F_{y,t_0}|$ as $F^* \in \mathcal{X}(D,\Omega)$. Then

$$\left|\frac{d(\psi^{F^*}_{y,t_0} - \psi^F_{y,t_0})}{dy}\right| = \left|\Theta(y+t_0,\psi^{F^*}_{y,t_0},F^*(t,\psi^{F^*}_{y,t_0}),\varepsilon,\mu) - \Theta(y+t_0,\psi^F_{y,t_0},F(t,\psi^F_{y,t_0}),\varepsilon,\mu)\right|$$
$$\le \theta(\varepsilon,\mu,D)\left[|\psi^{F^*}_{y,t_0} - \psi^F_{y,t_0}| + |F^*(t,\psi^{F^*}_{y,t_0}) - F(t,\psi^F_{y,t_0})|\right]$$
$$\le \theta(\varepsilon,\mu,D)\left[|\psi^{F^*}_{y,t_0} - \psi^F_{y,t_0}| + |F^*(t,\psi^{F^*}_{y,t_0}) - F^*(t,\psi^F_{y,t_0})|\right.$$
$$\left. + |F^*(t,\psi^F_{y,t_0}) - F(t,\psi^F_{y,t_0})|\right]$$
$$\le \theta(\varepsilon,\mu,D)\left[|\psi^{F^*}_{y,t_0} - \psi^F_{y,t_0}| + \Omega|\psi^{F^*}_{y,t_0} - \psi^F_{y,t_0}| + \|F^* - F\|\right]$$
$$= \theta(\varepsilon,\mu,D)(1+\Omega)|\psi^{F^*}_{y,t_0} - \psi^F_{y,t_0}| + \theta(\varepsilon,\mu,D)\|F^* - F\|.$$

Using standard first order differential inequalities (see [67, pp. 36 – 37] for details), we conclude that

$$|\psi^{F^*}_{y,t_0} - \psi^F_{y,t_0}| \le |\psi^*_0 - \psi_0|e^{\theta(\varepsilon,\mu,D)(1+\Omega)|y|} + \frac{\|F^* - F\|}{1+\Omega}\left[e^{\theta(\varepsilon,\mu,D)(1+\Omega)|y|} - 1\right]$$
$$= \left(|\psi^*_0 - \psi_0| + \frac{\|F^* - F\|}{1+\Omega}\right)e^{\theta(\varepsilon,\mu,D)(1+\Omega)|y|} - \frac{\|F^* - F\|}{1+\Omega} \tag{2.7.5}$$

Then

$$|\mathcal{L}_{\psi^*_0,t_0}(F^*) - \mathcal{L}_{\psi_0,t_0}(F)| \le \varepsilon \int_{-\infty}^{\infty} |K(\varepsilon y)| \left|\Lambda(y+t_0,\psi^{F^*}_{y,t_0},F^*(y+t_0,\psi^{F^*}_{y,t_0}),\varepsilon,\mu)\right.$$
$$\left. - \Lambda(y+t_0,\psi^F_{y,t_0},F(y+t_0,\psi^F_{y,t_0}),\varepsilon,\mu)\right| dy$$
$$\le \varepsilon \int_{-\infty}^{\infty} e^{-\alpha\varepsilon|y|}\lambda(\varepsilon,\mu,D)\left[|\psi^{F^*}_{y,t_0} - \psi^F_{y,t_0}|\right.$$
$$\left. + \left|F^*(y+t_0,\psi^{F^*}_{y,t_0}) - F(y+t_0,\psi^F_{y,t_0})\right|\right] dy$$
$$\le \varepsilon \int_{-\infty}^{\infty} e^{-\alpha\varepsilon|y|}\left[(1+\Omega)|\psi^{F^*}_{y,t_0} - \psi^F_{y,t_0}| + \|F^* - F\|\right] dy$$
$$= \varepsilon\lambda(\varepsilon,\mu,D)\left[(1+\Omega)\int_{-\infty}^{\infty} e^{-\alpha\varepsilon|y|}|\psi^{F^*}_{y,t_0} - \psi^F_{y,t_0}|\,dy + \frac{2}{\alpha\varepsilon}\|F^* - F\|\right].$$

Using (2.7.5), we obtain

$$\begin{aligned}
&\int_{-\infty}^{\infty} e^{-\alpha\varepsilon|y|}|\psi_{y,t_0}^{F^*} - \psi_{y,t_0}^{F}|\,dy \\
&\quad\le \int_{-\infty}^{\infty}\left(|\psi_0^* - \psi_0| + \frac{\|F^* - F\|}{1+\Omega}\right) e^{(\theta(\varepsilon,\mu,D)(1+\Omega)-\alpha\varepsilon)|y|}\,dy - \frac{\|F^* - F\|}{1+\Omega}\int_{-\infty}^{\infty} e^{-\alpha\varepsilon|y|}\,dy \\
&\quad= 2\left(|\psi_0^* - \psi_0| + \frac{\|F^* - F\|}{1+\Omega}\right)\int_0^{\infty} e^{(\theta(\varepsilon,\mu,D)(1+\Omega)-\alpha\varepsilon)y}\,dy - 2\frac{\|F^* - F\|}{1+\Omega}\int_0^{\infty} e^{-\alpha\varepsilon y}\,dy \\
&= \frac{2}{\theta(\varepsilon,\mu,D)(1+\Omega)-\alpha\varepsilon}\left(|\psi_0^* - \psi_0| + \frac{\|F^* - F\|}{1+\Omega}\right)\left[\lim_{b\to\infty} e^{(\theta(\varepsilon,\mu,D)(1+\Omega)-\alpha\varepsilon)b} - 1\right] - \frac{2}{\alpha\varepsilon}\frac{\|F^* - F\|}{1+\Omega}.
\end{aligned}$$

However, $\theta(\varepsilon,\mu,D)(1+\Omega) - \alpha\varepsilon < \frac{\alpha\varepsilon}{2} - \alpha\varepsilon = -\frac{\alpha\varepsilon}{2} < 0$ according to (2.7.1). Then

$$\int_{-\infty}^{\infty} e^{-\alpha\varepsilon|y|}|\psi_{y,t_0}^{F^*} - \psi_{y,t_0}^{F}|\,dy \le \frac{2}{\alpha\varepsilon - \theta(\varepsilon,\mu,D)(1+\Omega)}\left(|\psi_0^* - \psi_0| + \frac{\|F^* - F\|}{1+\Omega}\right) - \frac{2}{\alpha\varepsilon}\frac{\|F^* - F\|}{1+\Omega},$$

and so

$$\begin{aligned}
|\mathcal{L}_{\psi_0^*,t_0}(F^*) - \mathcal{L}_{\psi_0,t_0}(F)| &\le \frac{2\varepsilon\lambda(\varepsilon,\mu,D)}{\alpha\varepsilon - \theta(\varepsilon,\mu,D)(1+\Omega)}\left[(1+\Omega)|\psi_0^* - \psi_0| + \|F^* - F\|\right] \\
&\le \frac{4}{\alpha}\lambda(\varepsilon,\mu,D)\left[(1+\Omega)|\psi_0^* - \psi_0| + \|F^* - F\|\right].
\end{aligned}$$

Then, using (2.7.2) and (2.7.3), we get

$$|\mathcal{L}_{\psi_0^*,t_0}(F^*) - \mathcal{L}_{\psi_0,t_0}(F)| \le \Omega|\psi_0^* - \psi_0| + \frac{\|F^* - F\|}{2}. \tag{2.7.6}$$

If $F^* = F$, then $|\mathcal{L}_{\psi_0^*,t_0}(F) - \mathcal{L}_{\psi_0,t_0}(F)| \le \Omega|\psi_0^* - \psi_0|$. Thus $\mathcal{L}_{\psi_0,t_0}(F) \in \mathrm{Lip}(\psi;\Omega)$.

Hence, $\mathcal{L}_{\psi_0,t_0}(F) \in \mathcal{X}(D,\Omega)$ for all ψ_0, t_0. Now let $F, F^* \in \mathcal{X}(D,\Omega)$. From (2.7.6) we get

$$|\mathcal{L}_{\psi_0,t_0}(F^*) - \mathcal{L}_{\psi_0,t_0}(F)| \le \Omega|\psi_0 - \psi_0| + \frac{\|F^* - F\|}{2} = \frac{1}{2}\|F^* - F\|.$$

This shows $\mathcal{L}_{\psi_0,t_0}$ is a contraction for all ψ_0, t_0. ∎

Chapter 3

The Center Bundle Equations

When the underlying reaction-diffusion system (RDS) undergoes forced translational symmetry-breaking, the equations that describe the essential dynamics of a rotating wave before its transition to a modulated rotating wave have a very nice structure, which can be exploited to describe various phenomena. We derive the basic (skew-product) bundle equations on the manifold $V_* = \mathbb{C} \times \mathbb{S}^1$ for a reaction-diffusion system with n translational symmetry-breaking terms, using the Center Manifolf Reduction Theorem of Sandstede, Scheel and Wulff described in Section 2.2 and [61, 62].[1]

3.1 General Form of the Perturbations

The parametrization of $\mathbb{SE}(2)$ that is used depends on the space over which the work is being done: either the physical space $\mathbb{R}^2$ or the center bundle V_*. In the former case, set $\mathbb{SE}(2) = \mathbb{SO}(2) \dot{+} \mathbb{R}^2$ with a multiplication defined by (2.1.8) and an action on $\mathbb{R}^2$ given by (2.1.7). In the latter case, set $\mathbb{SE}(2) = \mathbb{C} \dot{+} \mathbb{S}^1$ with a multiplication defined by (2.2.4) and an action on V_* given by (2.2.5). Set $\mathsf{Y} = \mathbb{R}^2$ or $\mathsf{Y} = \mathbb{C}$ accordingly.

For $\xi \in \mathsf{Y}$, denote the group of **Euclidean rotations around** ξ by $\mathbb{SO}(2)_\xi$.[2] With the natural association, it is clear that $\mathbb{SO}(2)_\xi \cong \mathbb{SO}(2) < \mathbb{SE}(2)$.

[1] The notation of Section 2.2 will be used throughout this chapter.

[2] We use the notation ξ to represent both the point centering the inhomogeneity in the physical space $\mathbb{R}^2$ and the corresponding point centering the perturbation in the **phase space** $\mathbb{C}$. As the equivalence between the RDS and the center bundle equations is not explicit, it's quite possible that $\xi \in \mathbb{R}^2$ and $\xi \in \mathbb{C}$ refer to different planar points, in spite of the notation. The same remark applies to λ in (3.1.1) and (3.1.2).

Equation (2.1.1) models a RDS in a homogeneous isotropic medium. Our goal is to study perturbations of systems that arise from multiple localized inhomogeneities in the medium. To this end, we will need to make a simplifying assumption on the nature of these inhomogeneities.

Hypothesis 3.1.1 *Each localized inhomogeneity, considered in isolation from the other inhomogeneities, is rotationally symmetric about some point in the medium.*

This modeling assumption simplifies the analysis considerably, although it undoubtedly does not represent the general physical reality of inhomogeneities in excitable media. Nevertheless, it will allow for the prediction of new and interesting behaviour for spiral wave dynamics; some of these predictions will be confirmed numerically in Chapter 7.

Let $\xi_1, \ldots, \xi_n$ be distinct points of $\mathbb{R}^2$ and consider the reaction-diffusion system

$$u_t = \tilde{D}\Delta u + f(u) + \sum_{j=1}^{n} \lambda_j \left[\hat{D}_j(\|x-\xi_j\|^2, \lambda)\Delta u + f_j(u, \|x-\xi_j\|^2, \lambda)\right], \qquad (3.1.1)$$

where $\lambda = (\lambda_1, \ldots, \lambda_n) \in \mathbb{R}^n$ and the diffusion and reaction terms $\hat{D}_j$ and f_j are smooth and bounded for $j = 1, \ldots, n$.

When λ is small and $\tilde{D}$ is invertible, (3.1.1) is a small perturbation of (2.1.1); such a system satisfies Hypothesis 3.1.1 and is a generalization of RDS that have been used in the literature to model the presence of a single localized inhomogeneity in an excitable medium [35, 51, 55].[3]

The semi-flow $\Phi_{t,\lambda}$ generated by (3.1.1) is $\mathbb{SE}(2)$-equivariant when $\lambda = 0$; but it is only $\mathbb{SO}(2)_{\xi_j}$-equivariant when $\lambda \neq 0$ is small and along the j^{th} coordinate axis, and (generically) trivially equivariant when λ is small and generic (see p. 40 for details).

To study the effects of forced symmetry-breaking on (normally hyperbolic) rotating waves, assume further that hypotheses 2.2.1 and 2.2.2 hold. Accordingly, there is a center-unstable manifold M^{cu} satisfying the conclusion of Theorem 2.2.3 which

[3]Strictly speaking, it could be argued that a general perturbation of (2.1.1) satisfying Hypothesis 3.1.1 is not necessarily a sum of perturbations, as in (3.1.1). For our purposes however, under appropriate hypotheses on the nature of perturbations, a Taylor expansion about $\lambda = 0$ reduces the analysis to such a sum.

contains the group orbit $\mathbb{SE}(2)u_*$. In particular,

$$M^{\text{cu}} = \{(1+\sigma)(R_\varphi, p)(u_*) : (R_\varphi, p) \in \mathbb{SE}(2)\},$$

where R_φ is the rotation by angle φ around the origin and $\sigma \in C^k(\mathbb{SE}(2)(u_*), Y)$ is close to zero. From Theorem 2.2.4 and Theorem 5 in [62], the substitution of

$$u(t) = (1+\sigma)(R_{\varphi(t)}, p(t))(u_*)$$

in (2.1.1) yields a reduced system of differential equations of the form (2.2.3). Since (3.1.1) is a small perturbation of (2.1.1), the equivalent vector field on V_* is a small perturbation of that system, namely, a system of the form

$$\begin{aligned} \dot{p} &= e^{i\varphi}\left[\nu + G^p(p, \overline{p}, \varphi, \lambda)\right] \\ \dot{\varphi} &= \omega_{\text{rot}} + G^\varphi(p, \overline{p}, \varphi, \lambda) \end{aligned} \tag{3.1.2}$$

on the center bundle V_*, where $(p, \varphi) \in \mathbb{C}\times\mathbb{S}^1$, $\nu \in \mathbb{C}$, $\omega_{\text{rot}} \in \mathbb{R}^\times$, $G^p(p, \overline{p}, \varphi, 0) \equiv 0$ and $G^\varphi(p, \overline{p}, \varphi, 0) \equiv 0$. Furthermore, the functions G^p and G^φ are smooth and uniformly bounded in p (see [51, 62] for details).

Proposition 3.1.2 *The system* (3.1.2) *is* $\mathbb{SE}(2)-$*equivariant when* $\lambda = 0$*; but it is only* $\mathbb{SO}(2)_{\xi_j}$*-equivariant when* $\lambda \neq 0$ *is small and along the* j^{th} *coordinate axis, and (generically) trivially equivariant when* λ *is small and generic.*

Proof: The conclusion holds since the flow on V_* described by (3.1.2) is equivalent to the semi-flow $\Phi_{t,\lambda}$ on M^{cu} [62, Theorem 5, p. 143]. ∎

If $\lambda = (\lambda_1, \ldots, \lambda_n)$ is small enough, $\omega_{\text{rot}} + G^\varphi(p, \overline{p}, \varphi, \lambda) \neq 0$ for all $p \in \mathbb{C}$ (since G^φ is bounded in p) and we can introduce a new time τ along orbits of (3.1.2), governed by

$$\frac{dt}{d\tau} = \frac{1}{\omega_{\text{rot}} + G^\varphi(p, \overline{p}, \varphi, \lambda)}.$$

With this time, (3.1.2) becomes

$$\begin{aligned} \frac{dp}{d\tau} &= \frac{e^{i\varphi}\left[\nu + G^p(p, \overline{p}, \varphi, \lambda)\right]}{\omega_{\text{rot}} + G^\varphi(p, \overline{p}, \varphi, \lambda)} \\ \frac{d\varphi}{d\tau} &= 1. \end{aligned} \tag{3.1.3}$$

A Taylor expansion of $\frac{dp}{d\tau}$ around $\lambda = 0$ yields

$$\frac{dp}{d\tau} = \frac{e^{i\varphi}}{\omega_{\text{rot}}}\big[\nu + \hat{G}(p, \overline{p}, \varphi, \lambda)\big], \tag{3.1.4}$$

where $\hat{G}$ is a suitable smooth and uniformly bounded function with $\hat{G}(p, \overline{p}, \varphi, 0) \equiv 0$ (see p. 40 for details). Setting $v = \frac{\nu}{\omega_{\text{rot}}}$ and $G = \frac{\hat{G}}{\omega_{\text{rot}}}$ and re-labeling τ by t yields

$$\begin{aligned} \dot{p} &= e^{i\varphi}\big[v + G(p, \overline{p}, \varphi, \lambda)\big] \\ \dot{\varphi} &= 1, \end{aligned} \tag{3.1.5}$$

where $v \in \mathbb{C}$, $G \in \mathfrak{P}^{2\pi}_{\varphi}$ is smooth, uniformly bounded and $G(p, \overline{p}, \varphi, 0) \equiv 0$.

As (3.1.5) also satisfies the equivariance conditions of proposition 3.1.2 (being equivalent to (3.1.2)), G is not completely arbitrary; determining its structure is the topic of the next section.

3.2 Specific Form of the Perturbations

Let $\xi \in \mathbb{C}$. In $\mathbb{SE}(2) = \mathbb{C}\dot{+}\mathbb{S}^1$, the group of rotations around ξ is

$$\mathbb{SO}(2)_\xi = \{\, (\xi, 0) \cdot (0, \theta) \cdot (-\xi, 0) \mid \theta \in \mathbb{S}^1 \,\} < \mathbb{SE}(2).$$

A typical element of $\mathbb{SO}(2)_\xi$ is of the form

$$(\xi, 0) \cdot (0, \theta) \cdot (-\xi, 0) = (\xi, 0)(-e^{i\theta}\xi, \theta) = (\xi(1 - e^{i\theta}), \theta),$$

where $\theta \in \mathbb{S}^1$. Then

$$(\xi(1 - e^{i\theta}), \theta) \cdot (p, \varphi) = ((p - \xi)e^{i\theta} + \xi, \varphi + \theta) \tag{3.2.1}$$

is an $\mathbb{SO}(2)_\xi$–action on the center bundle V_* (see p. 41 for details).

Proposition 3.2.1 *Let N be a system of differential equations which commutes with (3.2.1) on V_*. Then N has the form*

$$\begin{aligned} \dot{p} &= N^p(p, \overline{p}, \varphi) = e^{i\varphi} H^p((p - \xi)e^{-i\varphi}, \overline{(p - \xi)}e^{i\varphi}) \\ \dot{\varphi} &= N^\varphi(p, \overline{p}, \varphi) = H^\varphi((p - \xi)e^{-i\varphi}, \overline{(p - \xi)}e^{i\varphi}). \end{aligned} \tag{3.2.2}$$

Proof: As N is $\mathbb{SO}(2)_\xi$–equivariant, solutions of N are transferred to solutions by the action (3.2.1). If $z(t) = (p(t), \varphi(t))$ is such a solution, then so is

$$y(t) = \big((p(t) - \xi)e^{i\theta} + \xi, \varphi(t) + \theta\big)$$

for any $\theta \in \mathbb{S}^1$. Differentiating $y(t)$ directly yields

$$\dot{y}(t) = (\dot{p}(t)e^{i\theta}, \dot{\varphi}(t)). \tag{3.2.3}$$

Since $z(t)$ is a solution, $p(t)$ and $\varphi(t)$ satisfy

$$\begin{aligned}\dot{p}(t) &= N^p(p(t), \overline{p}(t), \varphi(t)),\\ \dot{\varphi}(t) &= N^\varphi(p(t), \overline{p}(t), \varphi(t)).\end{aligned}$$

In particular, (3.2.3) becomes

$$\dot{y}(t) = \begin{pmatrix}\dot{p}(t)e^{i\theta}\\ \dot{\varphi}(t)\end{pmatrix} = \begin{pmatrix}e^{i\theta}N^p(p(t), \overline{p}(t), \varphi(t))\\ N^\varphi(p(t), \overline{p}(t), \varphi(t))\end{pmatrix}. \tag{3.2.4}$$

But $y(t)$ is itself a solution of the system. Hence

$$\dot{y}(t) = \begin{pmatrix}N^p((p(t) - \xi)e^{i\theta} + \xi, \overline{(p(t) - \xi)}e^{-i\theta} + \overline{\xi}, \varphi(t) + \theta)\\ N^\varphi((p(t) - \xi)e^{i\theta} + \xi, , \overline{(p(t) - \xi)}e^{-i\theta} + \overline{\xi}, \varphi(t) + \theta)\end{pmatrix}. \tag{3.2.5}$$

Since (3.2.4) and (3.2.5) are equal,

$$\begin{aligned}N^p\big((p - \xi)e^{i\theta} + \xi, \overline{(p - \xi)}e^{-i\theta} + \overline{\xi}, \varphi + \theta\big) &= e^{i\theta}N^p(p, \overline{p}, \varphi)\\ N^\varphi\big((p - \xi)e^{i\theta} + \xi, \overline{(p - \xi)}e^{-i\theta} + \overline{\xi}, \varphi + \theta\big) &= N^\varphi(p, \overline{p}, \varphi)\end{aligned} \tag{3.2.6}$$

where the time dependence has been dropped to lighten the text. Now, define

$$H^p(p, \overline{p}, \varphi) = e^{-i\varphi}N^p\big(pe^{i\varphi} + \xi, \overline{p}e^{-i\varphi} + \overline{\xi}, \varphi\big).$$

Then

$$\begin{aligned}H^p(p, \overline{p}, \varphi + \theta) &= e^{-i(\varphi+\theta)}N^p\big(pe^{i(\varphi+\theta)} + \xi, \overline{p}e^{-i(\varphi+\theta)} + \overline{\xi}, \varphi + \theta\big)\\ &= e^{-i\varphi}e^{-i\theta}N^p\big((pe^{i\varphi} + \xi - \xi)e^{i\theta} + \xi, (\overline{p}e^{-i\varphi} + \overline{\xi} - \overline{\xi})e^{-i\theta} + \overline{\xi}, \varphi + \theta\big)\\ &= e^{-i\varphi}e^{-i\theta}e^{i\theta}N^p\big(pe^{i\varphi} + \xi, \overline{p}e^{-i\varphi} + \overline{\xi}, \varphi\big)\\ &= e^{-i\varphi}N^p\big(pe^{i\varphi} + \xi, \overline{p}e^{-i\varphi} + \overline{\xi}, \varphi\big) = H^p(p, \overline{p}, \varphi),\end{aligned}$$

for all $\theta \in \mathbb{S}^1$ according to (3.2.6). Thus $N^p\big(pe^{i\varphi} + \xi, \overline{p}e^{-i\varphi} + \overline{\xi}, \varphi\big) = e^{i\varphi}H^p(p, \overline{p})$ and so

$$N^p(p, \overline{p}, \varphi) = e^{i\varphi}H^p\big((p - \xi)e^{-i\varphi}, \overline{(p - \xi)}e^{i\varphi}\big).$$

Using $H^{\varphi}(p,\overline{p},\varphi) = N^{\varphi}\left(pe^{i\varphi}+\xi,\overline{p}e^{-i\varphi}+\overline{\xi},\varphi\right)$ we obtain, in the same manner, the general form for the $\varphi-$component of (3.2.2). ∎

Consider system (3.1.5). Since $G(p,\overline{p},\varphi,0)\equiv 0$, Taylor's Theorem implies that there are smooth and uniformly bounded functions $G_1,\ldots,G_n$ such that

$$G(p,\overline{p},\varphi,\lambda) = \sum_{j=1}^{n}\lambda_j G_j(p,\overline{p},\varphi,\lambda).$$

Re-write (3.1.5) as

$$\begin{aligned}\dot{p} &= e^{i\varphi}\left[v+\sum_{j=1}^{n}\lambda_j G_j(p,\overline{p},\varphi,\lambda)\right]\\ \dot{\varphi} &= 1.\end{aligned} \tag{3.2.7}$$

When $\lambda = \lambda_j \mathbf{e}_j$, where $\mathbf{e}_j$ is the j^{th} vector of the canonical basis of $\mathbb{R}^n$, (3.2.7) is $\mathbb{SO}(2)_{\xi_j}-$equivariant, by equivalence with (3.1.2). Applying Proposition 3.2.1, it can be concluded that there are smooth functions $H_1,\ldots,H_n$ satisfying

$$G_j(p,\overline{p},\varphi,\lambda_j\mathbf{e}_j) = H_j((p-\xi_j)e^{-i\varphi},\overline{(p-\xi_j)}e^{i\varphi},\lambda_j), \qquad \text{for } j=1,\ldots,n.$$

Thus, the essential dynamics of the semi-flow $\Phi_{t,\lambda}$ generated by (3.1.1) (near the normally hyperbolic rotating wave u_*) are described by **center bundle equations** of the form

$$\begin{aligned}\dot{p} &= e^{i\varphi}\left[v+\sum_{j=1}^{n}\lambda_j H_j((p-\xi_j)e^{-i\varphi},\overline{(p-\xi_j)}e^{i\varphi},\lambda_j)\right]\\ \dot{\varphi} &= 1,\end{aligned} \tag{3.2.8}$$

where $\lambda=(\lambda_1,\ldots,\lambda_n)\in\mathbb{R}^n$, $v\in\mathbb{C}$, and H_j is smooth and uniformly bounded in p for all $j=1,\ldots,n$.[4]

[4]Strictly speaking, the center bundle equations take the form

$$\dot{p} = e^{it}\left[v+\sum_{j=1}^{n}\lambda_j H_j((p-\xi_j)e^{-it},\overline{(p-\xi_j)}e^{it},\lambda_j)+\sum_{j\neq k}\lambda_j\lambda_k\mathcal{H}_{j,k}(p,\overline{p},\xi_j,\xi_k,t,\lambda)\right], \tag{3.2.9}$$

where $\mathcal{H}_{j,k}\in\mathfrak{P}_t^{2\pi}$ are such that Proposition 3.1.2 holds. However, the analysis in what follows is independent of the "mixed" perturbation terms $\mathcal{H}_{j,k}$, when $\|\lambda\|$ is small enough: in particular, it is generically the case that if (3.2.9) has a $2\pi-$periodic solution, so does (3.2.8), with the same stability. The argument depends on the Taylor expansion of an associated time-2π map. In Section 5.4, we show explicitly what happens in the case $n=2$; the case $n>2$ is handled similarly.

The CMRT yields the existence of the functions H_j, $j = 1, \ldots, n$, but it does not provide a method to explicitly compute them; the only thing that can be said is that the flows of (3.2.8) and (3.1.1) are equivalent near u_* for small λ, which is admittedly quite informative. In particular, "interesting" phenomena in the center bundle equations map to "interesting" behaviours in the reaction-diffusion system.[5]

3.3 Appendix: Technical Details

Technical Result 2 The reaction-diffusion system (3.1.1) is $\mathbb{SE}(2)$−equivariant for $\lambda = 0$, but it is generally only $\mathbb{SO}(2)_{\xi_j}$−equivariant when λ is small and along the j^{th} coordinate axis.

Proof: Since Δ and the reaction term f are both $\mathbb{SE}(2)$-equivariant (see Chapter 2, p. 18), it remains only to show that $\hat{D}_j$ and f_j commute with rotations about ξ_j, *i.e* with the following action of $\mathbb{SO}(2)_{\xi_j}$:

$$\begin{aligned} R \cdot \left(v(x,t), \|x - \xi_j\|^2\right) &= \left(v\left(R^{-1}(x), t\right), \|R^{-1}(x) - \xi_j\|^2\right) \\ &= \left(v\left(R^{-1}(x), t\right), \|x - \xi_j\|^2\right). \end{aligned}$$

Let u be a solution of (3.1.1) and set $h_j^\lambda(x,t) = f_j(u(x,t), \|x - \xi_j\|^2, \lambda)$. Then

$$\begin{aligned} R \cdot f_j(u(x,t), \|x - \xi\|^2, \lambda) &= R \cdot h_j^\lambda(x,t) \\ &= h_j^\lambda(R^{-1}(x), t) \\ &= f_j\left(u(R^{-1}(x), t), \|R^{-1}(x) - \xi_j\|^2, \lambda\right) \\ &= f_j\left(u(R^{-1}(x), t), \|x - \xi_j\|^2, \lambda\right) \\ &= f_j\left(R \cdot (u(x,t), \|x - \xi_j\|^2), \lambda\right). \end{aligned}$$

Since rotations act as the identity on the $\|x - \xi_j\|^2$−component of the above action, the diffusion terms $\hat{D}_j$ are similarly shown to commute with rotations. ∎

Technical Result 3 The function $\hat{G}$ in (3.1.4) is smooth and uniformly bounded in p.

Proof: By Taylor's Theorem, there is a smooth and uniformly bounded function $\hat{G}^\varphi$ satisfying $\hat{G}^\varphi(p, \overline{p}, \varphi, 0) \equiv 0$ and

$$\frac{1}{\omega_{\text{rot}} + G^\varphi(p, \overline{p}, \varphi, \lambda)} = \frac{1}{\omega_{\text{rot}}} + \hat{G}^\varphi(p, \overline{p}, \varphi, \lambda).$$

[5]For instance, hyperbolic 2π−periodic solutions of (3.2.8) represent spiral anchoring in (3.1.1); these 2π−periodic solutions will sometimes be referred to as **perturbed rotating waves** to emphasize that they need not have $\mathbb{SO}(2)$−symmetry.

Hence the right-hand side of (3.1.3) becomes

$$\begin{aligned}\frac{e^{i\varphi}\left[\nu + G^p(p,\overline{p},\varphi,\lambda)\right]}{\omega_{\text{rot}} + G^\varphi(p,\overline{p},\varphi,\lambda)} &= e^{i\varphi}\left(\frac{1}{\omega_{\text{rot}}} + \hat{G}^\varphi(p,\overline{p},\varphi,\lambda)\right)\left[v + G^p(p,\overline{p},\varphi,\lambda)\right] \\ &= \frac{e^{i\varphi}}{\omega_{\text{rot}}}\left[\nu + G^p(p,\overline{p},\varphi,\lambda) + \omega_{\text{rot}}\hat{G}^\varphi(p,\overline{p},\varphi,\lambda)\big(v + G^p(p,\overline{p},\varphi,\lambda)\big)\right] \\ &= \frac{e^{i\varphi}}{\omega_{\text{rot}}}\left[\nu + \hat{G}(p,\overline{p},\varphi,\lambda)\right]\end{aligned}$$

about $\lambda = 0$. By construction, $\hat{G}(p,\overline{p},\varphi,\lambda)$ is smooth and uniformly bounded in p (since both G^p and $\hat{G}^\varphi$ also are) and $\hat{G}(p,\overline{p},\varphi,0) \equiv 0$. ∎

Technical Result 4 Let $\xi \in \mathbb{C}$, $(p,\varphi) \in V_*$. Then (3.2.1) defines a $\mathbb{SO}(2)_\xi$–action on V_*.

Proof: As $\xi \in \mathbb{C}$ is fixed, (3.2.1) is parameterized by $\theta \in \mathbb{S}^1 \cong \mathbb{R}/\mathbb{Z}$. Since

$$0 \cdot (p,\varphi) = \big((p-\xi)e^{i\cdot 0} + \xi, \varphi + 0\big) = (p - \xi + \xi, \varphi) = (p,\varphi)$$

and

$$\begin{aligned}\theta_1 \cdot (\theta_2 \cdot (p,\varphi)) = \theta_1 \cdot \big((p-\xi)e^{i\theta_2} + \xi, \varphi + \theta_2\big) &= \Big(\big((p-\xi)e^{i\theta_2} + \xi - \xi\big)e^{i\theta_1} + \xi, \big(\varphi + \theta_2\big) + \theta_1\Big) \\ &= \big((p-\xi)e^{i\theta_2}e^{i\theta_1} + \xi, \varphi + (\theta_2 + \theta_1)\big) = \big((p-\xi)e^{i(\theta_1+\theta_2)} + \xi, \varphi + (\theta_1 + \theta_2)\big) \\ &= (\theta_1 + \theta_2) \cdot (p,\varphi)\end{aligned}$$

for all $\theta_1, \theta_2 \in \mathbb{S}^1$, (3.2.1) is indeed an action of $\mathbb{SO}(2)_\xi$ on V_*. ∎

Chapter 4

Analysis of the Center Bundle Equations

Let $\xi_1, \ldots, \xi_n$ be n distinct complex numbers. In this chapter, we provide a detailed analysis of the system

$$\begin{aligned} \dot{p} &= e^{i\varphi}\left[v + \sum_{j=1}^{n} \lambda_j H_j((p-\xi_j)e^{-i\varphi}, \overline{(p-\xi_j)}e^{i\varphi}, \lambda_j)\right] \\ \dot{\varphi} &= 1, \end{aligned} \tag{4.0.1}$$

where $\lambda = (\lambda_1, \ldots, \lambda_n) \in \mathbb{R}^n$ is small, $v \in \mathbb{C}$ and each H_j is smooth and uniformly bounded in p, which we derived previously as the center bundle equations describing the essential dynamics of the semi-flow $\Phi_{t,\lambda}$ of a reaction-diffusion system modeling an excitable medium with numerous inhomogeneities. Each translational symmetry-breaking term H_j in this system preserves rotations around the center ξ_j. Generically, (4.0.1) does not have global Euclidean symmetry.

The case $n = 1$ has been studied extensively by LeBlanc and Wulff [51]; their paper is discussed in the introduction and in appendix A, pp. 147−150. They show that spiral waves will generically anchor at (or be repelled by) the (single) inhomogeneity and that under certain non-generic conditions, boundary drifting will take place.

One might think that the combination of many perturbations would just combine the effects of each perturbation, so that spirals would be observed anchoring at each of the centers, but we shall see that this is not usually so: the study of the case $n > 1$ provides a number of surprising results [15], which we will discuss presently.

The $\dot{\varphi}$ equation in (4.0.1) yields $\varphi(t) = t + \varphi_0$. We can assume, without loss of generality, that $\varphi_0 = 0$. Then, system (4.0.1) re-writes as

$$\dot{p} = e^{it}\left[v + \sum_{j=1}^{n} \lambda_j H_j((p-\xi_j)e^{-it}, \overline{(p-\xi_j)}e^{it}, \lambda_j)\right]. \tag{4.0.2}$$

4.1 Spiral Anchoring

Consider a $2\pi-$periodic solution p_λ of (4.0.2). Define the average value

$$[p_\lambda]_A = \frac{1}{2\pi}\int_0^{2\pi} p_\lambda(t)\,dt. \tag{4.1.1}$$

If the Floquet multipliers of p_λ all lie within the unit circle, we shall say that $[p_\lambda]_A$ is the **center of anchoring** of p_λ.

Let $j_0 \in \{1,\ldots,n\}$. We can set $j_0 = 1$ by re-labeling if necessary; this enables us to temporarily shift our point of view so that ξ_1 plays the central role in the following analysis. Considering (4.0.2) under the co-rotating frame of reference $z = p - \xi_1 + ie^{it}v$, we obtain

$$\dot{z} = \dot{p} - e^{it}v = e^{it}\sum_{j=1}^{n} \lambda_j H_j\big((z-\zeta_j)e^{-it} - iv, \overline{(z-\zeta_j)}e^{it} + i\overline{v}, \lambda_j\big), \tag{4.1.2}$$

where $\zeta_j = \xi_j - \xi_1$ for $j = 1,\ldots,n$.

When $\lambda_1 \neq 0$ and $\lambda_2 = \cdots = \lambda_n = 0$, we find ourselves in the situation described by LeBlanc and Wulff [51]. Now, set $\varepsilon = \lambda_1$, $\mu_1 = 1$ and $\lambda_j = \mu_j\varepsilon$ for $j = 2,\ldots,n$ and $\mu = (\mu_2,\ldots,\mu_n) \in \mathbb{R}^{n-1}$. Then (4.1.2) can be viewed as a perturbation of the corresponding equation in the case $n = 1$. Note that $\zeta_1 = 0$ and $\lambda = (1,\mu)\varepsilon$.

Equation (4.1.2) can then be rewritten as

$$\dot{z} = \varepsilon e^{it}\sum_{j=1}^{n} \mu_j H_j\big((z-\zeta_j)e^{-it} - iv, \overline{(z-\zeta_j)}e^{it} + i\overline{v}, \mu_j\varepsilon\big). \tag{4.1.3}$$

Let $\hat{H}_j(w,\overline{w},\varepsilon,\mu) = H_j\big(w - iv, \overline{w} + i\overline{v}, \mu_j\varepsilon\big)$ for $j = 1,\ldots n$. Then (4.1.3) becomes

$$\dot{z} = \varepsilon e^{it}K(ze^{-it}, \overline{z}e^{it}, t, \varepsilon, \mu) \tag{4.1.4}$$

where $K(w,\overline{w},t,\varepsilon,\mu)=\sum_{j=1}^{n}\mu_j\hat{H}_j(w-\zeta_j e^{-it},\overline{w}-\overline{\zeta}_j e^{it},\varepsilon,\mu)$ is $2\pi-$periodic in t.

Set $\alpha_1=D_1H_1(-iv,i\overline{v},0)$. The Poincaré map P of (4.1.4) is given by

$$P(z,\overline{z},\varepsilon,\mu)=z+2\pi\varepsilon\Big[\alpha_1 z+O\big(|z|^2\big)+O\big(\varepsilon,\mu_2,\ldots,\mu_n\big)\Big] \tag{4.1.5}$$

near $z=0$ and $(\varepsilon,\mu)=(0,0)$ (see p. 61 for details).[1] Hyperbolic fixed points of (4.1.5) correspond to hyperbolic $2\pi-$periodic solutions of (4.1.4), and so to perturbed rotating waves in (4.0.1). As $z=0$ is not generally a fixed point of (4.1.5), these perturbed rotating waves may not be centered at ξ_1. Indeed, let

$$B(z,\overline{z},\varepsilon,\mu)=\alpha_1 z+O\big(|z|^2\big)+O\big(\varepsilon,\mu_2,\ldots,\mu_n\big) \tag{4.1.6}$$

be the function inside the square brackets in (4.1.5). Note that $B(0,0,0,0)=0$ and that, generically, $D_1B(0,0,0,0)=\alpha_1\neq 0$. By the Implicit Function Theorem, there is a unique smooth function $z(\varepsilon,\mu)$ defined near $(\varepsilon,\mu)=(0,0)$ with $z(0,0)=0$ and

$$B\big(z(\varepsilon,\mu),\overline{z}(\varepsilon,\mu),\varepsilon,\mu\big)\equiv 0 \tag{4.1.7}$$

near $z=0$. This leads to the following theorem.

Theorem 4.1.1 *Let α_1 be as in the preceding discussion, with $\mathrm{Re}(\alpha_1)\neq 0$. If the parameters are small enough to satisfy the conditions outlined in the proof below, the Poincaré map (4.1.5) has a unique family of hyperbolic fixed points, whose stability is exactly determined by the sign of $\varepsilon\,\mathrm{Re}(\alpha_1)$.*

Proof: Write $z=x+iy$, where $x,y\in\mathbb{R}$ and set $\alpha_1=\mathrm{Re}(\alpha_1)+i\,\mathrm{Im}(\alpha_1)$. In these real coordinates, P becomes

$$P(x,y,\varepsilon,\mu)=\begin{pmatrix}x\\y\end{pmatrix}+2\pi\varepsilon\begin{pmatrix}\mathrm{Re}(\alpha_1)x-\mathrm{Im}(\alpha_1)y\\ \mathrm{Im}(\alpha_1)x+\mathrm{Re}(\alpha_1)y\end{pmatrix}+\varepsilon M_1, \tag{4.1.8}$$

where $M_1=O(x^2,xy,y^2,\varepsilon,\mu_2,\ldots,\mu_n)$. Then

$$DP(x,y,\varepsilon,\mu)=\begin{pmatrix}1+2\pi\varepsilon\,\mathrm{Re}(\alpha_1)+\varepsilon M_{1,1} & -2\pi\varepsilon\,\mathrm{Im}(\alpha_1)+\varepsilon M_{1,2}\\ 2\pi\varepsilon\,\mathrm{Im}(\alpha_1)+\varepsilon M_{2,1} & 1+2\pi\varepsilon\,\mathrm{Re}(\alpha_1)+\varepsilon M_{2,2}\end{pmatrix},$$

[1] The time-2π map one derives from (3.2.9) has exactly the same form, whence the comment in footnote 4 on page 39.

where $M_{i,j} = O(x, y, \varepsilon, \mu_2, \ldots, \mu_n)$ for $i, j = 1, 2$. The eigenvalues of $DP(x, y, \varepsilon, \mu)$ are

$$\eta_{1,2} = 1 + 2\pi\varepsilon \operatorname{Re}(\alpha_1) + \varepsilon M_3 \pm \frac{|\varepsilon|}{2}\sqrt{-16\pi^2 \operatorname{Im}(\alpha_1)^2 + M_4},$$

where $M_3, M_4 = O(x, y, \varepsilon, \mu_2, \ldots, \mu_n)$.

Let B be as in (4.1.6) and $z(\varepsilon, \mu) = x(\varepsilon, \mu) + iy(\varepsilon, \mu)$ be the unique continuous function solving the equation $B = 0$ for small parameter values, as asserted above. When $\varepsilon = 0$, any point in $\mathbb{R}^2$ is a non-hyperbolic fixed point of P and so, from now on, we will assume that $\varepsilon \neq 0$.

If ε and $\mu_2, \ldots, \mu_n$ are small enough, then $(x(\varepsilon, \mu), y(\varepsilon, \mu))$ is a fixed point of (4.1.8) and $x(\varepsilon, \mu)$ and $y(\varepsilon, \mu)$ are each near 0, so that all the terms of order $O(x, y, \varepsilon, \mu)$ can be made as small as desired. As a result, we will suppose that ε and $\mu_2, \ldots, \mu_n$ are small enough to satisfy whatever need we have for them: in particular, we may assume that

$$-16\pi^2 \operatorname{Im}(\alpha_1)^2 + M_4 < 0.$$

Let $\eta_{1,2}(\varepsilon, \mu)$ be the eigenvalues of $DP(x(\varepsilon, \mu), y(\varepsilon, \mu), \varepsilon, \mu)$. Then

$$\begin{aligned}
(\operatorname{Re}\eta_{1,2}(\varepsilon, \mu))^2 &= (1 + 2\pi\varepsilon \operatorname{Re}(\alpha_1) + \varepsilon M_3)^2 \\
(\operatorname{Im}\eta_{1,2}(\varepsilon, \mu))^2 &= \left(\frac{|\varepsilon|}{2}\sqrt{16\pi^2 \operatorname{Im}(\alpha_1)^2 - M_4}\right)^2
\end{aligned}$$

and

$$\begin{aligned}
|\eta_{1,2}(\varepsilon, \mu)|^2 &= (1 + 2\pi\varepsilon \operatorname{Re}(\alpha_1) + \varepsilon M_3)^2 + \left(\frac{|\varepsilon|}{2}\sqrt{16\pi^2 \operatorname{Im}(\alpha_1)^2 - M_4}\right)^2 \\
&= 1 + 4\pi\varepsilon \operatorname{Re}(\alpha_1) + \varepsilon M_5,
\end{aligned}$$

where $M_5 = O(x, y, \varepsilon, \mu)$. By hypothesis, $\operatorname{Re}(\alpha_1) \neq 0$, so we may assume $4\pi\varepsilon \operatorname{Re}(\alpha_1) + \varepsilon M_5 \neq 0$. In other words,

$$|\eta_{1,2}(\varepsilon, \mu)|^2 = 1 + 4\pi\varepsilon \operatorname{Re}(\alpha_1) + \varepsilon M_5 \neq 1,$$

i.e., the eigenvalues do not lie on the unit circle: the fixed point $(x(\varepsilon, \mu), y(\varepsilon, \mu))$ is then hyperbolic. When $\varepsilon \operatorname{Re}(\alpha_1) < 0$, the eigenvalues lie inside the unit circle and the fixed point is asymptotically stable; otherwise, it is unstable. ∎

We are now able to formulate and prove the following result.

Theorem 4.1.2 *Suppose the hypotheses of Theorem* 4.1.1 *are satisfied. Then there exists a wedge-shaped region near* $\lambda = 0$ *of the form*

$$\mathcal{W}_1 = \{(\lambda_1, \ldots, \lambda_n) \in \mathbb{R}^n : |\lambda_j| < W_{1,j}|\lambda_1|, \ W_{1,j} > 0, \ \text{ for } j \neq 1 \text{ and } \lambda_1 \text{ near } 0\}$$

such that for all $0 \neq \lambda \in \mathcal{W}_1$, (4.0.1) *has a unique perturbed rotating wave* $\mathcal{S}^1_\lambda$, *with center* $[\mathcal{S}^1_\lambda]_A$ *generically away from* ξ_1. *Furthermore,* $[\mathcal{S}^1_\lambda]_A$ *is a center of anchoring when* $\lambda_1 \operatorname{Re}(\alpha_1) < 0$.

Proof: For $j \neq 1$, let $W_{1,j} > 0$ be such that the conclusion of Theorem 4.1.1 holds for any μ_j with $|\mu_j| < W_{1,j}$. Let $\mathcal{W}_1$ be as stated in the hypothesis. If (ε, μ) is such that the Poincaré map (4.1.5) has a hyperbolic fixed point $z(\varepsilon, \mu)$ near 0, then (4.1.3) has a hyperbolic $2\pi-$periodic orbit $\tilde{z}_{\varepsilon,\mu}(t)$ centered at a point near $z = \zeta_1 = 0$.

Let $\lambda_1 = \varepsilon \neq 0$ be small enough and set $\lambda_j = \mu_j \varepsilon$, for $j \neq 1$. Then $\lambda \in \mathcal{W}_1$, as

$$|\lambda_j| = |\mu_j||\varepsilon| < W_{1,j}|\lambda_1| \quad \text{for } j \neq 1,$$

and $\tilde{z}_{\varepsilon,\mu}(t)$ is a $2\pi-$periodic orbit for the parameter λ, which we denote by $z_\lambda(t)$. Since $p = z - ie^{it}v + \xi_1$, (4.0.1) has a unique perturbed rotating wave $\mathcal{S}^1_\lambda$, with

$$[\mathcal{S}^1_\lambda]_A = \frac{1}{2\pi}\int_0^{2\pi} \left(z_\lambda(t) - ie^{it}v + \xi_1\right) dt = \xi_1 + [z_\lambda]_A.$$

If $0 \neq \lambda \in \mathcal{W}$ is such that $\mu_j = \frac{\lambda_j}{\varepsilon} \neq 0$ is fixed for $j = 2, \ldots, n$, then $[z_\lambda]_A = O(1)$ as $\lambda_1 \to 0$ (see p. 62 for details) and so $[\mathcal{S}^1_\lambda]_A \neq \xi_1$, generically. The conclusion about the stability of $\mathcal{S}^1_\lambda$ follows directly from Theorem 4.1.1. ∎

Remark: When λ approaches the λ_1-axis away from the origin, $[\mathcal{S}^1_\lambda]_A \to \xi_1$. On the other hand, when the parameter values stray outside of $\mathcal{W}_1$, all that can generically be said with certainty is that solutions of (4.0.1) do not anchor at ξ_1. After drifting, the spiral may very well get anchored at some point away ξ_1, depending on the global nature of the perturbation functions H_j in (4.0.1). Richer dynamics can also take place; we will investigate this further in Section 4.3 and chapter 5.

The preceding results have been achieved by considering (4.0.1) under a co-rotating frame of reference around ξ_1. Corresponding results must also be achieved, in exactly the same manner, when the viewpoint shifts to another ξ_k.

For $j = 1, \ldots, n$, let $\alpha_j = D_1 H_j(-iv, i\overline{v}, 0)$ be the **anchoring coefficients** of (4.0.1).

Theorem 4.1.3 *Let $k \in \{1, \ldots, n\}$. If $\mathrm{Re}(\alpha_k) \neq 0$, then there exists a wedge-shaped region near $\lambda = 0$ of the form*

$$\mathcal{W}_k = \{(\lambda_1, \ldots, \lambda_n) \in \mathbb{R}^n : |\lambda_j| < W_{k,j}|\lambda_k|, \ W_{k,j} > 0, \text{ for } j \neq k \text{ and } \lambda_k \text{ near } 0\}$$

such that for all $0 \neq \lambda \in \mathcal{W}_k$, (4.0.1) has a unique perturbed rotating wave $\mathcal{S}^k_\lambda$, with center $[\mathcal{S}^k_\lambda]_A$ generically away from ξ_k. Furthermore, $[\mathcal{S}^k_\lambda]_A$ is a center of anchoring when $\lambda_k \,\mathrm{Re}(\alpha_k) < 0$.

Proof: The anchoring coefficient α_k is exactly the coefficient that would appear in the statement of Theorem 4.1.1 had the preceding analysis been done around ξ_k. Theorems 4.1.1 and 4.1.2 can then be applied directly to obtain the desired result. ∎

Clearly, the remark that appears after the proof of Theorem 4.1.2 still holds.

4.2 Epicyclic Drifting

In experiments, spirals are sometimes observed to either be attracted to an inhomogeneity (if the spiral tip is located close enough to it), or repelled by the inhomogeneity (if the spiral tip is located beyond a certain distance from it) [55]. In other circumstances, spirals can be affected by the physical boundary of the experiments, or yet again meander in a non-linear fashion. LeBlanc and Wulff have explained these observations in the case $n = 1$. We give a simple sufficient condition on (4.0.1) under which these phenomena can occur when $n > 1$.

Suppose the manipulations of the previous section have been carried out to system (4.0.1) to yield (4.1.4). Consider the near-identity change of variables

$$z = w + \varepsilon\kappa(w, \overline{w}, t, \varepsilon, \mu) \tag{4.2.1}$$

where $\kappa \in \mathfrak{P}^{2\pi}_t$ is differentiable in all of its variables. Then

$$\dot{z} = \dot{w} + \varepsilon\left(\frac{\partial\kappa}{\partial t} + \frac{\partial\kappa}{\partial w}\dot{w} + \frac{\partial\kappa}{\partial\overline{w}}\dot{\overline{w}}\right).$$

Introducing the equivalent complex conjugate equation, this last system becomes

$$\left[I_2 + \varepsilon \begin{pmatrix} \kappa_w & \kappa_{\overline{w}} \\ \overline{\kappa}_w & \overline{\kappa}_{\overline{w}} \end{pmatrix}\right] \begin{pmatrix} \dot{w} \\ \dot{\overline{w}} \end{pmatrix} = \begin{pmatrix} \dot{z} \\ \dot{\overline{z}} \end{pmatrix} - \varepsilon \begin{pmatrix} \kappa_t \\ \overline{\kappa}_t \end{pmatrix}, \tag{4.2.2}$$

where κ_w, $\kappa_{\overline{w}}$, κ_t, $\overline{\kappa}_w$, $\overline{\kappa}_{\overline{w}}$, $\overline{\kappa}_t$ are used to denote the partial derivatives of κ and $\overline{\kappa}$. Set

$$\mathcal{I} = I_2 + \varepsilon \begin{pmatrix} \kappa_w & \kappa_{\overline{w}} \\ \overline{\kappa}_w & \overline{\kappa}_{\overline{w}} \end{pmatrix}.$$

Combining (4.2.2) with (4.1.4) yields

$$\begin{pmatrix} \dot{w} \\ \dot{\overline{w}} \end{pmatrix} = \varepsilon \mathcal{I}^{-1} \begin{pmatrix} e^{it} K\left((w+\varepsilon\kappa)e^{-it}, (\overline{w}+\varepsilon\overline{\kappa})e^{it}, t, \varepsilon, \mu\right) - \kappa_t \\ e^{-it}\overline{K}\left((w+\varepsilon\kappa)e^{-it}, (\overline{w}+\varepsilon\overline{\kappa})e^{it}, t, \varepsilon, \mu\right) - \overline{\kappa}_t \end{pmatrix} \tag{4.2.3}$$

By Taylor's Theorem, there are appropriate continuous bounded functions A_1, A_2 and $A_3 \in \mathfrak{P}_t^{2\pi}$ satisfying

$$e^{it}K\left((w+\varepsilon\kappa)e^{-it}, (\overline{w}+\varepsilon\overline{\kappa})e^{it}, t, \varepsilon, \mu\right) = e^{it}K\left(we^{-it}, \overline{w}e^{it}, t, 0, \mu\right) + \varepsilon A_1(w, \overline{w}, t, \varepsilon, \mu)$$
$$\kappa_t(w, \overline{w}, t, \varepsilon, \mu) = \kappa_t(w, \overline{w}, t, 0, \mu) + \varepsilon A_2(w, \overline{w}, t, \varepsilon, \mu)$$

and

$$\mathcal{I}^{-1} = \begin{pmatrix} 1-\varepsilon\kappa_w^0 & -\varepsilon\kappa_{\overline{w}}^0 \\ -\varepsilon\overline{\kappa}_w^0 & 1-\varepsilon\overline{\kappa}_{\overline{w}}^0 \end{pmatrix} + \varepsilon^2 A_3(w, \overline{w}, t, \varepsilon, \mu),$$

where

$$\kappa_w^0 = \kappa_w(w, \overline{w}, t, 0, \mu) \quad \text{and} \quad \kappa_{\overline{w}}^0 = \kappa_{\overline{w}}(w, \overline{w}, t, 0, \mu).$$

With these, (4.2.3) rewrites (upon dropping the equivalent complex conjugate equation) as

$$\dot{w} = \varepsilon\left(e^{it}K(we^{-it}, \overline{w}e^{it}, t, 0, \mu) - \kappa_t(w, \overline{w}, t, 0, \mu)\right) + \varepsilon^2\mathcal{H}(w, \overline{w}, t, \varepsilon, \mu), \tag{4.2.4}$$

where $\mathcal{H} \in \mathfrak{P}_t^{2\pi}$ is bounded and continuous in all its variables. Denote the average value of $e^{it}K(we^{-it}, \overline{w}e^{it}, t, 0, \mu)$ by

$$M^1(w, \overline{w}, \mu) = \frac{1}{2\pi}\int_0^{2\pi} e^{it}K(we^{-it}, \overline{w}e^{it}, t, 0, \mu)\, dt. \tag{4.2.5}$$

Then

$$e^{it}K(we^{-it}, \overline{w}e^{it}, t, 0, \mu) = M^1(w, \overline{w}, \mu) + F(w, \overline{w}, t, \mu),$$

where $F \in \mathfrak{P}_t^{2\pi}$ is uniformly continuous and

$$\int_0^{2\pi} F(w, \overline{w}, t, \mu)\, dt = 0. \tag{4.2.6}$$

Let κ be an antiderivative of F with respect to t. Then $\kappa \in \mathfrak{P}_t^{2\pi}$ by (4.2.6) and

$$F(w, \overline{w}, t, \mu) - \kappa_t(w, \overline{w}, t, 0, \mu) = 0.$$

With such a κ, (4.2.4) simplifies to

$$\dot{w} = \varepsilon M^1(w, \overline{w}, \mu) + \varepsilon^2 \mathcal{H}(w, \overline{w}, t, \varepsilon, \mu). \tag{4.2.7}$$

As $M^1(w, \overline{w}, 0)$ is $\mathbb{S}^1-$equivariant (see p. 64 for details), there exists a continuous function $L_1 : \mathbb{R} \to \mathbb{C}$ such that $M^1(w, \overline{w}, 0) = wL_1(w\overline{w})$ (see [33], p. 360 for details).

By Taylor's Theorem, there are appropriate continuous bounded functions M_j, for $j = 2, \ldots, n$, such that

$$M^1(w, \overline{w}, \mu) = M^1(w, \overline{w}, 0) + \sum_{j=2}^{n} \mu_j M_j(w, \overline{w}, \mu)$$

and so (4.2.7) becomes

$$\dot{w} = \varepsilon w L_1(w\overline{w}) + \varepsilon W(w, \overline{w}, t, \varepsilon, \mu), \tag{4.2.8}$$

where

$$W(w, \overline{w}, t, \varepsilon, \mu) = \sum_{j=2}^{n} \mu_j M_j(w, \overline{w}, \mu) + \varepsilon \mathcal{H}(w, \overline{w}, t, \varepsilon, \mu). \tag{4.2.9}$$

Differentiating the polar coordinates $w = \rho e^{-i(\psi - t)}$ yields

$$\begin{aligned} \dot{\rho} &= \operatorname{Re}\left[\dot{w} e^{i(\psi - t)}\right] \\ \dot{\psi} &= 1 - \frac{1}{\rho} \operatorname{Im}\left[\dot{w} e^{i(\psi - t)}\right]. \end{aligned}$$

But

$$\begin{aligned} \dot{w} e^{i(\psi - t)} &= \left(\varepsilon w L_1(w\overline{w}) + \varepsilon W(w, \overline{w}, t, \varepsilon, \mu)\right) e^{i(\psi - t)} \\ &= \left(\varepsilon \rho e^{-i(\psi - t)} L_1(\rho^2) + \varepsilon W(\rho e^{-i(\psi - t)}, \rho e^{i(\psi - t)}, t, \varepsilon, \mu)\right) e^{i(\psi - t)} \\ &= \varepsilon \rho L_1(\rho^2) + \varepsilon e^{i(\psi - t)} W(\rho e^{-i(\psi - t)}, \rho e^{i(\psi - t)}, t, \varepsilon, \mu) \end{aligned}$$

and so

$$\begin{aligned} \dot{\rho} &= \varepsilon R_0^1(\rho) + \varepsilon R(t, \psi, \rho, \varepsilon, \mu) \\ \dot{\psi} &= 1 + \varepsilon \Psi_0(\rho) + \varepsilon \Psi(t, \psi, \rho, \varepsilon, \mu), \end{aligned} \tag{4.2.10}$$

where $R_0^1(\rho) = \rho \operatorname{Re}[L_1(\rho^2)]$, $\Psi_0(\rho) = -\operatorname{Im}[L_1(\rho^2)]$ and

$$\begin{aligned} R(t, \psi, \rho, \varepsilon, \mu) &= \operatorname{Re}\left[e^{i(\psi - t)} W(\rho e^{-i(\psi - t)}, \rho e^{i(\psi - t)}, t, \varepsilon, \mu)\right] \\ \Psi(t, \psi, \rho, \varepsilon, \mu) &= -\frac{1}{\rho} \operatorname{Im}\left[e^{i(\psi - t)} W(\rho e^{-i(\psi - t)}, \rho e^{i(\psi - t)}, t, \varepsilon, \mu)\right]. \end{aligned} \tag{4.2.11}$$

Note that $R, \Psi \in \mathfrak{P}_t^{2\pi} \cap \mathfrak{P}_\psi^{2\pi}$ and that Ψ is not defined at $\rho = 0$.

We now give sufficient conditions for the existence of an invariant torus in (4.2.10).

Theorem 4.2.1 *Assume that R and Ψ, as defined in* (4.2.11), *are C^1 on intervals away from $\rho = 0$ and that the averaged equation*

$$\dot{\rho} = \varepsilon R_0^1(\rho) \tag{4.2.12}$$

has an equilibrium $\rho_1 > 0$ with $D_\rho R_0^1(\rho_1) = \gamma_1 \neq 0$. If the parameters are small enough to satisfy the conditions outlined in the proof below, then (4.2.10) *has an invariant torus $\hat{\mathcal{E}}_{\varepsilon,\mu}$, whose stability is exactly determined by the sign of $\varepsilon\gamma_1$.*

Proof: By the Implicit Function Theorem, there is a neighbourhood

$$U = (-\varepsilon_*, \varepsilon_*) \times \prod_{j=2}^{n} (-\mu_{j,*}, \mu_{j,*})$$

in parameter space and a continuous function $\rho : U \to \mathbb{R}^+$ such that $\rho(0,0) = \rho_1$,

$$\varepsilon R_0^1(\rho(\varepsilon, \mu)) \equiv 0 \quad \text{and} \quad D_\rho R_0^1(\rho(\varepsilon, \mu)) = \gamma_{\varepsilon,\mu} \neq 0,$$

where $\gamma_{\varepsilon,\mu}\gamma_1 > 0$ for all $(\varepsilon, \mu) \in U$, *i.e.*, the stability of the equilibria $\rho(\varepsilon, \mu)$ is the same as that of ρ_1 for all $(\varepsilon, \mu) \in U$. Due to the form of (4.2.12), we see that $\rho(\varepsilon, \mu) \equiv \rho_1$ and $\gamma_{\varepsilon,\mu} \equiv 1$.

When $\varepsilon = 0$, the phase space of (4.2.10) is foliated by invariant tori and so, from now on, we will assume that $\varepsilon \neq 0$. Consider the change of variables $\rho = \rho_1 + x$ in (4.2.10). Differentiating the new coordinates, we get $\dot{x} = \dot{\rho}$ and the equivalent system

$$\begin{aligned} \dot{x} &= \varepsilon R_0^1(\rho_1 + x) + \varepsilon R(t, \psi, \rho_1 + x, \varepsilon, \mu) \\ \dot{\psi} &= 1 + \varepsilon \Psi_0(\rho_1 + x) + \varepsilon \Psi(t, \psi, \rho_1 + x, \varepsilon, \mu). \end{aligned}$$

By Taylor's Theorem, there are continuously differentiable functions B_1 and B_2 such that

$$\begin{aligned} R_0^1(\rho_1 + x) &= R_0^1(\rho_1) + D_x R_0^1(\rho_1)x + B_1(x)x^2 \\ \Psi_0(\rho_1 + x) &= \Psi_0(\rho_1) + B_2(x)x. \end{aligned}$$

Since $R_0^1(\rho_1) \equiv 0$ and $D_x R_0^1(\rho_1) = \gamma_{\varepsilon,\mu}$, we obtain the new system

$$\begin{aligned} \dot{x} &= \varepsilon\gamma_1 x + \varepsilon\Lambda(t, \psi, x, \varepsilon, \mu) \\ \dot{\psi} &= d(\varepsilon) + \Theta(t, \psi, x, \varepsilon, \mu), \end{aligned} \tag{4.2.13}$$

where

$$\begin{aligned} \Lambda(t, \psi, x, \varepsilon, \mu) &= B_1(x)x^2 + R(t, \psi, \rho_1 + x, \varepsilon, \mu) \\ \Theta(t, \psi, x, \varepsilon, \mu) &= \varepsilon B_2(x)x + \varepsilon\Psi(t, \psi, \rho_1 + x, \varepsilon, \mu) \\ d(\varepsilon) &= 1 + \varepsilon\Psi_0(\rho_1) \end{aligned}$$

are at least C^1 by hypothesis.

Let $U^+ = \{\varsigma \in U : \varsigma_i > 0 \text{ for all } i = 1, \ldots, n\}$ and $(\varepsilon_0, \mu_0) \in U^+$. Define

$$S_0 = [-\varepsilon_0, \varepsilon_0] \times \prod_{j=2}^{n} [-\mu_{0,j}, \mu_{0,j}].$$

Set $\sigma_0 = \frac{1}{2}\rho_1 > 0$. If $x \geq -\sigma_0$, then

$$\rho = \rho_1 + x \geq \rho_1 - \sigma_0 \geq \tfrac{1}{2}\rho_1.$$

In that case, Θ and Λ are continuously differentiable, as R and Ψ are continuously differentiable in ρ on $[\frac{1}{2}\rho_1, \infty)$. Note further that $\Theta, \Lambda \in \mathfrak{P}_t^{2\pi} \cap \mathfrak{P}_\psi^{2\pi}$.

Set $\Sigma_0 = \mathbb{R} \times \mathbb{R} \times \{0\} \times S_0$, and $\Sigma_\sigma = \mathbb{R} \times \mathbb{R} \times [-\sigma, \sigma] \times S_0$. Then

1. Θ and Λ are bounded by a function $\Xi(\varepsilon, \mu) = O(\varepsilon, \mu_2, \ldots, \mu_n)$ over Σ_0 (see p. 64 for details), and

2. for all $0 \leq \sigma \leq \sigma_0$, Θ and Λ are Lipschitz in Hale's sense (with Lipschitz constants $\theta(\varepsilon, \mu, \delta) = O(\varepsilon, \mu_2, \ldots, \mu_n, \delta)$ and $\lambda(\varepsilon, \mu, \delta) = O(\varepsilon, \mu_2, \ldots, \mu_n, \delta)$, respectively) over Σ_σ (see p. 66 for details).

Accordingly, Theorem 2.3.1 can be applied to show there is a neighbourhood $S_1 \subseteq S_0$ of the origin in parameter space for which (4.2.10) (since it is equivalent to (4.2.13)) has an

invariant torus $\hat{\mathcal{T}}_{\varepsilon,\mu}$ when $(\varepsilon,\mu) \in S_1$. Furthermore, the stability of $\hat{\mathcal{T}}_{\varepsilon,\mu}$ is the same as that of the hyperbolic equilibrium ρ_1, which is given by $\varepsilon\gamma_1$. ∎

The invariant torus $\hat{\mathcal{T}}_{\varepsilon,\mu}$ can be parameterized by a relation of the form $x = \Upsilon_{\varepsilon,\mu}(\theta_1,\theta_2)$, where $\theta_1,\theta_2 \in \mathbb{S}^1$. Let

$$\langle \hat{\mathcal{T}}_{\varepsilon,\mu} \rangle = \frac{1}{4\pi^2}\int_0^{2\pi}\int_0^{2\pi} \Upsilon_{\varepsilon,\mu}(\theta_1,\theta_2)\, d\theta_1 d\theta_2 \tag{4.2.14}$$

be the **center** of $\hat{\mathcal{T}}_{\varepsilon,\mu}$. After applying the changes of variables of this section, $\hat{\mathcal{T}}_{\varepsilon,\mu}$ becomes an invariant set $\hat{\mathcal{E}}_{\varepsilon,\mu}$ for (4.1.4), in which all solutions are epicycles when projected upon the $z-$plane. Such a set is called an **epicycle manifold**.

By analogy with (4.1.1), define the average value

$$[\hat{\mathcal{E}}_{\varepsilon,\mu}]_{\mathrm{D}} = \frac{1}{4\pi^2}\int_0^{2\pi}\int_0^{2\pi} \Big(\big(\rho_1 + \langle \hat{\mathcal{T}}_{\varepsilon,\mu}\rangle\big) e^{-i(\psi - t)} + \varepsilon\kappa\Big(\big(\rho_1 + \langle \hat{\mathcal{T}}_{\varepsilon,\mu}\rangle\big)e^{-i(\psi-t)}, \text{c.c.}, t, \varepsilon, \mu\Big)\Big)\, d\psi dt. \tag{4.2.15}$$

If $\hat{\mathcal{T}}_{\varepsilon,\mu}$ is stable (in the sense of Section 2.3), we shall say that $[\hat{\mathcal{E}}_{\varepsilon,\mu}]_{\mathrm{D}}$ is the **center of drifting** of $\hat{\mathcal{E}}_{\varepsilon,\mu}$.

Theorem 4.2.2 *Suppose the hypotheses of Theorem* 4.2.1 *are satisfied. Then there exists a wedge-shaped region near* $\lambda = 0$ *of the form*

$$\mathcal{V}_1 = \{(\lambda_1,\ldots,\lambda_n) \in \mathbb{R}^n \,:\, |\lambda_j| < V_{1,j}|\lambda_1|,\ V_{1,j} > 0, \text{ for } j \neq 1 \text{ and } \lambda_1 \text{ near } 0\}$$

such that for all $0 \neq \lambda \in \mathcal{V}_1$, (4.0.1) *has an epicycle manifold* $\mathcal{E}^1_\lambda$, *with* $[\mathcal{E}^1_\lambda]_{\mathrm{D}}$ *near, but generically not at,* ξ_1. *Furthermore,* $[\mathcal{E}^1_\lambda]_{\mathrm{D}}$ *is a center of drifting when* $\lambda_1\gamma_1 < 0$.

Proof: According to Theorem 4.2.1, there are constants $\varepsilon_1, \mu_{1,2}, \ldots, \mu_{1,n} > 0$ and a neighbourhood

$$S_1 = [-\varepsilon_1,\varepsilon_1] \times \prod_{j=2}^{n} [-\mu_{1,j},\mu_{1,j}]$$

such that (4.2.10) has an integral manifold $\hat{\mathcal{E}}_{\varepsilon,\mu}$ whenever $(\varepsilon,\mu) \in S_1$.

For $j \neq 1$, set $\lambda_1 = \varepsilon \neq 0$, $\lambda_j = \mu_j\varepsilon$ and $V_{1,j} = \mu_{1,j}$. Then $\lambda \in \mathcal{V}_1$ as

$$|\lambda_j| \leq |\mu_j| \cdot |\lambda_1| \leq V_{1,j}|\lambda_1| \quad \text{for } j \neq 1,$$

and (4.0.1) has an integral manifold $\mathcal{E}^1_\lambda = \xi_1 - ie^{it}v + \hat{\mathcal{E}}_{\varepsilon,\mu}$. Furthermore, $[\mathcal{E}^1_\lambda]_D = \xi_1 + O(\lambda_1)$ (see p. 67 for details), and so $[\mathcal{E}^1_\lambda]_D \neq \xi_1$ for a generic $0 \neq \lambda \in \mathcal{V}_1$. The conclusion on the stability of $\mathcal{E}^1_\lambda$ then follows directly from Theorem 4.2.1. ∎

These isolated epicycle manifolds need not in general be unique for a given $\lambda \in \mathcal{V}_1$ as $R^1_0(\rho) = 0$ may have any number of hyperbolic solutions.

Remark: When the parameter values stray outside of $\mathcal{V}_1$, all that can generically be said is that the center of drifting of the epicycle manifolds in (4.0.1) is near ξ_1. Richer dynamics and interactions with rotating waves can also take place; in Section 7.2.3, we will provide an example in which the epicycle manifold collapses at a saddle-node bifurcation of rotating waves.

The preceding results have been achieved by considering (4.0.1) under a co-rotating frame of reference around ξ_1. Of course, corresponding results must also be achieved, in exactly the same manner, when the viewpoint shifts to another ξ_k.

For $j = 1, \ldots, n$, define the average functions

$$M^j(w, \overline{w}) = \frac{1}{2\pi} \int_0^{2\pi} e^{it} \hat{H}_j(we^{-it}, \overline{w}e^{it}, 0, 0)\, dt;$$

each M^j is $\mathbb{S}^1-$equivariant (see p. 64 for details) and so, as before, there exist continuous functions $L_j : \mathbb{R} \to \mathbb{C}$ such that $M^j(w, \overline{w}) = wL_j(w\overline{w})$. Let

$$R^j_0(\rho) = \rho \operatorname{Re}\left[L_j(\rho^2)\right]$$

be the **epicycle functions** of (4.0.1).

Theorem 4.2.3 *Let $k \in \{1, \ldots, n\}$. If $\rho_k > 0$ is such that*

$$R^k_0(\rho_k) = 0 \quad \textit{and} \quad D_\rho R^k_0(\rho_k) = \gamma_k \neq 0,$$

then there exists a wedge-shaped region near $\lambda = 0$ of the form

$$\mathcal{V}_k = \{(\lambda_1, \ldots, \lambda_n) \in \mathbb{R}^n \,:\, |\lambda_j| < V_{k,j}|\lambda_k|,\ V_{k,j} > 0, \text{ for } j \neq k \text{ and } \lambda_k \text{ near } 0\}$$

such that for all $0 \neq \lambda \in \mathcal{V}_k$, (4.0.1) has an epicycle manifold $\mathcal{E}^k_\lambda$, with $[\mathcal{E}^k_\lambda]_D$ near, but generically not at, ξ_k. Furthermore, $[\mathcal{E}^k_\lambda]_D$ is a center of drifting when $\lambda_k\gamma_k < 0$.

Proof: The function R_0^k is exactly the function that would appear in (4.2.12) had the preceding analysis been done around ξ_k. Theorems 4.2.1 and 4.2.2 can then be applied directly to obtain the desired result. ∎

Clearly, the remarks appearing after the proof of Theorem 4.2.2 still hold. There is one last statement to be made concerning epicycle manifolds: Theorem 4.2.3 only gives sufficient conditions for their existence in (4.0.1). In Section 7.2.3, we will provide an example showing that they are not, in fact, necessary.

4.3 Higher Codimension Phenomena

In this section, we discuss how the center bundle equations (4.0.1) can give rise to hysteresis and chaos, which are common occurrences in physiology and cardiology [9].

Suppose the manipulations of Section 4.1 have been carried out to (4.0.1) to yield

$$\dot{z} = e^{it}K^*(ze^{-it}, \overline{z}e^{it}, t, \lambda), \tag{4.3.1}$$

where

$$K^*(w, \overline{w}, t, \lambda) = \sum_{j=1}^{n} \lambda_j H_j(w - \zeta_j e^{-it} - iv, \overline{w} - \overline{\zeta}_j e^{it} + i\overline{v}, \lambda).$$

Note that $K^* \in \mathfrak{P}_t^{2\pi}$ and $\zeta_1 = 0$. The time-2π map of (4.3.1) near $(z, \lambda) = (0, 0)$ is

$$\Pi(z, \lambda) = z + \sum_{j=1}^{n} \lambda_j \left[E_j + A_j z + B_j \overline{z}\right] + O\left(|\lambda| \cdot |z|^2\right) + O\left(|\lambda|^2\right), \tag{4.3.2}$$

where

$$\begin{aligned} A_j &= \int_0^{2\pi} D_1 H_j(-\zeta_j e^{-is} - iv, -\overline{\zeta}_j e^{is} + i\overline{v}, 0)\, ds \\ B_j &= \int_0^{2\pi} e^{2is} D_2 H_j(-\zeta_j e^{-is} - iv, -\overline{\zeta}_j e^{is} + i\overline{v}, 0)\, ds \\ E_j &= \int_0^{2\pi} e^{is} H_j(-\zeta_j e^{-is} - iv, -\overline{\zeta}_j e^{is} + i\overline{v}, 0)\, ds \end{aligned} \tag{4.3.3}$$

for $j = 1, \ldots, n$, with $B_1 = E_1 = 0$ (see p. 67 for details).

Write $z = x + iy$ and set $r = (x, y)^\top$. In these cartesian coordinates, the Poincaré map Π near $(r, \lambda) = (0, 0)$ is given by

$$\Pi^*(r, \lambda) = r + \mathsf{C}(\lambda)r + \mathsf{E} \cdot \lambda^\top + O\left(|\lambda| \cdot |r|^2\right) + O\left(|\lambda|^2\right), \tag{4.3.4}$$

where

$$\mathsf{C}(\lambda) = \begin{pmatrix} \operatorname{Re}\left(\sum_{j=1}^{n} \lambda_j (A_j + B_j)\right) & -\operatorname{Im}\left(\sum_{j=1}^{n} \lambda_j (A_j - B_j)\right) \\ \operatorname{Im}\left(\sum_{j=1}^{n} \lambda_j (A_j + B_j)\right) & \operatorname{Re}\left(\sum_{j=1}^{n} \lambda_j (A_j - B_j)\right) \end{pmatrix}$$

and

$$\mathsf{E} = \begin{pmatrix} \operatorname{Re}(E_1) & \cdots & \operatorname{Re}(E_n) \\ \operatorname{Im}(E_1) & \cdots & \operatorname{Im}(E_n) \end{pmatrix}.$$

For all $j = 1, \ldots, n$, let $\lambda_j = \mu\varepsilon_j$, where $\|(\varepsilon_1, \ldots, \varepsilon_n)\|^2 = 1$. Write $\varepsilon = (\varepsilon_1, \ldots, \varepsilon_n)$ and define $\tilde{\Pi} : \mathbb{R}^2 \times \mathbb{R} \times \mathbb{R}^n \to \mathbb{R}^2$ by $\tilde{\Pi}(r, \mu, \varepsilon) = \Pi^*(r, \mu\varepsilon)$. Then

$$\tilde{\Pi}(r, \mu, \varepsilon) = r + \mu\left[\mathsf{C}(\varepsilon)r + \mathsf{E} \cdot \varepsilon^\top + O\left(\varepsilon|r|^2\right) + O\left(\mu\varepsilon_1^2, \ldots, \mu\varepsilon_n^2\right)\right]. \tag{4.3.5}$$

Let $n \geq 4$. Define the maps $\mathsf{P}_1 : \mathbb{R}^n \to \mathbb{R}^4$ and $\mathsf{P}_2 : \mathbb{R}^n \to \mathbb{R}^5$ by

$$\mathsf{P}_1(\varepsilon) = \begin{pmatrix} \mathsf{E} \cdot \varepsilon^\top \\ \det\left(\mathsf{C}(\varepsilon)\right) \\ \|\varepsilon\|^2 - 1 \end{pmatrix} \quad \text{and} \quad \mathsf{P}_2(\varepsilon) = \begin{pmatrix} \mathsf{E} \cdot \varepsilon^\top \\ \det\left(\mathsf{C}(\varepsilon)\right) \\ \operatorname{tr}\left(\mathsf{C}(\varepsilon)\right) \\ \|\varepsilon\|^2 - 1 \end{pmatrix}. \tag{4.3.6}$$

Let $\mathsf{A} = \begin{pmatrix} \operatorname{Re}(A_1) & \cdots & \operatorname{Re}(A_n) \end{pmatrix}$ and define $\mathsf{Q} \in \mathbb{M}_n(\mathbb{R})$ by

$$\mathsf{Q}_{jk} = \left(\operatorname{Re}(A_j)\operatorname{Re}(A_k) + \operatorname{Im}(A_j)\operatorname{Im}(A_k)\right) - \left(\operatorname{Re}(B_j)\operatorname{Re}(B_k) + \operatorname{Im}(B_j)\operatorname{Im}(B_k)\right)$$

for all $j, k \in \{1, \ldots, n\}$.

The zero-level sets of the components of P_1 and P_2 can be expressed in terms of kernels and quadric hypersurfaces:

$$\begin{aligned} \mathsf{E}\varepsilon^\top = 0 &\iff \varepsilon^\top \in \ker \mathsf{E} \\ \operatorname{tr}\left(\mathsf{C}(\varepsilon)\right) = 0 &\iff \varepsilon^\top \in \ker \mathsf{A} \\ \det\left(\mathsf{C}(\varepsilon)\right) = 0 &\iff \varepsilon\mathsf{Q}\varepsilon^\top = 0 \\ \|\varepsilon\|^2 - 1 = 0 &\iff \varepsilon\varepsilon^\top = 1. \end{aligned} \tag{4.3.7}$$

Let $\mathcal{Z}_{\mathsf{E}}, \mathcal{Z}_{\mathrm{tr}}, \mathcal{Z}_{\det}, \mathcal{Z}_1, \mathcal{Z}_2 \subset \mathbb{C}^{3n-2}$ be the maximal subsets satisfying respectively

- $\forall (A_1, A_2, B_2, E_2, \ldots, A_n, B_n, E_n) \in \mathcal{Z}_{\mathsf{E}}$, $\mathrm{rank}(\mathsf{E}) = 2$ and $\dim(\ker(\mathsf{E})) = n-2$;
- $\forall (A_1, A_2, B_2, E_2, \ldots, A_n, B_n, E_n) \in \mathcal{Z}_{\mathrm{tr}}$, $\mathrm{rank}(\mathsf{A}) = 1$ and $\dim(\ker(\mathsf{A})) = n-1$,
- $\forall (A_1, A_2, B_2, E_2, \ldots, A_n, B_n, E_n) \in \mathcal{Z}_{\det}$, the quadric hypersurface $\varepsilon \mathsf{Q} \varepsilon^{\top} = 0$ has dimension $n-1$ and it intersects the unit sphere transversally in $\mathbb{R}^n$;
- $\forall (A_1, A_2, B_2, E_2, \ldots, A_n, B_n, E_n) \in \mathcal{Z}_j$, the mapping P_j is t-regular, for $j = 1, 2$ (see Chapter 2, p. 29 for definition).

Whenever $n \geq 2$, all of these sets are non-empty and open. Furthermore, $\mathcal{Z}_{\mathsf{E}}$, $\mathcal{Z}_{\mathrm{tr}}$ and $\mathcal{Z}_j$, $j = 1, 2$, are dense in $\mathbb{C}^{3n-2}$ (see [25], Theorem 10.3.2, pp.83–84).

Proposition 4.3.1 *Let $n \geq 4$. There is a non-empty open subset $\mathcal{Z}_{\mathrm{SN}} \subset \mathbb{C}^{3n-2}$ such that for any $(A_1, A_2, B_2, E_2, \ldots, A_n, B_n, E_n) \in \mathcal{Z}_{\mathrm{SN}}$, there is a compact $n-4$ dimensional manifold $\mathcal{M}_{\mathrm{SN}} \subset \mathbb{R}^n$ consisting entirely of regular solutions of $P_1 = 0$.*

Proof: Set $\mathcal{Z} = \mathcal{Z}_{\mathsf{E}} \cap \mathcal{Z}_1 \cap \mathcal{Z}_{\det} \neq \varnothing$ and let $\mathcal{Z}_{\mathrm{SN}}$ be the maximal open subset of $\mathcal{Z}$ in which $\mathsf{P}_1 = 0$ has a solution. Since $\mathsf{P}_1 = 0$ is undetermined or exactly determined when $n \geq 4$, $\mathcal{Z}_{\mathrm{SN}} \neq \varnothing$.

Let $(A_1, A_2, B_2, E_2, \ldots, A_n, B_n, E_n) \in \mathcal{Z}_{\mathrm{SN}}$. Then $\mathsf{P}_1 = 0$ has at least one solution $\varepsilon^* \in \mathbb{R}^n$; in particular $\mathsf{P}_1^{-1}(\{0\}) \neq \varnothing$ is closed in $\mathbb{R}^n$ as P_1 is smooth. Since P_1 is t–regular at the origin, the pre-image $\mathcal{M}_{\mathrm{SN}} = \mathsf{P}_1^{-1}(\{0\})$ is a smooth manifold with $\dim(\mathcal{M}_{\mathrm{SN}}) = n-4$. But $\mathcal{M}_{\mathrm{SN}}$ is a closed subset of the unit ball in $\mathbb{R}^n$; it is then compact by the Heine-Borel Theorem. This completes the proof. ∎

Proposition 4.3.2 *Let $n \geq 5$. There is a non-empty open subset $\mathcal{Z}_{\mathrm{BT}} \subset \mathcal{Z}_{\mathrm{SN}}$ such that for any $(A_1, A_2, B_2, E_2, \ldots, A_n, B_n, E_n) \in \mathcal{Z}_{\mathrm{BT}}$, there is a compact $n-5$ dimensional manifold $\mathcal{M}_{\mathrm{BT}} \subset \mathcal{M}_{\mathrm{SN}} \subset \mathbb{R}^n$ consisting entirely of regular solutions of $P_2 = 0$.*

Proof: As in the proof of the previous proposition, $\mathcal{Z} = \mathcal{Z}_{\mathsf{E}} \cap \mathcal{Z}_1 \cap \mathcal{Z}_{\mathrm{tr}} \cap \mathcal{Z}_{\det} \neq \varnothing$ has a maximal open subset $\mathcal{Z}_{\mathrm{BT}} \subset \mathcal{Z}$ in which $\mathsf{P}_2 = 0$ has a solution. Since $\mathsf{P}_2 = 0$ is undetermined or exactly determined when $n \geq 5$, $\mathcal{Z}_{\mathrm{BT}} \neq \varnothing$. As any solution of $\mathsf{P}_2 = 0$ is also a solution of $\mathsf{P}_1 = 0$, $\mathcal{Z}_{\mathrm{BT}} \subset \mathcal{Z}_{\mathrm{SN}}$. The rest of the proof proceeds exactly as in Proposition 4.3.1, with the added property $\mathcal{M}_{\mathrm{BT}} \subset \mathcal{M}_{\mathrm{SN}}$. ∎

We are now in position to state and prove the following results.

Theorem 4.3.3 *Let $n \geq 4$, and $\mathcal{Z}_{\mathrm{SN}}$ and $\mathcal{M}_{\mathrm{SN}}$ be as in Proposition 4.3.1. Then there exists an open neighbourhood U_{SN} of the origin in $\mathbb{R}^2 \times \mathbb{R}$ and a smooth mapping $S_{\mathrm{SN}} : U_{\mathrm{SN}} \times \mathcal{M}_{\mathrm{SN}} \to \mathbb{R}^n$ such that $S_{\mathrm{SN}}((x, y, \mu), \mathcal{M}_{\mathrm{SN}})$ is diffeomorphic to $\mathcal{M}_{\mathrm{SN}}$ for all $(x, y, \mu) \in U_{\mathrm{SN}}$. Then for all λ on the manifold*

$$\widetilde{\mathcal{M}}_{\mathrm{SN}} = \{\mu S_{\mathrm{SN}}((x, y, \mu), \varepsilon) : ((x, y, \mu), \varepsilon) \in U_{\mathrm{SN}} \times \mathcal{M}_{\mathrm{SN}},\ \mu \neq 0\},$$

(4.3.2) *has a non-hyperbolic fixed point near $z = 0$. Generically, this singularity is a saddle-node.*

Proof: Let $\mathsf{F}_1 : \mathbb{R}^2 \times \mathbb{R} \times \mathbb{R}^n \to \mathbb{R}^4$ be the smooth function defined by

$$\mathsf{F}_1(r, \mu, \varepsilon) = \begin{pmatrix} Q(r, \mu, \varepsilon) \\ \det(D_r Q(r, \mu, \varepsilon)) \\ \|\varepsilon\|^2 - 1 \end{pmatrix},$$

where

$$\begin{aligned} Q(r, \mu, \varepsilon) &= \mathsf{C}(\varepsilon) r + \mathsf{E} \cdot \varepsilon^{\top} + O\left(\varepsilon |r|^2\right) + O\left(\mu\varepsilon_1^2, \ldots, \mu\varepsilon_n^2\right) \\ D_r Q(r, \mu, \varepsilon) &= \mathsf{C}(\varepsilon) + O\left(\varepsilon |r|\right) + O\left(\mu\varepsilon_1^2, \ldots, \mu\varepsilon_n^2\right) \end{aligned}$$

are as in (4.3.5). Let $(r_*, \mu_*, \varepsilon_*)$ be a solution of $\mathsf{F}_1 = 0$. Then

$$\tilde{\Pi}(r_*, \mu_*, \varepsilon_*) = r_* + \mu_* Q(r_*, \mu_*, \varepsilon_*) = r_*, \tag{4.3.8}$$

$$D_r \tilde{\Pi}(r_*, \mu_*, \varepsilon_*) = I_2 + \mu_* D_r Q(r_*, \mu_*, \varepsilon_*), \text{ and}$$

$$\det\left(D_r \tilde{\Pi}(r_*, \mu_*, \varepsilon_*) - I_2\right) = \mu_*^2 \det\left(D_r Q(r_*, \mu_*, \varepsilon_*)\right) = 0, \tag{4.3.9}$$

and so $(r_*, \mu_*, \varepsilon_*)$ corresponds to a non-hyperbolic fixed point of (4.3.5), with one of its multipliers equal to 1.

If $\varepsilon_* \in \mathcal{M}_{\mathrm{SN}}$, then $Q(0, 0, \varepsilon_*) = \mathsf{E} \cdot \varepsilon_*^{\top}$ and $D_r Q(0, 0, \varepsilon_*) = \mathsf{C}(\varepsilon_*)$; thus

$$\mathsf{F}_1(0, 0, \varepsilon_*) = \mathsf{P}_1(\varepsilon_*) \quad \text{and} \quad \operatorname{rank}(D_\varepsilon \mathsf{P}_1(\varepsilon_*)) = 4$$

according to proposition 4.3.1. By the Implicit Function Theorem, there is a neighbourhood U_{SN} of the origin in $\mathbb{R}^2 \times \mathbb{R}$ and a smooth mapping $S_{\mathrm{SN}} : U_{\mathrm{SN}} \times \mathcal{M}_{\mathrm{SN}} \to \mathbb{R}^n$ such that $S_{\mathrm{SN}}(0, 0, \varepsilon) = \varepsilon$ and $\mathsf{F}(r, \mu, S_{\mathrm{SN}}(r, \mu, \varepsilon)) \equiv 0$ on $U_{\mathrm{SN}} \times \mathcal{M}_{\mathrm{SN}}$. Furthermore, $S_{\mathrm{SN}}(r, \mu, \mathcal{M}_{\mathrm{SN}})$ is diffeomorphic to $\mathcal{M}_{\mathrm{SN}}$ for all $(r, \mu) \in U_{\mathrm{SN}}$.

Then for all $(A_1, A_2, B_2, E_2, \ldots, A_n, B_n, E_n) \in \mathcal{Z}_{\mathrm{SN}}$ and for all $(r, \mu, \varepsilon) \in U_{\mathrm{SN}} \times \mathcal{M}_{\mathrm{SN}}$ with $\mu \neq 0$, (4.3.2) has a fixed point $z = x + iy$ (where $r = (x, y)^{\mathsf{T}}$) near $z = 0$ for $\lambda = \mu S(r, \mu, \varepsilon)$, with one of its multipliers equal to 1. Generically, this multiplier is simple and the terms of order $O\left(|\lambda| \cdot |r|^2\right)$ in (4.3.2) do not vanish on the eigenspace of the fixed point z associated to the critical multiplier; hence (4.3.2) undergoes a saddle-node bifurcation of fixed points near $z = 0$ for parameter values λ arbitrarily close to the origin (see [32] and chapter 2, p. 25 for details). ∎

The condition $n \geq 4$ is not necessary in order for (4.3.2) to undergo a saddle-node bifurcation of fixed points (see pp. 121 – 124 for an example), however, it is necessary in order for (4.3.2) to undergo a saddle-node bifurcation of fixed points near $z = 0$ for λ *arbitrarily* close to the origin in parameter space.

Theorem 4.3.4 *Let $n \geq 5$, and $\mathcal{Z}_{\mathrm{BT}}$ and $\mathcal{M}_{\mathrm{BT}}$ be as in Proposition* 4.3.2. *Then there exists an open neighbourhood U_{BT} of the origin in $\mathbb{R}^2 \times \mathbb{R}$ and a smooth mapping $S_{\mathrm{BT}} : U_{\mathrm{BT}} \times \mathcal{M}_{\mathrm{BT}} \to \mathbb{R}^n$ such that $S_{\mathrm{BT}}\left((x, y, \mu), \mathcal{M}_{\mathrm{BT}}\right)$ is diffeomorphic to $\mathcal{M}_{\mathrm{BT}}$ for all $(x, y, \mu) \in U_{\mathrm{BT}}$. Then for all λ on the manifold*

$$\widetilde{\mathcal{M}}_{\mathrm{BT}} = \{\mu S_{\mathrm{BT}}((x, y, \mu), \varepsilon) : ((x, y, \mu), \varepsilon) \in U_{\mathrm{BT}} \times \mathcal{M}_{\mathrm{BT}},\ \mu \neq 0\},$$

(4.3.2) *has a non-hyperbolic fixed point near $z = 0$. Generically, this singularity is of Bogdanov-Takens type.*

Proof: Let $\mathsf{F}_2 : \mathbb{R}^2 \times \mathbb{R} \times \mathbb{R}^n \to \mathbb{R}^5$ be the smooth function defined by

$$\mathsf{F}_2(r, \mu, \varepsilon) = \begin{pmatrix} Q(r, \mu, \varepsilon) \\ \det(D_r Q(r, \mu, \varepsilon)) \\ \mathrm{tr}(D_r Q(r, \mu, \varepsilon)) \\ \|\varepsilon\|^2 - 1 \end{pmatrix},$$

where

$$\begin{aligned} Q(r, \mu, \varepsilon) &= \mathsf{C}(\varepsilon) r + \mathsf{E} \cdot \varepsilon^{\mathsf{T}} + O\left(\varepsilon |r|^2\right) + O\left(\mu\varepsilon_1^2, \ldots, \mu\varepsilon_n^2\right) \\ D_r Q(r, \mu, \varepsilon) &= \mathsf{C}(\varepsilon) + O\left(\varepsilon |r|\right) + O\left(\mu\varepsilon_1^2, \ldots, \mu\varepsilon_n^2\right) \end{aligned}$$

are as in (4.3.5).

Let $(r_*, \mu_*, \varepsilon_*)$ be a solution of $\mathsf{F}_2 = 0$. Then

$$\begin{aligned}
\tilde{\Pi}(r_*, \mu_*, \varepsilon_*) &= r_* + \mu_* Q(r_*, \mu_*, \varepsilon_*) = r_*, \\
D_r\tilde{\Pi}(r_*, \mu_*, \varepsilon_*) &= I_2 + \mu_* D_r Q(r_*, \mu_*, \varepsilon_*), \\
\det\left(D_r\tilde{\Pi}(r_*, \mu_*, \varepsilon_*) - I_2\right) &= \mu_*^2 \det\left(D_r Q(r_*, \mu_*, \varepsilon_*)\right) = 0, \text{ and} \\
\operatorname{tr}\left(D_r\tilde{\Pi}(r_*, \mu_*, \varepsilon_*)\right) &= 2 + \mu_*^2 \operatorname{tr}\left(D_r Q(r_*, \mu_*, \varepsilon_*)\right) = 2
\end{aligned}$$

and so $(r_*, \mu_*, \varepsilon_*)$ corresponds to a non-hyperbolic fixed point of (4.3.5), where both multipliers are 1.

If $\varepsilon_* \in \mathcal{M}_{\mathrm{BT}}$, then $Q(0,0,\varepsilon_*) = \mathsf{E} \cdot \varepsilon_*^{\top}$ and $D_r Q(0,0,\varepsilon_*) = \mathsf{C}(\varepsilon_*)$; thus

$$\mathsf{F}_2(0,0,\varepsilon_*) = \mathsf{P}_2(\varepsilon_*) \quad \text{and} \quad \operatorname{rank}(D_\varepsilon \mathsf{P}_2(\varepsilon_*)) = 5$$

according to proposition 4.3.2. The rest of the proof proceeds exactly as in Theorem 4.3.3 (see [32] and Chapter 2, p. 27 for details). ∎

The preceding results have been achieved by considering (4.0.1) under a co-rotating frame of reference around ξ_1. Of course, since the choice for ξ_1 was arbitrary, corresponding results must also be achieved, in exactly the same manner, when the viewpoint shifts to another ξ_k.

For $j = 1, \ldots, n$, let $\mathsf{P}_1^j : \mathbb{R}^n \to \mathbb{R}^4$ and $\mathsf{P}_2^j : \mathbb{R}^n \to \mathbb{R}^5$ be the maps obtained in (4.3.6) by carrying out the manipulations at the start of this section to (4.0.1) around ξ_j, and $\mathcal{Z}_{\mathrm{SN}}^j$, $\mathcal{M}_{\mathrm{SN}}^j$, $\mathcal{Z}_{\mathrm{BT}}^j$ and $\mathcal{M}_{\mathrm{BT}}^j$ be the appropriate sets guaranteed when Propositions 4.3.1 and 4.3.2 are applied to these maps with $n \geq 4$ and $n \geq 5$.

Since fixed points of (4.3.2) correspond to $2\pi-$periodic solutions of (4.0.1), we have the two following results.

Theorem 4.3.5 *Let $n \geq 4$ and $k \in \{1, \ldots, n\}$. There exists an open neighbourhood U_{SN}^k of the origin in $\mathbb{R}^2 \times \mathbb{R}$ and a smooth mapping $S_{\mathrm{SN}}^k : U_{\mathrm{SN}}^k \times \mathcal{M}_{\mathrm{SN}}^k \to \mathbb{R}^n$ such that $S_{\mathrm{SN}}^k\left((x,y,\mu), \mathcal{M}_{\mathrm{SN}}^k\right)$ is diffeomorphic to $\mathcal{M}_{\mathrm{SN}}^k$ for all $(x,y,\mu) \in U_{\mathrm{SN}}^k$. Then for all λ on the manifold*

$$\widetilde{\mathcal{M}}_{\mathrm{SN}}^k = \{\mu S_{\mathrm{SN}}^k((x,y,\mu),\varepsilon) : ((x,y,\mu),\varepsilon) \in U_{\mathrm{SN}}^k \times \mathcal{M}_{\mathrm{SN}}^k,\ \mu \neq 0\},$$

the center bundle equations (4.0.1) *has a non-hyperbolic periodic orbit* $\mathcal{Q}^k_{\mathrm{SN},\lambda}$, *with center* $[\mathcal{Q}^k_{\mathrm{SN},\lambda}]_{\mathrm{A}}$ *near* ξ_k, *around which a saddle-node bifurcation of periodic solutions is organized.*

In physical systems, varying parameters slightly often results in a sudden "jump" to a distinct branch of stable equilibria. This phenomenon is known as **hysteresis**, and it is linked to the collapse of two saddle-node bifurcation at a cusp singularity [47]. Suppose the semi-flow $\Phi_{t,\lambda}$ is generated by a reaction-diffusion system of the form (3.1.1) having a (normally hyperbolic) rotating spiral wave for $\lambda = 0$. If $n \geq 4$ and if the coefficients (4.3.3) lie in $\mathcal{Z}^k_{\mathrm{SN}}$ for some $k \in \{1, \ldots, n\}$, then a saddle-node bifurcation of rotating waves can be observed in (3.1.1); reversing the parameter path may lead to hysteresis of rotating waves.

Theorem 4.3.6 *Let* $n \geq 5$ *and* $k \in \{1, \ldots, n\}$. *There exists an open neighbourhood* U^k_{BT} *of the origin in* $\mathbb{R}^2 \times \mathbb{R}$ *and a smooth mapping* $S^k_{\mathrm{BT}} : U^k_{\mathrm{BT}} \times \mathcal{M}^k_{\mathrm{BT}} \to \mathbb{R}^n$ *such that* $S^k_{\mathrm{BT}}\left((x, y, \mu), \mathcal{M}^k_{\mathrm{BT}}\right)$ *is diffeomorphic to* $\mathcal{M}^k_{\mathrm{BT}}$ *for all* $(x, y, \mu) \in U^k_{\mathrm{BT}}$. *Then for all* λ *on the manifold*

$$\widetilde{\mathcal{M}}^k_{\mathrm{BT}} = \{\mu S^k_{\mathrm{BT}}((x, y, \mu), \varepsilon) : ((x, y, \mu), \varepsilon) \in U^k_{\mathrm{BT}} \times \mathcal{M}^k_{\mathrm{BT}},\ \mu \neq 0\},$$

the center bundle equations (4.0.1) *has a non-hyperbolic periodic orbit* $\mathcal{Q}^k_{\mathrm{BT},\lambda}$, *with center* $[\mathcal{Q}^k_{\mathrm{BT},\lambda}]_{\mathrm{A}}$ *near* ξ_k, *around which a Bogdanov-Takens bifurcation of periodic solutions is organized.*

In the two-dimensional unfolding of the Bogdanov-Takens singularity (or strong 1:1 resonance) for a planar map, there is a thin cusp-shaped region where the map has a homoclinic tangle; consequently, it also entertains chaotic dynamics (see [47, pp. 364 – 368] and Chapter 2, p. 27 for details). Suppose the semi-flow $\Phi_{t,\lambda}$ is generated by a reaction-diffusion system of the form (3.1.1) having a (normally hyperbolic) rotating spiral wave for $\lambda = 0$. If $n \geq 5$ and if the coefficients (4.3.3) lie in $\mathcal{Z}^k_{\mathrm{BT}}$ for some $k \in \{1, \ldots, n\}$, then, Theorem 4.3.6 implies that the spiral tip will meander chaotically for small amplitudes of the inhomogeneities lying in some non-zero measure set.

4.4 Appendix: Technical Details

Technical Result 5 The Poincaré map P of (4.1.4) near $z = 0$, $(\varepsilon, \mu) = (0,0)$ is given by (4.1.5).

Proof: Let $z_{\varepsilon,\mu}(t; z_0)$ denote the solution of (4.1.4) through z_0 at time t. Denote the right-hand side of (4.1.4) by $F(z, \overline{z}, t, \varepsilon, \mu)$. Then $z_{\varepsilon,\mu}$ must satisfy the integral equation

$$z_{\varepsilon,\mu}(t; z_0) = z_0 + \int_0^t F(z_{\varepsilon,\mu}(s; z_0), \text{c. c.}, s, \varepsilon, \mu)\, ds.$$

The Poincaré map P of (4.1.4) is the time-2π map, so

$$P(z_0, \varepsilon, \mu) = z_{\varepsilon,\mu}(2\pi; z_0).$$

A Taylor expansion of P around $(\varepsilon, \mu) = (0,0)$ yields

$$P(z_0, \varepsilon, \mu) = z_{0,0}(2\pi; z_0) + \varepsilon \frac{\partial}{\partial \varepsilon} z_{0,0}(2\pi; z_0) + \sum_{j=2}^{n} \mu_j \frac{\partial}{\partial \mu_j} z_{0,0}(2\pi; z_0) + O(\varepsilon^2, \varepsilon|\mu|, |\mu|^2),$$

where $O(\varepsilon^2, \varepsilon|\mu|, |\mu|^2)$ stands for $O(\varepsilon^2, \varepsilon\mu_2, \ldots, \varepsilon\mu_n, \mu_2^2, \mu_2\mu_3, \ldots, \mu_n^2)$.

Let $m_2, \ldots, m_\nu \in \mathbb{N}$ such that $|m| = m_2 + \cdots + m_\nu = \nu$. Now, $F(z, \overline{z}, s, 0, 0) \equiv 0$ and

$$\frac{\partial^\nu}{\partial \mu_2^{m_2} \cdots \partial \mu_n^{m_\nu}} F(z_{0,0}(s; z_0), \text{c. c.}, s, 0, 0) \equiv 0.$$

Indeed, since

$$F\big(z_{\varepsilon,\mu}(s; z_0), \text{c. c.}, s, \varepsilon, \mu\big) = \varepsilon e^{is} K\big(z_{\varepsilon,\mu}(s; z_0)e^{-is}, \text{c. c.}, s, \varepsilon, \mu\big),$$

then

$$\frac{\partial^\nu}{\partial \mu^m} F\big(z_{\varepsilon,\mu}(s; z_0), \text{c. c.}, s, \varepsilon, \mu\big) = \varepsilon e^{is} \frac{\partial^\nu}{\partial \mu^m} K\big(z_{\varepsilon,\mu}(s; z_0)e^{-is}, \text{c. c.}, s, \varepsilon, \mu\big)$$

and

$$\frac{\partial}{\partial \varepsilon} F\big(z_{\varepsilon,\mu}(s; z_0), \text{c. c.}, s, \varepsilon, \mu\big) = e^{is} K\big(z_{\varepsilon,\mu}(s; z_0)e^{-is}, \text{c. c.}, s, \varepsilon, \mu\big) + \varepsilon e^{is} \frac{\partial}{\partial \varepsilon} K\big(z_{\varepsilon,\mu}(s; z_0)e^{-is}, \text{c. c.}, s, \varepsilon, \mu\big).$$

In particular, when $\varepsilon = 0$ and $\mu = 0$, then $\frac{\partial^\nu}{\partial \mu_2^{m_2} \cdots \partial \mu_n^{m_\nu}} F\big(z_0, \overline{z_0}, s, 0, 0\big) \equiv 0$ and

$$\frac{\partial}{\partial \varepsilon} F\big(z_0, \overline{z_0}, s, 0, 0\big) = e^{is} K\big(z_0 e^{-is}, \overline{z}_0 e^{is}, s, 0, 0\big) = e^{is} \hat{H}_1(z_0 e^{-is}, \overline{z}_0 e^{is}, 0, 0).$$

Thus

$$z_{0,0}(t; z_0) = z_0 + \int_0^t F(z_{0,0}(s; z_0), \text{c. c.}, s, 0, 0)\, ds \equiv z_0$$

and

$$\frac{\partial^\nu}{\partial\mu_2^{m_2}\cdots\partial\mu_n^{m_\nu}} z_{0,0}(t;z_0) = \int_0^t \frac{\partial^\nu}{\partial\mu_2^{m_2}\cdots\partial\mu_n^{m_\nu}} F(z_{0,0}(s;z_0), \text{c. c.}, s, 0, 0)\, ds \equiv 0.$$

Hence $z_{0,0}(2\pi;z_0) = z_0$ and $\frac{\partial^\nu}{\partial\mu_2^{m_2}\cdots\partial\mu_n^{m_\nu}} z_{0,0}(2\pi;z_0) = 0$, and the Poincaré map P has the form

$$P(z_0,\varepsilon,\mu) = z_0 + \varepsilon\left[\frac{\partial}{\partial\varepsilon} z_{0,0}(2\pi;z_0) + O(\varepsilon,\mu_2,\ldots,\mu_n)\right].$$

However, since

$$\frac{\partial}{\partial\varepsilon} F(z_{0,0}(s;z_0), \text{c. c.}, s, 0, 0) = e^{is}\hat{H}_1(z_0e^{-is}, \text{c. c.}, 0, 0),$$

then

$$\begin{aligned}\frac{\partial}{\partial\varepsilon} z_{0,0}(2\pi;z_0) &= \int_0^{2\pi} \frac{\partial}{\partial\varepsilon} F(z_{0,0}(s,z_0), \text{c. c.}, s, 0, 0)\, ds = \int_0^{2\pi} e^{is}\hat{H}_1(z_0e^{-is}, \text{c. c.}, 0, 0)\, ds,\\ &= \int_0^{2\pi} e^{is}H_1(z_0e^{-is} - iv, \text{c. c.}, 0)\, ds.\end{aligned}$$

Set $c_1 = H_1(-iv, i\overline{v}, 0)$, $\alpha_1 = D_1H_1(-iv, i\overline{v}, 0)$, and $\beta_1 = D_2H_1(-iv, i\overline{v}, 0)$.

Generically, $\mathrm{Re}(\alpha_1) \neq 0$. Near $z_0 = 0$, a Taylor expansion of H_1 yields

$$H_1(z_0e^{-is} - iv, \overline{z}_0e^{is} + i\overline{v}, 0) = c_1 + \alpha_1 z_0 e^{-is} + \beta_1\overline{z}_0e^{is} + O(|z_0|^2),$$

and so

$$\begin{aligned}\frac{\partial}{\partial\varepsilon} z_{0,0}(2\pi;z_0) &= \int_0^{2\pi} e^{is}H_1(z_0e^{-is} - iv, \overline{z}_0e^{is} + i\overline{v}, 0)\, ds\\ &= \int_0^{2\pi}\left[e^{is}c_1 + \alpha_1 z_0 + \beta_1\overline{z}_0e^{2is}\right] ds + O(|z_0|^2) = 2\pi\alpha_1 z_0 + O(|z_0|^2),\end{aligned}$$

which completes the proof. ∎

Technical Result 6 If $0 \neq \lambda \in \mathcal{W}$ is such that each $\mu_j \neq 0$ is fixed, then $[z_\lambda]_A = O(1)$ as $\lambda_1 \to 0$.

Proof: Let $0 \neq \lambda = (1,\mu)\varepsilon \in \mathcal{W}_1$. Since P in (4.1.5) is the Poincaré map of (4.1.4), the 2π−periodic orbit $z_\lambda(t) = \tilde{z}_{\varepsilon,\mu}(t)$ actually goes trough $z(\varepsilon,\mu)$, where $z(\varepsilon,\mu)$ solves $P(z,\overline{z},\varepsilon,\mu) \equiv 0$ for small parameter values and $z(0,0) = 0$.

A Taylor expansion of $\tilde{z}_{\varepsilon,\mu}$ around $(\varepsilon,\mu)=0$ yields

$$\tilde{z}_{\varepsilon,\mu}(t;z(\varepsilon,\mu))=\tilde{z}_{0,0}(t;0)+\varepsilon\frac{\partial}{\partial\varepsilon}\tilde{z}_{0,0}(t;0)+\sum_{j=2}^{n}\mu_j\frac{\partial}{\partial\mu_j}\tilde{z}_{0,0}(t;0)+O(\varepsilon^2,\varepsilon|\mu|,|\mu|^2).$$

Since $\tilde{z}_{0,0}(t;0)$ satisfies (4.1.4) when $\varepsilon=0$, then $\tilde{z}_{0,0}(t;0)=0$. Furthermore,

$$\tilde{z}_{\varepsilon,\mu}(t;z(\varepsilon,\mu))=z(\varepsilon,\mu)+\int_0^t\varepsilon e^{is}K(\tilde{z}_{\varepsilon,\mu}(s;z(\varepsilon,\mu))e^{-is},\text{c. c.},s,\varepsilon,\mu)\,ds.$$

Differentiating separately by ε and μ_j, $j=2,\ldots,n$, and evaluating at $(\varepsilon,\mu)=0$ gives

$$\begin{aligned}\frac{\partial}{\partial\varepsilon}\tilde{z}_{0,0}(t;0)&=\frac{\partial}{\partial\varepsilon}z(0,0)+\int_0^t e^{is}H_1(-iv,i\overline{v},0)\,ds=\frac{\partial}{\partial\varepsilon}z(0,0)+\frac{c_1}{i}e^{it}\\ \frac{\partial}{\partial\mu_j}\tilde{z}_{0,0}(t;0)&=\frac{\partial}{\partial\mu_j}z(0,0).\end{aligned}$$

Then

$$\tilde{z}_{\varepsilon,\mu}(t;z(\varepsilon,\mu))=\varepsilon\left(\frac{\partial}{\partial\varepsilon}z(0,0)+\frac{c_1}{i}e^{it}\right)+\sum_{j=2}^{n}\mu_j\frac{\partial}{\partial\mu_j}z(0,0)+O(\varepsilon^2,\varepsilon|\mu|,|\mu|^2).$$

But $\frac{\partial}{\partial\varepsilon}z(0,0)$ and $\frac{\partial}{\partial\mu_j}z(0,0)$, $j=2,\ldots,n$ can be computed from (4.1.7). Since

$$\alpha_1 z(\varepsilon,\mu)+O\left(|z(\varepsilon,\mu)|^2\right)+O(\varepsilon,\mu_2,\ldots,\mu_n)\equiv 0$$

for small enough $\varepsilon,\mu_2,\ldots,\mu_n$ then

$$\begin{aligned}\alpha_1\frac{\partial}{\partial\varepsilon}z(\varepsilon,\mu)+O(|z(\varepsilon,\mu)|)+O(\mu_2,\ldots,\mu_n)+O(1)\equiv 0\\ \alpha_1\frac{\partial}{\partial\mu_j}z(\varepsilon,\mu)+O(|z(\varepsilon,\mu)|)+O(\varepsilon,\mu_2\ldots,\mu_{j-1},\mu_{j+1},\ldots,\mu_n)+O(1)\equiv 0,\end{aligned}$$

for $j=2,\ldots,n$, where the $O(1)$ terms come from differentiating $O(\varepsilon,\mu_2,\ldots,\mu_n)$ with respect to ε and μ_j, $j=2,\ldots,n$, respectively. When $(\varepsilon,\mu)=0$, $z(0,0)=0$ and so

$$\frac{\partial}{\partial\varepsilon}z(0,0)=\frac{1}{\alpha_1}C_1\quad\text{and}\quad\frac{\partial}{\partial\mu_j}z(0,0)=\frac{1}{\alpha_1}C_j$$

where $C_j\in\mathbb{C}$ for $j=1,\ldots,n$.

Then

$$\tilde{z}_{\varepsilon,\mu}(t;z(\varepsilon,\mu))=\varepsilon\left(\frac{C_1}{\alpha_1}+\frac{c_1}{i}e^{it}\right)+\sum_{j=2}^{n}\mu_j\frac{C_j}{\alpha_1}+O(\varepsilon^2,\varepsilon|\mu|,|\mu|^2).$$

Since $\varepsilon = \lambda_1 \neq 0$ and $\mu_j = \frac{\lambda_j}{\lambda_1}$ for $j = 1, \ldots, n$, then

$$z_\lambda(t) = \lambda_1 \left(\frac{C_1}{\alpha_1} + \frac{c_1}{i} e^{it} \right) + \sum_{j=2}^{n} \frac{\lambda_j}{\lambda_1} \frac{C_j}{\alpha_1} + O\left(\lambda_1^2, \lambda_2, \ldots, \lambda_n, \frac{\lambda_2^2}{\lambda_1^2}, \frac{\lambda_2 \lambda_3}{\lambda_1^2}, \ldots, \frac{\lambda_n^2}{\lambda_1^2} \right)$$

and so the center $[z_\lambda]_A$ is

$$\begin{aligned}
[z_\lambda]_A &= \frac{1}{2\pi} \int_0^{2\pi} z_\lambda(t)\, dt \\
&= \frac{1}{2\pi} \int_0^{2\pi} \left(\lambda_1 \left(\frac{C_1}{\alpha_1} + \frac{c_1}{i} e^{it} \right) + \sum_{j=2}^{n} \frac{\lambda_j}{\lambda_1} \frac{C_j}{\alpha_1} + O\left(\lambda_1^2, \lambda_2, \ldots, \lambda_n, \frac{\lambda_2^2}{\lambda_1^2}, \frac{\lambda_2 \lambda_3}{\lambda_1^2}, \ldots, \frac{\lambda_n^2}{\lambda_1^2} \right) \right) dt \\
&= \frac{1}{\alpha_1} \left(\lambda_1 C_1 + \frac{1}{\lambda_1} \sum_{j=2}^{n} \lambda_j C_j \right) + O\left(\lambda_1^2, \lambda_2, \ldots, \lambda_n, \frac{\lambda_2^2}{\lambda_1^2}, \frac{\lambda_2 \lambda_3}{\lambda_1^2}, \ldots, \frac{\lambda_n^2}{\lambda_1^2} \right) \\
&= O\left(\lambda_1, \frac{\lambda_2}{\lambda_1}, \ldots, \frac{\lambda_n}{\lambda_1} \right).
\end{aligned}$$

When $0 \neq \lambda \in \mathcal{W}$ is such that $\mu_j = \frac{\lambda_j}{\lambda_1} \neq 0$ is fixed, then $0 \neq \frac{|\lambda_j|}{|\lambda_1|} < W_{1,j}$ for $j = 2, \ldots, n$, and so the last term above is $O(1)$ as $\lambda_1 \to 0$. ∎

Technical Result 7 The function $M^1(w, \overline{w}, 0)$ defined in (4.2.5) is $\mathbb{S}^1-$equivariant.

Proof: Recall that $\hat{H}_1$ is $\mathbb{S}^1-$equivariant by construction. Then

$$\begin{aligned}
M^1(we^{-i\theta}, \overline{w}e^{i\theta}, 0) &= \frac{1}{2\pi} \int_0^{2\pi} e^{it} K(we^{-i\theta}e^{-it}, \overline{w}e^{i\theta}e^{it}, t, 0, 0)\, dt \\
&= \frac{1}{2\pi} \int_0^{2\pi} e^{it} \hat{H}_1(we^{-it}e^{-i\theta}, \overline{w}e^{it}e^{i\theta}, 0, 0)\, dt \\
&= \frac{1}{2\pi} \int_0^{2\pi} e^{it} e^{i\theta} \hat{H}_1(we^{-it}, \overline{w}e^{it}, 0, 0)\, dt \\
&= e^{i\theta} M^1(w, \overline{w}, 0),
\end{aligned}$$

that is, M^1 is $\mathbb{S}^1-$equivariant. ∎

Technical Result 8 Let all terms, variables and functions be as in Theorem 4.2.1. In particular, the functions R and Ψ are C^1 on intervals away from $\rho = 0$. Denote

$$\begin{aligned}
\Sigma_0^r &= [0, 2\pi] \times [0, 2\pi] \times \{0\} \times S_0 \\
\Sigma_\sigma^r &= [0, 2\pi] \times [0, 2\pi] \times [-\sigma, \sigma] \times S_0.
\end{aligned}$$

Note that these spaces, as well as the spaces Σ_0 and Σ_σ from Theorem 2.3.1, are convex. The functions Θ and Λ satisfy the following conditions:

1. Θ and Λ are bounded by a function $\Xi(\varepsilon,\mu) = O(\varepsilon,\mu_2,\ldots,\mu_n)$ over Σ_0, and

2. for all $0 \le \sigma \le \sigma_0$, Θ and Λ are Lipschitz in Hale's sense (with Lipschitz constants $\theta(\varepsilon,\mu,\sigma) = O(\varepsilon,\mu_2,\ldots,\mu_n,\sigma)$ and $\lambda(\varepsilon,\mu,\sigma) = O(\varepsilon,\mu_2,\ldots,\mu_n,\sigma)$, respectively) over Σ_σ.

Proof: Since $\Theta,\Lambda \in \mathfrak{P}_t^{2\pi} \cap \mathfrak{P}_\psi^{2\pi}$, we need only show that the first statement holds over Σ_0^r and the second over Σ_σ^r, for all $0 \le \sigma \le \sigma_0$. For $j = 1,\ldots,n$, there are appropriate functions $R_j, \Psi_j \in \mathfrak{P}_t^{2\pi} \cap \mathfrak{P}_\psi^{2\pi}$, C^1 on intervals away from $\rho = 0$, such that

$$\begin{aligned} \Psi(t,\psi,\rho,\varepsilon,\mu) &= \varepsilon\Psi_1(t,\psi,\rho,\varepsilon,\mu) + \sum_{j=2}^{n} \mu_j \Psi_j(t,\psi,\rho,\mu) \\ R(t,\psi,\rho,\varepsilon,\mu) &= \varepsilon R_1(t,\psi,\rho,\varepsilon,\mu) + \sum_{j=2}^{n} \mu_j R_j(t,\psi,\rho,\mu), \end{aligned} \tag{4.4.1}$$

according to (4.2.9).

1. Over Σ_0^r, we have $x = 0$ and so

$$\begin{aligned} \Theta(t,\psi,0,\varepsilon,\mu) &= \varepsilon\Psi(t,\psi,\rho_1,\varepsilon,\mu) \\ &= \varepsilon^2\Psi_1(t,\psi,\rho_1,\varepsilon,\mu) + \varepsilon\sum_{j=2}^{n} \mu_j \Psi_j(t,\psi,\rho_1,\varepsilon,\mu) \end{aligned} \tag{4.4.2}$$

and

$$\begin{aligned} \Lambda(t,\psi,0,\varepsilon,\mu) &= R(t,\psi,\rho_1,\varepsilon,\mu) \\ &= \varepsilon R_1(t,\psi,\rho_1,\varepsilon,\mu) + \sum_{j=2}^{n} \mu_j R_j(t,\psi,\rho_1,\varepsilon,\mu) \end{aligned} \tag{4.4.3}$$

according to (4.4.1).

For $j = 1,\ldots,n$, the continuous functions $|R_j|$ and $|\varepsilon\Psi_j|$ reach their maximum C_j and E_j, respectively, on the compact set $[0,2\pi] \times \{0\}$ for $j = 1,\ldots,n$. Then

$$|\varepsilon\Psi_j(t,\psi,\rho_1,\varepsilon,\mu)| \le E_j \quad \text{and} \quad |R_j(t,\psi,\rho_1,\varepsilon,\mu)| \le C_j$$

over Σ_0^r for $j = 1,\ldots,n$. According to (4.4.2) and (4.4.3),

$$\begin{aligned} |\Theta(t,\psi,0,\varepsilon,\mu)| &\le |\varepsilon|E_1 + \sum_{j=2}^{n} |\mu_j|E_j = Q_1(\varepsilon,\mu) \\ |\Lambda(t,\psi,0,\varepsilon,\mu)| &\le |\varepsilon|C_1 + \sum_{j=2}^{n} |\mu_j|C_j = Q_2(\varepsilon,\mu) \end{aligned}$$

over Σ_0^r. Set

$$\Xi(\varepsilon,\mu) = \max\{Q_1(\varepsilon,\mu), Q_2(\varepsilon,\mu)\}.$$

Then Λ and Θ are bounded by $\Xi(\varepsilon,\mu) = O(\varepsilon,\mu_2,\ldots,\mu_n)$ over Σ_0^r.

2. Let $(\psi_1,x_1),(\psi_2,x_2) \in \mathbb{R}\times[-\sigma,\sigma]$ for $0 \le \sigma \le \sigma_0$. By one of the mean value theorems, there exist points $(\psi^*,x^*),(\psi_*,x_*) \in [0,2\pi]\times[-\sigma,\sigma]$ on the line joining (ψ_1,x_1) and (ψ_2,x_2) such that

$$|\Theta(t,\psi_1,x_1,\varepsilon,\mu) - \Theta(t,\psi_2,x_2,\varepsilon,\mu)| = |\widehat{\Theta}(t,\psi^*,x^*,\varepsilon,\mu)|\big[|\psi_1-\psi_2| + |x_1-x_2|\big]$$
$$|\Lambda(t,\psi_1,x_1,\varepsilon,\mu) - \Lambda(t,\psi_2,x_2,\varepsilon,\mu)| = |\widehat{\Lambda}(t,\psi_*,x_*,\varepsilon,\mu)|\big[|\psi_1-\psi_2| + |x_1-x_2|\big],$$

where

$$\begin{aligned}
\widehat{\Theta}(t,\psi,x,\varepsilon,\mu) &= D_x\Theta(t,\psi,x,\varepsilon,\mu) + D_\psi\Theta(t,\psi,x,\varepsilon,\mu)\\
&= xK_0^\Psi(x,\varepsilon,\mu) + \varepsilon K_1^\Psi(t,\psi,x,\varepsilon,\mu) + \sum_{j=2}^n \mu_j K_j^\Psi(t,\psi,x,\varepsilon,\mu)\\
\widehat{\Lambda}(t,\psi,x,\varepsilon,\mu) &= D_x\Lambda(t,\psi,x,\varepsilon,\mu) + D_\psi\Lambda(t,\psi,x,\varepsilon,\mu)\\
&= xK_0^R(x,\varepsilon,\mu) + \varepsilon K_1^R(t,\psi,x,\varepsilon,\mu) + \sum_{j=2}^n \mu_j K_j^R(t,\psi,x,\varepsilon,\mu),
\end{aligned}$$

where

$$\begin{aligned}
K_0^\Psi(x,\varepsilon,\mu) &= \varepsilon D_x B_2(x)\\
K_0^R(x,\varepsilon,\mu) &= \varepsilon\left(D_x B_1(x)x + 2B_1(x)\right)\\
K_1^\Psi(t,\psi,x,\varepsilon,\mu) &= B_2(x) + \varepsilon\left(D_x\Psi_1(t,\psi,\rho_1+x,\varepsilon,\mu) + D_\psi\Psi_1(t,\psi,\rho_1+x,\varepsilon,\mu)\right)\\
K_1^R(t,\psi,x,\varepsilon,\mu) &= \varepsilon\left(D_x R_1(t,\psi,\rho_1+x,\varepsilon,\mu) + D_\psi R_1(t,\psi,\rho_1+x,\varepsilon,\mu)\right)\\
K_j^\Psi(t,\psi,x,\varepsilon,\mu) &= \varepsilon\left(D_x\Psi_j(t,\psi,\rho_1+x,\varepsilon,\mu) + D_\psi\Psi_j(t,\psi,\rho_1+x,\varepsilon,\mu)\right)\\
K_j^R(t,\psi,x,\varepsilon,\mu) &= \varepsilon\left(D_x R_j(t,\psi,\rho_1+x,\varepsilon,\mu) + D_\psi R_j(t,\psi,\rho_1+x,\varepsilon,\mu)\right),
\end{aligned}$$

with Ψ_j and R_j are as in (4.4.1). Since Θ and Λ are continuously differentiable, $\widehat{\Theta}$ and $\widehat{\Lambda}$ are continuous on Σ_σ^r, as are K_j^Ψ and K_j^R for $j = 0,\ldots,n$.

In particular, the functions $|K_j^\Psi|$ and $|K_j^\Psi|$ each reach their respective maximum k_j^Ψ and k_j^R on Σ_σ^r for $j = 0,\ldots,n$. Then, note that $|x^*|, |x_*| \le \sigma$,

$$\begin{aligned}
|\widehat{\Theta}(t,\psi^*,x^*,\varepsilon,\mu)| &\le |x^*||K_0^\Psi(x^*,\varepsilon,\mu)| + |\varepsilon||K_1^\Psi(t,\psi^*,x^*,\varepsilon,\mu)| + \sum_{j=2}^n |\mu_j||K_j^\Psi(t,\psi^*,x^*,\varepsilon,\mu)|\\
&\le |x^*|k_0^\Psi + |\varepsilon|k_1^\Psi + \sum_{j=2}^n |\mu_j|k_j^\Psi \le \sigma k_0^\Psi + |\varepsilon|k_1^\Psi + \sum_{j=2}^n |\mu_j|k_j^\Psi = \theta(\varepsilon,\mu,\sigma)
\end{aligned}$$

and

$$|\widehat{\Lambda}(t,\psi_*,x_*,\varepsilon,\mu)| \le |x_*||K_0^R(x_*,\varepsilon,\mu)| + |\varepsilon||K_1^R(t,\psi_*,x_*,\varepsilon,\mu)| + \sum_{j=2}^{n} |\mu_j||K_j^R(t,\psi_*,x_*,\varepsilon,\mu)|$$
$$\le |x_*|k_0^R + |\varepsilon|k_1^R + \sum_{j=2}^{n} |\mu_j|k_j^R \le \sigma k_0^R + |\varepsilon|k_1^R + \sum_{j=2}^{n} |\mu_j|k_j^R = \lambda(\varepsilon,\mu,\sigma).$$

In particular

$$|\Theta(t,\psi_1,x_1,\varepsilon,\mu) - \Theta(t,\psi_2,x_2,\varepsilon,\mu)| \le \theta(\varepsilon,\mu_2,\ldots,\mu_n,\sigma)\big[|\psi_1-\psi_2| + |x_1-x_2|\big]$$
$$|\Lambda(t,\psi_1,x_1,\varepsilon,\mu) - \Lambda(t,\psi_2,x_2,\varepsilon,\mu)| \le \lambda(\varepsilon,\mu_2,\ldots,\mu_n,\sigma)\big[|\psi_1-\psi_2| + |x_1-x_2|\big],$$

where $\theta(\varepsilon,\mu,\sigma), \lambda(\varepsilon,\mu,\sigma) = O(\varepsilon,\mu_2,\ldots,\mu_n,\sigma)$. Hence Θ and Λ are Lipschitz in Hale's sense.

This completes the proof. ∎

Technical Result 9 If $0 \neq \lambda \in \mathcal{V}_1$, then $[\mathcal{E}_\lambda^1]_D = \xi_1 + O(\lambda_1)$.

Proof: Let $0 \neq \lambda = (1,\mu)\varepsilon \in \mathcal{V}_1$. Note that $\{\hat{T}_{\varepsilon,\mu}\} = O(\varepsilon,\mu)$ since $\hat{T}_{\varepsilon,\mu}$ is bounded by a term of order 1 in (ε,μ) (see Theorem 2.3.1 for details). Then

$$[\hat{\mathcal{E}}_{\varepsilon,\mu}]_D = \frac{1}{4\pi^2}\int_0^{2\pi}\int_0^{2\pi}\big((\rho_1 + \{\hat{T}_{\varepsilon,\mu}\})e^{-i(\psi-t)} + \varepsilon\kappa\big((\rho_1 + \{\hat{T}_{\varepsilon,\mu}\})e^{-i(\psi-t)}, \text{c.c.}, t, \varepsilon, \mu\big)\big)\, d\psi dt$$
$$= \frac{1}{4\pi^2}\int_0^{2\pi}\int_0^{2\pi}\big((\rho_0 + O(\varepsilon,\mu))e^{-i(\psi-t)} + O(\varepsilon)\big)\, d\psi dt$$
$$= 0 + O(\varepsilon) = O(\varepsilon).$$

Accordingly,

$$[\mathcal{E}_{(1,\mu)\varepsilon}]_D = [\xi_1 - ie^{it}v]_D + [\hat{\mathcal{E}}_{\varepsilon,\mu}]_D = \frac{1}{4\pi^2}\int_0^{2\pi}\int_0^{2\pi}\big(\xi_1 - ie^{it}v\big)\, d\psi dt + O(\varepsilon) = \xi_1 + O(\varepsilon).$$

Thus, $[\mathcal{E}_\lambda^1]_D = \xi_1 + O(\lambda_1)$. ∎

Technical Result 10 The Poincaré map Π of (4.3.1) near $z = 0$, $\lambda = 0$ is given by (4.3.2).

Proof: Let $z_\lambda(t;z_0)$ denote the solution of (4.3.1) through z_0 at time t. Then z_λ must satisfy the integral equation

$$z_\lambda(t;z_0) = z_0 + \int_0^t e^{is}K^*(z_\lambda(s;z_0)e^{-is}, \text{c. c.}, s, \lambda)\, ds. \tag{4.4.4}$$

The Poincaré map Π of (4.3.1) is the time-2π map, so $\Pi(z_0,\lambda) = z_\lambda(2\pi; z_0)$. A Taylor expansion of Π around $\lambda = 0$ yields

$$\Pi(z_0,\lambda) = z_{\lambda=0}(2\pi; z_0) + \sum_{j=1}^{n} \lambda_j \frac{\partial}{\partial \lambda_j}\left[z_{\lambda=0}(2\pi; z_0)\right] + O\left(|\lambda|^2\right).$$

Note that $K^*(w,\overline{w},s,0) \equiv 0$, $D_1K^*(w,\overline{w},s,0) \equiv 0$ and $D_2K^*(w,\overline{w},s,0) \equiv 0$, by definition of K^*. In particular, when $\lambda = 0$, (4.4.4) becomes

$$z_{\lambda=0}(t; z_0) = z_0 + \int_0^t e^{is} K^*(z_{\lambda=0}(s; z_0), \text{c. c.}, s, 0)\, ds \equiv z_0$$

and so $z_{\lambda=0}(2\pi; z_0) = z_0$. Now, let $j \in \{1,\ldots,n\}$. Differentiating (4.4.4) with respect to λ_j yields

$$\begin{aligned}
\frac{\partial}{\partial \lambda_j} z_\lambda(t; z_0) &= \int_0^t \frac{\partial}{\partial \lambda_j}\left[e^{is} K^*(z_\lambda(s; z_0)e^{-is}, \text{c. c.}, s, \lambda)\right] ds \\
&= \int_0^t e^{is}\Big[D_1K^*(z_\lambda(s; z_0)e^{-is}, \text{c. c.}, s, \lambda)\frac{\partial}{\partial \lambda_j} z_\lambda(s; z_0)e^{-is} \\
&\qquad + D_2K^*(z_\lambda(s; z_0)e^{-is}, \text{c. c.}, s, \lambda)\frac{\partial}{\partial \lambda_j}\overline{z_\lambda(s; z_0)}e^{is} \\
&\qquad + H_j\left((z_\lambda(s; z_0) - \zeta_j)e^{-is} - iv, \text{c. c.}, \lambda\right) + O(\lambda)\Big]\, ds.
\end{aligned} \tag{4.4.5}$$

Setting $\lambda = 0$ in (4.4.5), we obtain

$$\frac{\partial}{\partial \lambda_j} z_{\lambda=0}(t; z_0) = \int_0^t e^{is} H_j\left((z_0 - \zeta_j)e^{-is} - iv, \text{c. c.}, 0\right)\, ds. \tag{4.4.6}$$

Near $z_0 = 0$, a Taylor expansion of H_j yields

$$\begin{aligned}
H_j((z_0 - \zeta_j)e^{-is} - iv, \text{c. c.}, 0) = {} & H_j\left(-\zeta_j e^{-is} - iv, \text{c. c.}, 0\right) + D_1H_j\left(-\zeta_j e^{-is} - iv, \text{c. c.}, 0\right) z_0 e^{-is} \\
& + D_2H_j\left(-\zeta_j e^{-is} - iv, \text{c. c.}, 0\right)\overline{z}_0 e^{is} + O\left(z_0^2, z_0\overline{z}_0, \overline{z}_0^2\right),
\end{aligned}$$

and so

$$\begin{aligned}
&\int_0^{2\pi} e^{is} H_j((z_0 - \zeta_j)e^{-is} - iv, \text{c. c.}, 0)\, ds = \\
&\qquad \int_0^{2\pi} e^{is} H_j\left(-\zeta_j e^{-is} - iv, \text{c. c.}, 0\right)\, ds + z_0 \int_0^{2\pi} D_1H_j\left(-\zeta_j e^{-is} - iv, \text{c. c.}, 0\right)\, ds \\
&\qquad\qquad + \overline{z}_0 \int_0^{2\pi} e^{2is} D_2H_j\left(-\zeta_j e^{-is} - iv, \text{c. c.}, 0\right)\, ds + O\left(z_0^2, z_0\overline{z}_0, \overline{z}_0^2\right).
\end{aligned}$$

Let A_j, B_j and E_j be as in (4.3.3). Then the Poincaré map Π takes the form

$$\Pi(z_0,\lambda) = z_0 + \sum_{j=1}^{n} \lambda_j\left[E_j + A_j z_0 + B_j \overline{z}_0\right] + O\left(|\lambda|^2\right) + O\left(z_0^2, z_0\overline{z}_0, \overline{z}_0^2\right).$$

As $E_1 = 0$ and $B_1 = 0$, this completes the proof.[2] ∎

[2] In fact, for $j = 1$, all the terms of order 2 in z_0 and $\overline{z}_0$ disappear.

Chapter 5

Characterization of Spiral Anchoring $(n = 2)$

In Chapter 4, we described the (local) behaviour of spiral anchoring in small wedges around the parameter coordinate axes. In the present chapter, we present a fuller characterization of spiral wave anchoring for the case $n = 2$.[1]

Let $0 \neq \xi \in \mathbb{R}^2$, $\Lambda_0 = (\lambda_1, 0), \Lambda_\xi = (0, \lambda_2) \in \mathbb{R}^2$ and let $P : \mathbb{R}^2 \times \mathbb{R}^2 \to \mathbb{R}^2$ be a real analytic map with $P(x, 0) = x$, $DP(x, 0) = I_2$ for all $x \in \mathbb{R}^2$, satisfying the following conditions: for $\eta \in \{0, \xi\}$,

(P1) $\exists\, \omega_* > 0$ such that $P(\eta, \Lambda_\eta) \equiv \eta$, for all $||\Lambda_\eta|| < \omega_*$;

(P2) the eigenvalues of $DP(\eta, \Lambda_\eta)$ lie both outside or both inside the unit circle for all $0 \neq ||\Lambda_\eta|| < \omega_*$;

(P3) there is a wedge region w_η surrounding the coordinate axis generated by Λ_η in parameter space (see Figure 5.1) in which P has a (locally) unique manifold $x_\eta(\lambda)$ such that, for all $\lambda \in \mathsf{w}_\eta$,

1. $P(x_\eta(\lambda), \lambda) \equiv x_\eta(\lambda)$;
2. $x_\eta(\lambda) \to \eta$ as λ approaches the coordinate axis away from the origin;
3. $x_\eta(\lambda)$ shares its stability with η in (P2).

[1] We believe that most of our analysis can be extended and adapted to the general case $n \geq 2$, but at the cost of substantial algebraic complications.

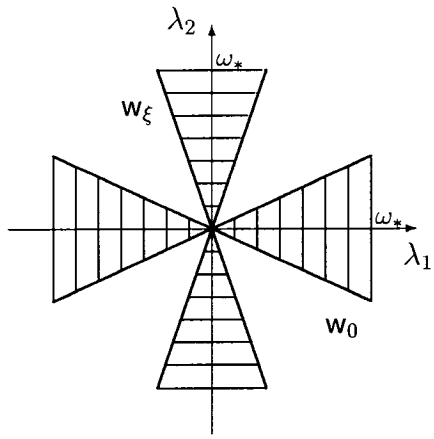

Figure 5.1: Wedges in parameter space corresponding to property (P3).

When the hypotheses of Theorem 4.1.3 hold, the associated Poincaré map (4.1.5) (viewed in real coordinates) satisfies (P1)−(P3). Numerous questions cannot be answered by the local analysis done in the previous chapter alone. For instance:

1. Can the wedges overlap? What does that imply for anchoring in (4.0.1)?
2. Can a wedge contain its "opposite" coordinate axis?
3. If the wedges do not overlap, what is the nature of their complement?
4. If there is a complement with non-trivial measure, what kinds of dynamics can be expected as the parameter vector λ traces a circle around the origin in parameter space?

We will provide answers to these questions by first studying a specific map, then extending our results to the general mapping.

5.1 A Specific Mapping

Consider the mapping $P : \mathbb{R}^2 \times \mathbb{R}^2 \to \mathbb{R}^2$ given by

$$P(x, \lambda) = x + 2\pi\big[\lambda_1 F_0(x) + \lambda_2 G_\xi(x)\big], \tag{5.1.1}$$

where $0 \neq \xi \in \mathbb{R}^2$, and F_0, G_ξ are real analytic functions of $x, \lambda \in \mathbb{R}^2$.

Such a map is obtained by truncating the $\lambda-$terms of order ≥ 2 from the Poincaré map (4.1.5), for instance. According to the form of the time-2π map appearing in the proof of Theorem 4.1.3, the jacobians $DF_0(0)$ and $DG_\xi(\xi)$ have a particular structure.

Proposition 5.1.1 *If* $F_0(0) = 0$, $G_\xi(\xi) = 0$, *and if*

$$DF_0(0) = \begin{pmatrix} a & -b \\ b & a \end{pmatrix} \quad \textit{and} \quad DG_\xi(\xi) = \begin{pmatrix} c & -d \\ d & c \end{pmatrix}$$

where $a, c \neq 0$, *then there exists* $\omega_* > 0$ *such that the map defined by* (5.1.1) *satisfies the conditions* (P1)$-$(P3).

Proof: By hypothesis, $P(x,0) = x$, $DP(x,0) = I_2$ for all $x \in \mathbb{R}^2$, and $P(\eta, \Lambda_\eta) \equiv \eta$ for all Λ_η, $\eta \in \{0, \xi\}$. Furthermore,

$$\begin{aligned} \det DF_0(0) &= a^2 + b^2 > 0, \quad \operatorname{tr} DF_0(0) = 2a \neq 0, \\ \det DG_\xi(\xi) &= c^2 + d^2 > 0, \quad \operatorname{tr} DG_\xi(\xi) = 2c \neq 0, \end{aligned}$$

as $a, c \neq 0$. Set

$$\omega_* = \min\left\{ \frac{|a|}{(a^2+b^2)\pi}, \frac{|c|}{(c^2+d^2)\pi} \right\} > 0. \tag{5.1.2}$$

Then

$$16\pi^2\lambda_1^2 \det DF_0(0)\big(\pi^2\lambda_1^2 \det DF_0(0) + \pi\lambda_1 \operatorname{tr} DF_0(0) + 1\big) > 0, \tag{5.1.3}$$

$$2\pi\lambda_1\big(\operatorname{tr} DF_0(0) + 2\pi\lambda_1 \det DF_0(0)\big) \neq 0, \tag{5.1.4}$$

$$16\pi^2\lambda_2^2 \det DG_\xi(\xi)\big(\pi^2\lambda_2^2 \det DG_\xi(\xi) + \pi\lambda_2 \operatorname{tr} DG_\xi(\xi) + 1\big) > 0, \tag{5.1.5}$$

$$2\pi\lambda_2\big(\operatorname{tr} DG_\xi(\xi) + 2\pi\lambda_2 \det DG_\xi(\xi)\big) \neq 0 \tag{5.1.6}$$

for all $0 \neq ||\Lambda_\eta|| < \omega_*$, $\eta \in \{0, \xi\}$ (see p. 90 for details). However,

$$\begin{aligned} \det DP(0,\Lambda_0) &= 1 + 2\pi\lambda_1 \operatorname{tr} DF_0(0) + 4\pi^2\lambda_1^2 \det DF_0(0), \\ \operatorname{tr} DP(0,\Lambda_0) &= 2 + 2\pi\lambda_1 \operatorname{tr} DF_0(0), \\ \det DP(\xi,\Lambda_\xi) &= 1 + 2\pi\lambda_2 \operatorname{tr} DG_\xi(\xi) + 4\pi^2\lambda_2^2 \det DG_\xi(\xi), \\ \operatorname{tr} DP(\xi,\Lambda_\xi) &= 2 + 2\pi\lambda_2 \operatorname{tr} DG_\xi(\xi), \end{aligned}$$

and so

$$\begin{aligned} \big(\det DP(0,\Lambda_0) - \operatorname{tr} DP(0,\Lambda_0) + 1\big) &= 4\pi^2\lambda_1^2 \det DF_0(0), \\ \big(\det DP(0,\Lambda_0) + \operatorname{tr} DP(0,\Lambda_0) + 1\big) &= 4\big(\pi^2\lambda_1^2 \det DF_0(0) + \pi\lambda_1 \operatorname{tr} DF_0(0) + 1\big), \\ \det DP(0,\Lambda_0) - 1 &= 2\pi\lambda_1\big(\operatorname{tr} DF_0(0) + 2\pi\lambda_1 \det DF_0(0)\big), \end{aligned}$$

$$\begin{aligned}
\big(\det DP(\xi,\Lambda_\xi) - \operatorname{tr} DP(\xi,\Lambda_\xi) + 1\big) &= 4\pi^2\lambda_2^2 \det DG_\xi(\xi),\\
\big(\det DP(\xi,\Lambda_\xi) + \operatorname{tr} DP(\xi,\Lambda_\xi) + 1\big) &= 4\big(\pi^2\lambda_2^2 \det DG_\xi(\xi) + \pi\lambda_2 \operatorname{tr} DG_\xi(\xi) + 1\big),\\
\det DP(\xi,\Lambda_\xi) - 1 &= 2\pi\lambda_2\big(\operatorname{tr} DG_\xi(\xi) + 2\pi\lambda_2 \det DG_\xi(\xi)\big).
\end{aligned}$$

Combining (5.1.3)-(5.1.6) with the last 6 equations yields

$$\begin{aligned}
\big(\det DP(0,\Lambda_0) - \operatorname{tr} DP(0,\Lambda_0) + 1\big)\big(\det DP(0,\Lambda_0) + \operatorname{tr} DP(0,\Lambda_0) + 1\big) > 0,\\
\big(\det DP(\xi,\Lambda_\xi) - \operatorname{tr} DP(\xi,\Lambda_\xi) + 1\big)\big(\det DP(\xi,\Lambda_\xi) + \operatorname{tr} DP(\xi,\Lambda_\xi) + 1\big) > 0,
\end{aligned}$$

$\det DP(0,\Lambda_0), \det DP(\xi,\Lambda_\xi) \neq 1$ for all $0 \neq ||\Lambda_\eta|| < \omega_*$, $\eta \in \{0,\xi\}$, and so (P2) is satisfied (see p. 90 for details).

The existence of the wedges and of the (locally) unique manifolds $x_0(\lambda)$ and $x_\xi(\lambda)$, as well as their limiting properties, can be shown exactly as in Theorems 4.1.1–4.1.3. ∎

5.2 The Search for Fixed Points

Let F_0, G_ξ be as in the statement of Proposition 5.1.1. Define $A : \mathbb{R}^2 \to \mathbb{M}_2(\mathbb{R})$ by

$$A(x) = \begin{bmatrix} F_0(x) & G_\xi(x) \end{bmatrix}. \tag{5.2.1}$$

Then, $\hat{x}$ is a fixed point of (5.1.1) for $\hat{\lambda} \in \mathbb{R}^2$ if and only if $A(\hat{x}) \cdot \hat{\lambda} = 0$, that is if and only if $\hat{\lambda} \in L_{\hat{x}} = \ker A(\hat{x})$. Let $(\hat{x}, \hat{\lambda})$ be such a pair. According to the Implicit Function Theorem, as long as

$$\det\Big(D_x P(\hat{x},\hat{\lambda}) - I\Big) = 4\pi^2 \det\Big(\hat{\lambda}_1 DF_0(\hat{x}) + \hat{\lambda}_2 DG_\xi(\hat{x})\Big) \neq 0,$$

there is a neighbourhood W of $\hat{\lambda}$ and a unique analytic function $X : W \to \mathbb{R}^2$ such that $X(\hat{\lambda}) = \hat{x}$ and $A(X(\lambda)) \cdot \lambda \equiv 0$ for all $\lambda \in W$. By construction, $X(\lambda)$ is a fixed point of (5.1.1) for all $\lambda \in W$.

If $\dim L_{\hat{x}} = 0$ as a manifold, then $L_{\hat{x}} = \{0\}$. Consequently, the preceding Implicit Function Theorem construction fails, which contradicts the existence of a wedge in property (P3). We need thus only investigate fixed points $\hat{x}$ for which $\dim L_{\hat{x}} \neq 0$, *i.e.*, fixed points for which $L_{\hat{x}} \neq \{0\}$ and $\operatorname{rank} A(\hat{x}) \neq 2$, thanks to the rank-nullity theorem.

Generically, amongst those $\hat{x}$, $\operatorname{rank} A(\hat{x}) \neq 0$, as otherwise, $\hat{x}$ would satisfy the four simultaneous equations $A_{j,k}(x) = 0$, $j,k = 1,2$. But each of these zero-level

sets consists of curves and/or points (since F_0 and G_ξ are real analytic). The generic intersection of four curves in $\mathbb{R}^2$ being empty, the remark follows. As a result, we will assume $\operatorname{rank} A(\hat{x}) = 1$ and $\dim L_{\hat{x}} = 1$ for the remainder of this chapter.

We now show how to optimally extend the wedge regions w_η using property (P3). Let $(x^*, \lambda^*), (x_*, \lambda_*) \in \mathbb{R}^2 \times (\mathbb{R}^2 - \{0\})$ be such that $\operatorname{rank} A(x^*) = \operatorname{rank} A(x_*) = 1$, $\lambda^* \in L_{x^*}, \lambda_* \in L_{x_*}$, $\det(D_x P(x^*, \lambda^*) - I) \neq 0$ and $\det(D_x P(x_*, \lambda_*) - I) \neq 0$.

According to the Implicit Function Theorem, there are open neighbourhoods W^*, W_* of $\lambda^*, \lambda_* \in \mathbb{R}^2$ respectively, and a pair of unique real analytic functions $X^* : W^* \to \mathbb{R}^2$, $X_* : W_* \to \mathbb{R}^2$ for which $X^*(\lambda^*) = x^*$, $X_*(\lambda_*) = x_*$ and

$$A(X^*(\Lambda)) \cdot \Lambda \equiv 0, \quad \text{for all } \Lambda \in W^*$$
$$A(X_*(\Lambda)) \cdot \Lambda \equiv 0, \quad \text{for all } \Lambda \in W_*.$$

Lemma 5.2.1 *If $\Lambda^*_* \in W^*_* = W^* \cap W_*$ is such that $X^*(\Lambda^*_*) = X_*(\Lambda^*_*)$, then*

$$X^*|_{W^*_*} = X_*|_{W^*_*}.$$

Proof: The assertion follows from the uniqueness of the real analytic functions X^*, X_* in the Implicit Function Theorem (see [41, lemma, p. 171] for a similar line of reasoning on extending solutions of a system of C^1 differential equations), and the sectorial nature of the domain in parameter space. ∎

Denote the punctured open disc of radius ω_* centered at the origin by $B(0, \omega_*)$. Let $\eta \in \{0, \xi\}$, $\omega_* > 0$ be as in proposition 5.1.1 and $0 \neq \Lambda_\eta \in \mathsf{w}_\eta$ be a point on the appropriate coordinate axis, as in properties (P1) and (P2). According to these same properties, η is a fixed point of (5.1.1) for Λ_η and $\det(D_x P(\eta, \Lambda_\eta) - I) \neq 0$.

Lemma 5.2.1 then implies the existence of a maximal open region W_η in $B(0, \omega_*)$ (and containing $\mathsf{w}_\eta \cap B(0, \omega_*)$) for which there is a unique real analytic function $\mathsf{X}_\eta : \mathsf{W}_\eta \to \mathbb{R}^2$ satisfying $x_\eta = \mathsf{X}_\eta|_{\mathsf{W}_\eta}$, where x_η is as in property (P3).

Since $\hat{x}$ is a fixed point of (5.1.1) for $0 \neq \hat{\lambda}$ whenever $\hat{\lambda} \in L_{\hat{x}}$, W_η is described (in polar coordinates) by either one of

$$\mathsf{W}_\eta = \{(r, \theta) : 0 < r < \omega_* \text{ and } s_\eta - \varphi^-_\eta < \theta < s_\eta + \varphi^+_\eta\} \tag{5.2.2}$$
$$\mathsf{W}_\eta = \{(r, \theta) : 0 < r < \omega_* \text{ and } \theta \in [0, 2\pi]\} \tag{5.2.3}$$

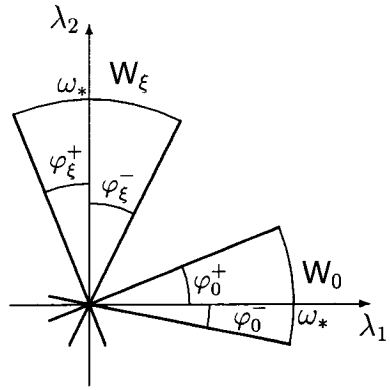

Figure 5.2: The four wedge angles in parameter space.

where $\varphi_\eta^-, \varphi_\eta^+ \in (0, \frac{\pi}{2}]$ and

$$s_\eta = \begin{cases} 0 & \text{if } \eta = 0, \\ \frac{\pi}{2} & \text{if } \eta = \xi. \end{cases}, \tag{5.2.4}$$

In the latter case, we will say that W_η is **catastrophe-free**. In the former case, the quantities $\varphi_\eta^-, \varphi_\eta^+ \in (0, \frac{\pi}{2}]$ are called the **fore-angle** and **post-angle** of W_η, respectively (see Figure 5.2).

The Implicit Function Theorem fails to extend $A(\mathsf{X}_\eta(\lambda)) \cdot \lambda \equiv 0$ (that is, it fails to extend W_η) at (x^*, λ^*) if either

(C1) $\det(\lambda_1^* DF_0(x^*) + \lambda_2^* DG_\xi(x^*)) = 0$ and $\mathsf{X}_\eta(\lambda) \to x^*$ as $\lambda \to \lambda^*$, or

(C2) $\|\mathsf{X}_\eta(\lambda)\| \to \infty$ as $\lambda \to \lambda^*$.

Such events will be referred to as **fold** and **∞−catastrophes**, respectively, or **catastrophes**, collectively.

Let $0 < \rho < \omega_*$ and set

$$\gamma_\rho(s) = \rho\,(\cos(s), \sin(s))^\top. \tag{5.2.5}$$

Assume W_η is not catastrophe-free. Starting at $(\rho, s_\eta) \in \mathsf{W}_\eta$, denote the angles in $(0, \frac{\pi}{2}]$ measuring the first clockwise and the first counter-clockwise occurrence of a catastrophe along γ_ρ by θ_η^- and θ_η^+ respectively. Then, $\varphi_\eta^\pm = s_\eta \pm \theta_\eta^\pm$.

Fold Bifurcation Points

Modulo a simple non-degeneracy condition (see below), (C1) is equivalent to the existence of a fold bifurcation curve in parameter space for (5.1.1). Indeed, in that case, (x^*, λ^*) is a solution of

$$\begin{aligned} P(x,\lambda) - x &= 0 \\ \det\left(D_x P(x,\lambda) - I\right) &= 0. \end{aligned} \tag{5.2.6}$$

If the (full) Jacobian of the left-hand side of (5.2.6) has rank 3 at that point, (5.2.6) has a fold bifurcation curve through λ^* [47]. Such solutions are in one-to-one correspondence with regular solutions of

$$\begin{aligned} A(x)\cdot\lambda &= 0 \\ \det\left(D_x\left[A(x)\cdot\lambda\right]\right) &= 0. \end{aligned} \tag{5.2.7}$$

Set

$$I_{10} = \begin{pmatrix} 1 & 0 \\ 0 & 0 \end{pmatrix}, \quad I_{01} = \begin{pmatrix} 0 & 0 \\ 0 & 1 \end{pmatrix}, \quad \hat{I} = \begin{pmatrix} 0 & 1 \\ 1 & 0 \end{pmatrix}, \quad e_1 = \begin{pmatrix} 1 \\ 0 \end{pmatrix} \quad \text{and} \quad e_2 = \begin{pmatrix} 0 \\ 1 \end{pmatrix},$$

and define $H_1, H_2 : \mathbb{R}^2 \to \mathbb{R}^2$ by

$$\begin{aligned} H_1(x) &= \left[I_{10}A(x) + I_{01}A(x)\hat{I}\right] e_1 \\ H_2(x) &= \left[I_{10}A(x) + I_{01}A(x)\hat{I}\right] e_2. \end{aligned} \tag{5.2.8}$$

A quick computation (see p. 91 for details) shows that (5.2.7) can be written as

$$\begin{aligned} A(x)\cdot\lambda &= 0 \\ \lambda^{\top} Q(x)\lambda &= 0, \end{aligned} \tag{5.2.9}$$

where

$$Q(x) = \begin{pmatrix} B(x) & \frac{1}{2}C(x) \\ \frac{1}{2}C(x) & E(x) \end{pmatrix} \tag{5.2.10}$$

and

$$\begin{aligned} B(x) &= \det DF_0(x) \\ C(x) &= \det DH_1(x) + \det DH_2(x) \\ E(x) &= \det DG_\xi(x). \end{aligned} \tag{5.2.11}$$

Denote

$$K_x = \{\lambda \in \mathbb{R}^2 : \lambda^\top Q(x)\lambda = 0\}. \tag{5.2.12}$$

For reasons similar to those presented on p. 72, only the fixed points x^* of (5.1.1) for which K_{x^*} has non-trivial dimension need to be investigated. Generically, $A(x^*) \neq 0$ and $\operatorname{rank} Q(x^*) \neq 0$ (again, see p. 72) and so K_{x^*} consists of a single line or a pair of intersecting lines through the origin in parameter space (see Section 2.4 for details).

Write $\mathsf{L}_x = L_x \cap B(0, \omega_*)$ and $\mathsf{K}_x = K_x \cap B(0, \omega_*)$. The following proposition summarizes the situation.

Proposition 5.2.2 *If (x^*, λ^*) is a regular solution of (5.2.7) with $\{0\} \neq \mathsf{L}_{x^*} \subseteq \mathsf{K}_{x^*}$, then (x^*, λ) is a fold bifurcation point of (5.1.1) for all $\lambda \in \mathsf{L}_{x^*}$.*

5.3 The Visual Criterion

Set $\mathfrak{Z} = \{(x, \lambda) \in \mathbb{R}^2 \times \mathbb{R}^2 : P(x, \lambda) = x \text{ and } \lambda \in \mathsf{L}_x \neq \{0\}\}$ and

$$\kappa(\mathfrak{Z}) = \{x \in \mathbb{R}^2 : \exists\, \lambda \neq 0 \in \mathbb{R}^2 \text{ such that } (x, \lambda) \in \mathfrak{Z}\}.$$

By construction, $\kappa(\mathfrak{Z}) = Z_{\mathbb{R}^2}(\det A(x))$ and $0, \xi \in \kappa(\mathfrak{Z})$. The nature of P is such that, generically, $\kappa(\mathfrak{Z})$ is a collection $\mathcal{C}$ of isolated planar curves, whose constituents come in two varieties: bounded or unbounded.[2] Denote this partition by $\mathcal{C} = \mathcal{C}_{\mathrm{B}} \sqcup \mathcal{C}_\infty$ and let C_0, C_ξ be the curves in $\mathcal{C}$ such that $0 \in C_0$ and $\xi \in C_\xi$.[3]

Let $\gamma_\rho : [0, 2\pi] \to \mathbb{R}^2$ be the circle of radius ρ around the origin, parameterized as in (5.2.5). For each $(x, \lambda) \in \mathfrak{Z}$, define L_x^ρ and K_x^ρ as the intersection of that circle with L_x and K_x, respectively, and let $P_\rho : \mathbb{R}^2 \times [0, 2\pi] \to \mathbb{R}^2$ be given by

$$P_\rho(x, s) = x + 2\pi\rho\big[\cos(s)F_0(x) + \sin(s)G_\xi(x)\big]. \tag{5.3.1}$$

Then L_x^ρ consists of two antipodal points $\{\pm\alpha_{x,\rho}\}$, and the fixed points (x, s) of P_ρ are in one-to-one correspondence with the 'lines' of fixed points (x, L_x) of P for which $\mathsf{L}_x \neq \{0\}$ (see proposition 5.2.2).

[2] Indeed, were any such curves to intersect at x_*, P would undergo a transcritical bifurcation along $\kappa^{-1}(x_*)$. Such bifurcations are not generically permitted by (C1) and (C2).

[3] There might be other curves in $\mathcal{C}$, but C_0 and C_ξ are the only ones whose existence can be guaranteed by properties (P1)–(P3). Note further that C_0 and C_ξ may be one and the same.

Set $\mathfrak{Z}_\rho = \{(x,s) \in \mathbb{R}^2 \times [0,2\pi] : P_\rho(x,s) = x \text{ and } \gamma_\rho(s) \in \mathsf{L}^\rho_x\}$ and

$$\kappa_\rho(\mathfrak{Z}_\rho) = \{x \in \mathbb{R}^2 : (x,s) \in \mathfrak{Z}_\rho\}.$$

By construction,

$$\kappa_\rho(\mathfrak{Z}_\rho) = \kappa(\mathfrak{Z}) = Z_{\mathbb{R}^2}(\det A(x)).$$

Thus for each $C \in \mathcal{C}$, $\kappa_\rho^{-1}(C)$ is a branch of fixed points in the bifurcation diagram of P_ρ. According to Section 5.2, the converse also holds: each branch of fixed points in the bifurcation diagram of P_ρ projects down *via* κ_ρ to a curve in $\mathcal{C}$.

The existence and location of fold catastrophes cannot be read directly from $\mathcal{C}$; the next Proposition remedies that situation.

Let $(x^*, \alpha) \in \mathbb{R}^2 \times (\mathbb{R}^2 - \{0\})$ be such that $\|\alpha\| = \rho$, $\alpha \in \mathsf{L}^\rho_{x^*} \subseteq \mathsf{K}^\rho_{x^*}$. Recall that $A(x^*) \neq 0$ by assumption. Then, there is some $j \in \{1,2\}$ for which $(A_{j,1}(x^*)\ A_{j,2}(x^*)) \neq 0$ and

$$L_{x^*} = \{\lambda \in \mathbb{R}^2 : A_{j,1}(x^*)\lambda_1 + A_{j,2}(x^*)\lambda_2 = 0\}.$$

The function $\Gamma_j : \mathbb{R}^2 \to \mathbb{R}^2$ defined by

$$\Gamma_j(x) = \left[A^2_{j,2}(x)B(x) - A_{j,1}(x)A_{j,2}(x)C(x) + A^2_{j,1}(x)E(x)\right], \tag{5.3.2}$$

where B, C and E are as in (5.2.11), is called the j**–fold bifurcation function** of (5.1.1). Set $\mathcal{R}_j = Z_{\mathbb{R}^2}(\Gamma_j(x))$.

Proposition 5.3.1 *Let $j \in \{1,2\}$. If x^* is a transverse intersection of $\kappa(\mathfrak{Z})$ and $\mathcal{R}_j$ such that $(A_{j,1}(x^*)\ A_{j,2}(x^*)) \neq 0$ and either*

1) *$B(x^*) = 0$ and $A_{j,1}(x^*)C(x^*) - A_{j,2}(x^*)E(x^*) = 0$ or*

2) *$B(x^*) \neq 0$ and $C(x^*)^2 - 4B(x^*)E(x^*) \geq 0$,*

then P_ρ undergoes a fold catastrophe at (x^*, s^*) for all s^* such that $\gamma_\rho(s^*) = \pm\alpha_{x^*,\rho}$.

Proof: By re-labeling the terms if necessary,[4] we may assume $A_{j,1} \neq 0$.[5]
1) If $B = 0$ and $A_{j,1}C - A_{j,2}E = 0$, then

$$K_{x^*} = \{\lambda \in \mathbb{R}^2 : \lambda_1\lambda_2 C + \lambda_2^2 E = 0\} = \{\lambda \in \mathbb{R}^2 : \lambda_2 = 0 \text{ or } \lambda_1 C + \lambda_2 E = 0\}.$$

[4] In that case also remembering to replace $B(x)$ by $E(x)$ and *vice-versa* throughout.
[5] The dependency on x^* is omitted to lighten the text.

i. If $\lambda_2 = 0$, then $L_{x^*} = \{(\lambda_1, 0) \in \mathbb{R}^2 : \lambda_1 A_{j,1} = 0\} = \{0\}$ since $A_{j,1} \neq 0$. But this contradicts the assumption $\dim L_{x^*} = 1$ (see p. 73).

ii. If $\lambda_1 C + \lambda_2 E = 0$, then

$$\operatorname{rank} \begin{pmatrix} A_{j,1} & A_{j,2} \\ C & E \end{pmatrix} = 1.$$

2) If $B \neq 0$ and $C^2 - 4BE \geq 0$, then

$$K_{x^*} = \left\{ \lambda \in \mathbb{R}^2 : \lambda_1 = \frac{-C \pm \sqrt{C^2 - 4BE}}{2B} \lambda_2 \right\}.$$

In this case,

$$\begin{aligned} 4B\Gamma_j &= (-2A_{j,2}B + A_{j,1}C)^2 - A_{j,1}^2(C^2 - 4BE) \\ &= \left(-2A_{j,2}B + A_{j,1}\left(C + \sqrt{C^2 - 4BE}\right)\right)\left(-2A_{j,2}B + A_{j,1}\left(C - \sqrt{C^2 - 4BE}\right)\right) = 0 \end{aligned}$$

and so

$$-\frac{A_{j,2}}{A_{j,1}} = \frac{-C + \sqrt{C^2 - 4BE}}{2B} \quad \text{or} \quad -\frac{A_{j,2}}{A_{j,1}} = \frac{-C - \sqrt{C^2 - 4BE}}{2B}.$$

In either cases, L_{x^*} is contained in K_{x^*}, and so $\{0\} \neq \mathsf{L}_{x^*} \subseteq \mathsf{K}_{x^*}$ and $\{0\} \neq \mathsf{L}^{\rho}_{x^*} \subseteq \mathsf{K}^{\rho}_{x^*}$. As x^* is a transverse intersection of $\kappa(\mathfrak{Z})$ and $\mathcal{R}_j$, it is also a regular solution of (5.2.9) (see p. 28); thus (x^*, L_{x^*}) consists of fold bifurcation points of (5.1.1), according to proposition 5.2.2. The desired conclusion then follows from the fact that $\{\pm\alpha_{x^*,\rho}\} = \mathsf{L}^{\rho}_{x^*} = \mathsf{L}_{x^*} \cap \gamma_\rho$ and from the correspondence between fixed points of P_ρ and 'lines' of fixed points of P. ∎

By construction, the bifurcation diagram of P_ρ is $2\pi-$periodic in s. Consequently, elements of $\mathcal{C}_{\mathrm{B}}$ must be (bounded) loops and elements of $\mathcal{C}_\infty$ must give rise to two $\infty-$catastrophes.

5.3.1 The Elowyn-Bonhomme Map

Set $\xi = (2, 2)^\top$, $a = 2$, $b = 1$, $c = -3$ and $d = \frac{1}{2}$. Consider

$$F_0(x) = \begin{pmatrix} 2x_1 - x_2 + x_1 x_2 - x_2^2 \\ x_1 + 2x_2 + x_1^2 \end{pmatrix}$$

and

$$G_\xi(x) = \begin{pmatrix} -3(x_1 - 2) - \frac{1}{2}(x_2 - 2) + (x_2 - 2)^2 \\ \frac{1}{2}(x_1 - 2) - 3(x_2 - 2) + (x_1 - 2)^2 + (x_1 - 2)(x_2 - 2) \end{pmatrix}.$$

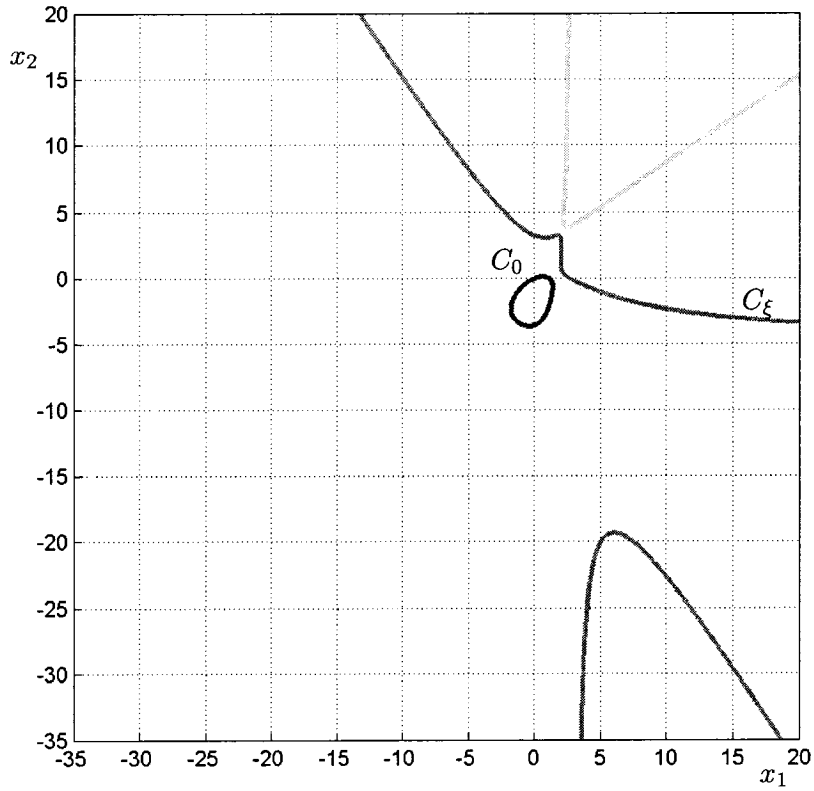

Figure 5.3: Zero-level set $\kappa(3)$ for the Elowyn-Bonhomme map.

Let P, $A(x)$, $B(x)$, $C(x)$, $E(x)$, $\kappa(3)$, $\Gamma_j(x)$ and $\mathcal{R}_j$, $j = 1, 2$, be defined as in the preceding subsection.[6] We refer to P as the **Elowyn-Bonhomme** (EB) map.

The fixed points $(\hat{x}, \hat{\lambda})$ of this map satisfy $\hat{x} \in \kappa(3)$ and $0 \neq \hat{\lambda} \in L_{\hat{x}}$; $\kappa(3)$ is shown in Figure 5.3. It consists of five isolated algebraic curves, of which C_0 is shown in blue and C_ξ in red. In this instance, $C_0 \in \mathcal{C}_B$ and $C_\xi \in \mathcal{C}_\infty$.

With the given values of a, b, c and d, we have $\omega_* = \frac{12}{37\pi}$. Let $\rho = 0.01 < \omega_*$. Using a pseudo-arc length continuation algorithm (see [10, 45] for details), a partial bifurcation diagram of P_ρ (ignoring all fixed point branches but those through η at $s = s_\eta$, for $\eta \in \{0, \xi\}$) is built: the results can be seen in figure 5.4.

Six fold catastrophes take place: two along C_0 and four along C_ξ. Two $\infty-$catastrophes occur on C_ξ.

[6]The length of some of the expressions involved is rather prohibitive. In the interest of clarity, they are not presented here.

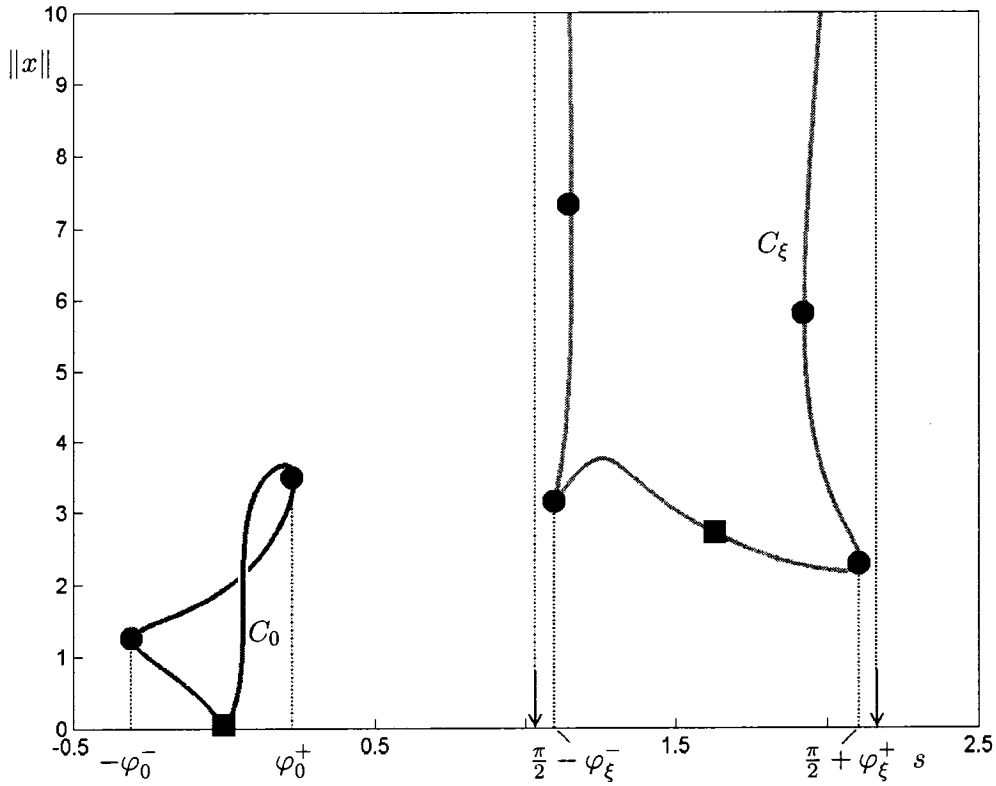

Figure 5.4: Fixed point branches of P_ρ for the Elowyn-Bonhomme problem: C_0 is shown in blue and C_ξ in red. The squares at $s = 0$ and $s = \frac{\pi}{2}$ represent 0 and ξ, respectively; the circles and arrows are fold and $\infty-$catastrophes, respectively. The apparent self-intersection on C_0 is due to a projection onto the $\|x\| - s$ plane.

By inspection, the corresponding wedge angles are found to be

$$\varphi_0^- \approx 0.3023, \quad \varphi_0^+ \approx 0.2308, \quad \varphi_\xi^- \approx 0.4688, \quad \varphi_\xi^+ \approx 0.5417.$$

It is readily seen that W_0 and W_ξ do not overlap as

$$\varphi_0^+ + \varphi_\xi^- \approx 0.6996 < \frac{\pi}{2} \quad \text{and} \quad \varphi_0^- + \varphi_\xi^+ \approx 0.8440 < \frac{\pi}{2}.$$

However, this information can be recovered directly from $\kappa(\mathfrak{Z})$ and $\mathcal{R}_j$, $j = 1, 2$, with the help of Proposition 5.3.1.

In Figure 5.5, the six intersections that satisfy the hypotheses of proposition 5.3.1 are marked with circles: they each correspond to one of the six fold catastrophes observed in figure 5.4.

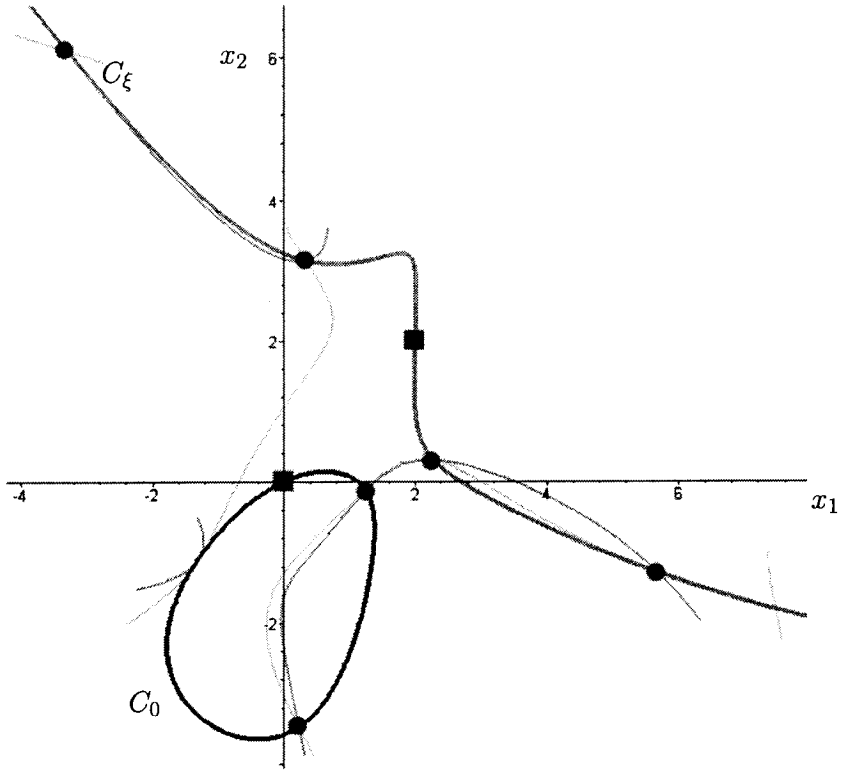

Figure 5.5: Intersections of the zero-level sets $\kappa(\mathfrak{Z})$ (in red and blue) and $\mathcal{R}_1$ and $\mathcal{R}_2$ (in green and magenta, respectively) of the Elowyn-Bonhomme problem. The squares represent 0 and ξ; the points that satisfy the hypotheses of Proposition 5.3.1 are marked with circles. The yellow region is part of the planar set for which $C(x)^2 - 4B(x)E(x) < 0$.

The wedge angles are linked to the $s-$values of four catastrophes: those occurring immediately before and after 0 and ξ along C_0 and C_ξ, respectively. In the EB map, these catastrophes are all of the fold type.

If $x^* \in \kappa(\mathfrak{Z})$ records a fold catastrophe, the corresponding s^*-values appearing in the conclusion of proposition 5.3.1 are easily computed.

As an example, consider the fold catastrophe occurring at $x^* \approx (2.2769, 0.2982)^\top$ along C_ξ: it gives rise to one of the wedge angles $\varphi_\xi^\pm$. Since $L_{x^*} = \ker A(x^*) = \langle v \rangle$, where $v \approx (-0.5156, 0.8568)^\top$, and since $\gamma_\rho(s)$ intersects L_{x^*} (in the upper half-plane) at $s^* \approx 2.1125 > \frac{\pi}{2}$, the corresponding wedge angle is $\varphi_\xi^+ = s^* - \frac{\pi}{2} \approx 0.5417$.

The fold catastrophes of P_ρ along C_0 and C_ξ are determined using this method; the results are compiled in Table 5.1.

x^*	s^*	**Wedge Angle**
$(1.2483, -0.1286)^\top$	5.9809	$\varphi_0^- \approx 0.3023$
$(0.2269, -3.4760)^\top$	0.2308	$\varphi_0^+ \approx 0.2308$
$(0.3371, 3.1473)^\top$	1.1020	$\varphi_\xi^- \approx 0.4688$
$(2.2769, 0.2982)^\top$	2.1125	$\varphi_\xi^+ \approx 0.5417$
$(-3.2933, 6.1024)^\top$	1.1581	n.a.
$(5.6733, -1.2807)^\top$	1.9267	n.a.

Table 5.1: Fold catastrophes of P_ρ along C_0 and C_ξ for the Elowyn-Bonhomme map.

The s^*-values of $\infty-$catastrophes cannot as easily be read from $\kappa(\mathfrak{Z})$, but the principle remains the same.

Consider the $\infty-$catastrophes occurring *via* C_ξ. Let (z_k) be a sequence of points on C_ξ such that $\|z_k\| \to \infty$ and such that the distance from ξ to z_k along C_ξ increases with k. For $k \in \mathbb{N}$, let s_k be the $s-$value in $(0, \pi)$ at which $\gamma_\rho(s)$ intersects L_{z_k}. Since P_ρ is real analytic, L_z vary continuously with z, and so do their intersections with γ_ρ (in the upper half-plane). In particular, if (s_k) converges to a value in $[0, \pi]$, the limit s^* does not depend on the choice of the original sequence (z_k). Using the sequences $\left(10^k, x_{2,k}\right), \left(x_{1,k}, 10^k\right) \in C_\xi$, where $x_{1,k}$ and $x_{2,k}$ are determined by the implicit equations

$$\det A\left(10^k, x_{2,k}\right) = \det A\left(x_{1,k}, 10^k\right) = 0,$$

the two $\infty-$catastrophes are found to occur at $s^* \approx 1.0172$ and $s^* \approx 2.3562$. These values do not give rise to wedge angles since they have all been found already.

5.3.2 Back to the Criterion

Based on the Elowyn-Bonhomme mapping and its analysis, we formulate the following visual criterion to determine the nature of W_0 and W_ξ.

Let P be a real analytic mapping of the form (5.1.1) satisfying the properties (P1)$-$(P3), together with its associated quantities. Generically, $A(x) = 0$ has no solution in $\mathbb{R}^2$. Let C be one of the curves in $\mathcal{C}$.

Clearly, an $\infty-$catastrophe can occur *via* C if and only if $C \in \mathcal{C}_\infty$; there are then exactly two such events.

Moreover, the number of fold catastrophes on any given $C \in \mathcal{C}_{\mathrm{B}}$ cannot be odd as C could not be a loop in that case; but there are no restrictions on the number of such events along $C \in \mathcal{C}_{\infty}$. Furthermore, catastrophes cannot occur at 0 or ξ as this would contradict (P2) and (P3).

Let C_0, C_ξ, s_0 and s_ξ be as defined previously. Set $\eta \in \{0, \xi\}$. By definition, C_η goes through η at $s = s_\eta$. By (P3), the wedges' angles $\varphi_\eta^{\pm}$ lie in $(0, \pi)$ or $(0, \pi]$ (when they exist), according to whether they record fold or $\infty-$catastrophes, respectively. Set $\nu_1 = \varphi_0^+ + \varphi_\xi^-$ and $\nu_2 = \varphi_0^- + \varphi_\xi^+$. Then W_0 and W_ξ overlap

1. in all four quadrants if and only if $\nu_1, \nu_2 > \frac{\pi}{2}$;
2. in the first and third quadrants if and only if $\nu_1 > \frac{\pi}{2}$ and $\nu_2 \leq \frac{\pi}{2}$, and in the second and fourth quadrants if and only if $\nu_1 \leq \frac{\pi}{2}$ and $\nu_2 > \frac{\pi}{2}$.

If $\nu_j = \frac{\pi}{2}$, the wedges do not overlap but their complement has zero measure in a neighbourhood of the origin.

When the wedge angles $\varphi_\eta^{\pm}$ do not exist, W_η is a deleted neighbourhood of the origin in parameter space.

If $C_0 \neq C_\xi$, it is sufficient to understand the bifurcation diagrams along a single curve: the full picture can then be obtained by combining the diagrams corresponding to C_0 and C_ξ.

When $C_\eta \in \mathcal{C}_{\mathrm{B}}$, there are two (essentially) distinct generic possibilities.

(i) If there is no fold catastrophe along C_η, then the angles $\varphi_\eta^{\pm}$ do not exist and W_η is catastrophe-free deleted neighbourhood of the origin in parameter space.

(ii) If there are $2k$ fold catastrophes along C_η, $k > 0$, then the angles $\varphi_\eta^{\pm}$ are well-defined: $s_\eta \mp \varphi_\eta^{\pm}$ are the $s-$values of the first fold catastrophes occurring respectively *before* and *after* η along C_η.

When $C_\eta \in \mathcal{C}_{\infty}$, there are two (essentially) distinct generic possibilities.

(i) If there is no fold catastrophe along C_η, then the angles $\varphi_\eta^{\pm}$ are well defined and $s_\eta \mp \varphi_\eta^{\pm}$ are the $s-$values of the $\infty-$catastrophes occurring respectively *before* and *after* η *via* C_η.

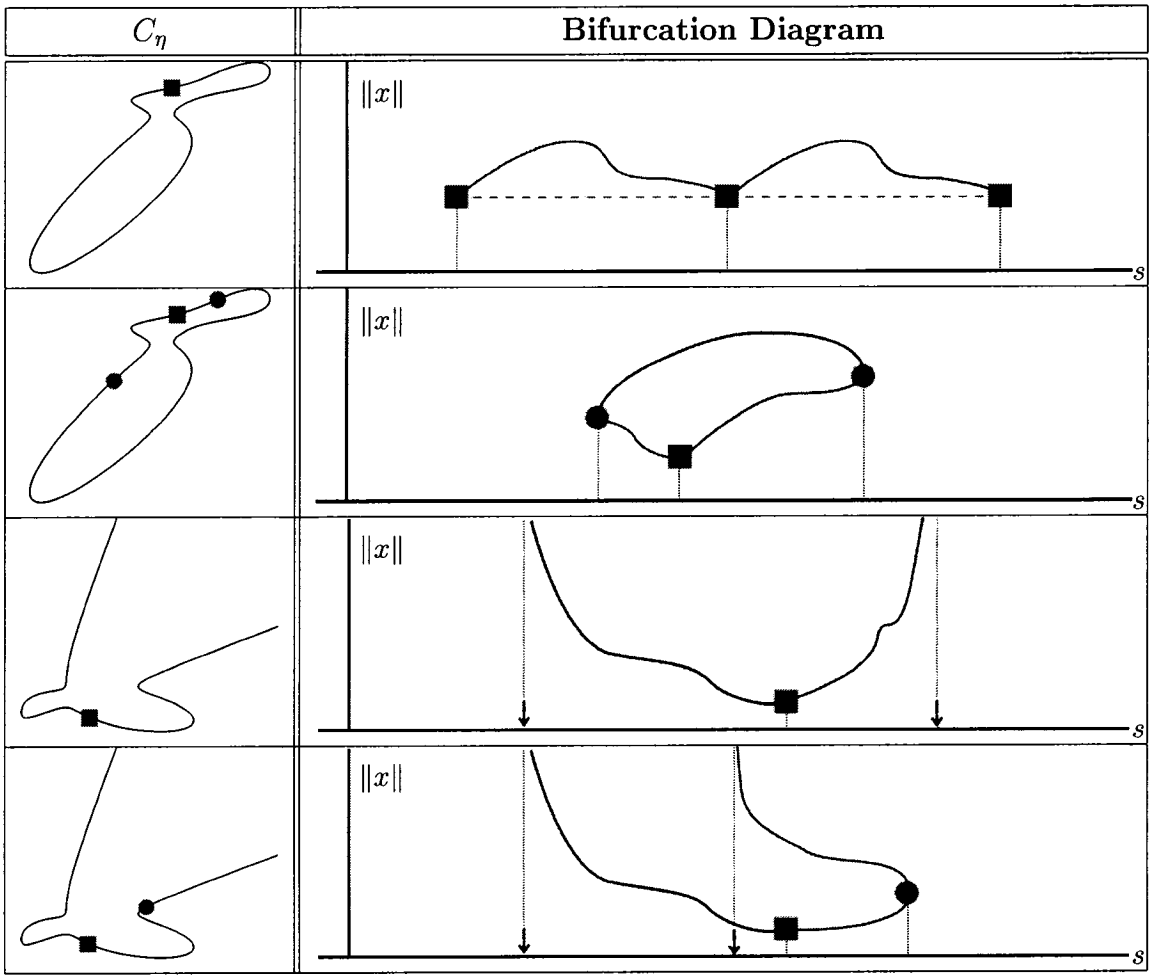

Table 5.2: Partial bifurcation diagrams of P_ρ when $C_0 \neq C_\xi$. Only the branch C_η is shown, for $\eta \in \{0, \xi\}$. The square represents η and the circles and arrows indicate fold and $\infty-$catastrophes, respectively.

(ii) If there are k fold catastrophes along C_η, $k > 0$, then the angles $\varphi_\eta^\pm$ are well-defined: if all the fold catastrophes lie on one side of η (say $s > s_\eta$) along C_η then $s_\eta \mp \varphi_\eta^\pm$ are the $s-$values of the $\infty-$catastrophes occurring *before* η and the first fold catastrophe *after* η along C_η, respectively (or *vice-versa*). Otherwise, $s_\eta \mp \varphi_\eta^\pm$ are the $s-$values of the first fold catastrophes occurring respectively *before* and *after* η along C_η.

Some corresponding qualitative bifurcation diagrams are shown in table 5.2.

If $C_0 = C_\xi$, the bifurcation diagram must pass through 0 at $s = 0$ and ξ at $s = \frac{\pi}{2}$.

When $C_0 = C_\xi \in \mathcal{C}_B$, the number of fold catastrophes along the curve is even; there are then three (essentially) distinct generic possibilities.

(i) If there is no fold catastrophe along $C_0 = C_\xi$, then the angles $\varphi_0^\pm$ and $\varphi_\xi^\pm$ do not exist and $\mathsf{W}_0 = \mathsf{W}_\xi$ are catastrophe-free deleted neighbourhoods of the origin in parameter space.

(ii) If there is an odd number of fold catastrophes between 0 and ξ along $C_0 = C_\xi$, then the angles $\mp\varphi_0^\pm$ and $\frac{\pi}{2} \mp \varphi_\xi^\pm$ are well-defined: they are the $s-$values of the first fold catastrophes occurring respectively *before* and *after* 0 and ξ *via* $C_0 = C_\xi$.

(iii) If there is an even number of fold catastrophes between 0 and ξ along $C_0 = C_\xi$, the situation is much as described in (ii), save for the fact that $C_0 = C_\xi$ is not a loop in the bifurcation diagram of P_ρ.

When $C_0 = C_\xi \in \mathcal{C}_\infty$, there are two (essentially) distinct generic possibilities.

(i) If there is no fold catastrophe along $C_0 = C_\xi$, then the angles $\varphi_0^\pm$ and $\varphi_\xi^\pm$ are well defined and $s_\eta \mp \varphi_\eta^\pm$ are the $s-$values of the $\infty-$catastrophes occurring respectively *before* and *after* 0 and ξ *via* $C_0 = C_\xi$.

(ii) If there are k fold catastrophes along $C_0 = C_\xi$, $k > 0$, then the angles $\varphi_0^\pm$ and $\varphi_\xi^\pm$ are well-defined: if no fold catastrophe lies between 0 and ξ along $C_0 = C_\xi$ then $\mp\varphi_0^\pm$ and $\frac{\pi}{2} \mp \varphi_\eta^\pm$ are determined as in the case $C_\eta \in \mathcal{C}_\infty$, (ii) (see p. 84). If there are fold catastrophes between 0 and ξ along $C_0 = C_\xi$, then φ_0^+ and $\frac{\pi}{2} - \varphi_\xi^-$ are the $s-$values of the first fold catastrophes occurring respectively *after* 0 and *before* ξ along C_ξ.

Some corresponding qualitative bifurcation diagrams are shown in table 5.3.

5.4 The General Mapping

The mapping (5.1.1) is not the most general mapping satisfying (P1)$-$(P3); one should instead study maps of the form

$$\mathcal{P}(x, \lambda) = x + 2\pi\big[\lambda_1 \mathcal{F}_0(x, \lambda_1) + \lambda_1\lambda_2 \mathcal{J}(x, \lambda) + \lambda_2 \mathcal{G}_\xi(x, \lambda_2)\big], \tag{5.4.1}$$

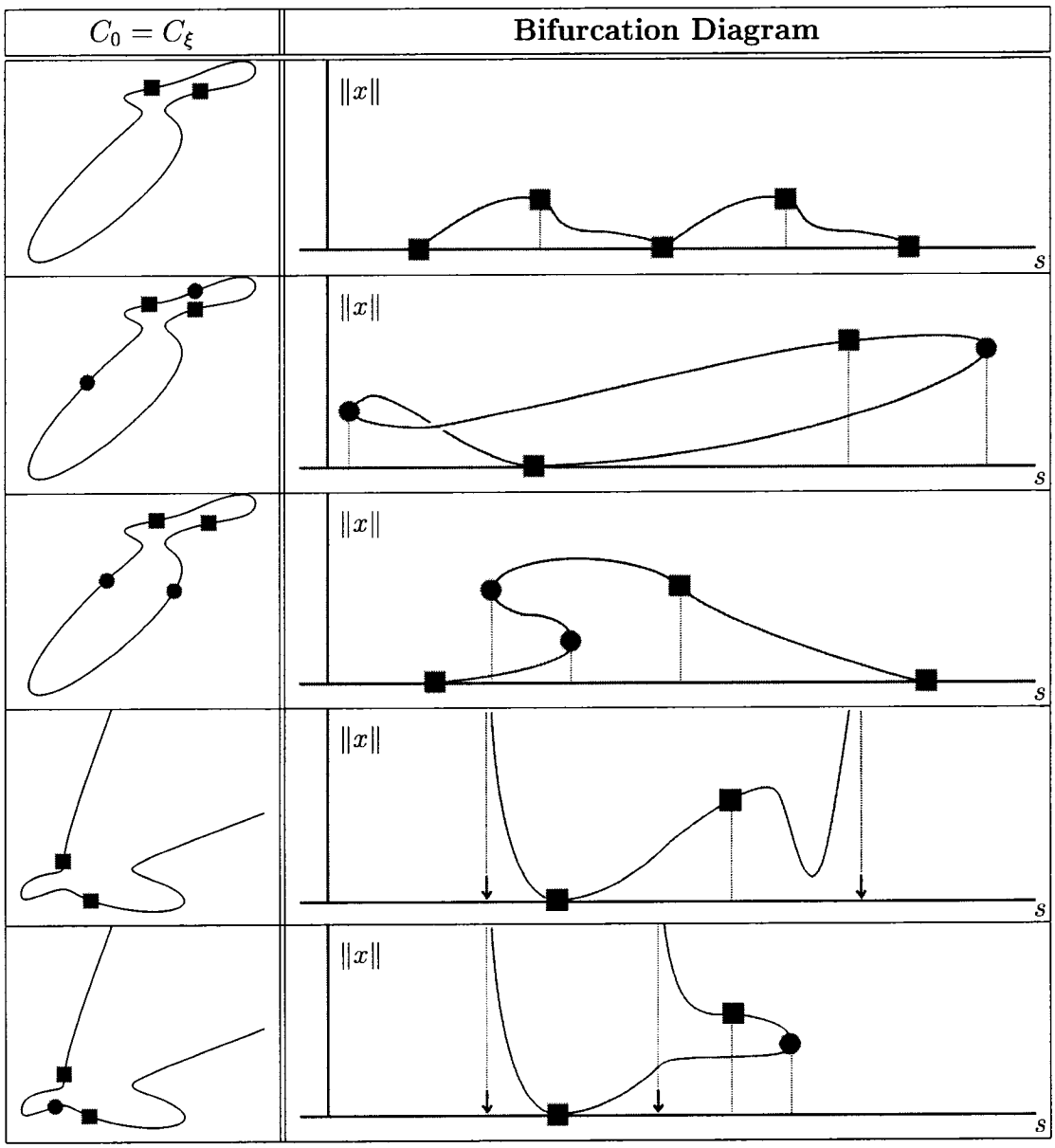

Table 5.3: Partial bifurcation diagrams of P_ρ when $C_0 = C_\xi$. The squares represent 0 and ξ, and the circles and arrows indicate fold and $\infty-$catastrophes, respectively. As before, self-intersections are only apparent and do not, in fact, occur.

where $\xi \neq 0 \in \mathbb{R}^2$, $\mathcal{F}_0$, $\mathcal{J}$ and $\mathcal{G}_\xi$ are real analytic in their variables and the jacobians $D_x\mathcal{F}_0(0, \lambda_1)$ and $D_x\mathcal{G}_\xi(\xi, \lambda_2)$ have the particular form prescribed by Proposition 5.4.1, which is analogous to Proposition 5.1.1 (so is its proof, which is omitted).

Proposition 5.4.1 *If* $\mathcal{F}(0,\lambda_1)\equiv 0$, $\mathcal{G}_\xi(\xi,\lambda_2)\equiv 0$, *and if*

$$D_x\mathcal{F}_0(0,\lambda_1)=\begin{pmatrix} a(\lambda_1) & -b(\lambda_1)\\ b(\lambda_1) & a(\lambda_1)\end{pmatrix} \quad \textit{and} \quad D_x\mathcal{G}_\xi(\xi,\lambda_2)=\begin{pmatrix} c(\lambda_2) & -d(\lambda_2)\\ d(\lambda_2) & c(\lambda_2)\end{pmatrix},$$

where $a,b,c,d:\mathbb{R}\to\mathbb{R}$ *are continuous in their variables and* $a(0),c(0)\neq 0$, *then there exists* $\omega_*>0$ *such that the map defined by* (5.4.1) *satisfies conditions* (P1)–(P3).

Define $\mathcal{A}:\mathbb{R}^2\times\mathbb{R}^2\to\mathbb{M}_2(\mathbb{R})$ by

$$\mathcal{A}(x,\lambda)=\Big[\mathcal{F}_0(x,\lambda_1)+\tfrac{\lambda_2}{2}\mathcal{J}(x,\lambda)\quad \tfrac{\lambda_1}{2}\mathcal{J}(x,\lambda)+\mathcal{G}_\xi(x,\lambda_2)\Big]; \tag{5.4.2}$$

fixed points of (5.4.1) are then in one-to-one correspondence with solutions of

$$\mathcal{A}(x,\lambda)\cdot\lambda=0. \tag{5.4.3}$$

Set $\mathfrak{F}(x,\lambda)=\det\mathcal{A}(x,\lambda)$. According to Taylor's Theorem, there are appropriate functions K_{10}, K_{01} such that $\mathfrak{F}(x,\lambda)=\mathfrak{F}(x,0)+\lambda_1K_{10}(x,\lambda)+\lambda_2K_{01}(x,\lambda)$.

Let $\hat{x}$ be such that $\mathfrak{F}(\hat{x},0)=0$, $\det D_x\mathfrak{F}(\hat{x},0)\neq 0$ and $\mathcal{A}(\hat{x},0)\neq 0$. Then, by the Implicit Function Theorem, there is a neighbourhood $\mathfrak{V}\subseteq\mathbb{R}^2$ of the origin and a unique analytic function $\mathfrak{X}:\mathfrak{V}\to\mathbb{R}^2$ such that $\mathfrak{X}(0)=\hat{x}$, $\mathfrak{F}(\mathfrak{X}(\lambda),\lambda)\equiv 0$ and $\operatorname{rank}\mathcal{A}(\mathfrak{X}(\lambda),\lambda)=1$ for all $\lambda\in\mathfrak{V}$.

Define $\mathfrak{L}_{\hat{x}}=\{\lambda\in\mathfrak{V}:\mathcal{A}(\mathfrak{X}(\lambda),\lambda)\cdot\lambda=0\}$. A simple rank argument shows that $\mathfrak{L}_{\hat{x}}$ is defined *via* a single equation in two real variables, with a regular solution at the origin (see p. 91 for details); consequently, as a manifold, $\mathfrak{L}_{\hat{x}}$ is one-dimensional.

Let $\mathcal{L}_{\hat{x}}=\ker\mathcal{A}(\hat{x},0)$. Then, there is a small neighbourhood $\mathfrak{U}\subseteq B(0,\omega_*)$ of the origin in parameter space for which

$$\{(\mathfrak{X}(\lambda),\lambda):\lambda\in\mathfrak{U}\cap\mathfrak{L}_{\hat{x}}\}\quad\text{is a deformation of}\quad\{(\hat{x},\lambda):\lambda\in\mathfrak{U}\cap\mathcal{L}_{\hat{x}}\}:$$

to wit, both 'curves' can be parameterized by the same λ_j, $j=1,2$.

The preceding discussion shows that the fixed points of (5.4.1) are in one-to-one correspondence with the fixed points of the truncated map

$$\mathcal{P}_{\mathrm{T}}(x,\lambda)=x+2\pi\big[\lambda_1\mathcal{F}_0(x,0)+\lambda_2\mathcal{G}_\xi(x,0)\big] \tag{5.4.4}$$

which we studied in Sections 5.1–5.2.

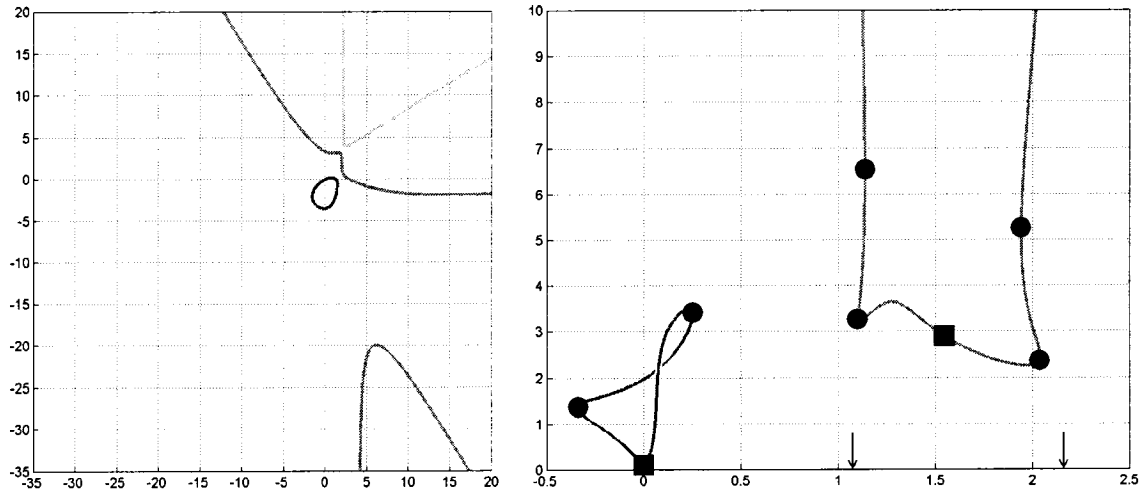

Figure 5.6: Fixed point branches of $\mathcal{P}_{0.01}$ for the perturbed Elowyn-Bonhomme problem. On the left, the fixed point branches of $\mathcal{P}_{0.01}$ are projected onto the $x-$plane; on the right, the norm of the branches through the origin (blue) and through ξ (red) are shown, plotted against s. The symbolism remains as it was in Section 5.3.

Fold bifurcations persist under small perturbations [36, 72]. Similarly, a generic unbounded curve remains unbounded under small perturbations (see p. 92 for details). Catastrophes thus generically persist: as a result, the bifurcation diagrams of (5.4.1) and (5.4.4) are (locally) topologically equivalent for small parameter values λ. Consequently, (5.4.1) has wedge-like regions $\mathfrak{W}_\eta$ corresponding to the wedge regions W_η of (5.1.1).

The Elowyn-Bonhomme Map Revisited

Let ξ, F_0 and G_ξ be as in the original EB map (see p. 78) and consider a small perturbation, defined *via*

$$\mathcal{F}_0(x,\lambda_1) = F_0(x) + \lambda_1 \begin{pmatrix} -\frac{28}{5}x_1 + 9x_2 - \frac{9}{5}x_1^2 - \frac{41}{10}x_1x_2 - \frac{57}{10}x_2^2 \\ -9x_1 - \frac{28}{5}x_2 - 9x_1^2 + \frac{49}{10}x_1x_2 - 10x_2^2 \end{pmatrix},$$

$$\mathcal{G}_\xi(x,\lambda_2) = G_\xi(x) + \lambda_2 \begin{pmatrix} 28 - 26x_1 + \frac{2}{5}x_2 + \frac{19}{2}x_1^2 - \frac{33}{10}x_1x_2 - \frac{2}{5}x_2^2 \\ \frac{2}{5} - \frac{38}{5}x_1 - 6x_2 + \frac{28}{5}x_1^2 - \frac{7}{2}x_1x_2 + \frac{23}{5}x_2^2 \end{pmatrix}$$

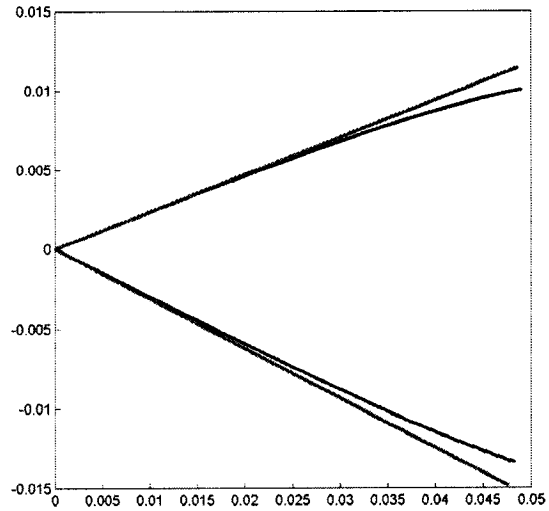

Figure 5.7: Wedges W_0 (in grey) and $\mathfrak{W}_0$ (in black) for the Elowyn-Bonhomme maps.

and

$$\mathcal{J}(x,\lambda) = \begin{pmatrix} \frac{67}{10} + \frac{32}{5}x_1 + \frac{18}{5}x_2 - \frac{33}{5}x_1^2 - x_1x_2 - \frac{8}{5}x_2^2 \\ \frac{59}{10} + \frac{31}{5}x_1 - \frac{46}{5}x_2 + \frac{5}{2}x_1^2 + \frac{79}{10}x_1x_2 + \frac{73}{10}x_2^2 \end{pmatrix}.$$

Then $\mathcal{F}_0(0,\lambda_1), \mathcal{G}_\xi(\xi,\lambda_2) \equiv 0$,

$$D_x\mathcal{F}_0(0,\lambda_1) = \begin{pmatrix} 2 - \frac{28}{5}\lambda_1 & -1 + 9\lambda_1 \\ 1 - 9\lambda_1 & 2 - \frac{28}{5}\lambda_1 \end{pmatrix}, D_x\mathcal{G}_\xi(\xi,\lambda_2) = \begin{pmatrix} -3 + \frac{27}{5}\lambda_2 & -\frac{1}{2} - \frac{39}{5}\lambda_2 \\ \frac{1}{2} + \frac{39}{5}\lambda_2 & -3 + \frac{27}{5}\lambda_2 \end{pmatrix},$$

$a(0) = 2$ and $c(0) = -3$. According to Proposition 5.4.1, $\mathcal{P}$ satisfies (P1)–(P3). By the preceding discussion, the bifurcation diagrams of the EB map P is topologically equivalent to that of $\mathcal{P}$ when λ is close enough to the origin.

As an example, let $0.01 < \omega_* = \frac{12}{37\pi}$ and define $\mathcal{P}_{0.01}$ as the restriction of $\mathcal{P}$ to the circle $\gamma_{0.01}(s) = 0.01\,(\cos(s), \sin(s))^\intercal$ in parameter space. Compare the diagrams shown in figures 5.3 and 5.4 to those of Figure 5.6: clearly, all the 'interesting' qualitative information regarding (5.4.1) for small parameter values λ is garnered from the (truncated) map (5.1.1) and the zero-set $\kappa(3)$.

Finally, note that since P is the 'linearization' of $\mathcal{P}$ at the origin with respect to λ, the wedge regions W_η of (5.1.1) provide tangential 'cones' for the corresponding wedge-like regions $\mathfrak{W}_\eta$ of (5.4.1). This phenomenon is illustrated in Figure 5.7, for both the original and the revisited EB maps.

5.5 Appendix: Technical Details

Technical Result 11 If ω_* is as in (5.1.2), (5.1.3)–(5.1.6) hold for all $0 \neq |\lambda_j| < \omega_*$, $j = 1, 2$.

Proof: We show (5.1.3) and (5.1.4) hold, the proof is similar for (5.1.5) and (5.1.6). Since $\det DF_0(0) = a^2 + b^2 > 0$ and $\operatorname{tr} DF_0(0) = 2a \neq 0$, (5.1.3) and (5.1.4) become

$$\pi^2\lambda_1^2 \det DF_0(0) + \pi\lambda_1 \operatorname{tr} DF_0(0) + 1 > 0, \tag{5.5.1}$$

$$\operatorname{tr} DF_0(0) + 2\pi\lambda_1 \det DF_0(0) \neq 0. \tag{5.5.2}$$

The discriminant $-4\pi^2 b^2$ of the left-hand term of (5.5.1) is negative if and only if $b \neq 0$. When $b = 0$, (5.5.1) holds as long as

$$\lambda_1 \neq -\frac{a}{(a^2+b^2)\pi} = -\frac{1}{a\pi}.$$

Thus (5.5.1) holds in general whenever λ_1 lies strictly between 0 and $\frac{|a|}{(a^2+b^2)\pi}$. As luck would have it, (5.5.2) also holds as long as

$$\lambda_1 \neq -\frac{a}{(a^2+b^2)\pi}.$$

In particular, both (5.5.1) and (5.5.2) hold whenever $0 \neq |\lambda_1| < \omega_*$. ∎

Technical Result 12 Let $A \in \mathbb{M}_2(\mathbb{R})$ and $\mu_{1,2}$ be the eigenvalues of A. If

$$(\det A - \operatorname{tr} A + 1) \cdot (\det A + \operatorname{tr} A + 1) > 0 \quad \text{and} \quad \det A \neq 1,$$

then μ_1 and μ_2 are either both inside or both outside the unit circle.

Proof: Recall that $\det A = \mu_1\mu_2$ and $\operatorname{tr} A = \mu_1 + \mu_2$. There are two possibilities.

1. If $\mu_1 = \overline{\mu_2} \notin \mathbb{R}$, then $\det A > 0$. The conclusion holds if and only if

   $$(|\mu_1|^2 - 1) \cdot (|\mu_2|^2 - 1) > 0,$$

   that is, if and only if $\det A = |\mu_1| \cdot |\mu_2| \neq 1$.

2. If $\mu_1, \mu_2 \in \mathbb{R}$, then $\mu_1^2 + \mu_2^2 = (\operatorname{tr} A)^2 - 2\det A$ and the following inequalities are equivalent:

$$\begin{gathered}(|\mu_1|^2 - 1) \cdot (|\mu_2|^2 - 1) > 0 \\ (\mu_1^2 - 1) \cdot (\mu_2^2 - 1) > 0 \\ \mu_1^2\mu_2^2 + 1 - (\mu_1^2 + \mu_2^2) > 0 \\ (\det A)^2 + 1 - (\operatorname{tr} A)^2 + 2\det A > 0 \\ (\det A + 1)^2 - (\operatorname{tr} A)^2 > 0 \\ (\det A - \operatorname{tr} A + 1) \cdot (\det A + \operatorname{tr} A + 1) > 0.\end{gathered}$$

The eigenvalues of A are complex conjugates if and only if $(\operatorname{tr} A)^2 - 4\det A < 0$. But this parabolic region is contained in the solution set of $(\det A - \operatorname{tr} A + 1) \cdot (\det A + \operatorname{tr} A + 1) > 0$ in the $(\det A, \operatorname{tr} A)$−plane, which yields the desired result. ∎

Technical Result 13 Let A, B, C and E be as in (5.2.1) and (5.2.11). Then (5.2.7) rewrites as (5.2.9).

Proof: Write

$$DF(x) = \begin{pmatrix} a & b \\ c & d \end{pmatrix} \quad \text{and} \quad DG_\xi(x) = \begin{pmatrix} e & f \\ g & h \end{pmatrix}.$$

Then

$$\begin{aligned}\det\big(\lambda_1 DF_0(x) + \lambda_2 DG_\xi(x)\big) &= \big(\lambda_1 a + \lambda_2 e\big)\big(\lambda_1 d + \lambda_2 h\big) - \big(\lambda_1 b + \lambda_2 f\big)\big(\lambda_1 c + \lambda_2 g\big) \\ &= \lambda_1^2\big(ad - bc\big) + \lambda_1\lambda_2\big(ah + de - bg - fc\big) + \lambda_2^2\big(eh - fg\big) \\ &= \lambda_1^2 B(x) + \lambda_1\lambda_2 C(x) + \lambda_2^2 E(x) \\ &= \lambda^\top Q(x)\lambda,\end{aligned}$$

which completes the proof. ∎

Technical Result 14 The origin is a regular point of $\mathfrak{L}_{\hat{x}}$.

Proof: Let j be the index of a non-zero row of $\mathcal{A}(\hat{x}, 0)$, and set $\mathcal{B}(\mathfrak{X}(\lambda), \lambda) = \mathcal{A}_j(\mathfrak{X}(\lambda), \lambda) \cdot \lambda$. Then the origin $\lambda = 0$ is a solution of $\mathcal{B}(\mathfrak{X}(\lambda), \lambda) = 0$; as such, it belongs to $\mathfrak{L}_{\hat{x}}$. Note that

$$\frac{\partial}{\partial\lambda_1}\mathcal{B}(\mathfrak{X}(0), 0) = \mathcal{A}_{j,1}(\hat{x}, 0) \quad \text{and} \quad \frac{\partial}{\partial\lambda_2}\mathcal{B}(\mathfrak{X}(0), 0) = \mathcal{A}_{j,2}(\hat{x}, 0).$$

Since $\mathcal{A}_j(\hat{x}, 0) \neq 0$, at least one of the partial derivatives above is non-zero; the origin is thus a regular point of $\mathfrak{L}_{\hat{x}}$. ∎

Technical Result 15 A generic unbounded planar curve remains unbounded under small perturbations.

Proof: In the real projective plane, an element of $\mathcal{C}_\infty$ meets the line at infinity in two points. Generically, these two points are distinct and a small perturbation will not change that fact, *i.e* the perturbed curve is still an element of $\mathcal{C}_\infty$. In the non-generic case where the two points at infinity are equal, a small perturbation will either cause the points to separate or to vanish entirely (reminiscent of a fold bifurcation of points at infinity), *i.e* the perturbed curve either stays in $\mathcal{C}_\infty$ or becomes finite. The classic example is a parabola, which can be perturbed into either an ellipse or a hyperbola. ∎

Chapter 6

Combined TSB and RSB Perturbations

In this chapter, we investigate another way in which Euclidean symmetry can be broken: combining rotational and translational symmetry breaking.

As a possible application, consider the following generalization of the bidomain equations describing the electrical properties of anisotropic cardiac tissue

$$\begin{aligned} u_t &= \tfrac{1}{\varsigma}(u - \tfrac{u^3}{3} - v) + \Delta u + \tfrac{\alpha\varepsilon}{1+\alpha(1-\varepsilon)}\Psi_{xx} \\ v_t &= \varsigma(u + \beta - \gamma v), \\ \Delta\Psi + \varepsilon g(\alpha,\varepsilon)\Psi_{yy} &= \varepsilon h(\alpha,\varepsilon)u_{yy}, \end{aligned} \tag{6.0.1}$$

where u is a transmembrane potential, v controls the recovery of the action potential, Ψ is an auxiliary potential (without obvious physical interpretation), x is the preferred direction in physical space in which tissue fibers align, ε is a measure of that preference, g and h are appropriate model functions, and α, ς, β and γ are model parameters [17, 50, 58]. If the tissue has equal anisotropy ratios (*i.e.*, $\varepsilon = 0$), (6.0.1) decouples into the FitzHugh-Nagumo equations for u and v, and Poisson's equation for Ψ [58].

Ignoring the boundaries, system (6.0.1) is $\mathbb{SE}(2)-$equivariant under the action of (2.1.8) when $\varepsilon = 0$, while it is only $\mathbb{R}^2\dot{+}\mathbb{Z}_2-$equivariant otherwise (see [50, section 2.2] for details).

Cardiac tissue is littered with inhomogeneities; let such a point be located at the origin in physical space. The situation is assumed[1] to be modeled by the (slightly) perturbed bidomain equations

$$\begin{aligned} u_t &= \tfrac{1}{\varsigma}(u - \tfrac{u^3}{3} - v) + \Delta u + \tfrac{\alpha\varepsilon}{1+\alpha(1-\varepsilon)}\Psi_{xx} + \mu g^u(x^2+y^2,\mu) \\ v_t &= \varsigma(u + \beta - \gamma v) + \mu g^v(x^2+y^2,\mu), \\ \Delta\Psi &+ \varepsilon g(\alpha,\varepsilon)\Psi_{yy} = \varepsilon h(\alpha,\varepsilon)u_{yy}, \end{aligned} \tag{6.0.2}$$

where μ is a small parameter and $g^{u,v}$ are smooth bounded functions.

The symmetry-breaking induced by anisotropy and the presence of the inhomogeneity at the origin then yields an equivariant structure on the semi-flow $\Phi_{t,\varepsilon,\mu}$ of (6.0.2):[2] it is $\mathbb{SE}(2)$−equivariant when $(\varepsilon,\mu)=0$; $\mathbb{Z}_2\dot{+}\mathbb{R}^2$−equivariant when $\varepsilon\neq 0$ is small and $\mu=0$; $\mathbb{SO}(2)$−equivariant when $\mu\neq 0$ is small and $\varepsilon=0$, and (generically) trivially equivariant when (ε,μ) is small and generic.[3]

Our study of forced Euclidean symmetry-breaking continues, along the lines presented in Chapters 3−5, with a generalization of this semi-flow.[4]

6.1 Center Bundle Equations

Set $\ell\in\mathbb{N}$. Let $\mathbb{C}\dot{+}\mathbb{Z}_\ell$ be the subgroup of $\mathbb{SE}(2)$ containing all translations and rotations by angle $\frac{2\pi k}{\ell}$, $k\in\mathbb{Z}$. Depending on the parametrization in use,

$$\mathbb{C}\dot{+}\mathbb{Z}_\ell = \left\{\left(R_{2\pi k/\ell}, S\right) : k\in\mathbb{Z}, S\in\mathbb{R}^2\right\}$$

acts on function spaces as in (2.1.8), or $\mathbb{C}\dot{+}\mathbb{Z}_\ell = \left\{\left(x, \frac{2\pi k}{\ell}\right) : k\in\mathbb{Z}, x\in\mathbb{C}\right\}$ acts on V_* as in (2.2.5).

Let $\Phi_{t,\varepsilon,\mu}$ be a semi-flow parameterized by the small vector $(\varepsilon,\mu)\in\mathbb{R}^2$. Suppose that $\Phi_{t,\varepsilon,\mu}$ is $\mathbb{SE}(2)$−equivariant when $(\varepsilon,\mu)=0$; $\mathbb{C}\dot{+}\mathbb{Z}_\ell$−equivariant when $\varepsilon\neq 0$ is small and $\mu=0$; $\mathbb{SO}(2)$−equivariant when $\mu\neq 0$ is small and $\varepsilon=0$, and (generically) trivially equivariant when (ε,μ) is small and generic.

[1] In much the same way as (3.1.1) was assumed to extend (2.1.1) in the presence of n TSB terms.
[2] The existence and uniqueness of such a semi-flow is shown in [22].
[3] This can be seen by slightly modifying the proof of Theorem 2.1.3, on p. 18.
[4] The proofs are often very similar and are omitted in an effort to avoid tedious repetitions.

To study the effects of combined symmetry-breaking on (normally hyperbolic) rotating waves, assume further that hypotheses 2.2.1 and 2.2.2 hold. Accordingly, there is a center-unstable manifold Q^{cu} satisfying the conclusion of Theorem 2.2.3, and which contains the group orbit $\mathbb{SE}(2)u_*$, and the dynamics on $\mathbb{SE}(2)u_*$ reduce to a system of differential equations

$$\begin{aligned} \dot{p} &= e^{i\varphi}\left[\nu + J^p(p,\overline{p},\varphi,\varepsilon,\mu)\right] \\ \dot{\varphi} &= \omega_{\text{rot}} + J^{\varphi}(p,\overline{p},\varphi,\varepsilon,\mu), \end{aligned} \tag{6.1.1}$$

on the center bundle V_* (which is diffeomorphic to Q^{cu}), where $(p,\varphi) \in \mathbb{C}\times\mathbb{S}^1$, $\nu \in \mathbb{C}$, $0 \neq \omega_{\text{rot}} \in \mathbb{R}$, $J^p(p,\overline{p},\varphi,0,0) \equiv 0$ and $J^{\varphi}(p,\overline{p},\varphi,0,0) \equiv 0$. Furthermore, the functions J^p and J^{φ} are smooth and uniformly bounded in p, and the flow on V_* described by (6.1.1) is equivalent to the semi-flow $\Phi_{t,\varepsilon,\mu}$ on Q^{cu} (see [48,62] for details).

Proposition 6.1.1 *System* (6.1.1) *is* $\mathbb{SE}(2)-$*equivariant when* $(\varepsilon,\mu) = 0$*; but it is only* $\mathbb{C}\dot{+}\mathbb{Z}_\ell-$*equivariant when* $\varepsilon \neq 0$ *is small and* $\mu = 0$*,* $\mathbb{SO}(2)-$*equivariant when* $\mu \neq 0$ *is small and* $\varepsilon = 0$*, and (generically) trivially equivariant when* (ε,μ) *is small and generic.*

After re-scaling time along orbits, (6.1.1) becomes

$$\begin{aligned} \dot{p} &= e^{i\varphi}\left[v + J(p,\overline{p},\varphi,\varepsilon,\mu)\right] \\ \dot{\varphi} &= 1, \end{aligned} \tag{6.1.2}$$

where $v \in \mathbb{C}$, $J \in \mathfrak{P}^{2\pi}_{\varphi}$ is smooth, uniformly bounded and $J(p,\overline{p},\varphi,0,0) \equiv 0$. As (6.1.2) also satisfies the equivariance conditions of proposition 6.1.1 (being equivalent to (6.1.1)), J is not completely arbitrary.

Proposition 6.1.2 *Let* N *be a system of differential equations which commutes with the action of* $\mathbb{C}\dot{+}\mathbb{Z}_\ell$ *on* V_**. Then* N *has the form*

$$\begin{aligned} \dot{p} &= N^p(p,\varphi) = e^{i\varphi}H^p(\varphi) \\ \dot{\varphi} &= N^{\varphi}(p,\varphi) = H^{\varphi}(\varphi), \end{aligned} \tag{6.1.3}$$

where $H^p, H^{\varphi} \in \mathfrak{P}^{2\pi/\ell}_{\varphi}$.

Since $J(p,\overline{p},\varphi,0,0) \equiv 0$, Taylor's Theorem implies there are smooth and uniformly bounded functions J_1, J_2 such that

$$J(p,\overline{p},\varphi,\varepsilon,\mu) = \varepsilon J_1(p,\overline{p},\varphi,\varepsilon,\mu) + \mu J_2(p,\overline{p},\varphi,\varepsilon,\mu).$$

Re-write (6.1.2) as

$$\begin{aligned} \dot{p} &= e^{i\varphi}\left[v + \varepsilon J_1(p,\overline{p},\varphi,\varepsilon,\mu) + \mu J_2(p,\overline{p},\varphi,\varepsilon,\mu)\right] \\ \dot{\varphi} &= 1. \end{aligned} \tag{6.1.4}$$

As (6.1.4) and (6.1.1) are equivalent, (6.1.4) is $\mathbb{C}\dot{+}\mathbb{Z}_\ell$–equivariant when $(\varepsilon,\mu) = (\varepsilon,0)$ and $\mathbb{SO}(2)$–equivariant when $(\varepsilon,\mu) = (0,\mu)$. Applying Propositions 3.2.1 and 6.1.2, we get, for some smooth and uniformly bounded functions $G \in \mathfrak{P}_\varphi^{2\pi/\ell}$ and H,

$$\begin{aligned} J(p,\overline{p},\varphi,\varepsilon,0) &= \varepsilon G(\varphi,\varepsilon) \\ J(p,\overline{p},\varphi,0,\mu) &= \mu H(pe^{-i\varphi},\overline{p}e^{i\varphi},\mu). \end{aligned}$$

Thus, adapting the contents of footnote 4 on page 39 to the situation at hand, the essential dynamics of the semi-flow $\Phi_{t,\varepsilon,\mu}$ (near the (normally hyperbolic) rotating wave u_*) are described by **center bundle equations** of the form

$$\begin{aligned} \dot{p} &= e^{i\varphi}\left[v + \varepsilon G(\varphi,\varepsilon) + \mu H(pe^{-i\varphi},\overline{p}e^{i\varphi},\mu)\right] \\ \dot{\varphi} &= 1, \end{aligned} \tag{6.1.5}$$

where $(\varepsilon,\mu) \in \mathbb{R}^2$, $v \in \mathbb{C}$ and $G \in \mathfrak{P}_\varphi^{2\pi/\ell}, H$ are smooth and uniformly bounded in p.

6.2 Analysis of the Center Bundle Equations

The cases $\varepsilon = 0$ and $\mu = 0$ have been studied extensively by LeBlanc and Wulff [51] and LeBlanc [48], respectively; their papers are discussed in the introduction and in appendix A, pp. 147–152.

We can assume, without loss of generality, that $\varphi(t) = t$. Then, system (6.1.5) re-writes as

$$\dot{p} = e^{it}\left[v + \varepsilon G(t,\varepsilon) + \mu H(pe^{-it},\overline{p}e^{it},\mu)\right], \tag{6.2.1}$$

where $G \in \mathfrak{P}_t^{2\pi/\ell}, H$ are smooth and uniformly bounded in p.

The specific value of ℓ will play a crucial role in the following analysis. Some of the results presented in this section are also found in [11,12].

6.2.1 The Case $\ell = 1$

As $G \in \mathfrak{P}_t^{2\pi}$, it can be written as the uniformly convergent Fourier series

$$G(t,\varepsilon) = \sum_{n\in\mathbb{Z}} g_n(\varepsilon)e^{int}. \tag{6.2.2}$$

Let $F_G : \mathbb{R}\times\mathbb{R} \to \mathbb{C}$ be defined by

$$F_G(t,\varepsilon) = e^{it}\Big[-iv + \varepsilon \sum_{n\neq -1} \frac{g_n(\varepsilon)e^{int}}{i(n+1)}\Big]. \tag{6.2.3}$$

Differentiating (6.2.3) yields

$$\dot{F}_G(t,\varepsilon) = e^{it}\big[v + \varepsilon G(t,\varepsilon) - \varepsilon g_{-1}(\varepsilon)\big]. \tag{6.2.4}$$

On V_*, the path $(F_G(t,\varepsilon),t)$ represents generically a discrete rotating wave around the origin with trivial spatio-temporal symmetry (see p. 106 for details). Set $z = p - F_G$. Then, using (6.2.4), (6.2.1) rewrites as

$$\begin{aligned}\dot{z} &= \dot{p} - \dot{F}_G \\ &= e^{it}\big[v + \varepsilon G(t,\varepsilon) + \mu H((z+F_G(t,\varepsilon))e^{-it}, \text{c.c.}, \mu)\big] - \dot{F}_G(t,\varepsilon) \\ &= \varepsilon g_{-1}(\varepsilon) + \mu e^{it} H((z+F_G(t,\varepsilon))e^{-it}, \text{c.c.}, \mu).\end{aligned} \tag{6.2.5}$$

Generically, $g_{-1}(0) \neq 0$ and so $g_{-1}(\varepsilon) \neq 0$ in some neighbourhood of the origin, by continuity. In particular, (6.2.5) does not have a periodic solution when $\mu = 0$ and $\varepsilon \neq 0$. However, (6.2.5) reduces to (4.0.1) with $n = 1$ when $\varepsilon = 0$.

Set $\varepsilon = \hat{\varepsilon}\mu$. Then (6.2.5) can be viewed as a perturbation of (4.0.1) with $n = 1$. Moreover, it transforms to

$$\dot{z} = \mu H_*(ze^{-it}, \overline{z}e^{it}, t, \hat{\varepsilon}, \mu), \tag{6.2.6}$$

where

$$H_*(w,\overline{w},t,\hat{\varepsilon},\mu) = \hat{\varepsilon}g_{-1}(\hat{\varepsilon}\mu) + e^{it}H(w + F_G(t,\hat{\varepsilon}\mu)e^{-it}, \text{c. c.}, \mu)$$

is $2\pi-$periodic in t, smooth and uniformly bounded in w.

Spiral Anchoring

Set $a_1 = D_1H(-iv, i\overline{v}, 0, 0)$. Near $(z, \hat{\varepsilon}, \mu) = (0, 0, 0)$, the Poincaré map P of (6.2.6) is given by

$$P(z, \hat{\varepsilon}, \mu) = z + 2\pi\mu\Big[\hat{\varepsilon}g_{-1}(0) + a_1 z + O\big(|z|^2\big) + O\big(\mu\big) + \text{h.o.t.}\Big]. \tag{6.2.7}$$

The fixed points of (6.2.7) correspond to $2\pi-$periodic solutions of (6.2.6), and so to discrete rotating waves with trivial spatio-temporal symmetry in (6.1.5). Let

$$B_*(z, \overline{z}, \hat{\varepsilon}, \mu) = \hat{\varepsilon}g_{-1}(0) + a_1 z + O\big(|z|^2\big) + O(\mu) + \text{h.o.t}$$

be the function inside the square brackets in (6.2.7). Note that $B_*(0, 0, 0, 0) = 0$ and that, generically, $D_1B_*(0, 0, 0, 0) = a_1 \neq 0$. By the Implicit Function Theorem, there is a unique smooth function $z(\hat{\varepsilon}, \mu)$ defined near $(\hat{\varepsilon}, \mu) = (0, 0)$ with $z(0, 0) = 0$ and

$$B_*\big(z(\hat{\varepsilon}, \mu), \overline{z}(\hat{\varepsilon}, \mu), \hat{\varepsilon}, \mu\big) \equiv 0$$

near $z = 0$. However $z = 0$ is not in general a solution of $B_* = 0$ for a small pair $(\hat{\varepsilon}, \mu)$, unless $g_{-1}(0) = 0$. Thus the generic behaviour of discrete rotating waves in (6.1.5) is to locally drift away from the origin. This leads to the following theorem.

Theorem 6.2.1 *Let $g_{-1}(0) \neq 0$ and a_1 be as above, with $\text{Re}(a_1) \neq 0$. Then there exists a wedge-shaped region near $(\varepsilon, \mu) = (0, 0)$ of the form*

$$\mathcal{W} = \{(\varepsilon, \mu) \in \mathbb{R}^2 : |\varepsilon| < K|\mu|, \ K > 0, \ \mu \text{ near } 0\}$$

such that for all $(\varepsilon, \mu) \in \mathcal{W}$ with $\varepsilon \neq 0$, (6.1.5) has a unique hyperbolic discrete rotating wave $\mathcal{D}^1_{\varepsilon,\mu}$ with trivial spatio-temporal symmetry with center $[\mathcal{D}^1_{\varepsilon,\mu}]_A$ near, but generically not at, the origin. Furthermore, $[\mathcal{D}^1_{\varepsilon,\mu}]_A$ is a center of anchoring when $\mu\,\text{Re}(a_1) < 0$.

When the parameter values stray outside of $\mathcal{W}$, all that can generically be said with certainty is that solutions of (6.1.5) do not anchor at the origin. After drifting, the spiral may very well get anchored at some point far from the origin, depending on the global nature of the perturbation function H in (6.1.5) (see Section 6.3 for more details).

To complete the picture, the situation would also need to be analyzed near the $\varepsilon-$axis. As this implies dealing with fixed points of (6.2.7) at ∞ (which introduces some complications, see [48, 51] for instance), it lies outside the scope of this thesis and will be investigated in detail at a later date.

Epicyclic Drifting

Consider the near-identity change of variables

$$z = w + \mu\varrho(w, \overline{w}, t, \varepsilon, \mu) \tag{6.2.8}$$

where $\varrho \in \mathfrak{P}_t^{2\pi}$ is continuous in all of its variables. This change of variables transform (6.2.6) into the equivalent system

$$\dot{w} = \mu\left(H_*(we^{-it}, \overline{w}e^{it}, t, \hat{\varepsilon}, 0) - \varrho_t(w, \overline{w}, t, \hat{\varepsilon}, 0)\right) + \mu^2\mathcal{H}_*(w, \overline{w}, t, \hat{\varepsilon}, \mu), \tag{6.2.9}$$

where $\mathcal{H}_* \in \mathfrak{P}_t^{2\pi}$ is bounded and continuous in all its variables. Denote the average value of $H_*(we^{-it}, \overline{w}e^{it}, t, \hat{\varepsilon}, 0)$ by

$$M_*(w, \overline{w}, \hat{\varepsilon}) = \frac{1}{2\pi}\int_0^{2\pi} H_*(we^{-it}, \overline{w}e^{it}, t, \hat{\varepsilon}, 0)\, dt.$$

But

$$\begin{aligned} H_*(we^{-it}, \overline{w}e^{it}, t, \hat{\varepsilon}, 0) &= \hat{\varepsilon}g_{-1}(0) + e^{it}H\left((w + F_G(t, 0, 0))e^{-it}, \text{c. c.}, 0\right) \\ &= \hat{\varepsilon}g_{-1}(0) + e^{it}H(we^{-it} - iv, \overline{w}e^{it} + i\overline{v}, 0), \end{aligned}$$

and so

$$M_*(w, \overline{w}, \hat{\varepsilon}) = \hat{\varepsilon}g_{-1}(0) + \frac{1}{2\pi}\int_0^{2\pi} e^{it}H(we^{-it} - iv, \overline{w}e^{it} + i\overline{v}, 0)\, dt.$$

Then

$$H_*(we^{-it}, \overline{w}e^{it}, t, \hat{\varepsilon}, 0) = M_*(w, \overline{w}, \hat{\varepsilon}) + F_*(w, \overline{w}, t, \hat{\varepsilon}),$$

where $F_* \in \mathfrak{P}_t^{2\pi}$ is uniformly continuous and

$$\int_0^{2\pi} F_*(w, \overline{w}, t, \hat{\varepsilon})\, dt = 0. \tag{6.2.10}$$

Let ϱ be an antiderivative of F_* with respect to t. Then $\varrho \in \mathfrak{P}_t^{2\pi}$ by (6.2.10) and

$$F_*(w, \overline{w}, t, \hat{\varepsilon}) - \varrho_t(w, \overline{w}, t, \hat{\varepsilon}, 0) = 0.$$

With such a ϱ, (6.2.9) simplifies to

$$\dot{w} = \mu M_*(w, \overline{w}, \hat{\varepsilon}) + \mu^2\mathcal{H}_*(w, \overline{w}, t, \hat{\varepsilon}, \mu). \tag{6.2.11}$$

As $M_*(w,\overline{w},0)$ is $\mathbb{S}^1-$equivariant (see p. 64 for details), there exists a continuous function $L_* : \mathbb{R} \to \mathbb{C}$ such that $M_*(w,\overline{w},0) = wL_*(w\overline{w})$ (see [33], p. 360 for details), and so (6.2.11) becomes

$$\dot{w} = \mu w L_*(w\overline{w}) + \mu W_*(w,\overline{w},t,\hat{\varepsilon},\mu), \tag{6.2.12}$$

where

$$W_*(w,\overline{w},t,\hat{\varepsilon},\mu) = \hat{\varepsilon} g_{-1}(0) + \mu \mathcal{H}_*(w,\overline{w},t,\hat{\varepsilon},\mu). \tag{6.2.13}$$

Differentiating the polar coordinates $w = \rho e^{-i(\psi - t)}$ and substituting in 6.2.12 yields

$$\begin{aligned} \dot{\rho} &= \mu R_*(\rho) + \mu R(t,\psi,\rho,\hat{\varepsilon},\mu) \\ \dot{\psi} &= 1 + \mu \Psi_*(\rho) + \mu \Psi(t,\psi,\rho,\hat{\varepsilon},\mu), \end{aligned} \tag{6.2.14}$$

where $R_*(\rho) = \rho \operatorname{Re}[L_*(\rho^2)]$, $\Psi_*(\rho) = -\operatorname{Im}[L_*(\rho^2)]$, $R, \Psi \in \mathfrak{P}_t^{2\pi} \cap \mathfrak{P}_\psi^{2\pi}$ and Ψ is not continuous at $\rho = 0$.

We now give sufficient conditions for the existence of an epicycle manifold in (6.1.5).

Theorem 6.2.2 *Assume that R and Ψ, as defined in* (6.2.14), *are C^1 on intervals away from $\rho = 0$ and that the averaged equation*

$$\dot{\rho} = \mu R_*(\rho) \tag{6.2.15}$$

has an equilibrium $\rho_0 > 0$ with $D_\rho R_*(\rho_0) = \gamma_0 \neq 0$. If the parameters are small enough, there exists a wedge-shaped region near $(\varepsilon,\mu) = (0,0)$ of the form

$$\mathcal{V} = \{(\varepsilon,\mu) \in \mathbb{R}^2 : |\varepsilon| < K|\mu|,\ K > 0,\ \mu \text{ near } 0\}$$

such that for all $(\varepsilon,\mu) \in \mathcal{V}$, $\mu \neq 0$, (6.1.5) *has an epicycle manifold $\mathcal{G}^1_{\varepsilon,\mu}$, with $[\mathcal{G}^1_{\varepsilon,\mu}]_D$ near, but generically not at, the origin. Furthermore, $[\mathcal{G}^1_{\varepsilon,\mu}]_D$ is a center of drifting when $\mu\gamma_0 < 0$.*

These epicycle manifolds need not in general be unique for a given $(\varepsilon,\mu) \in \mathcal{V}$ as $R_*(\rho) = 0$ may have any number of hyperbolic solutions.

When the parameter values stray outside of $\mathcal{V}$, all that can generically be said is that the center of drifting of the epicycle manifolds in (6.1.5) is near the origin.

The remark following Theorem 6.2.1 concerning the behaviour near the $\varepsilon-$axis also applies to epicycle manifolds.

6.2.2 The Case $\ell > 1$

Let $C^0_{\mathbb{R}}(\mathbb{C})$ and $C^1_{\mathbb{R}}(\mathbb{C})$ be the spaces of continuous and continuously differentiable functions from $\mathbb{R}$ to $\mathbb{C}$, respectively. Then

$$C^0_{2\pi/\ell} = \{f : f \in \mathfrak{P}_t^{2\pi/\ell} \cap C^0_{\mathbb{R}}(\mathbb{C})\} \quad \text{and} \quad C^1_{2\pi/\ell} = \{f : f \in \mathfrak{P}_t^{2\pi/\ell} \cap C^1_{\mathbb{R}}(\mathbb{C})\}$$

are Banach spaces when endowed with the respective norms

$$||u||_0 = \sup\{|u(x)| : x \in [0, \tfrac{2\pi}{\ell}]\} \quad \text{and} \quad ||u||_1 = ||u||_0 + ||u'||_0,$$

and the linear operator $\mathcal{Y} : C^1_{2\pi/\ell} \to C^0_{2\pi/\ell}$ defined by $\mathcal{Y}(u) = iu + u'$ is bounded, invertible and has bounded inverse (see [60] for details).

As $G \in \mathfrak{P}_t^{2\pi/\ell}$, it can be written as the Fourier series

$$G(t, \varepsilon) = \sum_{n \in \mathbb{Z}} g_n(\varepsilon) e^{in\ell t}. \tag{6.2.16}$$

Define the nonlinear operator $\mathcal{H}_G : C^1_{2\pi/\ell} \times \mathbb{R}^2 \to C^0_{2\pi/\ell}$ by

$$\mathcal{H}_G(u, \varepsilon, \mu) = \mathcal{Y}(u) - \mu H\left(u - iv + \varepsilon \sum_{n \in \mathbb{Z}} \frac{g_n(\varepsilon) e^{in\ell t}}{i(n\ell + 1)}, \text{c.c.}, \mu\right). \tag{6.2.17}$$

Note that $\mathcal{H}_G(0, 0, 0) = 0$ and $D_1\mathcal{H}_G(0, 0, 0) = i + \frac{d}{dt} \neq 0$. Thus, by the Implicit Function Theorem, there is a neighbourhood $\mathcal{N}$ of the origin in $\mathbb{R}^2$ and a unique smooth function $U : \mathbb{R}^2 \to C^1_{2\pi/\ell}$ satisfying $U(0, 0) = 0$ and $\mathcal{H}_G(U(\varepsilon, \mu), \varepsilon, \mu) \equiv 0$ for all $(\varepsilon, \mu) \in \mathcal{N}$.

Let $F_G : \mathbb{R} \times \mathbb{R}^2 \to \mathbb{C}$ be defined by

$$F_G(t, \varepsilon, \mu) = e^{it}\Big[- iv + \varepsilon \sum_{n \in \mathbb{Z}} \frac{g_n(\varepsilon) e^{in\ell t}}{i(n\ell + 1)} + U(\varepsilon, \mu)(t)\Big]. \tag{6.2.18}$$

Then

$$\mathcal{Y}(U(\varepsilon, \mu))(t) = \mu H\left(F_G(t, \varepsilon, \mu) e^{-it}, \text{c.c.}, \mu\right) \tag{6.2.19}$$

and

$$\dot{F}_G(t, \varepsilon, \mu) = e^{it}\big[v + \varepsilon G(t, \varepsilon) + \mathcal{Y}\left(U(\varepsilon, \mu)\right)(t)\big]. \tag{6.2.20}$$

On V_*, the path $(F_G(t,\varepsilon,\mu),t)$ represents a discrete rotating wave around the origin with $\mathbb{Z}_\ell$–spatio-temporal symmetry (see p. 106 for details). Set $z = p - F_G$. Then, using (6.2.19) and (6.2.20), (6.2.1) rewrites as

$$\begin{aligned}\dot{z} &= \dot{p} - \dot{F}_G \\ &= e^{it}\big[v + \varepsilon G(t,\varepsilon) + \mu H((z + F_G(t,\varepsilon,\mu))e^{-it}, \text{c.c.}, \mu)\big] - \dot{F}_G(t,\varepsilon,\mu) \\ &= \mu e^{it}\big[H((z + F_G(t,\varepsilon,\mu))e^{-it}, \text{c.c.}, \mu) - H(F_G(t,\varepsilon,\mu)e^{-it}, \text{c.c.}, \mu))\big],\end{aligned} \tag{6.2.21}$$

which reduces to

$$\dot{z} = \mu e^{it}\widehat{H}(ze^{-it}, \overline{z}e^{it}, t, \varepsilon, \mu), \tag{6.2.22}$$

where $\widehat{H} \in \mathfrak{P}_t^{2\pi/\ell}$ is defined by

$$\widehat{H}(w,\overline{w},t,\varepsilon,\mu) = H(w + F_G(t,\varepsilon)e^{-it}, \text{c.c.}, \mu) - H(F_G(t,\varepsilon)e^{-it}, \text{c.c.}, \mu).$$

Spiral Anchoring

Near $(z,\varepsilon,\mu) = (0,0,0)$, the Poincaré map P of (6.2.22) is given by

$$P(z,\varepsilon,\mu) = z + 2\pi\mu\Big[(a_1 + O(\varepsilon,\mu))z + O(\varepsilon,\mu)\overline{z} + O\big(|z|^2\big)\Big], \tag{6.2.23}$$

where a_1 is as defined in Section 6.2.1. The fixed points of (6.2.23) correspond to 2π–periodic solutions of (6.2.22), and so to discrete rotating waves with $\mathbb{Z}_\ell$–spatio-temporal symmetry in (6.1.5). Let

$$B^*(z,\overline{z},\varepsilon,\mu) = (a_1 + O(\varepsilon,\mu))z + O(\varepsilon,\mu)\overline{z} + O\big(|z|^2\big)$$

be the function inside the square brackets in (6.2.23). Note that $B^*(0,0,0,0) = 0$ and that, generically, $D_1B^*(0,0,0,0) = a_1 \neq 0$. By the Implicit Function Theorem, there is a unique smooth function $z(\varepsilon,\mu)$ defined near $(\varepsilon,\mu) = (0,0)$ with $z(0,0) = 0$ and

$$B^*\big(z(\varepsilon,\mu), \overline{z}(\varepsilon,\mu), \varepsilon, \mu\big) \equiv 0$$

near $z = 0$. But $z = 0$ is always a solution of $B^* = 0$; hence $z(\varepsilon,\mu) = 0$ for all small enough (ε,μ). This leads to the following theorem.

Theorem 6.2.3 *Let a_1 be as in the preceding discussion, with $\mathrm{Re}(a_1) \neq 0$. If (ε,μ) is in a (small enough) deleted neighbourhood $\mathcal{W}^\ell$ of the origin, (6.1.5) has a unique hyperbolic discrete rotating wave $\mathcal{D}^\ell_{\varepsilon,\mu}$ with $\mathbb{Z}_\ell$–spatio-temporal symmetry and center $[\mathcal{D}^\ell_{\varepsilon,\mu}]_A = 0$. Furthermore, $\mathcal{D}^\ell_{\varepsilon,\mu}$ is anchored at the origin if $\mathrm{Re}(a_1)\mu < 0$.*

Epicyclic Drifting

Combining the methods of the previous sections, (6.2.22) becomes

$$\begin{aligned} \dot{\rho} &= \mu R_*(\rho) + \mu R(t, \psi, \rho, \varepsilon, \mu) \\ \dot{\psi} &= 1 + \mu \Psi_*(\rho) + \mu \Psi(t, \psi, \rho, \varepsilon, \mu), \end{aligned} \tag{6.2.24}$$

where $R_*(\rho) = \rho \operatorname{Re}[L_*(\rho^2)]$, $\Psi_*(\rho) = -\operatorname{Im}[L_*(\rho^2)]$, $R, \Psi \in \mathfrak{P}_t^{2\pi} \cap \mathfrak{P}_\psi^{2\pi}$ and Ψ is not continuous at $\rho = 0$.

Theorem 6.2.4 *Assume that R and Ψ, as defined in* (6.2.24), *are C^1 on intervals away from $\rho = 0$ and that the averaged equation*

$$\dot{\rho} = \mu R_*(\rho) \tag{6.2.25}$$

has an equilibrium $\rho_0 > 0$ with $D_\rho R_*(\rho_0) = \gamma_0 \neq 0$. If the parameters are in a (small enough) deleted neighbourhood $\mathcal{V}^\ell$ of the origin, (6.1.5) *has an epicycle manifold $\mathcal{G}^\ell_{\varepsilon,\mu}$, with $[\mathcal{G}^\ell_{\varepsilon,\mu}]_{\mathrm{D}} = 0$. Furthermore, the origin is a center of drifting when $\mu\gamma_0 < 0$.*

These epicycle manifolds need not in general be unique for an admissible (ε, μ) as $R_*(\rho) = 0$ may have any number of hyperbolic solutions.

Note further that the epicycle manifolds do *not* have $\mathbb{Z}_\ell$–spatio-temporal symmetry as the averaged system defined by (6.2.24) is only $\frac{2\pi}{\ell}$–periodic in t when $R \equiv 0$ and $\Psi \equiv 0$, which is not generically the case; however, the epicycles themselves possess this symmetry in an appropriate rotating frame of reference.

6.3 Characterization of Spiral Anchoring ($\ell = 1$)

We now provide a characterization of spiral anchoring in the case $\ell = 1$.

Let $P : \mathbb{R}^2 \times \mathbb{R}^2 \to \mathbb{R}^2$ be a real analytic map with $P(x, 0) = x$, $DP(x, 0) = I_2$ for all $x \in \mathbb{R}^2$, satisfying the following conditions:

(Q1) $\exists \omega_* > 0$ such that $P(0, (0, \mu)) \equiv 0$ for all $|\mu| < \omega_*$;

(Q2) if $\mu = 0$ and $\varepsilon \neq 0$, P has no fixed point;

(Q3) the eigenvalues of $DP(0,(0,\mu))$ lie both outside or both inside the unit circle for all $0 \neq |\mu| < \omega_*$;

(Q4) there is an open wedge region w surrounding the coordinate axis μ in parameter space in which P has a (locally) unique manifold $x(\varepsilon,\mu)$ such that, for all $(\varepsilon,\mu) \in \mathsf{w}$,

1. $P(x(\varepsilon,\mu) \equiv x(\varepsilon,\mu)$;
2. $x(\varepsilon,\mu) \to 0$ as $\varepsilon \to 0$, $\mu \neq 0$;
3. $x(\varepsilon,\mu)$ shares its stability with the origin in (Q3).

For instance, when the hypotheses of Theorem 6.2.1 hold, the associated Poincaré map (6.2.7) (viewed in real coordinates) satisfies (Q1)–(Q4).

The Visual Criterion Revisited

Consider the mapping $P : \mathbb{R}^2 \times \mathbb{R}^2 \to \mathbb{R}^2$ given by

$$P(x,\varepsilon,\mu) = x + 2\pi\big[\varepsilon\aleph + \mu H(x)\big], \tag{6.3.1}$$

where $\aleph \neq 0 \in \mathbb{R}^2$ and H is a real analytic function of $x \in \mathbb{R}^2$. Such a map is obtained by truncating the parameter terms of order ≥ 2 from the Poincaré map (6.2.7), for instance.

Proposition 6.3.1 *If* $\aleph \neq 0$, $H(0) = 0$ *and*

$$DH(0) = \begin{pmatrix} a & -b \\ b & a \end{pmatrix}$$

where $a \neq 0$, *then there exists* $\omega_* > 0$ *such that the map defined by* (6.3.1) *satisfies the conditions* (Q1)–(Q4).

Define $A : \mathbb{R}^2 \to \mathbb{M}_2(\mathbb{R})$ by

$$A(x) = \big[\aleph \;\; H(x)\big], \tag{6.3.2}$$

and let L_x, $B(0,\omega_*)$, L_x, ρ, P_ρ and $\mathsf{L}_x^\rho = \{\pm\alpha_{x,\rho}\}$ be defined as in Chapter 5, but using (6.3.2) instead of (5.2.1). Set $\varpi(\mathfrak{Z}) = Z_{\mathbb{R}^2}(\det A(x))$ and $\mathcal{R} = Z_{\mathbb{R}^2}(\det DH(x))$. By construction, $0 \in \varpi(\mathfrak{Z})$.

The following result is analogous to Proposition 5.3.1.

Proposition 6.3.2 *If x^* is a transverse intersection of $\varpi(\mathfrak{Z})$ and $\mathcal{R}$, then P_ρ undergoes a fold catastrophe at (x^*, s^*) for all s^* such that $\gamma_\rho(s^*) = \pm\alpha_{x^*,\rho}$.*

The visual criterion can then be applied to $\varpi(\mathfrak{Z})$ exactly as it was applied to $\kappa(\mathfrak{Z})$ in section 5.3 to provide a bifurcation diagram for P_ρ and a maximal open wedge region W for (6.3.1).

Property (Q2) not only implies that the wedge angles $\varphi^\pm$ are well-defined, but it also allows us to locate them in $(0, \frac{\pi}{2})$, when they record a fold catastrophe, or in $(0, \frac{\pi}{2}]$ otherwise. Thus, W is guaranteed to never overlap the $\mu-$axis in parameter space; this is in marked contrast with the situation described in chapter 5.

The General Mapping

The mapping (6.3.1) is not the most general mapping satisfying (Q1)$-$(Q4); one should instead study maps of the form

$$\mathcal{P}(x, \lambda) = x + 2\pi\big[\varepsilon\Upsilon(\varepsilon) + \varepsilon\mu\mathcal{K}(x, \varepsilon, \mu) + \mu\mathcal{H}(x, \mu)\big], \tag{6.3.3}$$

where $0 \neq \Upsilon(0) \in \mathbb{R}^2$, $\Upsilon, \mathcal{K}, \mathcal{H}$ are real-analytic in their variables and the jacobian $D_x\mathcal{H}(0, \mu)$ has the particular form prescribed by Proposition 6.3.3, which is analogous to Proposition 6.3.1.

Proposition 6.3.3 *If $\mathcal{H}(0, \mu) \equiv 0$ and*

$$D_x\mathcal{H}(0, \mu) = \begin{pmatrix} a(\mu) & -b(\mu) \\ b(\mu) & a(\mu) \end{pmatrix}$$

where $a, b : \mathbb{R} \to \mathbb{R}$ are continuous and $a(0) \neq 0$, then there exists $\omega_* > 0$ such that the map defined by (6.3.3) *satisfies the conditions* (Q1)$-$(Q4).

Following the arguments of Section 5.4, it is possible to show that the bifurcation diagrams of (6.3.3) and

$$\mathcal{P}_{\mathrm{T}}(x, \varepsilon, \mu) = x + 2\pi\big[\varepsilon\Upsilon(0) + \mu\mathcal{H}(x, 0)\big],$$

which is of the form (6.3.1), are (locally) topologically equivalent for small parameter values (ε, μ). Consequently, (6.3.3) has a wedge-like region $\mathfrak{W}$ corresponding to the (tangential) wedge region W described above.

6.4 Appendix: Technical Details

Technical Result 16 F_G gives rise to a discrete rotating wave around the origin, with trivial spatio-temporal symmetry.

Proof: Let $k \in \mathbb{Z}$. The element $\overline{k} \in \mathbb{C}\dot{+}\mathbb{Z}_1$ acts on V_* as the identity $\overline{k}\cdot(p,\varphi) = (p,\varphi)$. In particular, $\overline{k}\cdot(F_G(t,\varepsilon),t) = (F_G(t,\varepsilon),t)$. The spatial action thus sends F_G to itself, without the need for time evolution. This completes the proof. ∎

Technical Result 17 F_G gives rise to a discrete rotating wave around the origin, with $\mathbb{Z}_\ell$–spatio-temporal symmetry.

Proof: Let $k \in \mathbb{Z}$. The element $\overline{k} = (0, \frac{2\pi k}{\ell}) \in \mathbb{C}\dot{+}\mathbb{Z}_\ell$ acts on V_* as

$$\overline{k}\cdot(p,\varphi) = \left(e^{2\pi ik/\ell}p, \varphi + \tfrac{2\pi k}{\ell}\right).$$

In particular,

$$\begin{aligned}
\overline{k}\cdot(F_G(t,\varepsilon,\mu),t) &= \left(e^{2\pi ik/\ell}F_G(t,\varepsilon,\mu), t+\tfrac{2\pi k}{\ell}\right)\\
&= \left(e^{2\pi ik/\ell}e^{it}\Big[-iv+\varepsilon\sum_{n\in\mathbb{Z}}\frac{g_n(\varepsilon,\mu)e^{in\ell t}}{i(n\ell+1)} + U(\varepsilon,\mu)(t)\Big], t+\tfrac{2\pi k}{\ell}\right)\\
&= \left(e^{i(t+2\pi k/\ell)}\Big[-iv+\varepsilon\sum_{n\in\mathbb{Z}}\frac{g_n(\varepsilon,\mu)e^{in\ell(t+2\pi k/\ell)}}{i(n\ell+1)} + U(\varepsilon,\mu)(t+\tfrac{2\pi k}{\ell})\Big], t+\tfrac{2\pi k}{\ell}\right)\\
&= \left(F_G(t+\tfrac{2\pi k}{\ell},\varepsilon,\mu), t+\tfrac{2\pi k}{\ell}\right),
\end{aligned}$$

since $U(\varepsilon,\mu) \in \mathfrak{P}_t^{2\pi/\ell}$. Thus the spatial action of $\overline{k}$ corresponds to time evolution by $\frac{2\pi k}{\ell}$. This completes the proof. ∎

Chapter 7

Examples and Simulations

In this chapter, we illustrate and interpret the results of Chapters 4, 5 and 6 through various examples. As such, the emphasis lies with qualitative observations rather than with precise numerical analysis. First, we study systems of PDE from a (naive) numerical perspective: we observe spiral anchoring, as well as hysteresis and homotopy of the spiral tip. We then show that these can, in a sense, be predicted from (4.0.1) and (6.1.5) by exhibiting center bundle systems in which they (and other interesting phenomena) occur. Finally, we provide various examples of mappings of the form (5.4.1) together with their zero-level sets and partial bifurcation diagrams.

7.1 PDE and Semi-Flows

In this section, we examine systems of partial differential equations giving rise to semi-flows satisfying the FESB equivariance described in Chapters 3 and 6.

The computations are carried out on a two-dimensional square domain [1] with Neumann boundary condition, using a 5-point Laplacian and i) the Euler forward integrator in section 7.1.1, and ii) Matsui's fourth-order Runge-Kutta code based on Barkley's `EZ-Spiral` in section 7.1.2. Throughout, centers of anchoring are found *via* fast Fourier transforms of the tip data.

Given appropriate initial conditions, the systems sustain spiral waves. We will characterize them by following a point on the wave front; when the spiral is a rotating wave, for instance, the tip path looks like the illustration on the right in Figure 7.1.

[1] More precisely, on the domain $[-30, 30]^2$ with 200 grid points to a side and time-step $\Delta t = 0.005$.

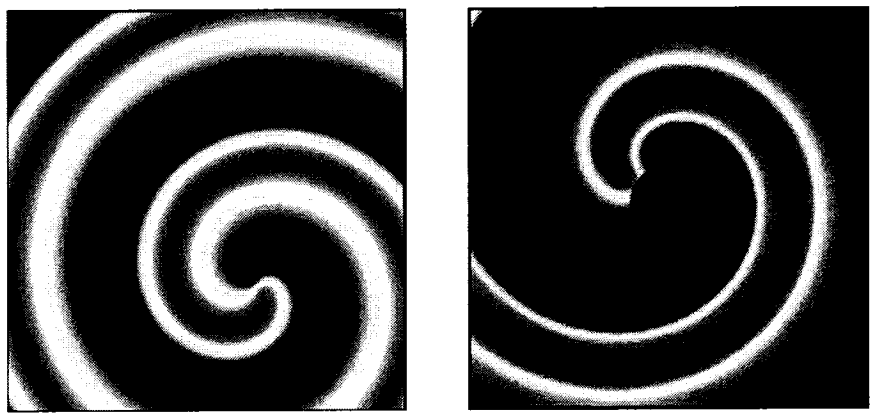

Figure 7.1: On the left, an isolated spiral in a reaction-diffusion system; the excited wave front is shown in red. On the right, the spiral tip path of a rotating wave.

7.1.1 Spiral Anchoring

In order to validate our numerical PDE solver and the subsequent results presented in this chapter, we start by reproducing a known result.

Consider the following reaction-diffusion system, which is a small perturbation of the FitzHugh-Nagumo equations:

$$\begin{aligned} u_t &= \tfrac{1}{\varsigma}\left(u - \tfrac{1}{3}u^3 - v\right) + \phi + \Delta u, \\ v_t &= \varsigma(u + \beta - \gamma v), \end{aligned} \tag{7.1.1}$$

where $\varsigma = 0.3$, $\beta = 0.6$, $\gamma = 0.5$ and ϕ is an inhomogeneous term which depends on $x \in \mathbb{R}^2$. When $\phi \equiv 0$, (7.1.1) has full Euclidean symmetry, being of the form (2.1.1). In this verification, ϕ is given by

$$\phi(x) = -0.12 \exp\left(-0.00086((x_1 - 9)^2 + x_2^2)\right). \tag{7.1.2}$$

Note that ϕ breaks translational symmetry but preserves rotational symmetries about $(9, 0)$, that it is uniformly bounded on $\mathbb{R}^2$ and that it approaches 0 as $\|x\| \to \infty$.

According to [51], spiral wave solutions of (7.1.1) should anchor at a rotating wave around $(9, 0)$; our code finds such a RW (see Figure 7.2).

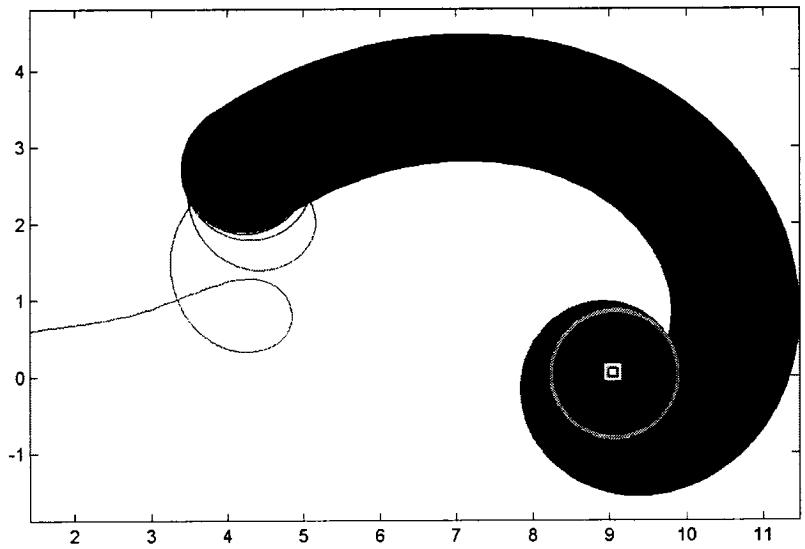

Figure 7.2: Anchoring in the FHN equations (7.1.1), with ϕ as in (7.1.2). The anchored rotating wave is shown in gray; the white square locates the perturbation center $(9, 0)$.

The Case $n = 2$

Consider the following reaction-diffusion system, which is also a small perturbation of the FitzHugh-Nagumo equations:

$$\begin{aligned} u_t &= \tfrac{1}{\varsigma}\left(u - \tfrac{1}{3}u^3 - v\right) + \phi + \Delta u, \\ v_t &= \varsigma(u + \beta - \gamma v), \end{aligned} \tag{7.1.3}$$

where $\varsigma = 0.3$, $\beta = 0.6$, $\gamma = 0.5$ and ϕ is an inhomogeneous term, which depends on $x \in \mathbb{R}^2$. When $\phi \equiv 0$, (7.1.3) has full Euclidean symmetry, being of the form (2.1.1). In the first simulation, ϕ is the sum of two perturbations:

$$\phi(x) = g_1(x) + g_2(x) = -0.25 f(x_1 - 9, x_2) + 1.9 f(x_1 + 10, x_2 - 5\sqrt{3}), \tag{7.1.4}$$

where $f(x) = \left(1.1 - \sin\left(0.4\sqrt{x_1^2 + x_2^2}\right)\right) \exp\left(-0.016\left(x_1^2 + x_2^2\right)\right)$.

Each $g_j(x)$, alone, breaks translational symmetry but preserves rotational symmetry about $(9, 0)$ (for $j = 1$) or $(-10, 5\sqrt{3})$ (for $j = 2$). Note that both perturbations are uniformly bounded on $\mathbb{R}^2$ and that they approach 0 as $\|x\| \to \infty$. Under these conditions, the flow of (7.1.3) near a normally hyperbolic rotating wave is equivalent to the flow of some center bundle equation (4.0.1).[2]

[2]With the exception of boundary effects: consider the case $n = 4$ on p. 114.

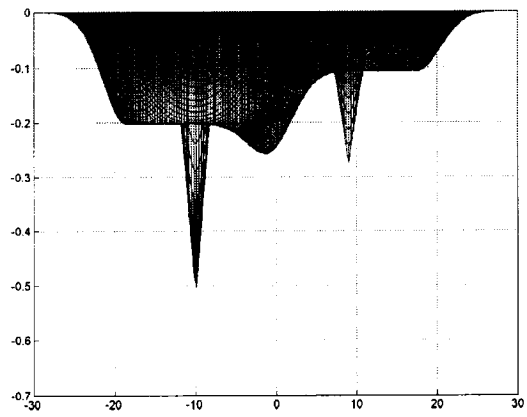

(a) Perturbation profile

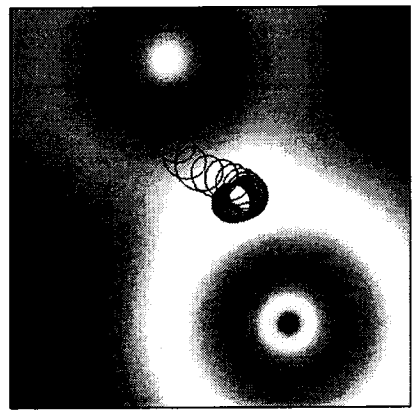

(b) Tip path and perturbation

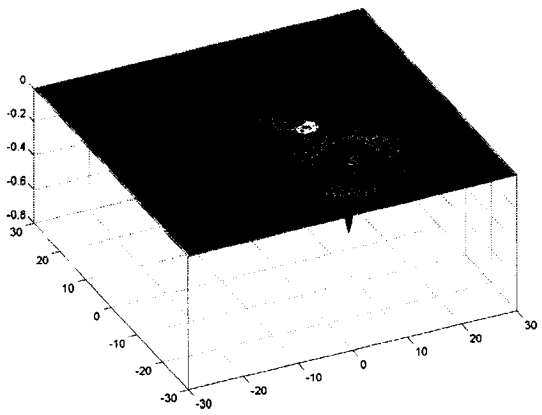

(c) Tip path and perturbation (3D)

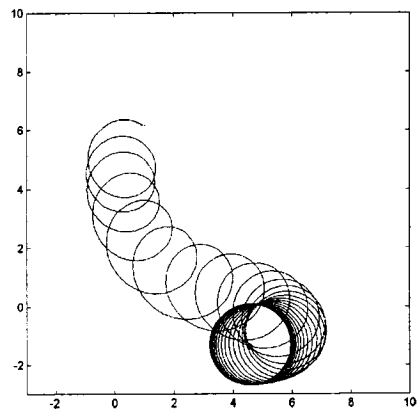

(d) Tip path and center

Figure 7.3: Anchoring in the FitzHugh-Nagumo equations (7.1.3) with ϕ as in (7.1.4). In (a), the profile of ϕ is plotted against x_2. Note the 'artificial' third bump located at approximately $x_2 = -1.35$. In (b) and (c), the path of the spiral tip is superimposed on a graph of the perturbation. In (d), the tip path alone is plotted; after the initial transient, the spiral wave is seen to anchor at approximately $(4.55, -1.35)$.

Accordingly, if spiral waves anchor at all, they will generically do so away from either perturbation center. This is confirmed in Figure 7.3. However, the spiral anchors at a relative minimum of ϕ that is "artificially" created by the superposition of g_1 and g_2.

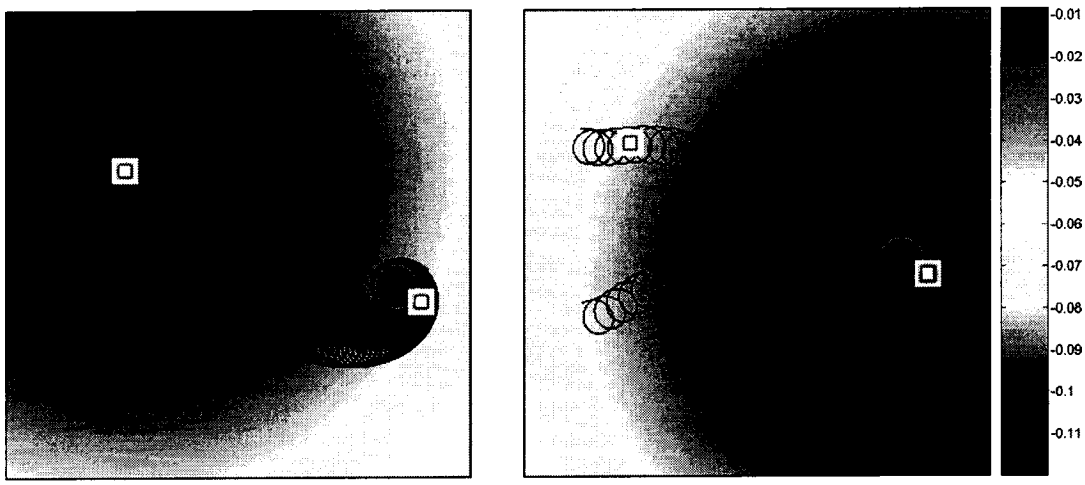

Figure 7.4: Anchoring in the FHN equations (7.1.5) with perturbations as in (7.1.6), for three different initial conditions. The spiral tip paths are plotted against a contour plot of ϕ_1 (on the left) and ϕ_2 (on the right). The anchored perturbed rotating wave is shown in red; the white squares indicate the location of the perturbation centers.

In the second simulation, each of the FHN equations is perturbed slightly, so that (7.1.3) becomes

$$\begin{aligned} u_t &= \tfrac{1}{\varsigma}\left(u - \tfrac{1}{3}u^3 - v\right) + \phi_1 + \Delta u, \\ v_t &= \varsigma(u + \beta - \gamma v - \phi_2), \end{aligned} \tag{7.1.5}$$

where

$$\phi_j(x) = 0.12 f(x_1 - c_{1,j}, x_2 - c_{2,j}),\ j = 1, 2 \tag{7.1.6}$$

$c_{1,1} = 9$, $c_{2,1} = 0$, $c_{1,2} = -10$, $c_{2,2} = 5\sqrt{3}$ and

$$f(x) = \exp\left(-0.00086\left(x_1^2 + x_2^2\right)\right).$$

Each $g_j(x)$, alone, breaks translational symmetry but preserves rotational symmetry about $(9, 0)$ (for $j = 1$) or $(-10, 5\sqrt{3})$ (for $j = 2$). Note that both perturbations are uniformly bounded on $\mathbb{R}^2$ and that they approach 0 as $\|x\| \to \infty$. Under these conditions, the flow of (7.1.5) near a normally hyperbolic rotating wave is equivalent to the flow of some center bundle equation (4.0.1).

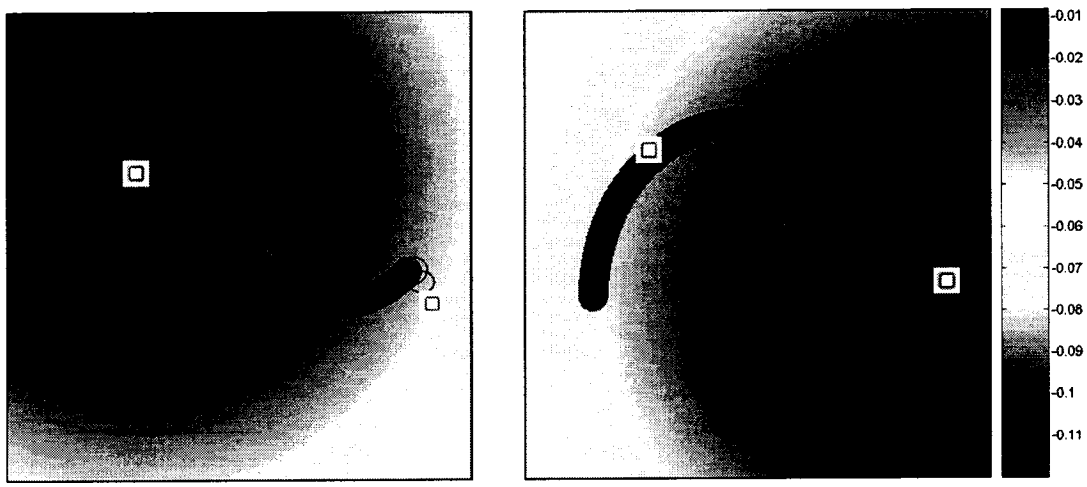

Figure 7.5: Anchoring in the FHN equations (7.1.5) with perturbations as in (7.1.7). The spiral tip paths are plotted against a contour plot of both perturbations. The anchored perturbed rotating wave is shown in red; the white squares indicate the location of the perturbation centers.

As in the first simulation, if spiral waves anchor at all, they will generically do so away from either perturbation center. This is confirmed in Figure 7.4, in which the transients anchor at what would be an otherwise unremarkable location.

Yet, one might wonder if this anchoring away from inhomogeneities could not be due to some quirk of the numerical Euler forward integrator: after all, while the spirals in Figure 7.4 anchor away from the inhomogeneities, they do so relatively close to the center of the second bump. In Figure 7.5, we present the results of another numerical simulation on (7.1.5), with perturbations given by

$$\sqrt{2}\cos(0.05\pi)\phi_j(x), \quad j = 1, 2, \tag{7.1.7}$$

where $\phi_j(x)$ is as in (7.1.6). The spirals are clearly seen to anchor away from the perturbation centers.

Finally, we present the result of an integration of (7.1.5) with perturbations as in (7.1.6), this time using an explicit Runge-Kutta 2−stage method of order two. Anchoring clearly takes place away from the perturbation centers (see figure 7.6): as such, this phenomenon is unlikely to be a numerical artifact.

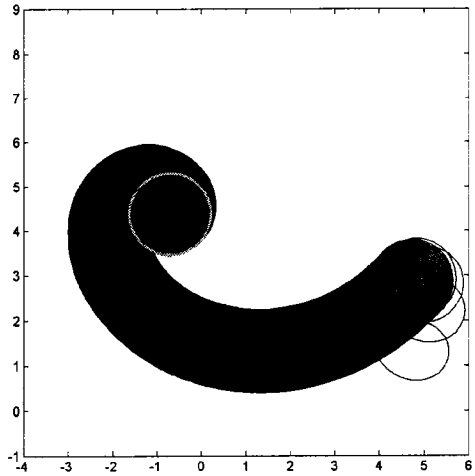

Figure 7.6: Anchoring in the FHN equations (7.1.5) with perturbations as in (7.1.6). A Runge-Kutta 2−stage scheme of order two is used to integrate the system. The anchored perturbed rotating wave is shown in gray; the perturbation centers are located outside the frame box, at $(9,0)$ and $(-10,5\sqrt{3})$, respectively (see figure 7.5 for comparison).

The Case $n > 2$

We now present the results of simulations on a small perturbation of the FitzHugh-Nagumo equations, this time with four bumps:

$$\begin{aligned} u_t &= \tfrac{1}{\varsigma}\left(u - \tfrac{1}{3}u^3 - v\right) + \phi_1 + \Delta u, \\ v_t &= \varsigma(u + \beta - \gamma v + \phi_2), \end{aligned} \tag{7.1.8}$$

where $\varsigma = 0.3$, $\beta = 0.6$, $\gamma = 0.5$, and where ϕ_1,ϕ_2 are inhomogeneous terms which depend on $x \in \mathbb{R}^2$ and are defined by

$$\begin{aligned} \phi_1(x) &= g_1(x) + g_2(x) = 0.12 f_1(x_1 - 9, x_2) - 0.10 f_2(x_1 + 1, x_2 - 10), \\ \phi_2(x) &= g_3(x) + g_4(x) = -0.12 f_1(x_1 + 10, x_2 - 5\sqrt{3}) + 0.08 f_3(x_1 - 10, x_2 - 10), \end{aligned}$$

where $A_1 = 0.12$, $A_2 = -0.10$, $B_1 = -0.12$, $B_2 = 0.08$,

$$f_j(x) = \exp\left(a_j(x_1^2 + x_2^2)\right), \quad j = 1,2,3,$$

$a_1 = -0.00086$, $a_2 = -0.0008$ and $a_3 = -0.0009$.

Each $g_j(x)$, alone, breaks translational symmetry but preserves rotational symmetry about $c_1 = (9,0)$ (for $j = 1$), $c_2 = (-1,10)$ (for $j = 2$), $c_3 = (-10,5\sqrt{3})$ (for

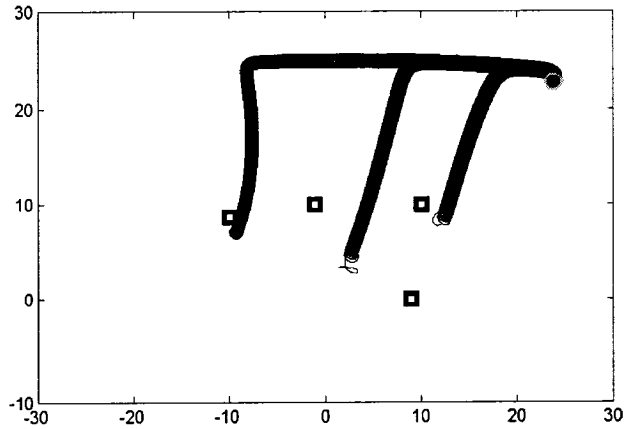

Figure 7.7: Anchoring in the FitzHugh-Nagumo equations (7.1.8). The spiral tip paths are plotted in black. The anchored perturbed rotating wave is shown in gray; the black squares indicate the location of the perturbation centers.

$j = 3$) and $c_4 = (10, 10)$ (for $j = 4$). Note that the four perturbations are uniformly bounded on $\mathbb{R}^2$ and that they approach 0 as $\|x\| \to \infty$. As was the case previously, anchoring takes place away from the c_j, $j = 1, \ldots, 4$.

Note the similarity between Figure 7.7 and parts of the epicycle manifolds shown on p. 126 and p. 128: the transients in Figure 7.7 appear to first (hyperbolically) approach some manifold along which they travel to the anchored perturbed rotating wave. Compare this with figure 7.6, where each transient seems to approach the anchored perturbed rotating wave on its own manifold. It is not clear from the figure whether the manifold is in fact a closed epicycle manifold; no doubt boundary effects are playing a role here. Further investigations will tell the tale.

The Case $\ell = 1$

A planar **reaction-diffusion-advection system** (RDAS) is a reaction-diffusion system to which an advection term has been added:

$$u_t = \tilde{D}\Delta u + \tilde{A}_1 u_{x_1} + \tilde{A}_2 u_{x_2} + f(u), \tag{7.1.9}$$

where $\tilde{A}_i \in \mathbb{M}_2(\mathbb{R})$ for $i = 1, 2$, and the other terms are as in (3.1.1).

Advection terms are used to model a directed flow or current through the excitable medium under consideration; for instance, the modified RDAS

$$u_t = \tilde{D}\Delta u + f(u) + \varepsilon\left[\tilde{A}_1(\varepsilon,\mu)u_{x_1} + \tilde{A}_2(\varepsilon,\mu)u_{x_2}\right] + \mu g(u, \|x-\xi\|^2, \varepsilon, \mu), \quad (7.1.10)$$

where $(\varepsilon,\mu) \in \mathbb{R}^2$ is small, $\tilde{A}_1, \tilde{A}_2 : \mathbb{R}^2 \to \mathbb{M}_2(\mathbb{R})$ are smooth functions and g is a smooth bounded function, could model membrane potentials in a piece of cardiac tissue subjected to a directed current, with an inhomogeneity located at ξ.

Let $\Phi_{t,\varepsilon,\mu}$ denote the semi-flow generated by (7.1.10): it is $\mathbb{SE}(2)-$equivariant when $(\varepsilon,\mu) = 0$; $\mathbb{C}\dot{+}\{1\}-$equivariant when $\varepsilon \neq 0$ is small and $\mu = 0$; $\mathbb{SO}(2)_\xi-$equivariant when $\mu \neq 0$ is small and $\varepsilon = 0$, and (generically) trivially equivariant when (ε,μ) is small and generic.[3]

Advection terms are covered by the CMRT (with a fractional space exponent given by $\alpha = \frac{3}{4} \in [\frac{1}{2}, 1)$), as such, Theorem 6.2.1 can be applied to (7.1.10) and the corresponding center bundle equations are of the form (6.1.1).

The following example shows that (6.1.1) captures the essential dynamics near a rotating wave when the semi-flow of the PDE has the general symmetry-breaking properties outlined above.

Consider the RDAS

$$\begin{aligned} u_t &= \tfrac{1}{\varsigma}\left(u - \tfrac{1}{3}u^3 - v\right) - 3\sqrt{2}\sin\left(\tfrac{0.03\pi}{2}\right)\phi_2 + \Delta u + 0.002u_{x_1}, \\ v_t &= \varsigma(u + \beta - \gamma v + \phi_2), \end{aligned} \quad (7.1.11)$$

where $\varsigma = 0.3$, $\beta = 0.6$, $\gamma = 0.5$ and ϕ_2 is as in (7.1.6). The results are shown in Figure 7.8: the spiral clearly anchors away from the perturbation center.

7.1.2 Homotopy and Hysteresis of Rotating Waves

Following [55], define the modified Oregonator

$$\begin{aligned} u_t &= \tfrac{1}{\varsigma}\left(u - u^2 - (fv + \phi)\tfrac{u-q}{u+q}\right) + \Delta u, \\ v_t &= (u - v) + 0.6\Delta v, \end{aligned} \quad (7.1.12)$$

where $f = 1.4$, $q = 0.002$, $\varsigma = 0.05$ and ϕ is an inhomogeneous term which depends on $x \in \mathbb{R}^2$. When $\phi \equiv 0$, (7.1.12) has full Euclidean symmetry.

[3] This can be seen by slightly modifying the proof of Theorem 2.1.3, on p. 18.

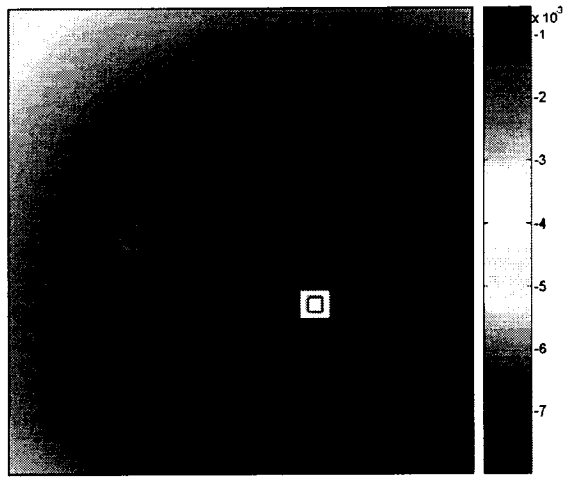

Figure 7.8: Anchoring in the RDAS equations (7.1.11). The spiral tip path is plotted in black. The anchored perturbed rotating wave is shown in red; the white square indicates the location of the perturbation center.

In the following simulations, ϕ is the sum of two Gaussian bells:

$$\begin{aligned}\phi(x) &= \alpha_1 g_1(x) + \alpha_2 g_2(x) \\ &= \alpha_1 \exp\left(-\frac{(x_1-15)^2+(x_2-15)^2}{{\beta_1}^2}\right) + \alpha_2 \exp\left(-\frac{(x_1-18.75)^2+(x_2-15)^2}{{\beta_2}^2}\right),\end{aligned}$$

with α_1, α_2, β_1, $\beta_2 \in \mathbb{R}$, and $\beta_1, \beta_2 \neq 0$. Each $g_j(x)$, alone, breaks translational symmetry but preserves rotational symmetry about $c_1 = (15, 15)$ (for $j = 1$) or $c_2 = (18.75, 15)$ (for $j = 2$). Note that both perturbations are uniformly bounded on $\mathbb{R}^2$ and that they approach 0 as $\|x\| \to \infty$.

When $\alpha = (\alpha_1, 0) \neq 0$, (7.1.12) is $\mathbb{SO}(2)_{c_1}$–equivariant with respect to the action of (2.1.8). Similarly, (7.1.12) is $\mathbb{SO}(2)_{c_2}$–equivariant when $\alpha = (0, \alpha_2) \neq 0$ and trivially equivariant when $\alpha_1, \alpha_2 \neq 0$.

Set $\beta_1 = \beta_2 = 1$ and $\rho_* = 0.01$. For each α along the path $\gamma_1(\tau) = \rho_* (\cos(\tau), \sin(\tau))^\top$, (7.1.12) has a unique anchored perturbed rotating wave whose tip path deforms continuously from a circle centered at c_1, when $\tau = 0 = 0°$, to a circle centered at c_2, when $\tau = \frac{\pi}{2} = 90°$ (see Figure 7.9). Let $\mathcal{W}_j$, $j = 1, 2$, be the anchoring wedges

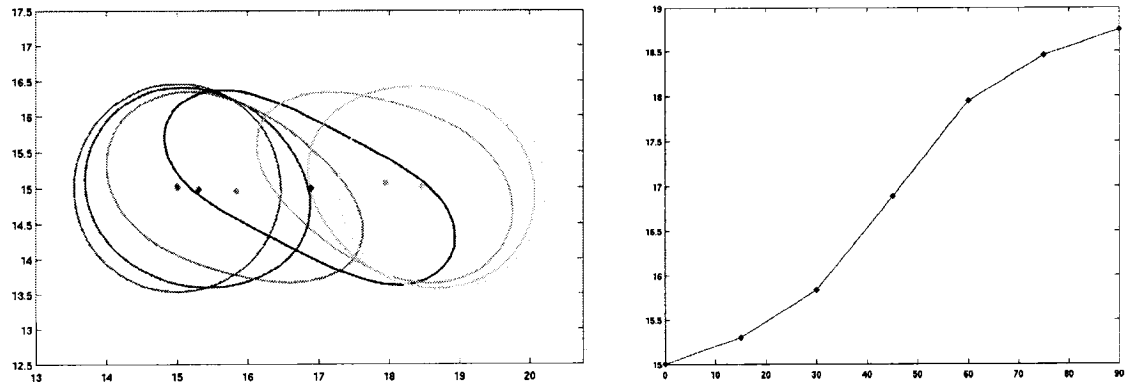

Figure 7.9: Homotopy of the spiral tip path in (7.1.12). On the left, anchored tip paths are plotted, together with their center of anchoring, against $\tau = 0°, 15°, 30°, 45°, 60°, 75°, 90°$, from left to right and purple to yellow. On the right, the corresponding x_1-coordinates of the anchoring centers are plotted against τ; compare this image with the first bifurcation diagram of Table 5.4, on p. 86.

in the equivalent center bundle equation (4.0.1) and let $\hat{\gamma}_1$ be the path in $\lambda-$space corresponding to γ_1. According to the preceding results, $\hat{\gamma}_1 \subseteq \overline{\mathcal{W}_1 \cup \mathcal{W}_2}$.

Along the path $\gamma_2(\tau) = \frac{\rho_*}{10}\gamma_1(\tau)$, however, the situation changes. As the parameters vary along the path, starting at $\tau = 0 = 0°$, (7.1.12) has an anchored perturbed rotating wave whose tip path deforms continuously from a circle centered at c_1. At $\aleph_1 \in \gamma_2$ (corresponding to $\tau \approx 49°$), the rotating wave jumps (discontinuously) to another anchored perturbed rotating wave, whose tip path center is close to c_2. As $\tau = \frac{\pi}{2} = 90°$ is approached on γ_2, the tip path of the anchored perturbed rotating wave deforms continuously, and approaches a circle centered at c_2.

Following γ_2 in the opposite direction leads to similar behaviour, this time with the discontinuous jump taking place at $\aleph_2 \in \gamma_2$ (corresponding this time to $\tau \approx 41°$), as can be seen in Figure 7.10. Consequently, there must be a third unstable rotating wave (which escapes detection by direct means) appearing and then disappearing at $\aleph_1$ and $\aleph_2$, respectively, in saddle-node bifurcations.

Let $\mathcal{W}_j$, $j = 1, 2$, be the anchoring wedges in the equivalent center bundle equation (4.0.1) and let $\hat{\gamma}_2$ be the path in $\lambda-$space corresponding to γ_2. According to the preceding results, $\hat{\gamma}_2$ leaves $\overline{\mathcal{W}_1 \cup \mathcal{W}_2}$ and we conclude that the wedges are separated by a region of non-zero measure.

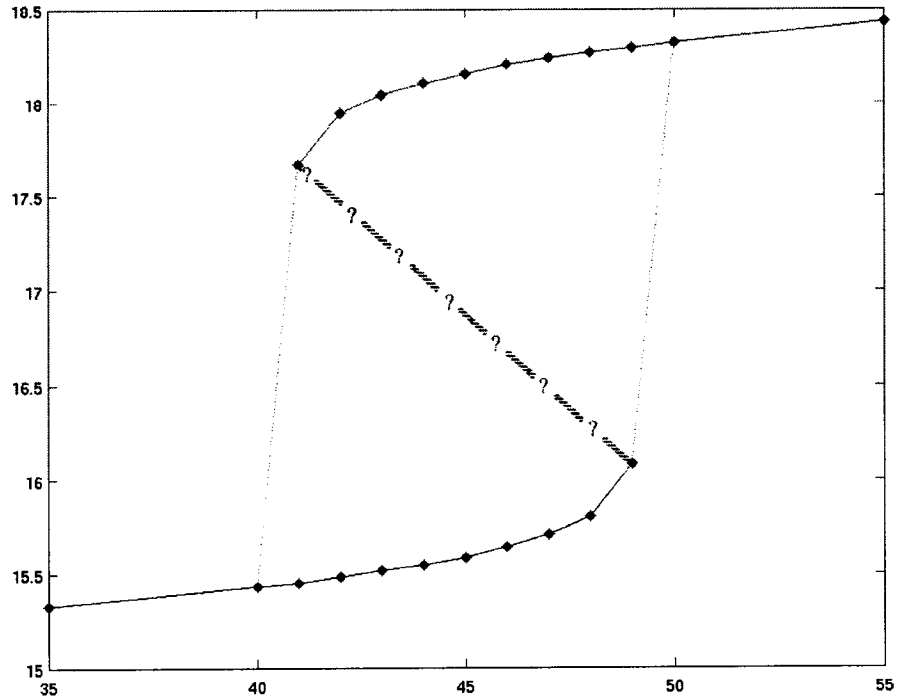

Figure 7.10: Hysteresis of the spiral tip path in (7.1.12). The first spatial coordinates of the spiral centers are plotted against $\tau = 35°, 40°, 41°, \ldots, 49°, 50°, 55°$. The dotted lines indicate the discontinuous jumps described in the text; the question marks interpolate (roughly) the unstable rotating waves. Compare this image with the third bifurcation diagram of table 5.4, on p. 86.

7.2 Dynamics on the Center Bundle

In this section, we present examples of center bundle equations of the form (4.0.1) or (6.1.5) and we examine various aspects of their dynamics.

Polynomial systems have numerous benefits, not the least of which is the significant ease in computing the coefficients related to spiral anchoring and epicyclic drifting. Unfortunately, such systems do not usually satisfy the requirement that they be bounded in p.

Nevertheless, we will at times take full advantage of polynomial simplicity by assuming that the vector field approaches 0 uniformly with $p \to \infty$, *via* a product with some cut-off function. Inside some central region, the cut-off function has no effect and the analysis can be applied to the polynomial system.

7.2.1 Anchoring at Infinity

The first example exhibits homotopic behaviour (compare with the same behaviour in Section 7.1.2) as well as $\infty-$catastrophes.

Let $n = 2$. Set $\xi_1 = 0$ and $\xi_2 \in \mathbb{C}^\times$. Following [51], set $H_1(x_1, x_2, x_3) = ax_1$ and $H_2(x_1, x_2, x_3) = bx_1$ in (4.0.1), with $a, b = \pm 1$. Then (4.0.1) becomes

$$\dot{p} = e^{it}\left[v + a\lambda_1 p e^{-it} + b\lambda_2(p - \xi_2)e^{-it}\right] = ve^{it} - b\lambda_2\xi_2 + (a\lambda_1 + b\lambda_2)p. \quad (7.2.1)$$

This system is integrable: when $a\lambda_1 + b\lambda_2 \neq 0$, its solution is

$$p(t) = \frac{ve^{it}}{i - (a\lambda_1 + b\lambda_2)} + \frac{b\lambda_2\xi_2}{a\lambda_1 + b\lambda_2} + \left(p_0 - \frac{v}{i - (a\lambda_1 + b\lambda_2)} - \frac{b\lambda_2\xi_2}{a\lambda_1 + b\lambda_2}\right) e^{(a\lambda_1 + b\lambda_2)t};$$

when $a\lambda_1 + b\lambda_2 = 0$, then the solution is

$$p(t) = p_0 + iv(1 - e^{it}) - b\lambda_2\xi_2 t$$

(see page 135 for details).

In the first case, (7.2.1) has exactly one $2\pi-$periodic solution:

$$p_\lambda(t) = \frac{ve^{it}}{i - (a\lambda_1 + b\lambda_2)} + \frac{b\lambda_2\xi_2}{a\lambda_1 + b\lambda_2} \quad (7.2.2)$$

through

$$p_0 = \frac{v}{i - (a\lambda_1 + b\lambda_2)} + \frac{b\lambda_2\xi_2}{a\lambda_1 + b\lambda_2} \quad (7.2.3)$$

with center

$$[p_\lambda]_A = \frac{1}{2\pi}\int_0^{2\pi}\left(\frac{ve^{it}}{i - (a\lambda_1 + b\lambda_2)} + \frac{b\lambda_2\xi_2}{a\lambda_1 + b\lambda_2}\right) dt = \frac{b\lambda_2\xi_2}{a\lambda_1 + b\lambda_2}. \quad (7.2.4)$$

Analysis

Let σ be a path joining some small but non-trivial points on the λ_1-axis and the λ_2-axis. Assume further that σ doesn't go through the origin $\lambda = 0$. Since

$$\alpha_j = D_1 H_j(-iv, i\overline{v}, 0) = \pm 1 \neq 0, \quad j = 1, 2,$$

Theorem 4.1.3 states that there are wedges $\mathcal{W}_1$ and $\mathcal{W}_2$ in parameter space near $\lambda = 0$ in each of which there is a unique $2\pi-$periodic solution $\mathcal{S}^j_\lambda$, with $[\mathcal{S}^j_\lambda]_A$ near ξ_j, $j = 1, 2$. By uniqueness, $\mathcal{S}^j_\lambda = p_\lambda(t)$ when $0 \neq \lambda \in \mathcal{W}_j$, $j = 1, 2$.

When $\lambda_2 \to 0$ and $\lambda_1 \neq 0$ on σ (*i.e.*, $\lambda \in \mathcal{W}_1$),

$$\mathcal{S}^1_\lambda = p_\lambda(t) = \frac{ve^{it}}{i - (a\lambda_1 + b\lambda_2)} + \frac{b\lambda_2\xi_2}{a\lambda_1 + b\lambda_2} \to \frac{ve^{it}}{i - a\lambda_1} = \mathcal{S}^1_{(\lambda_1,0)},$$

which is a $2\pi-$periodic solution with $[\mathcal{S}^1_{(\lambda_1,0)}]_A = \xi_1 = 0$. When $\lambda_2 \neq 0$ and $\lambda_1 \to 0$ on σ (*i.e.*, $\lambda \in \mathcal{W}_2$),

$$\mathcal{S}^2_\lambda = p_\lambda(t) = \frac{ve^{it}}{i - (a\lambda_1 + b\lambda_2)} + \frac{b\lambda_2\xi_2}{a\lambda_1 + b\lambda_2} \to \frac{ve^{it}}{i - b\lambda_2} + \xi_2 = \mathcal{S}^2_{(0,\lambda_2)},$$

which is a $2\pi-$periodic solution with $[\mathcal{S}^2_{(0,\lambda_2)}]_A = \xi_2$.

There are then two possibilities:

1. If σ doesn't intersect the line $a\lambda_1 + b\lambda_2 = 0$, the periodic solution $p_\lambda(t)$ varies continuously from $\mathcal{S}^1_{(\lambda_1,0)}$ to $\mathcal{S}^2_{(0,\lambda_2)}$, without a change in stability. The weight of the perturbations determines where the center $[p_\lambda]$ given by (7.2.4) lands on the straight line between $\xi_1 = 0$ and ξ_2.

2. If σ intersects the line $a\lambda_1 + b\lambda_2 = 0$, the periodic solution $p_\lambda(t)$ shoots off to infinity as $a\lambda_1 + b\lambda_2 \to 0$ along σ.

   To fully understand the transition, note that (7.2.3) rewrites as

   $$p_0 = \frac{b\lambda_2\xi_2}{a\lambda_1 + b\lambda_2} - iv + O(a\lambda_1 + b\lambda_2) \tag{7.2.5}$$

   when $|a\lambda_1 + b\lambda_2| < 1$. In the inverted plane $p = \frac{1}{\varsigma}$, (7.2.5) becomes

   $$\varsigma_0 = \frac{1}{p_0} = \frac{a\lambda_1 + b\lambda_2}{b\lambda_2\xi_2 + O(a\lambda_1 + b\lambda_2)}.$$

   As $a\lambda_1 + b\lambda_2 \to 0$ and $\lambda_2 \not\to 0$,[4] $\varsigma_0 \to 0$. Hence, the p_λ meanders to infinity as λ approaches the fateful line. Furthermore, it is asymptotically stable if $a\lambda_1 + b\lambda_2 < 0$ and unstable if $a\lambda_1 + b\lambda_2 > 0$.

[4]Thus the pair (λ_1, λ_2) is *away* from the origin.

In fact, a transcritical bifurcation of periodic solutions (one of which stays at infinity) takes place along the line $a\lambda_1 + b\lambda_2 = 0$.

Based on the results of Chapter 5, we conclude that the line $a\lambda_1 + b\lambda_2 = 0$ is a curve of $\infty-$catastrophes and that while the wedges $\mathcal{W}_1, \mathcal{W}_2$ do not overlap, the complement of their union has trivial measure.

7.2.2 Saddle-Node Bifurcation of Rotating Waves

The second example exhibits a saddle-node bifurcation, a process that often accompanies hysteresis or bi-stability (see Section 7.1.2), although it is neither a sufficient nor a necessary condition: consider the 'generalized' saddle-node bifurcation [72, pp. 281 – 282], for instance.

Let $n = 2$. Set $\xi_1 = 0$ and $\xi_2 \in \mathbb{C}^\times$. For some suitable functions g_1 and g_2, set $H_j(x_1, x_2, x_3) = g_j(x_1, x_2)$ in (4.0.1), for $j = 1, 2$. With $z = p + ie^{it}v$, $\lambda_2 = \varepsilon$, and $\lambda_1 = \mu\varepsilon$, (4.0.1) becomes

$$\dot{z} = \varepsilon e^{it} K(ze^{-it}, \overline{z}e^{it}, t, \varepsilon, \mu), \tag{7.2.6}$$

where $K(w, \overline{w}, t, \varepsilon, \mu) = \mu g_1(w - iv, \text{c. c.}) + g_2(w - iv - \xi_2 e^{-it}, \text{c. c.})$.

If $z_{\varepsilon,\mu}(t; z_0)$ is the solution of (7.2.6) through z_0, then the Poincaré map is given by $P(z_0, \varepsilon, \mu) = z_{\varepsilon,\mu}(2\pi; z_0)$. The Taylor series of P about $(\varepsilon, \mu) = (0, 0)$ is

$$P(z_0, \varepsilon, \mu) = \sum_{0 \le k,m \le 2} D_{\varepsilon^k \mu^m} z_{0,0}(2\pi; z_0)\varepsilon^k \mu^m + O(\varepsilon^3, \varepsilon^2\mu, \varepsilon\mu^2, \mu^3). \tag{7.2.7}$$

Then

$$\begin{aligned}
z_{0,0}(2\pi; z_0) &= z_0 \\
D_{\mu^m} z_{0,0}(2\pi; z_0) &= 0 \quad \text{for } m \ge 1, \\
D_\varepsilon z_{0,0}(2\pi; z_0) &= \int_0^{2\pi} e^{is} g_2((z_0 - \xi_2)e^{-is} - iv, \text{c. c.})\, ds \\
D_{\varepsilon\mu} z_{0,0}(2\pi; z_0) &= \int_0^{2\pi} e^{is} g_1(z_0 e^{-is} - iv, \text{c. c.})\, ds \\
D_{\varepsilon\varepsilon} z_{0,0}(2\pi; z_0) &= 2\int_0^{2\pi} \big[D_1 g_2((z_0 - \xi_2)e^{-is} - iv, \text{c. c.}) D_\varepsilon z_{0,0}(s; z_0) \\
&\qquad + D_2 g_2((z_0 - \xi_2)e^{-is} - iv, \text{c. c.}) D_\varepsilon \overline{z_{0,0}(s; z_0)} e^{2is}\big]\, ds,
\end{aligned} \tag{7.2.8}$$

where $D_\varepsilon z_{0,0}(s; z_0)$ is given by

$$D_\varepsilon z_{0,0}(s; z_0) = \int_0^s e^{i\tau} g_2((z_0 - \xi_2)e^{-i\tau} - iv, \text{c. c.})\, d\tau$$

(see page 136 for details).

Proposition 7.2.1 *Set $g_1(x_1, x_2) = x_1^2 x_2$ and $g_2(x_1, x_2) = -x_1$. Let P_{TS} be the map obtained from P by truncating all terms of order ≥ 3 in (ε, μ). Set $v = 1 + i$ and $\xi_2 = 4 + 4i$. Then there is a curve in parameter space along which P_{TS} undergoes a fold bifurcation.*

Proof: In this case, $D_1 g_2(x_1, x_2) = -1$, $D_2 g_2(x_1, x_2) = 0$ and

$$D_\varepsilon z_{0,0}(t; z_0) = -\int_0^t e^{is}\big((z_0 - \xi_2)e^{-is} - iv\big)\, ds = -t(z_0 - \xi_2) - v(e^{-it} - 1)$$

$$D_{\varepsilon\mu} z_{0,0}(2\pi; z_0) = \int_0^{2\pi} e^{is}(z_0 e^{-is} - iv)^2(\overline{z_0}e^{is} + i\overline{v})\, ds = 2\pi z_0(|z_0|^2 + 2|v|^2).$$

Hence $D_\varepsilon z_{0,0}(2\pi; z_0) = -2\pi(z_0 - \xi_2)$ and

$$D_{\varepsilon\varepsilon} z_{0,0}(2\pi; z_0) = -\int_0^{2\pi} D_\varepsilon z_{0,0}(s; z_0)\, ds = \int_0^{2\pi} \big(s(z_0 - \xi_2) + ve^{-is} - v\big)\, ds = 2\pi(\pi(z_0 - \xi_2) - v),$$

and so

$$P_{\text{TS}}(z, \varepsilon, \mu) = z_0 + 2\pi\varepsilon\left[4 + 4i - z + \mu z(|z|^2 + 4) + \varepsilon(\pi(z - 4 - 4i) - 1 - i)\right]. \tag{7.2.9}$$

Let $z = x + iy$, where $x = \operatorname{Re} z$ and $y = \operatorname{Im} z$. In these coordinates, (7.2.9) becomes

$$P_{\text{TS}}(x, y, \varepsilon, \mu) = \begin{pmatrix} x \\ y \end{pmatrix} + 2\pi\varepsilon \begin{pmatrix} 4 - x + \mu(x^2 + y^2 + 4)x + \varepsilon(\pi(x - 4) - 1) \\ 4 - y + \mu(x^2 + y^2 + 4)y + \varepsilon(\pi(y - 4) - 1) \end{pmatrix},$$

whence

$$DP_{\text{TS}}(x, y, \varepsilon, \mu) - I = 2\pi\varepsilon \begin{pmatrix} -1 + \mu(3x^2 + y^2 + 4) + \varepsilon\pi & 2\mu xy \\ 2\mu xy & -1 + \mu(x^2 + 3y^2 + 4) + \varepsilon\pi \end{pmatrix}.$$

The Jacobian of P_{TS} at a fold bifurcation of fixed points has 1 as a multiplier; its second multiplier is not equal to 1. To find such a bifurcation point, one must start by solving the system

$$\begin{aligned} P_{\text{TS}}(x, y, \varepsilon, \mu) - \begin{pmatrix} x \\ y \end{pmatrix} &= 0 \\ \det\left(DP_{\text{TS}}(x, y, \varepsilon, \mu) - I\right) &= 0. \end{aligned} \tag{7.2.10}$$

Note that

$$\det\left(DP_{\mathrm{TS}}(x,y,\varepsilon,\mu)-I\right)=4\pi^2\varepsilon^2\big(\varepsilon\pi-1+\mu(3x^2+3y^2+4)\big)\big(\varepsilon\pi-1+\mu(x^2+y^2+4)\big).$$

Consider the related system

$$\begin{aligned}4-x+\mu(x^2+y^2+4)x+\varepsilon(\pi(x-4)-1)&=0\\ 4-y+\mu(x^2+y^2+4)y+\varepsilon(\pi(y-4)-1)&=0\\ \big(\varepsilon\pi-1+\mu(3x^2+3y^2+4)\big)\big(\varepsilon\pi-1+\mu(x^2+y^2+4)\big)&=0\end{aligned}\tag{7.2.11}$$

Any solution of (7.2.11) is also a solution of (7.2.10). Set $\varepsilon=\varepsilon_0=\frac{1}{1000}$. From the third equation of (7.2.11), we obtain

$$\mu=\frac{1000-\pi}{1000(3x^2+3y^2+4)}\quad\text{or}\quad\mu=\frac{1000-\pi}{1000(x^2+y^2+4)}.$$

The second of these expressions must be discarded as it leads to an inconsistent system. With the first expression for μ, (7.2.11) becomes

$$\begin{aligned}4-x+\frac{1000-\pi}{1000(3x^2+3y^2+4)}(x^2+y^2+4)x+\frac{1}{1000}(\pi(x-4)-1)&=0\\ 4-y+\frac{1000-\pi}{1000(3x^2+3y^2+4)}(x^2+y^2+4)y+\frac{1}{1000}(\pi(y-4)-1)&=0,\end{aligned}$$

or equivalently,

$$\begin{aligned}(2\pi-2000)x^3+(2\pi-2000)xy^2+(11997-12\pi)x^2+(11997-12\pi)y^2+15996-16\pi&=0\\ (2\pi-2000)y^3+(2\pi-2000)x^2y+(11997-12\pi)x^2+(11997-12\pi)y^2+15996-16\pi&=0\end{aligned}$$

This system has at least one real solution, approximated by $x_0=y_0\approx 6.105763500$. In this case, $\mu_0=0.004378290878$, and $(x_0,y_0,\varepsilon_0,\mu_0)$ is a solution of (7.2.10).

Let $J\in\mathbb{M}_{3,4}(\mathbb{R})$ be the Jacobian of the left hand side of (7.2.10) with respect to (x,y,ε,μ). If J is of rank 3 at $(x_0,y_0,\varepsilon_0,\mu_0)$, then P_{TS} undergoes a fold bifurcation there, and there is a curve of fold bifurcation points in parameter space emanating from (ε_0,μ_0) (see [47, pp. 348 – 349] for details).

The reduced row-echelon form of J at $(x_0,y_0,\varepsilon_0,\mu_0)$ is approximately

$$\left(\begin{array}{ccc|c}1&0&0&0.458451113\\0&1&0&0.458451113\\0&0&1&72.42665285\end{array}\right);$$

accordingly, a curve of fold bifurcation points for P_{TS} passes through $(x_0,y_0,\varepsilon_0,\mu_0)$. ∎

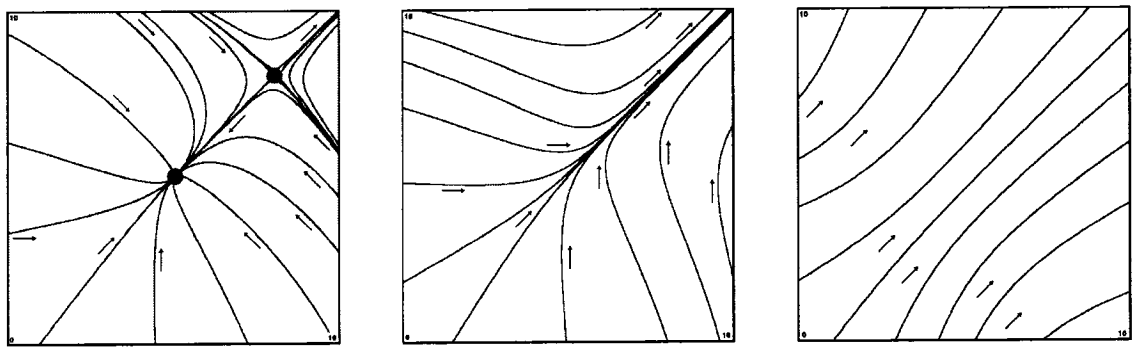

(a) $\mu = 0.004$ (b) $\mu = 0.005$ (c) $\mu = 0.01$

Figure 7.11: Projection (in the z-plane) of the phase diagrams of (7.2.6) with g_1, g_2 as in Proposition 7.2.1, for $\varepsilon = 0.001$. The arrows represent the direction of the flow.

Analysis

As (7.2.6) cannot be solved explicitly for the choices of g_1 and g_2 in proposition 7.2.1, we cannot be certain that the truncated map P_{TS} captures the essential dynamics of the Poincaré map P for the above parameter values. However, due to the relatively small size of (ε_0, μ_0), that is certainly a possibility.

If it does, the data relating to the fold bifurcation found in the proof of Proposition 7.2.1 will lead to a saddle-node bifurcation of periodic orbits in (7.2.6), *near* $z_0 = x_0 + iy_0$, ε_0 and μ_0.

A study of the time-evolution of (7.2.6) (with DSTOOL) for various parameter values shows that a saddle-node bifurcation of periodic solutions does indeed take place near the prescribed values. In Figure 7.11, some solutions of (7.2.6) are projected on the $z-$plane, for $\varepsilon = \varepsilon_0$ and three different values of μ. As μ approaches the critical value $\mu_* \approx \mu_0$ from below, the 'saddle' and the 'node' come together and annihilate: the bifurcation takes place between (a) and (b).

Due to the simple algebraic nature of the functions g_1 and g_2, it is possible to find an explicit expression for the curve along which P_{TS} undergoes fold bifurcations (see page 138 for details). In light of the evidence presented above, it seems safe to assume that P_{TS} and P are topologically equivalent for small enough parameter values, included amongst which is (ε_0, μ_0).

7.2.3 Collapse of the Epicycle Manifold

We have shown previously that, under certain conditions, (4.0.1) can have epicycle manifolds for small parameter values in a wedge near the origin. However, our results do not provide information concerning the flow of (4.0.1) in this invariant set.

The third and fourth examples are systems in which the flow on the epicycle manifolds are essentially different.

Let $n = 2$. Set $\xi_1 = 0$, $\xi_2 = 4 + 4i$, $v = 1 + i$,

$$H_1(x_1, x_2, x_3) = -x_3 x_1^2 - x_1^2 x_2 + 80x_1,$$
$$H_2(x_1, x_2, x_3) = -x_2$$

in (4.0.1), which then becomes

$$\dot{p} = e^{it}\big[v - \lambda_1(\lambda_1 p^2 e^{-2it} + |p|^2 p e^{-it} - 80pe^{-it}) - \lambda_2\overline{(p - \xi_2)}e^{it}\big]. \tag{7.2.12}$$

Analysis

The average function M^1 is given by

$$\begin{aligned} M^1(w, \overline{w}) &= \frac{1}{2\pi}\int_0^{2\pi} e^{it} H_1(we^{-it} - iv, \overline{w}e^{it} + i\overline{v}, 0)\, dt \\ &= \frac{1}{2\pi}\int_0^{2\pi} e^{it}\big[- (we^{-it} - iv)^2(\overline{w}e^{it} + i\overline{v}) + 80(we^{-it} - iv)\big]\, dt \\ &= w(76 - |w|^2). \end{aligned}$$

Then $L_1(w\overline{w}) = 76 - w\overline{w}$ and so $R_0^1(\rho) = \mathrm{Re}\,[M^1(\rho, \rho)] = \rho(76 - \rho^2)$, which in turn implies $D_\rho R_0^1(\rho) = 76 - 3\rho^2$. The only positive solution of $R_0^1(\rho) = 0$ is $\rho_0 = \sqrt{76}$, for which

$$\gamma_0 = D_\rho R_0^1(\rho_0) = 76 - 3\rho_0^2 = -152.$$

Then, Theorem 4.2.3 states that there is a wedge $\mathcal{V}_1$ near $\lambda = 0$ in parameter space for which (7.2.12) has an attractive epicycle manifold $\mathcal{E}_\lambda$ with $[\mathcal{E}_\lambda]_D$ *near* $\xi_1 = 0$ for all $\lambda \in \mathcal{V}_1$. Furthermore, since

$$D_1 H_1(x_1, x_2, x_3) = -2x_3 x_1 - 2x_1 x_2 + 80$$

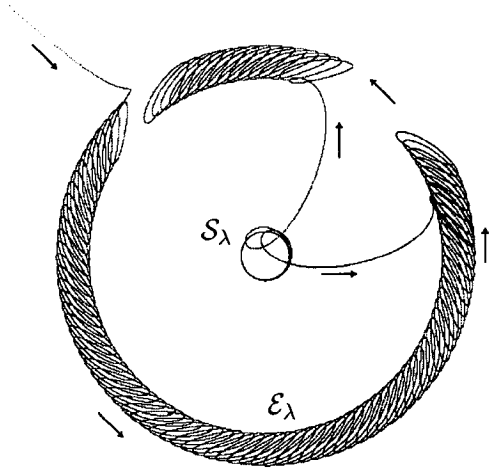

Figure 7.12: Projection (in the $p-$plane) of the stable epicycle manifold $\mathcal{E}_\lambda$ and repelling rotating wave $\mathcal{S}_\lambda$ of (7.2.12), for $\lambda = (0.01, 0.001)$. The arrows direct the flow.

---

and

$$\mathrm{Re}(\alpha_1) = \mathrm{Re}\,(D_1 H_1(-iv, i\overline{v}, 0)) = \mathrm{Re}\,\big(-2|1+i|^2 + 80\big) = 76 > 0,$$

there is a wedge $\mathcal{W}_1$ near $\lambda = 0$ in parameter space for which (7.2.12) has a unique repelling rotating wave $\mathcal{S}_\lambda$, according to Theorem 4.1.3, with $[\mathcal{S}_\lambda]_A$ *near* $\xi_1 = 0$ for all $\lambda \in \mathcal{W}_1$.

Thus there is an overlapping region in which (7.2.12) has both an epicycle manifold and a unique rotating wave solution. The parameter vector $\lambda \in (0.01, 0.001)$ lies in the overlapping region, as can be seen in figure 7.12.

In the next example, the flow along the epicycle manifold is significantly richer.

Let $n = 2$. Set $\xi_1 = 0$, $\xi_2 = 4 + 4i$, $v = 1 + i$, $H_1(x_1, x_2, x_3) = -x_1^2 x_2$ and $H_2(x_1, x_2, x_3) = x_1$ in (4.0.1). Note that

$$M^1(w, \overline{w}) = \frac{1}{2\pi}\int_0^{2\pi} e^{it}\big[-(we^{-it} - iv)^2(\overline{w}e^{it} + i\overline{v})\big]\,dt = -w(|w|^2 + 4i)$$

and

$$M^2(w, \overline{w}) = \frac{1}{2\pi}\int_0^{2\pi} e^{it}(we^{-it} - iv)\,dt = w.$$

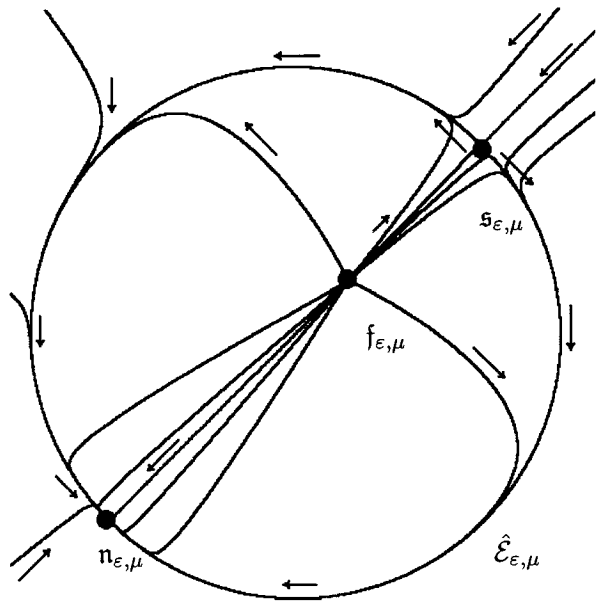

Figure 7.13: Projection (in the $z-$plane) of the stable epicycle manifold $\hat{\mathcal{E}}_{\varepsilon,\mu}$ and the three rotating waves $\mathfrak{s}_{\varepsilon,\mu}$, $\mathfrak{n}_{\varepsilon,\mu}$ and $\mathfrak{f}_{\varepsilon,\mu}$ of (7.2.13), for $\varepsilon = 0.01$ and $\mu < 0.00437$.

Then $L_1(w\overline{w}) = -|w|^2 - 4i$ and $L_2(w\overline{w}) = 1$ and so

$$R_0^1(\rho) = \text{Re}\left[M^1(\rho,\rho)\right] = -\rho^3 \quad \text{and} \quad R_0^2(\rho) = \text{Re}\left[M^2(\rho,\rho)\right] = \rho.$$

None of the solutions of $R_0^1(\rho) = 0$ or $R_0^2(\rho) = 0$ are positive: thus Theorem 4.2.3 cannot be applied. Yet there is a parameter region in which interesting epicycle manifolds exist.

Analysis

Set $z = p + ie^{it}v$, $\lambda_2 = \varepsilon$, and $\lambda_1 = \mu\varepsilon$ in (4.0.1) to obtain

$$\dot{z} = \varepsilon e^{it} K(ze^{-it}, \overline{z}e^{it}, t, \varepsilon, \mu), \tag{7.2.13}$$

where $K(w, \overline{w}, t, \varepsilon, \mu) = -\mu(w - iv)^2(\overline{w} + i\overline{v}) + w - iv - \xi_2 e^{-it}$.

When $\varepsilon = 0.01$ and $\mu = 0.0005$, (7.2.13) has a stable epicycle manifold $\hat{\mathcal{E}}_{\varepsilon,\mu}$ and three rotating waves: a "saddle" $\mathfrak{s}_{\varepsilon,\mu}$, a "node" $\mathfrak{n}_{\varepsilon,\mu}$ and a "source" $\mathfrak{f}_{\varepsilon,\mu}$. Note that $\mathfrak{s}_{\varepsilon,\mu}, \mathfrak{n}_{\varepsilon,\mu} \in \hat{\mathcal{E}}_{\varepsilon,\mu}$ (see Figure 7.13).

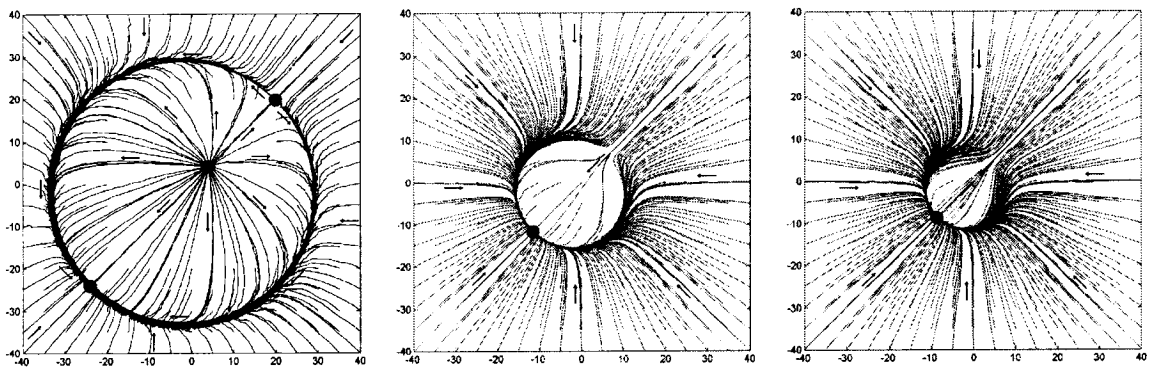

(a) $\mu = 0.001$ (b) $\mu = 0.005$ (c) $\mu = 0.01$

Figure 7.14: Projection (in the z–plane) of the collapse of the epicycle manifold $\hat{\mathcal{E}}_{\varepsilon,\mu}$ at the saddle-node bifurcation of the rotating waves $\mathfrak{s}_{\varepsilon,\mu}$ and $\mathfrak{f}_{\varepsilon,\mu}$ of (7.2.13), for $\varepsilon = 0.01$.

A study of the time-evolution of (7.2.13) (with Matlab's `ode45`) for various parameter values shows that the epicycle manifold collapses at a saddle-node bifurcation of rotating waves; when $\varepsilon = 0.01$, the collapse occurs for $\mu \approx 0.00437$ (see figure 7.14).

It should come as no surprise that this parameter value is exactly the one found in the study of the saddle-node bifurcation of rotating waves in (7.2.6), since both systems are essentially the same (modulo a time-reversal). Consequently, there is a curve in parameter space along which the epicycle manifold $\hat{\mathcal{E}}_{\varepsilon,\mu}$ collapses at a saddle-node bifurcation of $\mathfrak{s}_{\varepsilon,\mu}$ and $\mathfrak{f}_{\varepsilon,\mu}$.

It should be noted that in general there is no reason to expect the collapse (or creation) of an epicycle manifold to be specifically linked to a saddle-node bifurcation of rotating waves.

7.2.4 Combined TSB and RSB Perturbations

We provide two examples illustrating anchoring and epicyclic drifting in (6.1.5).

Set $v = 1$, $G(t, \varepsilon, \mu) = e^{-it}$, $\zeta = pe^{-it} + i$ and

$$H(z, \overline{z}, \varepsilon, \mu) = -0.0865ize^{-0.6|\zeta|^2} - \zeta(-0.6 + \arctan(3|\zeta| - 4.5))e^{-0.4|\zeta|^2} \qquad (7.2.14)$$

in (6.2.1).

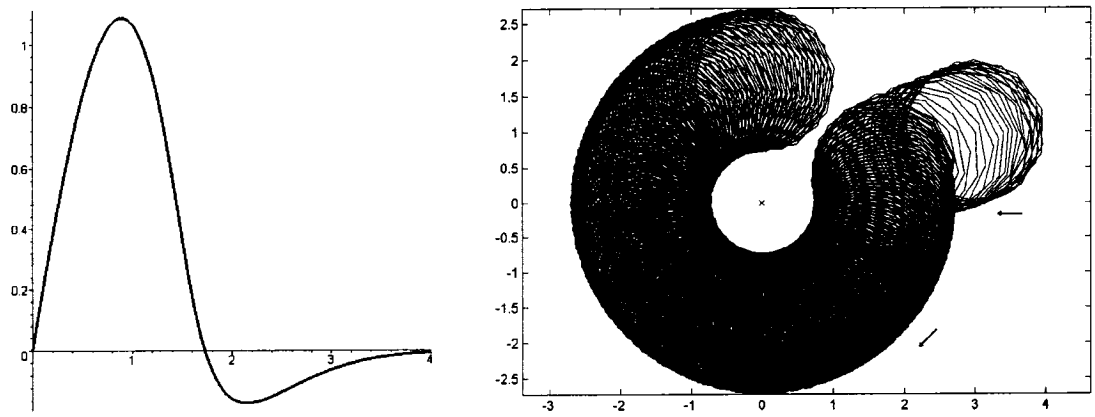

(a) $R_*(\rho)$ (b) Epicycle manifold

Figure 7.15: On the left, numerical values of $R_*(\rho)$ on the interval $[0,4]$, for H as in (7.2.14). On the right, projection (in the $p-$plane) of the attracting epicycle manifold $\mathcal{G}^1_{\varepsilon,\mu}$ in (6.1.5), for H as in (7.2.14) and $(\varepsilon,\mu) = (0.001, 0.1)$.

Analysis

Clearly, $G \in \mathfrak{P}_t^{2\pi}$; the averaged function $R_*(\rho)$ associated to (7.2.14) is plotted in figure 7.15; it has a positive root at $\rho_0 \approx 1.72804$, with $\gamma_0 = D_\rho R_*(\rho_0) \approx -1.06951 < 0$. Note that $g_{-1}(0,0) = 1 \neq 0$. According to Theorem 6.2.2, (6.1.5) has an attracting epicycle manifold $\mathcal{G}^1_{\varepsilon,\mu}$, with $[\mathcal{G}^1_{\varepsilon,\mu}]_{\mathrm{D}}$ slightly off the origin, whenever $(\varepsilon,\mu) \in \mathcal{V}$; Figure 7.15 shows such a manifold for $(\varepsilon,\mu) = (0.001, 0.1)$.

For the second example, set $v = 1 + i$, G and H such that (6.2.1) becomes

$$\dot{p} = e^{it}\big[v + \varepsilon(e^{-\ell it} + 2\sin(3\ell t) + i\cos(5\ell t)) + \mu p e^{-it}(\mu p e^{-it} + |p|^2 - 80)\big]. \qquad (7.2.15)$$

Analysis

Clearly, $G \in \mathfrak{P}_t^{2\pi/\ell}$ and

$$\mathrm{Re}(a_1) = \mathrm{Re}(D_1 H(-iv, i\overline{v}, 0, 0)) = \mathrm{Re}(2|1+i|^2 - 80) = -76 < 0.$$

To simplify the numerical simulations, let $\ell = 5$. According to Theorem 6.2.3, there is a deleted neighbourhood $\mathcal{W}^5$ of the origin in parameter space such that (7.2.15) has

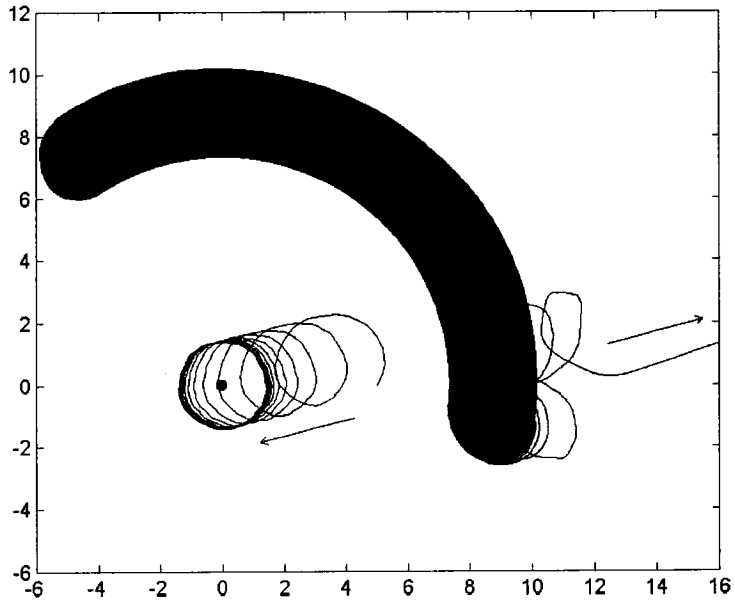

Figure 7.16: Projection (in the p−plane) of the anchored rotating wave $\mathcal{D}^5_{0.1,0.001}$ and the unstable epicycle manifold $\mathcal{G}^5_{0.1,0.001}$ in (7.2.15). Note the pentagonal shape of the anchored perturbed rotating wave.

a rotating wave $\mathcal{D}^5_{\varepsilon,\mu}$ with $\mathbb{Z}_5$−spatio-temporal symmetry and centered at the origin whenever $(\varepsilon,\mu) \in \mathcal{W}^5$. Figure 7.16 shows such a rotating wave.

Furthermore, since $R_*(\rho) = -\rho(76-\rho^2)$ (see p. 125 for details), (7.2.15) has a repelling epicycle manifold $\mathcal{G}^5_{\varepsilon,\mu}$ for all $(\varepsilon,\mu) \in \mathcal{V}^5$. Indeed, the cercle $\rho_* \approx \sqrt{76}$ provides a boundary outside of which the solutions of (7.2.15) meander away from the origin.[5]

7.3 Wedges and Catastrophes

In this final section, we provide a partial catalogue of (partial) bifurcation diagrams for mappings of the form

$$P(x,\lambda) = x + 2\pi\big[\lambda_1 F_0(x) + \lambda_2 G_\xi(x)\big], \tag{7.3.1}$$

[5]While it is next to impossible to directly detect an unstable epicycle manifold in a reaction-diffusion system, it is easy to do so in the center bundle equations: one only needs to reverse the direction of time and look for a stable epicycle manifold.

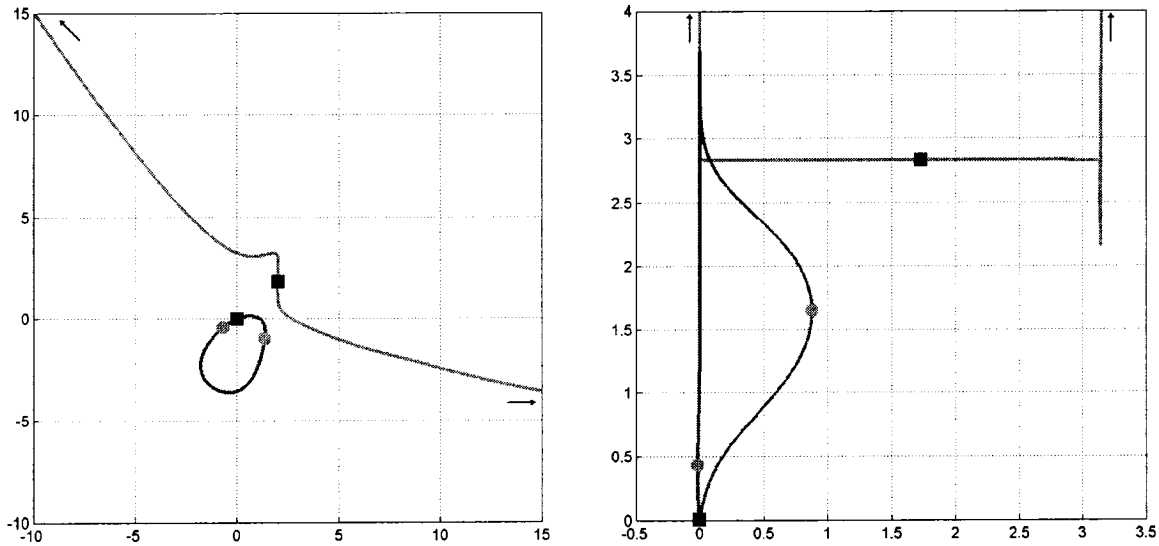

Figure 7.17: Wedges and catastrophes: the first example.

where $\lambda \in \mathbb{R}^2$, $\xi = (2,2)^\top$,

$$F_0(x) = \begin{pmatrix} 2x_1 - x_2 + \sum a_{i,j} x_1^i x_2^j \\ x_1 + 2x_2 + \sum b_{i,j} x_1^i x_2^j \end{pmatrix} \cdot f_0(x),$$

$$G_\xi(x) = \begin{pmatrix} 7 - 3x_1 - \frac{x_2}{2} + \sum c_{i,j} (x_1 - 2)^i (x_2 - 2)^j \\ 5 - 3x_1 + \frac{x_2}{2} + \sum d_{i,j} (x_1 - 2)^i (x_2 - 2)^j \end{pmatrix} \cdot g_\xi(x),$$

$a_{i,j}, b_{i,j}, c_{i,j}, d_{i,j} \in \mathbb{R}$, $i + j > 1$, and f_0 and g_ξ are continuous functions such that (7.3.1) satisfies Proposition 5.1.1; we can then use the visual criterion of Section 5.3 to understand the nature of the bifurcation diagram of the associated map $P_{0.01}$. Furthermore, the wedge angles can be read directly from the bifurcation diagram.

For each of the following examples, we give F_0 and G_ξ as well as two associated Figures: on the left is shown $\kappa(3)$, while the corresponding bifurcation diagram of $P_{0.01}$ appears on the right.

In each figure, C_0 is shown in blue and C_ξ in red unless $C_0 = C_\xi$, in which case it appears in purple. Fold catastrophes are indicated by green circles and $\infty-$catastrophes by arrows. The squares represent the origin and ξ.

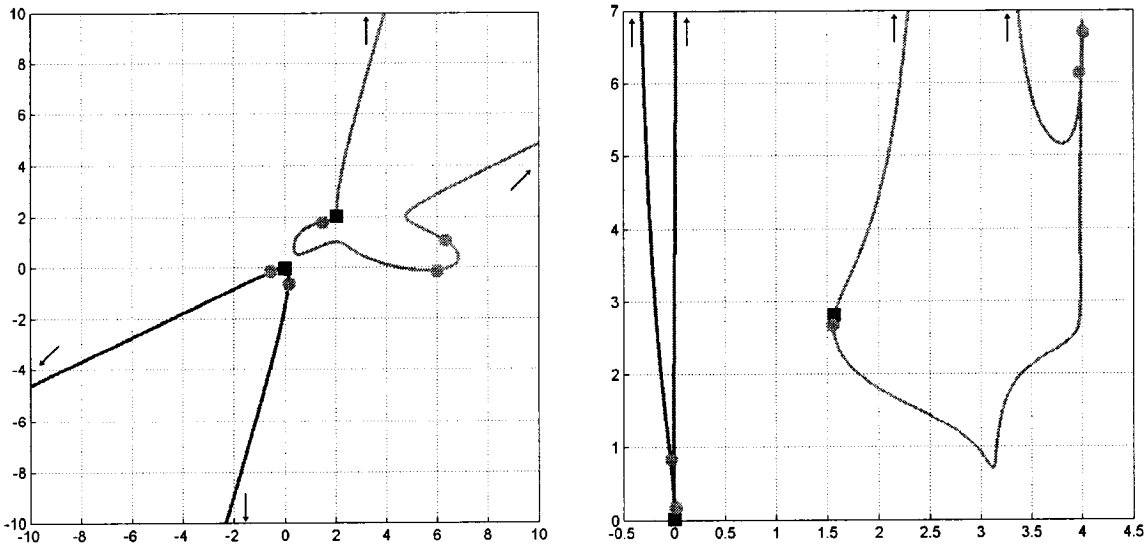

Figure 7.18: Wedges and catastrophes: the second example.

The First Example

$$a_{2,0} = 0 \quad a_{1,1} = 1 \quad a_{0,2} = -1 \quad b_{2,0} = 1 \quad b_{1,1} = 0 \quad b_{0,2} = 0$$
$$c_{2,0} = 0 \quad c_{1,1} = 0 \quad c_{0,2} = 1 \quad d_{2,0} = 1 \quad d_{1,1} = 1 \quad d_{0,2} = 0$$

$$f_0(x) = \exp\left(-\tfrac{x_1^2+x_2^2}{10}\right) \qquad g_\xi(x) = \exp\left(-\tfrac{(x_1-2)^2+(x_2-2)^2}{14}\right)$$

See Figure 7.17 for a portion of $\kappa(3)$ and a partial bifurcation diagram of $P_{0.01}$. By construction, the zero-level set for this first example is exactly the zero-level set of the EB map; however, their bifurcation diagrams are not topologically equivalent (see Figures 5.3 and 5.4). In this instance, the wedge angles record fold catastrophes on $C_0 \in \mathcal{C}_B$ and $\infty-$catastrophes on $C_\xi \in \mathcal{C}_\infty$. Note further that this map provides an instance when the anchoring wedges overlap.

The Second Example

$$a_{2,0} = \tfrac{2}{5} \quad a_{1,1} = \tfrac{43}{10} \quad a_{0,2} = -\tfrac{17}{2} \quad b_{2,0} = \tfrac{51}{10} \quad b_{1,1} = -\tfrac{91}{10} \quad b_{0,2} = -\tfrac{12}{5}$$
$$c_{2,0} = -\tfrac{16}{5} \quad c_{1,1} = -\tfrac{99}{10} \quad c_{0,2} = -\tfrac{48}{5} \quad d_{2,0} = -\tfrac{53}{10} \quad d_{1,1} = \tfrac{61}{10} \quad d_{0,2} = -\tfrac{99}{10}$$

$$f_0(x) = 1 \qquad g_\xi(x) = 1$$

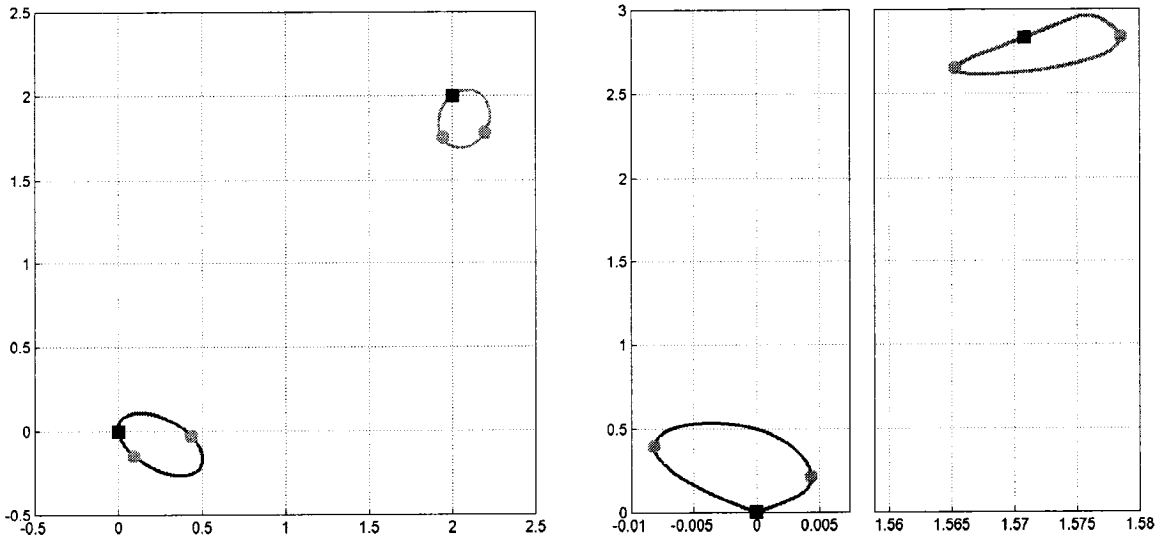

Figure 7.19: Wedges and catastrophes: the third example.

See Figure 7.18 for a portion of $\kappa(3)$ and a partial bifurcation diagram of $P_{0.01}$. In this instance, $C_0, C_\xi \in \mathcal{C}_\infty$, and $\varphi_0^\pm, \varphi_\xi^-$ record fold catastrophes while φ_ξ^+ records an $\infty-$catastrophe.

The Third Example

$$a_{2,0} = -\tfrac{53}{10} \quad a_{1,1} = -\tfrac{28}{5} \quad a_{0,2} = -9 \quad b_{2,0} = -\tfrac{9}{5} \quad b_{1,1} = -\tfrac{41}{10} \quad b_{0,2} = -\tfrac{57}{10}$$
$$c_{2,0} = \tfrac{22}{5} \quad c_{1,1} = \tfrac{21}{5} \quad c_{0,2} = -\tfrac{3}{2} \quad d_{2,0} = -9 \quad d_{1,1} = \tfrac{49}{10} \quad d_{0,2} = -10$$
$$f_0(x) = 1 \quad g_\xi(x) = 1$$

See Figure 7.19 for a portion of $\kappa(3)$ and a partial bifurcation diagram of $P_{0.01}$. In this instance, $C_0, C_\xi \in \mathcal{C}_\mathrm{B}$, and the wedge angles all record fold catastrophes.

The Fourth Example

$$a_{2,0} = 2 \quad a_{1,1} = \tfrac{13}{5} \quad a_{0,2} = -\tfrac{13}{10} \quad b_{2,0} = \tfrac{16}{5} \quad b_{1,1} = -\tfrac{21}{10} \quad b_{0,2} = \tfrac{3}{5}$$
$$c_{2,0} = -\tfrac{4}{5} \quad c_{1,1} = -\tfrac{3}{10} \quad c_{0,2} = -\tfrac{29}{10} \quad d_{2,0} = -\tfrac{9}{10} \quad d_{1,1} = \tfrac{7}{10} \quad d_{0,2} = -\tfrac{3}{2}$$
$$f_0(x) = 1 \quad g_\xi(x) = 1$$

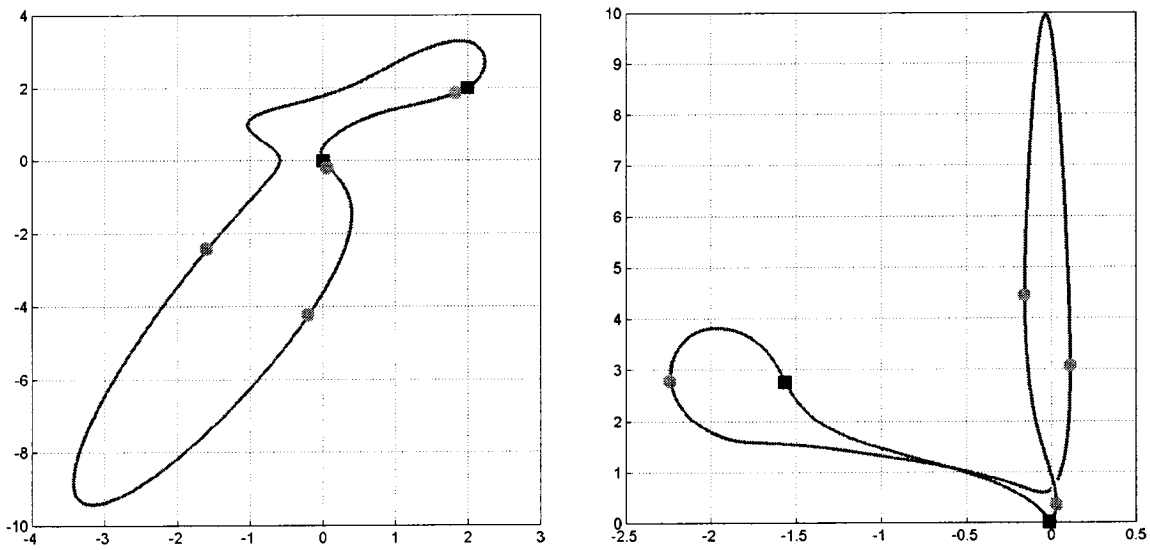

Figure 7.20: Wedges and catastrophes: the fourth example.

See Figure 7.20 for a portion of $\kappa(3)$ and a partial bifurcation diagram of $P_{0.01}$. In this instance, $C_0 = C_\xi \in \mathcal{C}_B$, the wedge angles all record fold catastrophes and the anchoring wedges overlap.

The Fifth Example

$$
\begin{array}{lllllll}
a_{2,0} = \frac{59}{10} & a_{1,1} = \frac{43}{10} & a_{0,2} = -7 & a_{3,0} = \frac{38}{5} & a_{2,1} = \frac{27}{5} & a_{1,2} = -\frac{59}{10} & a_{0,3} = -\frac{1}{5} \\
b_{2,0} = -\frac{37}{5} & b_{1,1} = -\frac{51}{10} & b_{0,2} = -\frac{9}{5} & b_{3,0} = \frac{63}{10} & b_{2,1} = \frac{41}{10} & b_{1,2} = -4 & b_{0,3} = \frac{43}{10} \\
c_{2,0} = \frac{11}{5} & c_{1,1} = -\frac{36}{5} & c_{0,2} = -\frac{38}{5} & c_{3,0} = -\frac{61}{10} & c_{2,1} = 2 & c_{1,2} = -\frac{4}{5} & c_{0,3} = -\frac{8}{5} \\
d_{2,0} = -\frac{49}{10} & d_{1,1} = -\frac{38}{5} & d_{0,2} = \frac{27}{10} & d_{3,0} = -\frac{79}{10} & d_{2,1} = \frac{69}{10} & d_{1,2} = -\frac{29}{5} & d_{0,3} = -\frac{41}{10}
\end{array}
$$

$$f_0(x) = 1 \qquad g_\xi(x) = 1$$

See Figure 7.21 for a portion of $\kappa(3)$ and a partial bifurcation diagram of $P_{0.01}$. In this instance, $C_0 = C_\xi \in \mathcal{C}_\infty$ and the wedge angles all record fold catastrophes.

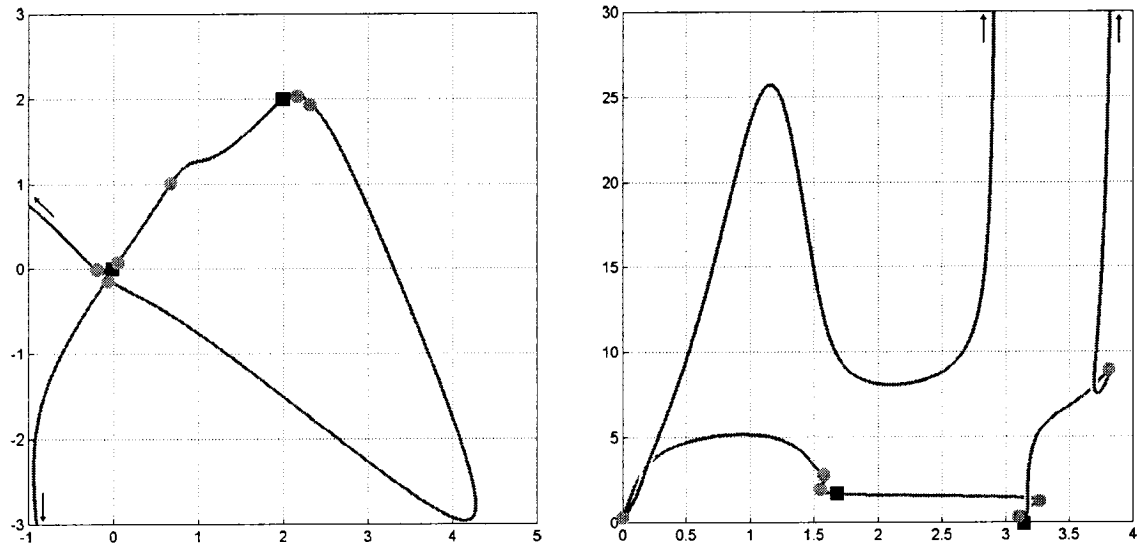

Figure 7.21: Wedges and catastrophes: the fifth example.

7.4 Appendix: Technical Details

Technical Result 18 We solve the ODE (7.2.1) using standard arguments.

Proof: If $a\lambda_1 + b\lambda_2 \neq 0$, set $y = (a\lambda_1 + b\lambda_2)p - b\lambda_2\xi_2$. Then $\dot{y} = (a\lambda_1 + b\lambda_2)\dot{p}$ and so (7.2.1) becomes

$$\frac{1}{a\lambda_1 + b\lambda_2}\dot{y} - y = ve^{it}. \tag{7.4.1}$$

The homogeneous equation is

$$\frac{1}{a\lambda_1 + b\lambda_2}\dot{y} - y = 0, \tag{7.4.2}$$

and its characteristic polynomial is $\frac{1}{a\lambda_1+b\lambda_2}\lambda - 1$; its only root is $\lambda = a\lambda_1 + b\lambda_2$. Thus, the homogeneous solution y_h of (7.4.2) is $y_h(t) = Ce^{(a\lambda_1+b\lambda_2)t}$, where C is a constant. Due to the form of the non-homogenous term, the particular solution y_p of (7.4.1) is $y_p(t) = Ke^{it}$, where K is a constant. The general solution of (7.4.1) is thus

$$y_g(t) = y_h(t) + y_p(t) = Ce^{(a\lambda_1+b\lambda_2)t} + Ke^{it}.$$

Since $p = \frac{y+b\lambda_2\xi_2}{a\lambda_1+b\lambda_2}$, the general solution of (7.2.1) is

$$p(t) = \frac{y_g(t) + b\lambda_2\xi_2}{a\lambda_1 + b\lambda_2} = \frac{1}{a\lambda_1 + b\lambda_2}\left(Ce^{(a\lambda_1+b\lambda_2)t} + Ke^{it} + b\lambda_2\xi_2\right).$$

To find the values of C and K, we differentiate the general solution $p(t)$ to obtain

$$\dot{p} = \frac{1}{a\lambda_1 + b\lambda_2}\left((a\lambda_1 + b\lambda_2)Ce^{(a\lambda_1+b\lambda_2)t} + iKe^{it}\right) = Ce^{(a\lambda_1+b\lambda_2)t} + \frac{iK}{a\lambda_1 + b\lambda_2}e^{it}.$$

Then

$$\dot{p} - (a\lambda_1 + b\lambda_2)p = \left(\frac{1}{a\lambda_1 + b\lambda_2} - 1\right)Ke^{it} - b\lambda_2\xi_2.$$

As p is the solution of (7.2.1), $\left(\frac{i}{a\lambda_1+b\lambda_2} - 1\right)K = v$, and so

$$K = \frac{v(a\lambda_1 + b\lambda_2)}{i - (a\lambda_1 + b\lambda_2)}.$$

Furthermore,

$$p_0 = \frac{y_{g0} + b\lambda_2\xi_2}{a\lambda_1 + b\lambda_2} = \frac{C + K + b\lambda_2\xi_2}{a\lambda_1 + b\lambda_2},$$

so $C = (a\lambda_1 + b\lambda_2) - K - b\lambda_2\xi_2 = (a\lambda_1 + b\lambda_2)\left[p_0 - \frac{v}{i-(a\lambda_1+b\lambda_2)}\right] - b\lambda_2\xi_2$ and

$$p(t) = \left(p_0 - \frac{v}{i - (a\lambda_1 + b\lambda_2)} - \frac{b\lambda_2\xi_2}{a\lambda_1 + b\lambda_2}\right)e^{(a\lambda_1+b\lambda_2)t} + \frac{v}{i - (a\lambda_1 + b\lambda_2)}e^{it} + \frac{b\lambda_2\xi_2}{a\lambda_1 + b\lambda_2}$$

is the solution of (7.2.1) through p_0.

If $a\lambda_1 + b\lambda_2 = 0$ then (7.2.1) becomes $\dot{p} = ve^{it} - b\lambda_2\xi_2$. Direct integration leads to

$$p(t) = -ive^{it} - b\lambda_2\xi_2 t + C.$$

Since $p_0 = -iv + C$, then $C = p_0 + iv$ and

$$p(t) = -ive^{it} - b\lambda_2\xi_2 t + p_0 + iv = p_0 + iv(1 - e^{it}) - b\lambda_2\xi_2 t.$$

This completes the proof. ∎

Technical Result 19 The coefficients of order ≤ 2 of (7.2.7) are given by (7.2.8).

Proof: For $z_0 \in \mathbb{C}$, let g_1, g_2 and $z_{\varepsilon,\mu}(t; z_0)$ be as defined on page 121. Then

$$K(w, \overline{w}, t, \varepsilon, \mu) = \mu g_1(w - iv, \text{c. c.}) + g_2(w - iv - \xi_2 e^{-it}, \text{c. c.})$$

and

$$z_{\varepsilon,\mu}(t; z_0) = z_0 + \varepsilon\int_0^t e^{is}K\left(z_{\varepsilon,\mu}(s; z_0)e^{-is}, \text{c. c.}, s, \varepsilon, \mu\right)ds. \tag{7.4.3}$$

We obtain the desired coefficients *via* appropriate differentiation of the integral equation (7.4.3).

1. Since $z_{0,0}(t;z_0) = 0$ for all t, $z(2\pi;z_0) = 0$.

2. Differentiating (7.4.3) with respect to ε yields

$$\begin{aligned} D_\varepsilon z_{\varepsilon,\mu}(t;z_0) = &\int_0^t e^{is} K\big(z_{\varepsilon,\mu}(s;z_0)e^{-is}, \text{c. c.}, s, \varepsilon, \mu\big)\, ds \\ &+ \varepsilon \int_0^t e^{is}\big[D_1 K\big(z_{\varepsilon,\mu}(s;z_0)e^{-is}, \text{c. c.}, s, \varepsilon, \mu\big) D_\varepsilon z_{\varepsilon,\mu}(s;z_0)e^{-is} \\ &\quad + D_2 K\big(z_{\varepsilon,\mu}(s;z_0)e^{-is}, \text{c. c.}, s, \varepsilon, \mu\big) D_\varepsilon \overline{z_{\varepsilon,\mu}(s;z_0)} e^{is} \\ &\quad + D_\varepsilon K\big(z_{\varepsilon,\mu}(s;z_0)e^{-is}, \text{c. c.}, s, \varepsilon, \mu\big)\big]\, ds. \end{aligned}$$

Then

$$D_\varepsilon z_{0,0}(t;z_0) = \int_0^t e^{is} K\big(z_0 e^{-is}, \text{c. c.}, s, 0, 0\big)\, ds \quad \text{for all } t \tag{7.4.4}$$

and so

$$D_\varepsilon z_{0,0}(2\pi;z_0) = \int_0^{2\pi} e^{is} K\big(z_0 e^{-is}, \text{c. c.}, s, 0, 0\big)\, ds = \int_0^{2\pi} e^{is} g_2\big((z_0 - \xi_2)e^{-is} - iv, \text{c. c.}\big)\, ds.$$

3. Differentiating (7.4.3) with respect to μ yields

$$\begin{aligned} D_\mu z_{\varepsilon,\mu}(t;z_0) = \varepsilon &\int_0^t e^{is}\big[D_1 K\big(z_{\varepsilon,\mu}(s;z_0)e^{-is}, \text{c. c.}, s, \varepsilon, \mu\big) D_\mu z_{\varepsilon,\mu}(s;z_0)e^{-is} \\ &\quad + D_2 K\big(z_{\varepsilon,\mu}(s;z_0)e^{-is}, \text{c. c.}, s, \varepsilon, \mu\big) D_\mu \overline{z_{\varepsilon,\mu}(s;z_0)} e^{is} \\ &\quad + D_\mu K\big(z_{\varepsilon,\mu}(s;z_0)e^{-is}, \text{c. c.}, s, \varepsilon, \mu\big)\big]\, ds. \end{aligned}$$

Then $D_\mu z_{0,0}(t;z_0) = 0$ for all t and so $D_\mu z_{0,0}(2\pi;z_0) = 0$.

4. Differentiating (7.4.3) twice with respect to ε yields

$$\begin{aligned} D_{\varepsilon\varepsilon} z_{\varepsilon,\mu}(t;z_0) = 2 &\int_0^t e^{is}\big[D_1 K\big(z_{\varepsilon,\mu}(s;z_0)e^{-is}, \text{c. c.}, s, \varepsilon, \mu\big) D_\varepsilon z_{\varepsilon,\mu}(s;z_0)e^{-is} \\ &\quad + D_2 K\big(z_{\varepsilon,\mu}(s;z_0)e^{-is}, \text{c. c.}, s, \varepsilon, \mu\big) D_\varepsilon \overline{z_{\varepsilon,\mu}(s;z_0)} e^{is} \\ &\quad + D_\varepsilon K\big(z_{\varepsilon,\mu}(s;z_0)e^{-is}, \text{c. c.}, s, \varepsilon, \mu\big)\big]\, ds + \varepsilon \int_0^t A_{2,0}(z_0, s, \varepsilon, \mu)\, ds, \end{aligned}$$

where $A_{2,0}$ is some function involving second derivatives of K. Then

$$\begin{aligned} D_{\varepsilon\varepsilon} z_{0,0}(2\pi;z_0) &= 2 \int_0^{2\pi} e^{is}\big[D_1 K\big(z_0 e^{-is}, \text{c. c.}, s, 0, 0\big) D_\varepsilon z_{0,0}(s;z_0)e^{-is} \\ &\quad + D_2 K\big(z_0 e^{-is}, \text{c. c.}, s, 0, 0\big) D_\varepsilon \overline{z_{0,0}(s;z_0)} e^{is} + D_\varepsilon K\big(z_0 e^{-is}, \text{c. c.}, s, 0, 0\big)\big]\, ds \\ &= 2 \int_0^{2\pi} \big[D_1 g_2((z_0 - \xi_2)e^{-is} - iv, \text{c. c.}) D_\varepsilon z_{0,0}(s;z_0) \\ &\quad + D_2 g_2((z_0 - \xi_2)e^{-is} - iv, \text{c. c.}) D_\varepsilon \overline{z_{0,0}(s;z_0)} e^{2is}\big]\, ds, \end{aligned}$$

where $D_\varepsilon z_{0,0}(s;z_0)$ is obtained from (7.4.4).

5. Differentiating (7.4.3) with respect to ε then with respect to μ yields

$$\begin{aligned} D_{\varepsilon\mu}z_{\varepsilon,\mu}(t;z_0) = \int_0^t e^{is}\big[&D_1K\big(z_{\varepsilon,\mu}(s;z_0)e^{-is},\text{c. c.},s,\varepsilon,\mu\big)D_\mu z_{\varepsilon,\mu}(s;z_0)e^{-is} \\ &+ D_2K\big(z_{\varepsilon,\mu}(s;z_0)e^{-is},\text{c. c.},s,\varepsilon,\mu\big)D_\mu\overline{z_{\varepsilon,\mu}(s;z_0)}e^{is} \\ &+ D_\mu K\big(z_{\varepsilon,\mu}(s;z_0)e^{-is},\text{c. c.},s,\varepsilon,\mu\big)\big]\,ds + \varepsilon\int_0^t A_{1,1}(z_0,s,\varepsilon,\mu)\,ds, \end{aligned}$$

where $A_{1,1}$ is some function involving second derivatives of K. Then

$$\begin{aligned} D_{\varepsilon\mu}z_{0,0}(2\pi;z_0) &= \int_0^{2\pi} e^{is}\big[D_1K\big(z_0e^{-is},\text{c. c.},s,0,0\big)D_\mu z_{0,0}(s;z_0)e^{-is} \\ &\quad + D_2K\big(z_0e^{-is},\text{c. c.},s,0,0\big)D_\mu\overline{z_{0,0}(s;z_0)}e^{is} + D_\mu K\big(z_0e^{-is},\text{c. c.},s,0,0\big)\big]\,ds \\ &= \int_0^{2\pi} e^{is}g_1(z_0e^{-is}-iv,\text{c. c.})\,ds, \end{aligned}$$

as $D_\mu z_{0,0}(s;z_0) = 0$ for all s.

6. Differentiating (7.4.3) twice with respect to μ yields

$$D_{\mu\mu}z_{\varepsilon,\mu}(t;z_0) = \varepsilon\int_0^t A_{0,2}(z_0,s,\varepsilon,\mu)\,ds,$$

where $A_{0,2}$ is some function involving second derivatives of K. Then

$$D_{\mu\mu}z_{0,0}(2\pi;z_0) = 0.$$

This completes the proof. ∎

Technical Result 20 There is an explicit expression for the fold bifurcation curve of P_{TS}.

Proof: Because of the inherent symmetry of the system, we look for fixed points on the line $y = x$. Let (7.2.11) and J be as in the proof of Proposition 7.2.1; fold bifurcation points are the solutions (x,x,ε,μ) of

$$\begin{aligned} 4 - x + 2\mu(x^2+2)x + \varepsilon(\pi(x-4) - 1) &= 0 \\ \varepsilon\pi - 1 + 2\mu(3x^2+2) &= 0 \end{aligned} \tag{7.4.5}$$

for which $\text{rank}(J) = 3$. The second of these equations is easily solved as

$$\mu = \mu(\varepsilon) = \frac{1-\varepsilon\pi}{2(3x^2+2)}.$$

The first equation in (7.4.5) then becomes

$$4 - x + \frac{1 - \varepsilon\pi}{3x^2 + 2}(x^2 + 2)x + \varepsilon(\pi(x - 4) - 1) = 0,$$

or equivalently

$$2(\varepsilon\pi - 1)x^3 + 3(4 - \varepsilon - 4\varepsilon\pi)x^2 + 2(4 - \varepsilon - 4\varepsilon\pi) = 0. \tag{7.4.6}$$

Write (7.4.6) as $F(x) = 0$. We first show that $F(x)$ has only one real root for small values of ε. The critical points of the cubic are the roots of its derivative

$$F'(x) = 6x\big((\varepsilon\pi - 1)x + (4 - \varepsilon - 4\varepsilon\pi)\big),$$

namely $x_1(\varepsilon) = 0$ and $x_2(\varepsilon) = -\frac{4-\varepsilon-4\varepsilon\pi}{\varepsilon\pi-1}$. Now,

$$\begin{aligned} F(x_1(\varepsilon)) &= 8 - 2\varepsilon - 8\varepsilon\pi \\ F(x_2(\varepsilon)) &= \frac{(4 - \varepsilon - 4\varepsilon\pi)^3}{(\varepsilon\pi - 1)^2} + 8 - 2\varepsilon - 8\varepsilon\pi. \end{aligned}$$

Clearly, $x_1(\varepsilon) < x_2(\varepsilon)$ and $F(x_1(\varepsilon)), F(x_2(\varepsilon)) > 0$ for small values of ε. Hence, $F(x)$ has only one real root $x_0(\varepsilon)$ when ε is small. We can find the root analytically using Cardano's formula for the cubic; first set $F(x) = ax^3 + bx^2 + cx + d$ and let

$$\begin{aligned} A &= -\frac{b^3}{27a^3} + \frac{bc}{6a^2} - \frac{d}{2a} \\ B &= \frac{c}{3a} - \frac{b^2}{9a^2} \\ C &= -\frac{b}{3a}. \end{aligned}$$

Then

$$x_0(\varepsilon) = \sqrt[3]{A + \sqrt{A^2 + B^3}} + \sqrt[3]{A - \sqrt{A^2 + B^3}} + C.$$

This completes the proof. ∎

Chapter 8

Conclusion

The application of forced Euclidean symmetry-breaking to the study of rotating waves in reaction-diffusion systems has yielded a number of interesting theorems. We finish with some conjectures concerning modulated rotating waves, followed by possible applications to the fields of cardiology and ecology, as well as a list of problems and questions, whose solutions would vastly improve our knowledge and understanding of spiral waves and excitable media.

8.1 Conjectures

The equations describing the essential dynamics of a normally hyperbolic modulated rotating wave are similar to those of rotating waves derived in Section 3.2. Near such a MRW, the basic (skew-product) bundle equations on the manifold $V^* = \mathbb{C} \times \mathbb{T}^2$ for a reaction-diffusion system with n translational symmetry-breaking terms take the form

$$\begin{aligned} \dot{p} &= e^{i\varphi}\left[v + \sum_{j=1}^{n} \lambda_j H_j^p((p-\xi_j)e^{-i\varphi}, \overline{(p-\xi_j)}e^{i\varphi}, t, \lambda_j)\right] \\ \dot{\varphi} &= \omega_{\text{rot}} + \sum_{j=1}^{n} \lambda_j H_j^{\varphi}((p-\xi_j)e^{-i\varphi}, \overline{(p-\xi_j)}e^{i\varphi}, t, \lambda_j), \end{aligned} \tag{8.1.1}$$

where $\lambda = (\lambda_1, \ldots, \lambda_n) \in \mathbb{R}^n$, $v \in \mathbb{C}$, $\omega_{\text{rot}} \neq 0$ and $H_j^{p,\varphi} \in \mathfrak{P}_t^{2\pi}$ are smooth and uniformly bounded in p for all $j = 1, \ldots, n$. As in Sections 3.2 and 6.1, it is conjectured that the higher order $\lambda_j\lambda_k$ terms do not influence the local analysis.

System (8.1.1) cannot be analyzed as easily as (4.0.1), but it seems nonetheless likely that the following generalizations of Theorems 4.1.3 and 4.2.3 hold.

Conjecture 8.1.1 *Let $k \in \{1,\dots,n\}$. Generically, there is a wedge-shaped region near $\lambda = 0$ of the form*

$$\mathcal{W}_k = \{(\lambda_1,\dots,\lambda_n) \in \mathbb{R}^n \,:\, |\lambda_j| < W_{k,j}|\lambda_k|,\ W_{k,j} > 0,\ \text{for } j \neq k \text{ and } \lambda_k \text{ near } 0\}$$

such that for all $0 \neq \lambda \in \mathcal{W}_k$, (8.1.1) has a unique hyperbolic modulated rotating wave $\mathfrak{S}^k_\lambda$ centered away from ξ_k.

Conjecture 8.1.2 *Let $k \in \{1,\dots,n\}$. Given a hyperbolic equilibrium of a related averaged system, there is a wedge-shaped region near $\lambda = 0$ of the form*

$$\mathcal{V}_k = \{(\lambda_1,\dots,\lambda_n) \in \mathbb{R}^n \,:\, |\lambda_j| < V_{k,j}|\lambda_k|,\ V_{k,j} > 0,\ \text{for } j \neq k \text{ and } \lambda_k \text{ near } 0\}$$

such that for all $0 \neq \lambda \in \mathcal{V}_k$, (8.1.1) has a hyperbolic 3–frequency epicycle manifold $\mathfrak{E}^k_\lambda$ centered near, but generically not at, ξ_k.

The center bundle equations on the manifold $V^* = \mathbb{C} \times \mathbb{T}^2$ for a reaction-diffusion system with a translational symmetry-breaking term and a rotational symmetry-breaking term take the form

$$\begin{aligned} \dot{p} &= e^{i\varphi}\left[v + \varepsilon G^p(\varphi,t,\varepsilon,\mu) + \mu H^p(pe^{-i\varphi},\overline{p}e^{i\varphi},t,\varepsilon,\mu)\right] \\ \dot{\varphi} &= \omega_{\text{rot}} + \varepsilon G^\varphi(\varphi,t,\varepsilon,\mu) + \mu H^\varphi(pe^{-i\varphi},\overline{p}e^{i\varphi},t,\varepsilon,\mu), \end{aligned} \tag{8.1.2}$$

where $(\varepsilon,\mu) \in \mathbb{R}^2$, $v \in \mathbb{C}$, $\omega_{\text{rot}} \neq 0$, $G^{p,\varphi} \in \mathfrak{P}^{2\pi/\ell}_\varphi, H^{p,\varphi}$ are smooth and uniformly bounded in p and 2π–periodic in t and $0 < \ell \in \mathbb{N}$. As above, it seems likely that the following generalizations of Theorems (6.2.1), (6.2.2), (6.2.3) and (6.2.4) will hold.

Conjecture 8.1.3 *Let $\ell = 1$. Generically, there is a wedge-shaped region near $(\varepsilon,\mu) = (0,0)$ of the form*

$$\mathcal{W} = \{(\varepsilon,\mu) \in \mathbb{R}^2 \,:\, |\varepsilon| < K|\mu|,\ K > 0,\ \mu \text{ near } 0\}$$

such that for all $(\varepsilon,\mu) \in \mathcal{W}$ with $\mu \neq 0$, (8.1.2) has a unique hyperbolic discrete modulated rotating wave $\mathfrak{D}^1_{\varepsilon,\mu}$, with trivial spatio-temporal symmetry, centered away from the origin.

Conjecture 8.1.4 *Let $\ell = 1$. Given a hyperbolic equilibrium of a related averaged system, there is a wedge-shaped region near $(\varepsilon, \mu) = (0,0)$ of the form*

$$\mathcal{V} = \{(\varepsilon, \mu) \in \mathbb{R}^2 : |\varepsilon| < K|\mu|, \ K > 0, \ \mu \text{ near } 0\}$$

such that for all $(\varepsilon, \mu) \in \mathcal{V}$ with $\mu \neq 0$, (8.1.2) has a hyperbolic 3–frequency epicycle manifold $\mathfrak{G}^1_{\varepsilon,\mu}$ centered near, but generically not at, the origin.

Conjecture 8.1.5 *Let $\ell > 1$. Generically, there is a deleted neighbourhood $\mathcal{W}^\ell$ of the origin such that for all $(\varepsilon, \mu) \in \mathcal{W}^\ell$, (8.1.2) has a unique hyperbolic discrete modulated rotating wave $\mathfrak{D}^\ell_{\varepsilon,\mu}$ with $\mathbb{Z}_\ell$–spatio-temporal symmetry centered at the origin.*

Conjecture 8.1.6 *Let $\ell > 1$. Given a hyperbolic equilibrium of a related averaged system, there is a deleted neighbourhood $\mathcal{V}^\ell$ of the origin such that for all $(\varepsilon, \mu) \in \mathcal{V}^\ell$, (8.1.2) has a hyperbolic 3–frequency epicycle manifold $\mathfrak{G}^\ell_{\varepsilon,\mu}$ centered at the origin.*

8.2 Remarks

The results presented in section 7.1 were naively qualitative, as we were mostly interested in demonstrating the validity of our results in an experimental setting.

In numerical experiments where we have attempted to produce a Bogdanov-Takens bifurcation as predicted in Section 4.3, the linear systems we encountered were invariably too ill-conditioned (with condition number to the order of $\sim 10^{15}$) for the results to be meaningful. It remains to be seen how this obstacle can be circumvented.

Finally, while numerical experiments show without the shadow of a doubt that spirals can anchor away from a center of inhomogeneity, we would find it very satisfying to see this result reproduced in the laboratory. From a resolutely profane perspective, the Belousov-Zhabotinsky reaction appears most likely to yield results, as it seems the easiest to control.

It should also be noted that the study of spirals does not start and end in the plane. For instance, Comanici used the dynamical system approach in her doctoral thesis to study spirals on spherical domains [23]. Scroll waves, the 3-dimensional analogues of spiral waves, have also attracted attention from physicists and cardiologists in recent years [1, 21, 65, 66].

8.3 Possible Applications

A Cardiac Forecast System

Ultimately, a complete understanding of spirals in excitable systems will be a major component in the eventual creation of what Leon Glass (a physiologist at McGill University) terms a 'cardiac forecast system' (CFS) [28]. A CFS would allow accurate prediction and prevention of fatal cardiac activity; however, a working CFS prototype is still "at least twenty years away [16]."

We have seen that (in the infinite plane) numerous sites of inhomogeneity can lead to spirals anchoring away from centers of high density or even chaos. Can these observations be of use when combining the different aspects of cardiology (electrical activity, blood flow, scroll waves, etc.) into an adequate mathematical model of the heart? [19, 29, 44]

Prey-Predator Pursuit and Evasion Waves

Reaction-diffusion systems are also used to model spatial interactions amongst prey and predator species [56, 57]. Consider for instance the modified Lotka-Volterra system

$$\begin{aligned} \frac{\partial U}{\partial t} &= AU\left(1-\frac{U}{K}\right) - BUV + D_1\Delta U \\ \frac{\partial V}{\partial t} &= CUV - DV + D_2\Delta V, \end{aligned} \tag{8.3.1}$$

where U and V represent the prey and predator populations, respectively, K is the prey carrying capacity, A, B, C, D are positive constants and D_1, D_2 are the diffusion coefficients.

In such a model, the wavefronts follow the prey species as it tries to evade the predators, and the predator species as it attempts to capture the preys. The model (8.3.1) can sustain rotating waves, as it is a reaction-diffusion system.[1]

Define an **oasis** as a point of high ecological 'density,' or rallying point, such as a lake or bay. Assume that there is a base habitat type and that it is uniformly spread in small neighbourhoods of these oases.[2] If the perturbations created by various oases

[1] The illustration from [4] on p. 2 shows such spirals.

[2] This is certainly the case in a desert, for instance.

are small with respect to the base habitat type, our results predict the appearance of an anchored pursuit and evasion rotating wave, generically not centered at an oasis.

8.4 Future and Related Work

MRW, TW and MTW

Previous authors were often able to study RW, MRW, TW and MTW in the same context (see [48, 51], for instance). In our treatment of full Euclidean symmetry-breaking, only RW and TW were found to be easily amenable to characterization, and even then, TW were not tackled in order to simplify the presentation. The next step then is to reproduce the work of this treatise as it applies to TW. Then, our approach will need to be suitably modified so as to accommodate the extra variable that appears in (8.1.1) and (8.1.2). Hopefully, we will then be able to fully characterize MRW and MTW under full Euclidean symmetry-breaking.

An Explicit Center Manifold Reduction Theorem

The CMRT does not provide the explicit relation between the center bundle equations system and the original PDE system.

When a specific center manifold system is studied, we thus have no way of knowing if it corresponds to a 'realizable' excitable system, *i.e.*, if it is 'attainable' in any way from such an excitable system *via* the CMRT.

Recent observations by Lajoie and LeBlanc [49] suggest that it might be possible to efficiently relate the coefficients of the RDS to those of the center manifold, near a traveling wave. Is there a direct and efficient way to compute the relevant coefficients of the center bundle equations directly from the PDE, near any type of relative equilibrium or relative periodic solution?

Spiral Groupings

So far, the model-independent approach based on the CMRT has only been used to study *isolated* spiral waves. Even though experiments by Li, Ouyang, Petrov and Swinney [52] have shown that spiral waves can be isolated with the help of a laser, they

are rarely found in that state in excitable media (see for instance the two illustrations on p. 2).

Spiral **groupings**, where two or more spirals rotate around a common center or one another, have much different dynamics, as is attested to by the recent numerical simulations of Pertsov and Zariski [78]. Some of the showcased interactions are somewhat analogous to this thesis' results on epicycle/boundary drifting, which begs the question: can our approach be altered to apply to spiral groupings as well?

Global Spiral Dynamics

Finally, the CMRT can only be applied to local neighbourhoods. Yet, many spiral interactions are global in nature (see [78] for details). As of now, there is little machinery short of numerical simulations to deal with spiral dynamics on a global level. How can this situation be remedied?

Appendix A

Article Summaries

A.1 Summary of [5]

In *Linear stability analysis of rotating spiral waves in excitable media*, Barkley studies the spectrum of the linearization of a reaction-diffusion model at a rotating wave.

Summary: Consider the Oregonator-like system of PDE

$$\begin{aligned}\frac{\partial u_1}{\partial t} &= \Delta u_1 + \frac{1}{\varepsilon} u_1(1-u_1)\left(u_1 - \frac{u_2+b}{a}\right)\\ \frac{\partial u_2}{\partial t} &= \delta \Delta u_2 + u_1 - u_2,\end{aligned}$$

where a, b, ε are parameters with ε small and δ taken to be a constant in $[0,1]$. In vector form, this system may be written as

$$\frac{\partial u}{\partial t} = \hat{\delta}\Delta u + f(u), \tag{A.1.1}$$

where $u = (u_1, u_2)^\top$, $\hat{\delta} = \mathrm{diag}(1, \delta)$ and f contains the remaining terms. The boundary condition $\partial_r u = 0$ is taken on a circle of radius $R > 0$. With this set-up, (A.1.1) has Euclidean symmetry under the action of (1.1.4) as $R \to \infty$.

To find RW solutions of (A.1.1), *i.e.*, solutions for which $(\partial_t + \omega\partial_\theta)u \equiv 0$ for some speed of rotation ω, it suffices to solve the eigenvalue problem

$$\begin{aligned}F(u) &= 0\\ DF(u)\tilde{u} &= \lambda\tilde{u},\end{aligned} \tag{A.1.2}$$

where $F(u) = \hat{\delta}\Delta u + \omega\partial_\theta u + f(u)$ and $DF(u) = \hat{\delta}\Delta + \omega\partial_\theta + Df(u)$. Any λ solving (A.1.2) will correspond to an eigenvalue of the linearization of (A.1.1) at the RW solution.
Using fast and efficient numerical methods, it can be shown that three of the five leading eigenvalues[1] lie on the imaginary axis. Indeed, the rotational symmetry of (A.1.1) forces $\lambda_R = 0$ (with corresponding eigenmode $\tilde{u}_R = \partial_\theta u$, where u is the spiral solution of the first equation in (A.1.2)); the translational symmetry of (A.1.1) imposes $\lambda_T = \pm i\omega$ (with corresponding eigenmode $\tilde{u}_T = \partial_x u \pm i\partial_y u$, where u is as above). Note that this holds in spite of the fact that the boundary condition breaks the Euclidean symmetry: for sufficiently large domain, the real part of λ_T is numerically indistinguishable from zero.[2]

There is yet a last pair of complex conjugate leading eigenvalues $\lambda_B = \alpha(a) \pm i\beta(a)$ that crosses the imaginary axis for some prescribed $a = a^*$, leading to a Hopf bifurcation or 'spiral wave instability', in which quasi-periodic behaviour is observed.

All the remaining eigenvalues have negative real part and so do not affect spiral dynamics. As a result, the five leading eigenvalues are isolated in the spectrum and so any pair (u, ω_{rot}) that solves (A.1.2) is *not* part of a continuum of solutions with continuously varying shapes or speed of rotation.

These results are in fact model-independent; as long as the reaction-diffusion equations governing the field u are $\mathbb{SE}(2)$−equivariant, the five leading eigenvalues will have the above properties. ∎

A.2 Summary of [51]

In *Translational Symmetry-Breaking for Spiral Waves*, LeBlanc and Wulff study small $\mathbb{SO}(2)$-equivariant perturbations of (1.1.6) taking the form (1.1.8).

Summary: Consider the system (1.1.8). For normally hyperbolic relative equilibria (*i.e.*, for $q = 0$ and the RW is not at the transition to a MRW), a center manifold reduction yields

$$\begin{aligned} \dot{p} &= e^{i\varphi}[v + \varepsilon G^p(pe^{-i\varphi}, \overline{p}e^{i\varphi}, \varepsilon)] \\ \dot{\varphi} &= \omega_{\text{rot}} + \varepsilon G^\varphi(pe^{-i\varphi}, \overline{p}e^{i\varphi}, \varepsilon), \end{aligned} \tag{A.2.1}$$

where $v \in \mathbb{C}^\times$ and $\omega_{\text{rot}} \in \mathbb{R}$.

[1] Eigenvalues with largest real part.
[2] Barkley provides some very strong estimates to that effect.

Under the change of variables $w = pe^{-i\varphi}$, (A.2.1) transforms to the equivalent system

$$\begin{aligned} \dot{w} &= v - i\omega_{\text{rot}} w + \varepsilon[G^p(w, \overline{w}, \varepsilon) - iwG^\varphi(w, \overline{w}, \varepsilon)] \\ \dot{\varphi} &= \omega_{\text{rot}} + \varepsilon G^\varphi(w, \overline{w}, \varepsilon). \end{aligned} \tag{A.2.2}$$

Generically, the w-equation in (A.2.2) has a unique smooth branch of equilibria $w^*(\varepsilon)$ for small ε when $\omega_{\text{rot}} \neq 0$. When $\varepsilon = 0$, $w^*(0)$ is a center and as such is surrounded by periodic orbits in the $w-$plane; otherwise, $w^*(\varepsilon)$ is a hyperbolic equilibrium whose stability is exactly determined by the sign of $\varepsilon \operatorname{Re}(a_1)$, where

$$a_1 = D_w G^p\left(\frac{v}{i\omega_{\text{rot}}}, -\frac{\overline{v}}{i\omega_{\text{rot}}}, 0\right) - iG^\varphi\left(\frac{v}{i\omega_{\text{rot}}}, -\frac{\overline{v}}{i\omega_{\text{rot}}}, 0\right) - \frac{v}{\omega_{\text{rot}}} D_w G^\varphi\left(\frac{v}{i\omega_{\text{rot}}}, -\frac{\overline{v}}{i\omega_{\text{rot}}}, 0\right).$$

These equilibria represent periodic solutions centered around the origin in the p-plane and are observable as anchored RW in the physical space.

Let

$$G^w(z, \overline{z}, \varepsilon) = G^p\left(z + \frac{v}{i\omega_{\text{rot}}}, \overline{z} - \frac{v}{i\omega_{\text{rot}}}, \varepsilon\right) - i\left(z + \frac{v}{i\omega_{\text{rot}}}\right) G^\varphi\left(z + \frac{v}{i\omega_{\text{rot}}}, \overline{z} - \frac{v}{i\omega_{\text{rot}}}, \varepsilon\right)$$

and $s = -\operatorname{sgn}(\omega_{\text{rot}})$. If ρ_0 is a non-trivial hyperbolic solution of

$$I(\rho) = \operatorname{Re}\left[\int_0^{2\pi} e^{-ist} G^w\left(\rho e^{ist} + \frac{v}{i\omega_{\text{rot}}}, \rho e^{-ist} - \frac{\overline{v}}{i\omega_{\text{rot}}}, 0\right) dt\right] = 0,$$

then the $w-$equation has a unique smooth branch of periodic solutions $w(t, \varepsilon)$, for small ε when $\omega_{\text{rot}} \neq 0$. When $\varepsilon = 0$,

$$w(t, 0) = \rho_0 e^{-i\omega_{\text{rot}} t} + \frac{v}{i\omega_{\text{rot}}};$$

otherwise, $w(t, \varepsilon)$ is a hyperbolic periodic solution whose stability is exactly determined by the sign of $\varepsilon I'(\rho_0)$. These periodic solutions represent quasi-periodic motion around the origin in the $p-$plane and are observable as epicycle-like motion in the physical space, with angular frequency $\omega_{\text{rot}} + O(\varepsilon)$, along a circular boundary.

TW can be thought of as orbits centered around infinity, *i.e.*, they lie on 'circles of infinite radius.' In [51], this is tackled by setting $z = w^{-1}$ in (A.2.2) and then considering the limiting case $\omega_{\text{rot}} \to 0$. The relevant system is given by

$$\dot{z} = -vz^2 + i\varepsilon z C^\varphi(z, \overline{z}, \varepsilon) - \varepsilon z^2 C^p(z, \overline{z}, \varepsilon), \tag{A.2.3}$$

where $C^\varphi(z, \overline{z}, \varepsilon) = G^\varphi(z^{-1}, \overline{z}^{-1}, \varepsilon)$ and $C^p(z, \overline{z}, \varepsilon) = G^p(z^{-1}, \overline{z}^{-1}, \varepsilon)$. If C^φ and C^p are smooth enough near $z = 0$, then for $\varepsilon \neq 0$ sufficiently small, (A.2.3) has two smooth

branches of equilibria: a center at $z = 0$ and a non-trivial source/sink $z^*(\varepsilon)$, who collide in a 'transcritical' bifurcation at $\varepsilon = 0$. The fixed $z = 0$ equilibria represent traveling waves in the $p-$plane and are observable as linear drifting in the physical space.

For normally hyperbolic relative periodic solutions (*i.e.*, the $q-$equation in (1.1.8) has a $2\pi-$periodic solution and the MRW is not at the transition to a RW), a center manifold reduction yields

$$\begin{aligned} \dot{p} &= \varepsilon G^p(pe^{-i\varphi}, \overline{p}e^{i\varphi}, \theta, \varepsilon) \\ \dot{\varphi} &= \omega_{\text{rot}} + \varepsilon G^\varphi(pe^{-i\varphi}, \overline{p}e^{i\varphi}, \theta, \varepsilon) \\ \dot{\theta} &= 1 + \varepsilon G^\theta(pe^{-i\varphi}, \overline{p}e^{i\varphi}, \theta, \varepsilon), \end{aligned} \tag{A.2.4}$$

where $\omega_{\text{rot}} \notin \mathbb{Z}$. After rescaling time so that $\dot{\theta} = 1$ and applying the change of variables $w = pe^{-i\varphi}$, (A.2.4) transforms to the equivalent system

$$\begin{aligned} \dot{w} &= -i\omega_{\text{rot}} w + \varepsilon H^w(w, \overline{w}, t, \varepsilon) \\ \dot{\varphi} &= \omega_{\text{rot}} + \varepsilon H^\varphi(w, \overline{w}, t, \varepsilon), \end{aligned} \tag{A.2.5}$$

where H^w and H^φ are $2\pi-$periodic in t. Generically, the time-2π map of (A.2.5) has a unique smooth branch of fixed points $w_*(\varepsilon)$ for small ε. When $\varepsilon = 0$, $w_*(0)$ is surrounded by a family of invariant circles, otherwise, $w_*(\varepsilon)$ is a hyperbolic fixed point, whose stability is exactly determined by the sign of $\varepsilon \operatorname{Re}\left[\int_0^{2\pi} h_1^w(t)dt\right]$, where

$$h_1^w(t) = D_w H^w(0, 0, t, 0).$$

These fixed points represent periodic solutions centered around the origin in the w-plane and are observable as MRW in the physical space.

If $\omega_{\text{rot}} \notin \mathbb{Q}$, consider the average value

$$M_{H,(\psi,\theta)}(\rho, \varepsilon) = \lim_{T\to\infty} \frac{1}{T} \int_0^T e^{i\omega_{\text{rot}}(\psi+t)} H^w\left(\rho e^{-i\omega_{\text{rot}}(\psi+t)}, \rho e^{i\omega_{\text{rot}}(\psi+t)}, \theta + t, \varepsilon\right) dt.$$

Then $M_{H,(\psi,\theta)}(\rho, \varepsilon)$ is independent of ψ and θ. If ρ_0 is a non-trivial hyperbolic solution of

$$J(\rho) = \operatorname{Re}\left[M_{H,(\psi,\theta)}(\rho, 0)\right] = 0,$$

then the $w-$equation of (A.2.5) has a unique smooth branch of invariant two-torii $T(\varepsilon)$ for small ε. When $\varepsilon = 0$, the flow on $T(0)$ is ergodic and every $w-$solution of (A.2.5) lies on its own two-torus; otherwise, $T(\varepsilon)$ is hyperbolic with stability exactly determined by the sign of $\varepsilon J'(\rho_0)$. Such an invariant two-torus represents an $O(\varepsilon)$ drift of a MRW (around a

point other than the origin) around its $\mathbb{SO}(2)$−orbit about 0 in (A.2.4) and is observable as a three-frequency motion in the physical space.

If $\omega_{\text{rot}} \in \mathbb{Q}$, with $\omega_{\text{rot}} = \frac{q}{\ell}$, $\gcd(q,\ell) = 1$ and $\ell > 1$, consider the average value

$$N_{H,\theta}(\xi,\overline{\xi},\varepsilon) = \lim_{T\to\infty} \frac{1}{T} \int_0^T e^{i\omega_{\text{rot}}(\theta+t)} H^w \left(\xi e^{-i\omega_{\text{rot}}(\theta+t)}, \overline{\xi} e^{i\omega_{\text{rot}}(\theta+t)}, \theta + t, \varepsilon\right) dt.$$

Then $N_{H,\theta}(\xi,\overline{\xi},\varepsilon)$ is independent of θ and is $\mathbb{Z}_\ell$−equivariant. If $\tilde{\xi}(t)$ is a hyperbolic periodic solution or an equilibrium point, respectively, of $\dot{\xi} = h_0(\xi,\overline{\xi})$, where

$$h_0(\xi,\overline{\xi}) = N_{H,\theta}(\xi,\overline{\xi},0),$$

then the w−equation of (A.2.5) has a unique smooth branch of invariant two-torii $\tilde{T}(\varepsilon)$ or $\frac{2\pi}{\ell}$−periodic solutions $\tilde{w}(t,\varepsilon)$, respectively, for small ε. In the case of the invariant two-torus, when $\varepsilon = 0$, $\tilde{T}(0)$ is foliated by $\frac{2\pi}{\ell}$−periodic solutions and every w−solution of (A.2.5) lies on its own two-torus; otherwise, $T(\varepsilon)$ is hyperbolic with stability as an invariant set exactly determined by the product of the sign of the stability of $\tilde{\xi}(t)$ with the sign of ε.

MTW are approached much the same way as TW. The relevant system is

$$\begin{aligned} \dot{p} &= e^{i\varphi}[v + \varepsilon G^p(pe^{-i\varphi}, \overline{p}e^{i\varphi}, \theta, \varepsilon)] \\ \dot{\varphi} &= \varepsilon G^\varphi(pe^{-i\varphi}, \overline{p}e^{i\varphi}, \theta, \varepsilon) \\ \dot{\theta} &= 1 + \varepsilon G^\theta(pe^{-i\varphi}, \overline{p}e^{i\varphi}, \theta, \varepsilon), \end{aligned} \tag{A.2.6}$$

where $v \in \mathbb{C}^\times$. After rescaling time so that $\dot{\theta} = 1$ and applying the change of variables $w = pe^{-i\varphi}$, (A.2.6) transforms to the equivalent system

$$\begin{aligned} \dot{w} &= v + \varepsilon H^w(w,\overline{w},t,\varepsilon) \\ \dot{\varphi} &= \varepsilon H^\varphi(w,\overline{w},t,\varepsilon), \end{aligned} \tag{A.2.7}$$

where H^w and H^φ are 2π−periodic in t and H^φ is real-valued. Setting $z = w^{-1}$ in (A.2.7) yields

$$\begin{aligned} \dot{z} &= -vz^2 + \varepsilon C^z(z,\overline{z},t,\varepsilon) \\ \dot{\varphi} &= \varepsilon C^\varphi(z,\overline{z},t,\varepsilon), \end{aligned} \tag{A.2.8}$$

where $C^z(z,\overline{z},t,\varepsilon) = -z^2 H^w(z^{-1},\overline{z}^{-1},t,\varepsilon)$ and $C^\varphi(z,\overline{z},t,\varepsilon) = H^\varphi(z^{-1},\overline{z}^{-1},t,\varepsilon)$. If C^z and C^φ are smooth-enough near $z = 0$, then for $\varepsilon \neq 0$ sufficiently small, the time−2π map of the z−equation in (A.2.8) has two smooth branches of fixed points: one at $z = 0$ and a non-trivial one at $z_*(\varepsilon)$, who collide in 'transcritical' bifurcation at $\varepsilon = 0$, as in the TW case. The trivial fixed points $z = 0$ represent MTW in the p−plane and are observable as linear meandering in the physical space. ∎

A.3 Summary of [48]

In *Rotational Symmetry-Breaking for Spiral Waves*, LeBlanc studies small $\mathbb{C}\dot{+}\mathbb{Z}_\ell$–equivariant perturbations of (1.1.6) taking the form (1.1.9).

Summary: Consider the system (1.1.9). For normally hyperbolic relative equilibria, a center manifold reduction yields

$$\begin{aligned} \dot{p} &= e^{i\varphi}[v + \varepsilon G^p(\varphi, \varepsilon)] \\ \dot{\varphi} &= \omega_{\text{rot}} + \varepsilon G^\varphi(\varphi, \varepsilon), \end{aligned} \tag{A.3.1}$$

where $v \in \mathbb{C}^\times$, $\omega_{\text{rot}} \in \mathbb{R}$ and G^p, G^φ are $\frac{2\pi}{\ell}$–periodic in φ, $\ell \geq 1$ an integer.

Let $\omega_{\text{rot}} \neq 0$. If $\varepsilon = 0$, all solutions of (A.3.1) are RW. If $\varepsilon \neq 0$ is sufficiently small, all solutions of (A.3.1) are $\frac{2\pi}{\ell}$–periodic in time with discrete $\mathbb{Z}_\ell$–symmetry, *i.e.*, evolution in time by $\frac{2\pi}{\ell^2}$ is the same as a spatial rotation by $\frac{2\pi}{\ell}$. These periodic solutions represent discrete RW in the physical space.

Now, consider the case $\omega_{\text{rot}} = 0$. If $\varepsilon = 0$, all solutions are TW. If $\varepsilon \neq 0$ is sufficiently small, there are two possibilities:

(i) if $G^\varphi(\varphi, 0) \neq 0$ for all $\varphi \in \mathbb{S}^1$, then all solutions of (A.3.1) are discrete RW, with large radii of the order of $\frac{1}{\varepsilon}$.

(ii) if there exists $\varphi^* \in [0, 2\pi)$ such that $G^\varphi(\varphi^*, 0) = 0$ and $D_\varphi G^\varphi(\varphi^*, 0) \neq 0$, then (A.3.1) has at least ℓ stable (*i.e.*, attracting) TW solutions and an equal number of unstable (*i.e.*, repelling) TW solutions. In that case, all solutions of (A.3.1) end up drifting linearly, after 'an initial transient period.'

For normally hyperbolic relative periodic solution, a center manifold reduction yields

$$\begin{aligned} \dot{p} &= e^{i\varphi}[F^p(\theta) + \varepsilon G^p(\varphi, \theta, \varepsilon)] \\ \dot{\varphi} &= \omega_{\text{rot}} + F^\varphi(\theta) + \varepsilon G^\varphi(\varphi, \theta, \varepsilon) \\ \dot{\theta} &= F^\theta(\theta) + \varepsilon G^\theta(\varphi, \theta, \varepsilon), \end{aligned} \tag{A.3.2}$$

where $\omega_{\text{rot}} \in \mathbb{R}$ and all functions are 2π–periodic in θ and $\frac{2\pi}{\ell}$–periodic in φ. If $F^\varphi(\theta) \neq 0$ for all $\theta \in \mathbb{S}^1$, time can be rescaled so that (A.3.2) transforms to the equivalent system

$$\begin{aligned} \dot{p} &= e^{i\varphi}[\tilde{F}^p(\theta) + \varepsilon \tilde{G}^p(\varphi, t, \varepsilon)] \\ \dot{\varphi} &= \omega_{\text{rot}} + \tilde{F}^\varphi(\theta) + \varepsilon \tilde{G}^\varphi(\varphi, t, \varepsilon), \end{aligned} \tag{A.3.3}$$

where all functions are 2π–periodic in θ and $\frac{2\pi}{\ell}$–periodic in φ. Furthermore it can be assumed that the average value of $\tilde{F}^\varphi$ is 0.[3]

[3] If it is not, it can simply be added to ω_{rot}.

If $\varepsilon = 0$, all solutions of (A.3.3) are discrete MRW (if $\omega_{\text{rot}} \notin \mathbb{Z}$) or MTW (if $\omega_{\text{rot}} \in \mathbb{Z}$). If $\varepsilon \neq 0$ is sufficiently small, the φ–equation in (A.3.3) defines a $\mathbb{Z}_\ell$–equivariant flow on a two-torus. The Poincaré map of this flow takes the form

$$P(\varphi; \omega_{\text{rot}}, \varepsilon) = \varphi + 2\pi\omega_{\text{rot}} + \varepsilon H(\varphi, \omega_{\text{rot}}, \varepsilon), \tag{A.3.4}$$

where H is $\frac{2\pi}{\ell}$–periodic in φ, and C^r for some $r \geq 3$. The map P is a circle map; its rotation number is denoted by $\rho_{\omega_{\text{rot}},\varepsilon}$.

Suppose $\rho_{\omega_{\text{rot}},\varepsilon} = \frac{m}{q}$, where $m, q \in \mathbb{Z}$ with $\gcd(m, q) = 1$ and $q > 0$. Set $k = \gcd(q, \ell)$. Phase-locking occurs when $(\omega_{\text{rot}}, \varepsilon)$ lies in the $m : q$ Arnol'd tongue of P. If $k \neq 1$, the p–component of solutions of (A.3.3) is a q–petaled $2\pi q$–periodic curve with $\mathbb{Z}_k$–spatial symmetry. If $k = 1$, then the p–component of solutions of (A.3.3) is a superposition of a motion as in the case $k \neq 1$ together with a 'slow' linear drift.

Suppose now $\rho_{\omega_{\text{rot}},\varepsilon} \notin \mathbb{Q}$. Then the flow on the two-torus described above is ergodic. If there exist $\sigma \in (0, 1)$ and $K > 0$ such that

$$\left| \rho_{\omega_{\text{rot}},\varepsilon} + \frac{k}{j} \right| \geq K|j|^{-(2+\sigma)}$$

for all non-trivial integer pairs (k, j) (which is almost always the case), then the p–component of solutions of (A.3.3) is quasi-periodic and the closure of its positive image has $\mathbb{Z}_\ell$–rotational symmetry. ∎

Appendix B

Spirals in the Literature

This appendix contains a selected bibliography of spiral pattern formation in excitable media and numerical experiments. Within each category, the articles are listed in chronological order.

BZ Reaction and the Oregonator: [52], [35], [80], [55].

Cardiac Tissue and the FHN Equations: [71], [77], [24], [59], [75], [43], [53].

Global Spiral Dynamics: [39], [78].

Surveys of Spiral Wave Behaviour: [42], [73], [13].

Dynamical System Approach: [8], [5], [7], [62], [30], [63], [31], [51], [48], [15], [12], [11], [14].

Bibliography

[1] Alonso, S., Sagués, F. and Mikhailov, A.S. [2003], Taming winfree turbulence of scroll waves in excitable media, *Science*, **299**, 1722–1725.

[2] Apollonius of Perga [1997], *Conics*, Green Lion Press, Santa Fe, edited by Densmore.

[3] Aptekarev, A.I., Kalyaguine, V. and van Assche, W. [1995], Criterion for the resolvent set of non-symmetric tridiagonal operators, *Proc. of Amer. Math. Soc.*, **123**, 2423–2430.

[4] Ball, P. [1994], *Designing the Molecular World: Chemistry At the Frontier*, Princeton University Press, Princeton.

[5] Barkley, D. [1992], Linear stability analysis of rotating spiral waves in excitable media, *Phys. Rev. Lett.*, **68**, 2090–2093.

[6] Barkley, D. [1994], Euclidean symmetry and the dynamics of rotating spiral waves, *Phys. Rev. Lett.*, **76**, 164–167.

[7] Barkley, D. and Kevrekedis, I.G. [1994], A dynamical system approach to spiral wave dynamics, *Chaos*, **4**, 453–460.

[8] Barkley, D., Kness, M. and Tuckerman, L.S. [1990], Spiral-wave dynamics in a simple model of excitable media: The transition from simple to compound rotation, *Phys. Rev. Lett.*, **42**, 2489–2492.

[9] Beuter, A., Glass, L., Mackey, M.C. and Titcombe, M.S. (eds.) [2003], *Nonlinear Dynamics in Physiology and Medecine*, Springer, New York.

[10] Boily, P. [2000], *Analyse numérique de bifurcations dans les systèmes d'équations différentielles paramétrées*, Master's thesis, University of Ottawa.

[11] Boily, P. [forthcoming], Epicyclic drifting in anisotropic excitable media with multiple inhomogeneities: a dynamical system approach, arXiv: math.DS/0602141, submitted to *SIADS*.

[12] Boily, P. [forthcoming], Spiral anchoring in anistropic media with multiple inhomogeneities: a dynamical system approach, arXiv: math.DS/0602142, submitted to *Nonlinearity*.

[13] Boily, P. [forthcoming], Spiral waves and the dynamical system approach, arXiv: math.DS/0601033.

[14] Boily, P. and Ethier, M. [forthcoming], Spiral anchoring in a modified bidomain model.

[15] Boily, P., LeBlanc, V.G. and Matsui, E. [forthcoming], Spiral anchoring in media with multiple inhomogeneities: a dynamical system approach, arXiv: math.DS/0512511, submitted to *J. Nonlin. Sc.*

[16] Bourgault, Y. [2003], personal communication.

[17] Bourgault, Y., Éthier, M. and LeBlanc, V.G. [2003], Simulation of electrophysiological waves with an unstructured finite element method, *ESAIM:M2AN*, **37**, 649–662.

[18] Braune, M., Schrader, A. and Engel, H. [1994], Entrainment and resonance of spiral waves in active media with periodically modulated excitability, *Chem. Phys. Lett.*, **222**, 358–362.

[19] Bub, G., Shrier, A. and Glass, L. [2002], Spiral wave generation in heterogeneous excitable media, *Phys. Rev. Lett.*, **88**, 0581011–0581014.

[20] Chang, H.C., He, W. and Prabhu, N. [2003], The analytic domain in the implicit function theorem, *J. Inequal. Pure Appl. Math.*, **4**, no assigned page numbers, document only available in electronic format.

[21] Chàvez, F., Kapral, R., Rousseau, G. and Glass, L. [2001], Scroll waves in spherical shell geometries, *Chaos*, **11**, 757–765.

[22] Colli Franzone, P. and Savaré, G. [2002], Degenerate evolution systems modeling the cardiac electric field at micro- and macroscopic level, in *Evolution equations, semigroups and functional analysis: in memory of Brunello Terreni* (Lorenzi and Ruf, eds.), Birkhäuser, Basel, 49–78.

[23] Comanici, A. [2004], *Spiral Waves on Spherical Domains: A Dynamical System Approach*, Ph.D. thesis, University of Ottawa.

[24] Davidenko, J.M., Persov, A.V., Salomonsz, R., Baxter, W. and Jalife, J. [1992], Stationary and drifting spiral waves of excitation in isolated cardiac muscle, *Nature*, **355**, 349–351.

[25] Dubrovin, B.A., Fomenko, A.T. and Novikov, S.P. [1985], *Modern Geometry – Methods and Applications (Part II: The Geometry and Topology of Manifolds)*, Springer, New York.

[26] Dym, H. and McKean, H.P. [1972], *Fourier Series and Integrals*, Academic Press, New York.

[27] Fiedler, B., Sandstede, B., Scheel, A. and Wulff, C. [1996], Bifurcation from relative equilibria of noncompact group actions: Skew products, meanders and drifts, *Doc. Math.*, **1**, 479–555.

[28] Glass, L. [2001], heard during the Applied Math Seminar (UO).

[29] Glass, L., Guevara, M.R., Shrier, A. and Perez, R. [1983], Bifurcation and chaos in a periodically stimulated cardiac cell oscillator, *Physica D*, 89–101.

[30] Golubitsky, M., LeBlanc, V.G. and Melbourne, I. [1997], Meandering of the spiral tip: An alternative approach, *J. Nonlin. Sc.*, **7**, 557–586.

[31] Golubitsky, M., LeBlanc, V.G. and Melbourne, I. [2000], Hopf bifurcation from rotating waves and patterns in physical space, *J. Nonlinear Sc.*, **10**, 69–101.

[32] Golubitsky, M. and Schaeffer, D.G. [1985], *Singularities and Groups in Bifurcation Theory, Volume I*, Springer-Verlag, Berlin.

[33] Golubitsky, M. and Stewart, D.G. I. et Schaeffer [1988], *Singularities and Groups in Bifurcation Theory, Volume II*, Springer-Verlag, Berlin.

[34] Greenberg, J.M., Hassard, N.D. and Hastings, S.P. [1978], Pattern formation and periodic structures in systems modeled by reaction-diffusion equations, *B. Am. Math. Soc.*, **84**, 1296–1326.

[35] Grill, S., Zykov, V.S. and Müller, S.C. [1996], Spiral wave dynamics under pulsatory modulation of excitability, *J. Phys. Chem.*, **100**, 19082–19088.

[36] Guckenheimer, J. and Holmes, P. [1983], *Nonlinear Oscillations, Dynamical Systems, and Bifurcations of Vector Fields*, Springer, New York.

[37] Hale, J.K. [1961], Integral manifolds of perturbed differential equations, *Ann. Math.*, **73**, 496–531.

[38] Hale, J.K. [1969], *Ordinary Differential Equations*, Wiley, New York.

[39] Hendrey, M., Ott, E. and Antonsen, T.M. [2000], Spiral wave dynamics in oscillatory inhomogeneous media, *Phys. Rev. E*, **61**, 4943–4953.

[40] Henry, D. [1981], *Geometric Theory of Semilinear Parabolic Equations*, Springer-Verlag, Berlin.

[41] Hircsh, M.W. and Smale, S. [1974], *Differential Equations, Dynamical Systems, and Linear Algebra*, Academic Press, San Diego.

[42] Jahnke, W. and Winfree, W.T. [1991], A survey of spiral-wave behaviors in the oregonator model, *Int. J. Bifur. Chaos*, **1**, 445–466.

[43] Jalife, J. [2000], Ventricular fibrillation: Mechanisms of initiation and maintenance, *Annu. Rev. Physiol.*, **62**, 25–50.

[44] Keener, J. and Sneyd, J. [1998], *Mathematical Physiology*, IAM, Springer, New York.

[45] Keller, H.B. [1977], Numerical solutions of bifurcation and nonlinear eigenvalue problems, in *Applications of Bifurcation Theory*, 359–384.

[46] Krupa, M. [1990], Bifurcations from relative equilibria, *SIAM J. Math. Anal.*, **21**, 1453–1486.

[47] Kuznetsov, Yu. [1995], *Elements of Applied Bifurcation Theory*, Springer-Verlag, Berlin.

[48] LeBlanc, V.G. [2002], Rotational symmetry-breaking for spiral waves, *Nonlinearity*, **15**, 1179–1203.

[49] LeBlanc, V.G. and Lajoie, G. [2005], personal communication.

[50] LeBlanc, V.G. and Roth, B.J. [2003], Meandering of spiral waves in anisotropic tissue, *Dynam. Contin. Discrete Impuls. Systems*, **B10**, 29–42.

[51] LeBlanc, V.G. and Wulff, C. [2000], Translational symmetry-breaking for spiral waves, *J. Nonlin. Sc.*, **10**, 569–601.

[52] Li, G., Ouyang, Q., Petrov, V. and Swinney, H.L. [1996], Transition from simple rotating chemical spirals to meandering and traveling spirals, *Phys. Rev. Lett.*, **77**, 2105–2109.

[53] Mackenzie, D. [2004], Making sense of a heart gone wild, *Science*, **303**, 786–787.

[54] Marsden, J.E. [1974], *Elementary Classical Analysis*, Freeman, New York.

[55] Muñuzuri, A.P., Pérez-Muñuzuri, V. and Pérez-Villar, V. [1998], Attraction and repulsion of spiral waves by localized inhomogeneities in excitable media, *Phys. Rev. E*, **58**, R2689–R2692.

[56] Murray, J.D. [2003], *Mathematical Biology - I: An Introduction*, Springer, New York, third edn.

[57] Murray, J.D. [2003], *Mathematical Biology - II: Spatial Models and Biomedical Applications*, Springer, New York, third edn.

[58] Roth, B.J. [1997], Approximate analytical solutions to the bidomain equations with unequal anisotropy ratios, *Phys. Rev. E*, **55**, 1819–1826.

[59] Roth, B.J. [1998], Frequency locking of meandering spiral waves in cardiac tissue, *Phys. Rev. E*, **57**, R3735–R3738.

[60] Rudin, W. [1987], *Real and Complex Analysis*, McGraw-Hill, Boston.

[61] Sandstede, B., Scheel, A. and Wulff, C. [1997], Center manifold reduction for spiral waves, *C. R. Acad. Sci.*, **324**, 153–158.

[62] Sandstede, B., Scheel, A. and Wulff, C. [1997], Dynamics of spiral waves on unbounded domains using center-manifold reductions, *J. Diff. Eq.*, **141**, 122–149.

[63] Sandstede, B., Scheel, A. and Wulff, C. [1999], Bifurcations and dynamics of spiral waves, *J. Nonlin. Sc.*, **9**, 439–478.

[64] Scheel, A. [1998], Bifurcation to spiral waves in reaction-diffusion systems, *SIAM J. Math. Anal.*, **29**, 1399–1418.

[65] Setayeshgar, S. and Bernoff, A.J. [2002], Scroll waves in the presence of slowly varying anisotropy with application to the heart, *Phys. Rev. Lett.*, **88**, 028101.

[66] Siegert, F. and Weijer, C.J. [1992], Three-dimensional scroll waves organize dictyostelium slugs, *Proc. Natl. Acad. Sci. USA*, **89**, 6433–6437.

[67] Szarski, J. [1965], *Differential Inequalities*, PWN-Polish Scientific Publishers, Warsaw.

[68] Taylor, M.E. [1996], *Partial Differential Equations, Volume III: Nonlinear Equations*, Springer, New York.

[69] Vanderbauwhede, A. [1982], *Local Bifurcation Theory and Symmetry*, Pitman, London.

[70] Vanderbauwhede, A. [1989], Centre manifolds, normal forms and bifurcations, in *Dynamics Reported, Vol. 2*, Wiley, New York.

[71] Wiener, N. and Rosenblueth, A. [1946], The mathematical formulation of the problem of conduction of impulses in a network of connected excitable elements, specifically in cardiac muscle, *Arch. Inst. Card. De Mexico*, **16**, 205–265.

[72] Wiggins, S. [1990], *Introduction to Applied Non-Linear Dynamical Systems and Chaos*, Springer, New York.

[73] Winfree, A.T. [1991], Varieties of spiral wave behavior: An experimentalist's approach to the theory of excitable media, *Chaos*, **1**, 303–334.

[74] Winfree, A.T. [1995], in *Cardiac Electrophysiology, From Cell to Bedside* (Zipes and Jalife, eds.), Saunders, Philadelphia, second edn., 379–389.

[75] Witkowski, F.X., Leon, L.J., Penkoske, P.A., Giles, W.R., Spanol, M.L., Ditto, W.L. and Winfree, A.T. [1998], Spatiotemporal evolution of ventricular fibrillation, *Nature*, **392**, 78–82.

[76] Wulff, C. [1996], *Theory of Meandering and Drifting Spiral Waves in Reaction-Diffusion Systems*, Ph.D. thesis, Freie Universität Berlin.

[77] Yermakova, Y.A. and Pertsov, A.M. [1987], Interaction of rotating spiral waves with a boundary, *Biophys.*, **31**, 932–940.

[78] Zaritski, R.M. and Pertsov, A.M. [2002], Stable spiral structures and their interaction in two-dimensional excitable media, *Phys. Rev. E*, **66**, 066120–1–066120–6.

[79] Zwillinger, D. (ed.) [1996], *Standard Mathematical Tables and Formulae*, CRC, Boca Raton, 30th edn.

[80] Zykov, V.S. and Müller, S.C. [1996], Spiral waves on circular and spherical domains of excitable medium, *Physica D*, **97**, 322–332.